UNIVERSITY OF SOUTHAMPTON

ASSESSING THE PERFORMANCE ENVELOPE OF TOTAL KNEE REPLACEMENT – AN EXPLICIT FINITE ELEMENT STUDY

Rachael Tan Kheng Hooi

A thesis submitted in partial fulfilment of the requirements for the degree of

Doctor of Philosophy

SCHOOL OF ENGINEERING SCIENCES
Bioengineering Science Research Group

May 2004

UNIVERSITY OF SOUTHAMPTON
ABSTRACT
FACULTY OF ENGINEERING AND APPLIED SCIENCES
BIOENGINEERING SCIENCE RESEARCH GROUP
Doctor of Philosophy

ASSESSING THE PERFORMANCE ENVELOPE OF TOTAL KNEE REPLACEMENT – AN EXPLICIT FINITE ELEMENT STUDY

by Kheng Hooi Tan

Total knee replacement (TKR) has proven long term success in elderly patients. During normal walking, the knee joint is subjected to an average force of 3 times body weight (BW). However, the knee joint is subjected to even higher forces, up to 7 times body weight while carrying out more vigorous activities. To date, many of the experimental and finite element studies have only investigated the kinematics and stresses within the TKR using a single idealised load case, typically that of level gait. Since the knee joint is routinely loaded with forces higher than 3 times BW, there is a need to investigate the performance of TKR for various activities. Clinical follow-up studies have shown that a significant portion of implanted knees exhibited highly variable kinematics for the same prosthesis design implanted in a group of patients. This wide range of kinematics from the same prosthesis suggests that they are dependent on patient related factors (gait patterns and loading conditions) and surgical related factors (alignment). Gait analysis combined with inverse dynamic calculations have shown variations in the magnitude of the joint contact forces *in vivo* within a group of subjects undergoing same activity. Although it is well understood that a TKR design will experience a range of loading conditions *in vivo*, at present, it is only evaluated using single load case *in vitro* and the potential influence of patient-to-patient variability ignored. Alignment of TKR components in the lower limb is essential in providing excellent kinematics outcome post-operatively. However, many of the biomechanical studies that investigate the performance of TKR assume an ideal prosthetic alignment. The effect of malalignment on the performance of TKR has not been investigated extensively.

Hence, the purpose of this study was to examine: 1) The performance of TKR for a variety of activities, 2) The performance of TKR under the influence of eccentric loading, 3) The performance envelope of TKR under subject specific loading, and 4) The effect of misalignment on the performance of TKR. Two TKR designs: PFC Σ and PFC PLI knees (DePuy) have been examined in this thesis. Simulations were performed using dynamic finite element method. In the first study, the TKR produced larger kinematics and contact pressures when simulated using more demanding loads from stair descent and squatting activities. Stair ascent and level gait activities were also simulated. Inclusion of other loading activities in wear studies could help in understanding wear observed *in vivo*. In the 2nd study, the influence of varus/valgus knee on the performance of TKR was simulated by offsetting the point of application of the axial load either medially or laterally. Medial eccentric loading was the most destructive for the TKR particularly when the collateral ligaments were not included. The femoral component rode up the anterior lip of the tibial insert and nearly subluxed. Lateral eccentric loading did not show significant kinematics variations as compared to medial eccentric loading, with or without the collateral ligaments. The femoral component did not ride up the anterior edge of the tibial insert. Both the medial and lateral eccentric loading should be avoided as they increased the contact stresses and would lead to accelerated wear. In the 3rd study, the simulations were performed by applying level gait loads obtained from 7 subjects and stair ascent loads from 9 subjects. Performance envelopes in the kinematics and contact pressures were obtained as a result of patient-to-patient variability. The kinematics for the PFC Σ and PLI designs were relatively insensitive to subject specific loading during level gait but greater variations during stair ascent. The contact pressures during level gait were largely dependent on the applied axial load; whereas during stair ascent, the contact pressures were also a function of the applied A-P forces and I-E torque. In the 4th study, simulations were performed by offsetting the TKR 3 mm in the proximal-distal and anterior-posterior directions with respect to the ligamentous structures. Varus/valgus tilt (5°) of the TKR and internal/external malrotation (5°) of the tibial insert relative to the femoral component were also simulated. The average loads during level gait and stair descent from subject specific loading were applied to the FE model. Overall, the kinematics of PFC Σ and PLI designs were less sensitive to the misalignment when the level gait loads were applied as compared to the stair ascent loads. The contact pressures for both the designs were influenced by malalignment, for both activities.

LIST OF CONTENTS

LIST OF FIGURES

Appendix A

Appendix B

LIST OF TABLES

ACKNOWLEDGEMENTS

I would like to take this opportunity to thank the following that have helped me and contributed to this thesis.

Dr. Mark Taylor, who has been very professional in advising and guiding me through my academic progress. Also, to his patience and unlimited kind support.

All my colleagues within the Bioengineering Science Research Group, who have been very supportive and managed to cheer me up during the stressful time of writing up.

Dr. Patrick Costigan, Queen's University, Canada for his contributions to the FE input data.

Dr. Ana Alonso Vázquez, Dr. Antonio Perillo-Marcone and Dr. Andy New, for their valuable ideas and helps, especially in the field of finite element modelling.

Cécile Schott, Ana Alonso, Dominique Mouazé, Katherine Brown and Ralitza Nikolova, who have been extremely supportive and understanding. You all have lightened up my life and I am very proud to have known you all.

My parents, brother and sister for always being beside me and listen to me.

Finally, I want to acknowledge DePuy International Ltd. (Leeds, UK) and the University of Southampton for funding this research.

UCAPAN TERIMA KASIH

Penulis ingin mengambil peluang ini untuk mengucapkan ribuan terima kasih kepada

Dr. Mark Taylor, penasihat projek ini, yang tidak bosan mengedit projek ini dan telah memberikan nasihat serta ide-ide untuk hasil akhir yang terbaik. Kapakaran beliau amat dihargai.

Rakan-rakan sekerja Kejuteraan Bioloji di Universiti Southampton, yang telah memberikan sokongan moral kepada penulis, terutamanya semasa penulisan projek ini.

Dr. Patrick Costigan, dari Universiti Queen's (Canada). Beliau telah menyumbangkan data-data untuk kegunaan dalam projek ini.

Dr. Ana Alonso Vázquez, Dr. Antonio Perillo-Marcone serta Dr. Andy New, yang telah aktif memberikan maklumat-maklumat terhadap penulisan projek ini. Kepakaran anda sekalian dalam 'finite element modelling' amat dihargai.

Cécile Schott, Ana Alonso, Dominique Mouazé, Katherine Brown serta Ralitza Nikolova. Sokongan dan ucapan dari rakan-rakan telah memberikan semangat dan keyakinan untuk meneruskan tugasan penulis. Kehadiran anda sekalian telah dan akan terus menjadi inspirasi dan semangat kepada penulis.

Ibuanda, ayahanda, adik perempuan serta adik lelaki atas doa-an dan dukungan-mu sekalian. Kasih saying yang tidak terhad dari mu telah memberikan kekuatan serta semangat pejuangan untuk mencapai matlamat penulis.

Akhir sekali, penulis ingin mengucapkan ribuan terima kasih kepada DePuy Int. Ltd. (Leeds, UK) serta Universiti Southampton keatas sumbangan kewangan dalam projek ini.

NOMENCLATURES

TKR	total knee replacement
BW	body weight
ACL	anterior cruciate ligament
PCL	posterior cruciate ligament
MCL	medial collateral ligament
LCL	lateral collateral ligament
FE	finite element
OA	osteoarthritis
RA	rheumatoid arthritis
LBA	load bearing axis
CH	condylar-hip angle
CP	condylar-plateau angle
PA	plateau-ankle angle
SD	standard deviation
A-P	anterior-posterior
I-E	internal-external
PMMA	polymethylmethacylate cement
MMA	methyl-methacrylate
PCR	posterior cruciate retaining
CAE	computer-aided engineering
UHMWPE	ultra high molecular weight polyethylene
PE	polyethylene
HLS	horizontal linear spring
RSA	radiostereometric analysis

THESIS OBJECTIVES

In an elderly population, total knee replacement (TKR) is generally a successful operation. However, failure of TKR does occur. The potential problems in TKR are polyethylene wear, loosening and infection. The number of TKR implanted into younger patients have increased in the recent years, particularly those involve in more physical demanding activities. Polyethylene wear rate in young, active patients are particularly of concern [8,14]. Wear is a function of kinematics and stresses. The amount and pattern of kinematics produced are dependent on TKR design, implant positioning in the lower limb and soft tissues balance. *In vivo* clinical studies using fluoroscopy have shown variable kinematics for the same design of prosthesis. This suggests that variability in the kinematics is also strongly dependent on the patient-to-patient variability. Implant positioning plays a substantial role in the outcome of the TKR after surgery. Improper implant orientation causes imbalancing in the soft tissues and ultimately affects the range of motion. Misalignment in the TKR also leads to uneven load distribution in the components. The aim of this thesis is to use an explicit FE model to study some of the factors, which may influence the performance of TKR by examining the kinematics and the polyethylene stresses. These factors include: eccentric loading study, subject specific loading and malorientation in the TKR.

In Chapter 1, a brief description of the anatomy and function of the knee joint and knee ligaments are presented, followed by an overview of the range of knee joint motion and knee joint forces in Chapter 2. Chapter 3 looks at the types of total knee design and discusses different wear modes of the polyethylene insert. Chapter 3 also focuses on the factors leading to failure of TKR and gives an overview of approaches to tackling the problems arising from TKR. Chapter 4 discusses about the assessment of finite element modelling parameters to test the convergence of parameters of interest with two TKR models that will be used in the study. Information regarding boundary conditions and material properties in the FE modelling are also described here. In chapter 5, comparisons are made on the performances of TKR during different daily activities. Chapter 6 analyses the influence of eccentric loading on the performance of TKR and Chapter 7 examines the variability in patient-to-patient loading on the performance of TKR. This chapter examines the influence of ligament modelling has on the predicted kinematics and stresses. To gain an understanding to the influence of malorientation on the performance of TKR and how it affects the soft tissues tension is performed in Chapter 8. Finally, in Chapter 9, a critical discussion of the finite element analyses performed is presented, followed by recommendations for future developments.

Chapter 1

ANATOMY OF THE KNEE

The knee is one of the most complex joints in the human body. This articulation has six degrees of freedom and mainly works in flexion-extension. Other movements that are encountered by the knee joint are: adduction, abduction, internal or external rotation, medial or lateral motion, anterior or posterior translation. The knee is principally loaded in compression under the force of gravity and muscle forces. From the mechanical point of view, in full extension, due to the position of the knee joint below the centre of gravity of the body, it supports large stresses due to the body weight. Various knee joint functions, such as walking, stair-ascent, stair-descent, running and etc. constantly subjected the knee joint to high forces and torque, making this joint vulnerable to injury. The stability of the knee depends upon the ligaments, the congruency and conformity of the articulating surfaces and as well as the surrounding muscles. Understanding this ingenious mechanical system is vital in understanding the whole mechanics of the total knee replacement. In the following section, the structures of the knee joint and the ligaments involve in the mobility of the knee joint will be discussed.

1.1 ANATOMY OF THE KNEE

In the knee joint, surface motion occurs in three planes simultaneously but is greatest by far in the sagittal plane [110]. Figure 1-1 shows the anatomical reference planes. The knee is a complex joint and involves three main bones. The femur (thigh bone) and the tibia (shin bone) meet to form a loose hinge joint. The joint is protected by the patella, which is also known as the kneecap. The patella is the moveable bone on the front of the knee and it is wrapped inside a large tendon that connects the large muscles on the front of the thigh, the quadriceps muscles, to the lower leg bone. This large tendon, when combined with the patella is called the quadriceps mechanism. The quadriceps mechanism allows one to straighten out the knee. The patella acts to increase the lever arm and hence, increases the force of the quadriceps muscle. The patellar glide is a special groove of the thigh bone (femur), called the patellar groove. Together the patella and the groove in the femur are called the patello-femoral mechanism. Just below and next to the tibia is the fibula, which runs parallel to the tibia. The fibula is situated on the lateral side of the tibia (Figure 1-2).

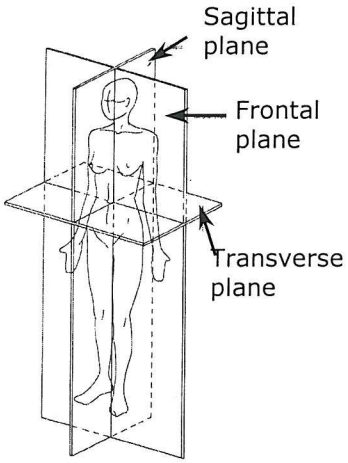

Sagittal plane: A longitudinal plane that divides the human body of a bilateral symmetrical into right and left sections.
Frontal plane: This plane is perpendicular to the sagittal plane and divides the body into front and back section.
Transverse plane: This plane is perpendicular to sagittal and frontal plane and divides the body into upper (proximal) and lower (distal) portions.

Figure 1-1: Anatomical plane [72].

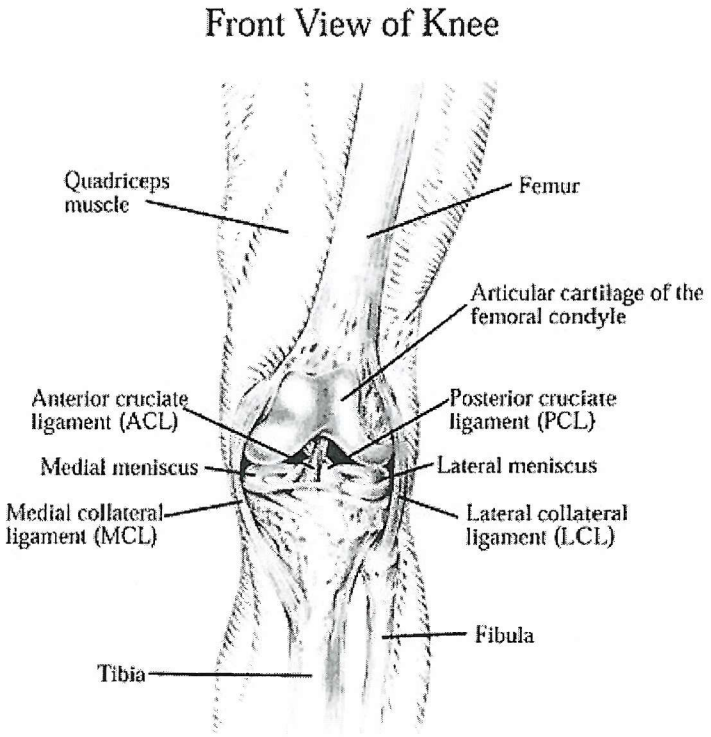

Figure 1-2: Anatomy of the knee joint. Picture obtained from http://cincinnatisportsmed.com/

The important internal parts of the knee include the articular cartilage, menisci, ligaments and tendons. The knee joint is cushioned by articular cartilage (Figure 1-2), a smooth and soft tissue that covers the ends of the femur and the tibia, as well as the back of the patella. The articular cartilage has a white, shiny appearance and rubbery consistency. Further supporting the knee joint are two structures called menisci that sit between the femur and tibia. The two menisci (medial and lateral) are also referred to as the semilunar

cartilages (Figure 1-3), and act to distribute the load more evenly in between the articular surfaces.

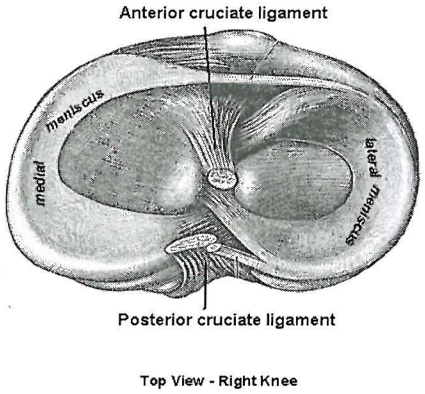

Figure 1-3: Medial and lateral menisci which act as padding to the femur and tibia. They help to distribute the load more evenly in between the articular surfaces [56].

Stability of the knee joint is provided by the ligamentous system in the joint. Four main ligaments can be found in the knee, the two collateral ligaments (medial and lateral) at the periphery of the joint and the two cruciate ligaments (anterior and posterior) inside the joint (Figure 1-2). The posterior cruciate ligament (PCL) is tight in extension and the anterior cruciate ligament (ACL) is tight in the flexion. The lateral collateral ligament (LCL) is attached to the head of the fibula and the lateral condyle of the femur. The medial collateral ligament (MCL) is longer and wider than the LCL and is attached to the medial condyle of the femur and tibia. The main muscles groups, which cross the knee joint, are the quadriceps and the hamstrings. The quadriceps muscles (Figure 1-2) are the large muscle group making up the front of the thigh. The muscle starts from the thigh bone, narrows down towards the knee to the kneecap and attaches to the bony eminence on the anterior of the proximal tibia, called the tibial tuberosity. The quadriceps are a very powerful muscle group and act to straighten (extend) the knee in such activities as standing up, going up stairs or running. The hamstrings make up the back of the thigh, coming from part of the pelvis and running down the thigh to attach to the back of the fibula and tibia just below the knee. This muscle group bends (flexes) the knee and straightens the hip. The hamstrings are essential to the activity of sprinting. These two major muscle groups control knee movement and are vital to the stability of the joint. There are other muscle groups, which affect knee movement, and stability but they are minor in contrast to the main groups.

1.2 STRUCTURES AND MECHANICAL PROPERTIES OF LIGAMENTS

The collateral ligaments and cruciate ligaments are part of the collagenous tissues [98,110,164]. The collagenous tissues are composed of three types of fibres, namely the collagen fibres, elastic fibres and reticulin fibres [164]. During knee motions, these ligaments are loaded in tension and compression. Their mechanical properties are influenced by the structural orientation of the fibres. The ligaments have a less consistent structural orientation and have a wavy configuration when they are not loaded [110]. This is shown in the Figure 1-4 below. These wavy configurations of fibres acted differently when loaded and unloaded. When these wavy fibres are tensile tested, the fibres that are oriented in the direction of loading sustain the most loads and straighten out first [110]. Meanwhile, those that are not oriented in the direction of loading sustain less or no loads.

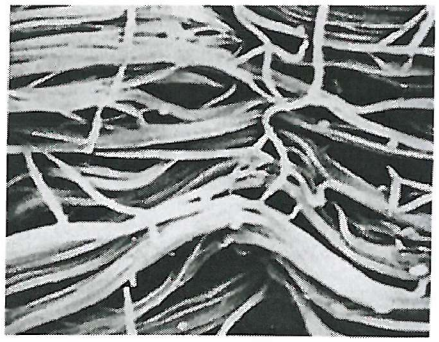

Figure 1-4: The wavy configurations of knee ligament fibres when in the unloaded state. Picture obtained from [110].

Two main factors that determine the strength of a ligament are the size (cross-sectional area) and the shape of the ligaments [110,164]. The fibre bundles in the ligaments consist mainly of collagen fibres [111]. These fibres bundles when tensile tested till failure; a stress-strain curve is obtained and it could be used to represent the mechanical behaviour of the knee ligament. An example of stress-strain curve for a knee ligament is shown in Figure 1-5. This curve is divided into several stages [110,111,164]. In the first stage (1), the wavy configurations of the fibre bundles will absorb some loads and start to straighten out. The first stage is also known as the 'toe' region. In the second stage (2), the fibres absorb more loads and these fibres tend to line up in the direction of loading. These fibres elongate more compare to when they are in the first stage. When proceeding to the third stage (3), the fibre bundles rapidly become stiff until the yield point is reached. After the yielding point (4), non-linear deformation takes place until the fibre bundles fail (ligament ruptures).

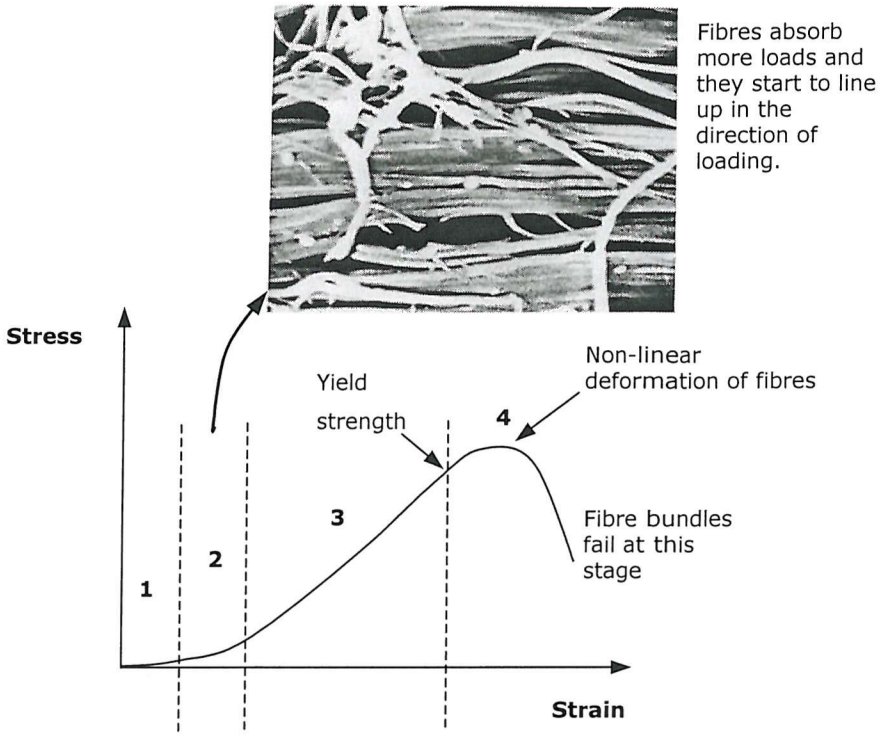

Figure 1-5: The stress-strain curve of a human knee ligament undergoing tensile testing until the ligament failed. The curve is divided into 4 stages. Pictures obtained from [110].

Tensile tests of the ligaments have been done with use of the bone-ligament-bone method [98]. Studies of tensile stiffness of knee ligaments have reported a high variability in values. The stiffness of the ACL has been reported to vary from 124 N mm^{-1} to 242 N mm^{-1} [97,99,111,120,145,160]. For the PCL, the stiffness varies from 183 N mm^{-1} to 258 N mm^{-1} [98,120,145], the MCL varies from 72 N mm^{-1} to 134 N mm^{-1} [98,145] and the LCL from 47 N mm^{-1} up to 114 N mm^{-1} [98,145].

The variability in stiffness values can be explained by differences in age and activity level of the specimen donors and by technical causes. The quality of ligament also affects the experimental results. Another potential cause of variability between the different studies is the bone-to-bone angle of the ligaments relative to the tensile direction [98]. For example, Momersteeg et al. [98] reported that the tensile stiffness of human knee ligaments is a function of the relative orientation of ligament insertion sites. Small variations in tilt and translation of the femoral bone relative to the tibial can change the tensile stiffness of knee ligaments.

1.3 LIGAMENTS FUNCTION

The four major ligaments of the knee act together to provide stability to the joint, to guide and prevent excessive joint motion. Each ligament has a particular function due to its position and shape. Each of the ligaments, except the LCL, can be divided into several fibre bundles. The PCL is a cord like ligament and can be divided into anterolateral and posterior-medial bands, whereas the ACL is divided into anterior and posterior bands [48,164]. The MCL is the largest ligament and has a flat geometry. It is composed of anterior, oblique and deep fibre bundles [164]. In a completely extended knee joint, both collateral ligaments and cruciate ligaments are taut. When the knee is hyper-extended, the anterior part of the knee menisci are held very tightly between the tibia and the femur. For both the cruciate ligaments, PCL and ACL, the posterior part is tight in extension and the anterior part is tight in flexion [48]. The actions of posterior and anterior parts of ACL and PCL are illustrated in Figure 1-6 and Figure 1-7.

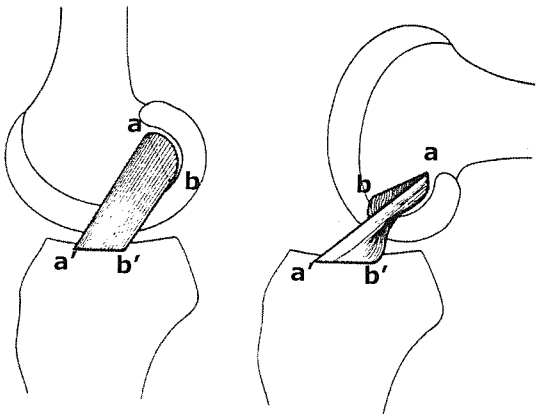

In extension, the posterior portion of the ACL (bb') is tight. When the knee flexes, the anterior part of the ACL (aa') is in tension and becomes tighter. At flexion, the posterior part (bb') is slack.

Figure 1-6: The tightening and slackening of anterior (aa') and posterior (bb') parts of the ACL, when the knee joint is in extension and flexion. Picture obtained from [48].

When the knee is in extension (Figure 1-7 a), the posterior part of the PCL (BB') is in tension. As the knee flexes (Figure 1-7 b), the tension transfers from posterior to the anterior part (AA') of the PCL. At deep flexion angle (Figure 1-7 c), the anterior portion of the PCL (AA') sustains more tension and extended more.

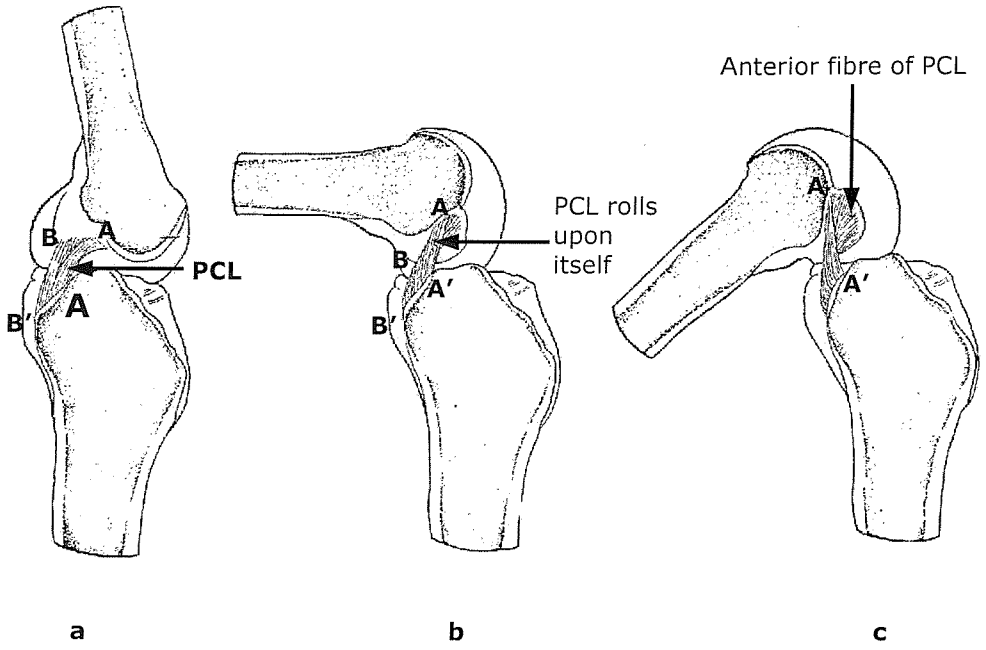

Figure 1-7: The tightening and slackening of anterior (AA') and posterior (BB') parts of the PCL, when the knee joint is in extension and flexion. Picture obtained from [22].

The LCL, with only one fibre bundle, is in tension during extension and the tension reduces as the knee flexes. For the MCL, then tension transfers from the posterior part (the oblique bundle) across the deep portion to the anterior part of the ligament when the knee flexes [22]. The transfer of tension across the width of the MCL is illustrated in Figure 1-8.

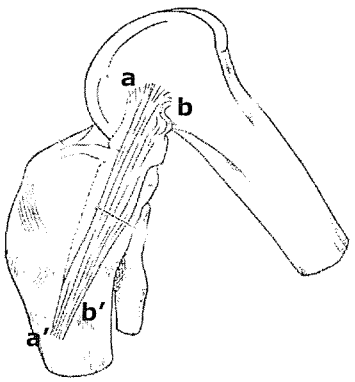

Figure 1-8: The anterior part of the MCL (aa') tightens and the posterior part (bb') slackens when the knee is in flexion [22].

1.3.1 Anterior Cruciate Ligament (ACL)

The ACL is the predominant restraint to the anterior tibial displacement relative to the femur (or prevents the femur from sliding too far backwards on the tibia). This ligament produces 75% of the anterior force at full extension and approximately 85% at 30 and 90 degrees of flexion [48]. Loss of the ACL causes excessive anterior displacement of the tibia relative to the femur in the range of 30° knee flexion to full extension [166]. The ACL can be divided into posterior and anterior fiber bundles. *In situ* observations show that the anterior bundles are loaded more frequently and more heavily than the posterior bundles. The detail functions of the ACL will not be discussed as in total knee replacement (TKR), the ACL is resected.

1.3.2 Posterior Cruciate Ligament (PCL)

The posterior cruciate ligament (PCL) plays a dominant role in the restriction of posterior motion. It controls the tibia so that it does not move backward too much, (or prevents the femur from sliding too far forward on the tibia). The PCL is composed of anterolateral and posteromedial fiber bands. It sustains 85 to 100% of the posterior force at both 30° and 90° of flexion [48]. During posterior translation, the lateral collateral ligament (LCL) and popliteus tendon are the secondary restraints. The medial collateral ligament (MCL) has lesser role. With the PCL intact, the moment arm of quadriceps is increased by 20 to 30% and this is important for stair climbing activity. Posterior displacement of the knee is also accompanied by external rotation and lateral translation [48,49]. According to several studies [49,54], posterior translation of 4 to 5 mm is seen with the application of 100 N posterior forces. If the PCL is resected but the other ligaments left intact, this will result in an increase in posterior translation to a maximum of 15 to 20 mm at 90° of flexion [49,54]. Furthermore, the posterior translation will not be accompanied by external rotation.

1.3.3 Lateral Collateral Ligament (LCL)

The LCL is the primary restraint to varus angulation and it resists approximately 55% of the applied varus load at full extension [48,54,58]. The cruciate ligaments only resist approximately 25% of moment during full extension. The LCL also acts to resist internal rotation forces. The LCL is the primary restraint to varus stress at 5 degrees and 25 degrees flexion and if the lateral collateral ligament is resected, this will result in an increase in varus opening [48]. External rotation of the tibia will also increase with the sectioning of this ligament [48,49].

1.3.4 Medial Collateral Ligament (MCL)

The medial collateral ligament is composed of superficial and deep portions of fiber bundles. Anatomically, the superficial MCL is the 2nd or middle layer of its medial compartment [48]. The MCL provides primary restraint to valgus stress at the knee [48]. At full extension, the MCL resists about 50% of the applied valgus moment, whereas the other 50% is shared between cruciate ligaments and other surrounding soft tissues. At 25° of flexion, the MCL provides 78% of the support to valgus stress and at 5° of flexion; it contributes 57% of the support against valgus stress. If the MCL is resected, this increases valgus instability markedly [58,88,90]. Normal coupled motions with an applied valgus load include lateral translation without noticeable internal-external rotation or anterior-posterior translation. Isolated sectioning of the ACL does not affect any of these coupled motions [48].

1.4 DISEASE OF KNEE

Normal knee function is needed to perform routinely everyday activities. However, disease or injury can disrupt the normal knee function, resulting in pain, muscle weakness and less function of the knee. The most common cause of chronic knee pain and disability is *arthritis*. Arthritis means an inflammation of a joint causing pain, swelling, stiffness, instability and often deformity. Severe arthritis interferes with a person's activities and limits his or her lifestyle. Osteoarthritis, rheumatoid arthritis and traumatic arthritis are the most common forms of arthritis. The differences of these arthritis are:

Osteoarthritis (OA) is a result of wear and tear arthritis, since the cartilage that cushions the bones of the knee simply wears out. When cartilage wears away, bone rubs on bone causing severe pain and disability. Osteoarthritis usually occurs after the age of 50 and in an individual with a family history of arthritis.

Rheumatoid arthritis (RA) is also known as inflammatory arthritis and it is a disease that attacks body joints and the surrounding tissues. *RA* is caused by dysfunction of the immune system. Abnormal anti-bodies are produced in the lining tissue of the knee joints (the synovium). This causes chronic inflammation and slow destruction of cartilage. [http://www.jri-oh.com/Knee_Arthritis.htm]

Post *traumatic arthritis* is a result of a serious knee injury. A bad fall or blow to the knee can injure the joint. If the injury does not heal properly, extra force may be place on the joint, which over time can cause the cartilage to wear away.

Reasons for total knee replacement (TKR):

The most common reason for TKR is severe arthritic pain. Pain cannot be measured and the degree of pain sufficient to warrant surgery should be decided by the patient and doctor together. Painful and arthritic knees are often become unstable and untrustworthy, causing falls and other injuries. The patient's independence is compromised and the quality of their life will decrease. Due to these reasons, TKR is performed on those who need it. The goal of TKR is to relief pain, to restore motion and eventually give the patients normal life again.

Chapter 2

BIOMECHANICS OF THE KNEE

The biomechanics of the knee joint provide an important basis for the rationale in the design and selection of appropriate total knee arthroplasty. The knee joint motion is a complex interaction between four bones [23] – the patella, femur, tibia and fibula – which can be simplified into three separate models of joint motion: the tibio-femoral joint, the patello-femoral joint and the tibio-fibular joint. The knee joint motion has been described in various ways in the literature and this chapter will introduce the kinematics as well as the kinetics of the normal knee.

2.1 TIBIO-FEMORAL JOINT

The primary motions of the knee are flexion and extension; however, anterior-posterior displacement, rotation and varus and valgus motions are also essential to its overall function. Extension is defined as the movement of the posterior aspect of the calf away from the posterior surface of the thigh. Flexion is the movement of the posterior aspect of the calf towards the posterior aspect of the thigh.

The range of motion of the knee joint varies according to the positions of the hip and also whether it is passive or active motion [4]. Passive motion of the knee joint is dependent on the interaction between the shape of the articular surfaces and the various ligaments crossing the knee joint. Passive motion is defined as the motions of a particular joint as a result of an external force without the involvement of the muscles forces. An example of a passive motion is the movements of a joint by a surgeon on the operating table. Conversely, active motion of a joint involves the action of muscles forces, but without the influence of external force. An example of active motion is walking. Flexion of the knee progresses as a combination of rolling, gliding and rotation of the femoral condyles over the tibial plateaus [72].

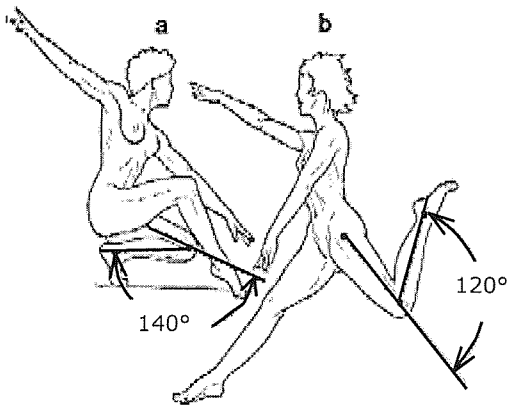

The magnitude of various active motions changes through the range of flexion. Flexion of about 140° [62,110] can be easily reached if the hip is already flexed; whereas only 120° if the hip is extended (Figure 2-1). The difference that occurs is due to the fact that the hamstrings (lower limb muscle groups) lose some of their efficiency with the extension of the hip.

Figure 2-1: The influence of hip position on the movement of the knee joint. (a) With the hip flexed. (b) With the hip extended [62].

In the sagittal plane, as the femur is flexed on a fixed tibia, the contact point of the femur on the tibia displaces posteriorly, controlled by the geometry of the four-bar linkage consisting of the cruciate ligaments and the joint surfaces [165]. The mechanical implications of this motion are that the lever arm of the posterior muscles is increased towards extension, thus providing an effective brake to hyperextension whereas in flexion, the lever arm of the quadriceps is increased for efficiency of activities such as stair climbing and rising from a seated position. In addition, the posterior displacement of the femur in high flexion allows clearance of the posterior structures, increasing the range of flexion. The contact point on the lateral plateau rolls a greater distance posteriorly, due to the larger radius of curvature of the lateral than the medial femoral condyle [4]. Condylar movement during flexion imposes internal rotation of the tibia. During the movement of the knee, the menisci actually move forward when the knee is extended and glide backward when the knee is flexed [62]. The shape of the menisci constrains the femoral condyles to induce rolling as the knee flexes.

During knee extension, when the knee is almost fully extended and the tibia fixed, the femur rotates medially (if the femur is fixed, the tibia rotates externally or laterally). This rotary movement is termed the 'screw-home' mechanism and 'locks' the knee joint firmly in place for standing [60,118]. Screw-home has been described as characteristic of healthy knee motion and its absence is often described as indicative of instability or joint damage such as meniscal tears [110,118,138,147]. Flexion of the knee is initiated by lateral rotation of the femur on the tibia. This 'unlocking' action is caused by the contraction of the popliteus muscle. Rotation of the knee is possible when the knee is flexed, but not when the knee is in locked positioned as in hyperextension. Beyond 90° of knee flexion the range of internal and external rotation decreases, primarily because the soft tissues restrict rotation movements. In the upright stance the knee joint is usually in a position of slight

hyperextension. The limit of this hyperextension is between 5° and 10° [62]. The femoral condyles contact on the tibial plateaus anteriorly during extension.

2.2 PATELLO-FEMORAL JOINT

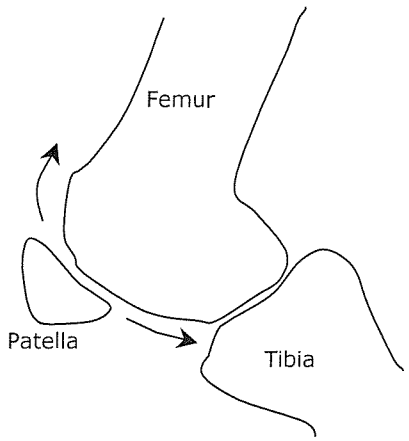

The patella is positioned at the frontal part of the femur, which is known as femoral groove (Figure 2-2). This groove allows the gliding motion of the patella. From full extension to full flexion of the knee the patella glides approximately 7 cm on the femoral groove [110].

Figure 2-2: The gliding motion of the patella at the femoral groove. View from sagittal plane.

Both the medial and lateral facets of the femur articulate with the patella from full extension to 90 degrees of flexion. Beyond 90 degrees of flexion the patella rotates externally and only the medial femoral facet articulates with the patella (Figure 2-3). At full flexion the patella sinks into the intercondylar groove (at the distal part of the femur) [110].

Figure 2-3: A) At full extension both the medial and lateral femoral facets articulate with the patella. B) Beyond 90 degrees of flexion the patella rotates externally and only the medial femoral facet articulates with the patella [110].

2.3 KNEE JOINT ALIGNMENT

Proper component and correct limb alignments are essential to achieve durable results after total knee arthroplasty. Misalignment after arthroplasty can lead to implant failure, loosening, and decreased range of motion [29]. Therefore, an understanding of normal limb alignment is essential. In a healthy non-arthritic adult, the mechanical axis of the lower extremity is a line projected from the centre of the femoral head to the centre of the ankle (Figure 2-4 a). This axis is also known as the load-bearing axis (LBA) [29] and should be closely aligned to the mechanical axis of each bone (i.e. femur and knee). The mechanical axis of the femur is a line from the centre of the femoral head to the centre of the knee (Figure 2-4 b). The mechanical axis of the tibia is a line from the centre of the knee to the centre of the ankle (Figure 2-4 b). For a 0° mechanical axis of the limb, the mechanical axis of the tibia and femur would be coincident. The tibiofemoral angle or axial alignment of the limb is formed by the intersection of lines along the centre of the femoral shaft (anatomic axis) and the femoral mechanical axis (Figure 2-4 b).

The joint line angle can be considered in reference to the femur or tibia. The femoral joint line angle is formed by a line tangential to the femoral condyles and a line projected along the anatomic axis of the femur (centre of the femoral shaft). The tibial joint line angle is formed by a line tangential to the tibial condyles and a line projected along the anatomic axis of the tibia (centre of the tibial shaft), (Figure 2-4 c). Negative tibial joint angle indicates the amount of varus and positive the amount of valgus.

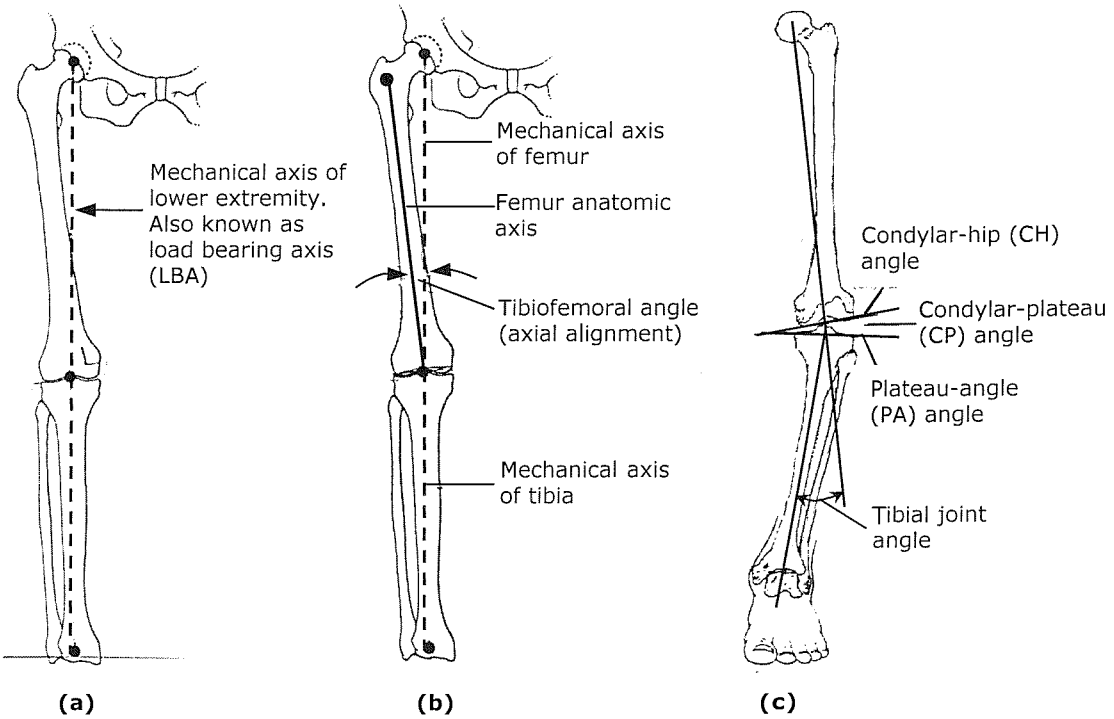

Figure 2-4: Angles between the longitudinal axes of the femur and tibia [77].

The articulating surfaces of the distal femur and proximal tibia are represented in the frontal plane (Figure 2-4 c). Two lines are defined, one as a tangent to the mechanical axis of the femoral condyles and the second as a line connecting the medial and lateral margins of the tibia plateau. The orientations of these lines with respect to the mechanical axes of the femur and tibia are defined as the condylar-hip (CH) and plateau-ankle (PA) angles. These angles are expressed as deviations from 90°, with negative values indicating varus (<90°), and positive ones indicating valgus (>90°) [30]. The angle between the knee joint surfaces is given by the condylar-plateau (CP) angle. CP is negative if the joint surfaces converge medially, positive if they converge laterally (Figure 2-5).

In healthy adults, the average of CH angle is 3° - 4° valgus (CH>0°); the mean of PA angle is 3° - 4°varus (PA<0°). The tangent of tibial plateaus generally parallels that of femoral condyles (CP = -1.7°). This accounts for the nearly co-linear alignment of non-arthritic knees with normal alignment (when mechanical axis of the limb = 0°) [30]. However, variations of these angles occur in non-arthritic knees [30], even more variation is evident in arthritic ones [30]. A clinical study by Ritter et al. [126] showed that patients with osteoarthrosis had anatomic valgus deformity as high as 20°. This condition should be corrected as soon as possible to avoid severe knee failure and pain.

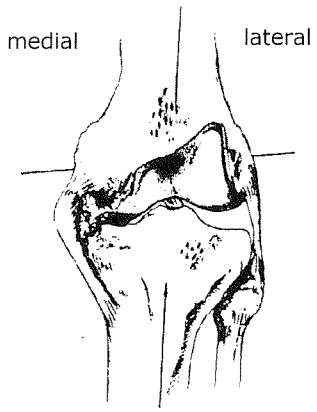

Figure 2-5: Illustration of varus medial compartmental OA with osteophytes. Medial joint space collapse and lateral joint space opening [29].

Normal limb alignment has been reported using different definitions by various authors. Furthermore, the measurement techniques used to assess orientation have varied. Some investigators have used clinical radiographs [17,77,126] whereas others have used anatomical specimens (such as cadaver specimens) [9]. These different techniques have led to differing conclusions about 'normal' limb alignment. An anatomical study of femoral anatomy in 32 specimens was performed [162]. The femoral joint line angle was 3.8° ± 2.1° of valgus [162]. The difference between the mechanical axis and anatomical axis of the femur was 5.4° of

valgus [162]. Another study of 100 radiographs found a difference between the mechanical and anatomical axes of the femur range from 4° to 8° of valgus [81]. Whiteside [157] suggested that the anatomic axis of the femur aligns in approximately 5° valgus to the mechanical axis of the lower extremity. The tibial joint angle (Figure 2-4 c) ranged between 2.5° and 3.5° of varus [81]. Whiteside [157] reported that this angle (tibial joint angle) was approximately 3° varus and was consistent with Krachow et al. [81] finding. Therefore, the normal joint line inclines slightly medially but with individual variation. The mechanical axis of the limb lies in the range of 2.5° to 3.5° of varus (medial to the centre of the knee) [81]. In another radiographic study [100] of normal subjects, the anatomic and mechanical axes of the femur were found to intersect in the supracondylar region of the femur. The mechanical axis of the limb was found to be in slight varus of 1.1° to 1.5°. The tibial joint angle was 2.6° to 3.0° of varus. The angle between the mechanical and anatomic axis of the femur was 5.8° ± 0.7° of valgus [100]. These knee joint angles are summarized in Table 2-1.

Authors	Angle between mechanical and anatomic axes of femur	Tibial joint angle
Yoshioka et al. [162]	5.4° of valgus	/
Krachow [81]	4° - 8° of valgus	2.5° - 3.5° of varus
Whiteside [157]	5° of valgus	3° of varus
Moreland et al. [100]	5.8° ± 0.7°	2.6 – 3.0°

Table 2-1: Various knee joint angles.

2.4 GAIT CYCLE

Walking, stairs climbing, walking down stairs, sitting, getting out of a chair and running are the most common activities encountered in daily living. The differences of these activities are on the speed of movement and the amount of the load applied at the lower limb. Here, walking activity will be discussed in details.

There are two main phases in the walking gait cycle (Figure 2-6). During *stance* phase, the foot is in contact with the ground, whereas in *swing* phase that same foot is no longer in contact with the ground and the leg is swinging through in preparation for the next foot strike. The *stance* phase can be further divided into five periods and the *swing* phase can be divided into three (Figure 2-7).

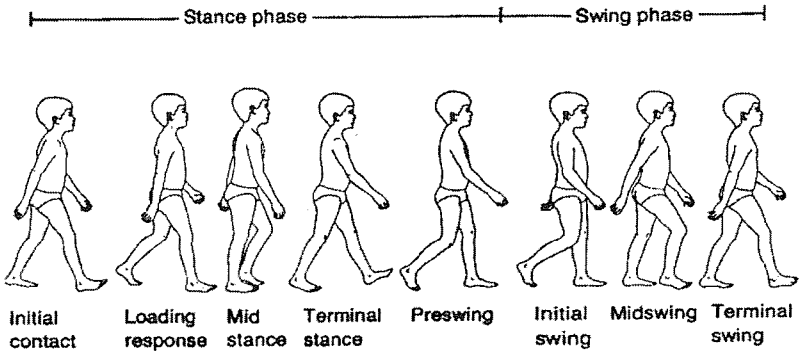

Figure 2-6: The normal walking (gait) cycle of a man [149].

The *stance* phase events (60% of the activity cycle) are as follows [149] (Figure 2-7):

1. *Heel strike* initiates the gait cycle and represents the point at which the body's centre of gravity is at its lowest position.
2. *Foot-flat* is the time when the plantar surface of the foot touches the ground.
3. *Midstance* occurs when the swinging foot passes the stance foot and the body's centre of gravity is at its highest position.
4. *Heel-off* occurs as the heel loses contact with the ground.
5. *Toe-off* terminates the stance phase as the foot leaves the ground.

The *swing* phase events (40% of the activity cycle) are as follows [149] (Figure 2-7):

1. *Acceleration* begins as soon as the foot leaves the ground and the subject activates the hip flexor muscles to accelerate the leg forward.
2. *Midswing* occurs when the foot passes directly beneath the body, coincidental with midstance for the other foot.
3. *Deceleration* describes the action of the muscles as to slow the leg and stabilize the foot in preparation for the next heel strike.

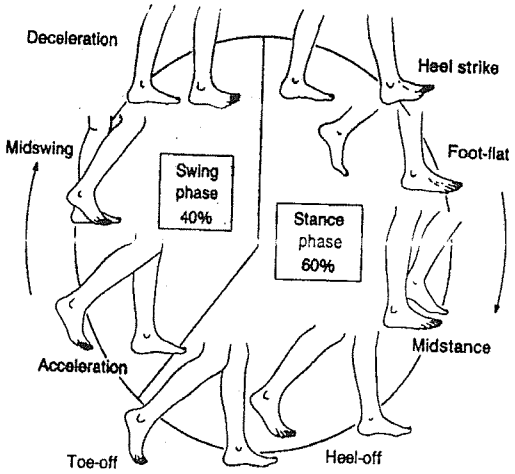

Figure 2-7: Breakdown events or periods for stance phase and swing phase [149].

2.5 RANGE OF MOTIONS OF THE TIBIOFEMORAL JOINT

2.5.1 Flexion/Extension

The range of tibiofemoral joint motion required for the performance of various physical activities can be determined from kinematic analyses. Motion of this joint during walking has been measured in all planes. The range of motion in the sagittal plane during level walking was measured with an electrogoniometer by Murray et al. [107]. During the entire gait cycle the knee was never fully extended. Near full extension (5 degrees of flexion) was noted at the beginning of the stance phase at heel strike and at the end of the stance phase just before toe-off. Maximum flexion, 75 degrees was observed during the middle of the swing phase

Lafortune et al. [82] reported similar trend during level gait, whereby the tibiofemoral joint flexed to average 35 degrees (S.D. 4.7 deg.) by toe-off and peak at average 60 degree (S.D. 3.1 deg) early into the swing phase. Lafortune et al. used target (shin) markers to identify positions of some bony landmarks at the lower limb and relative motion between tibia and femur was measured. The problem of using target markers was the risk of target markers being put at wrong bony landmarks and errors in skin movement as these markers were attached to the skin.

Values for the range of motion of the tibiofemoral joint in the sagittal plane during several common activities are presented in Table 2-2. Maximal knee flexion occurs during lifting. A range of motion from full extension to at least 117° of flexion appears to be required in order for an individual to carry out the activities of daily living in a normal manner. Any restriction of knee motion is compensated for by increased motion in other joints. Tying a shoelace also requires quite high degree of knee flexion, with recorded value of 106°. Sitting down into a chair involves slight bending in the upper body and the knee flexes to approximately 90°. In studying the range of tibiofemoral joint motion during various activities, Kettelkamp and co-workers [74] noted a significant relationship between the length of the lower leg and the range of motion in the sagittal plane. The longer the leg was, the greater the range of motion. An increased speed of movement requires a greater range of motion in the tibiofemoral joint [116]. As the pace accelerates from walking slowly to running, progressively more knee flexion is needed during the stance phase.

Kinematics studies have shown that a larger range of knee motion is required during stair climbing than during level walking [3,4,31,80,95]. Using electrogoniometers, Laubenthal et al. [83] observed that about 83 degrees of knee flexion is required for going up and down stairs. Andriacchi et al. [3] and Costigan et al. [31] performed stair climbing gait tests on healthy men and women. They found that the average maximum flexion-extension angle at the knee joint during this activity was approximately 85°.

Activity	Range of motion from knee extension to knee flexion (degrees)
Walking [104,107]	0 – 67
Stair climbing [31,83]	0 - 88
Descending stairs [83]	0 - 80
Sitting down in a chair [109]	0 – 90
Tying a shoe [110]	0 - 106
Lifting an object	0 - 117

Table 2-2: Range of tibiofemoral joint motion in the sagittal plane during common activities.

2.5.2 Internal/External Rotation

The range of knee joint rotation varies according to the degree of knee flexion. From *in vivo* test [143], at 90 degrees of knee flexion, total tibial rotation (direction not given) of approximately 7 and 13 degrees were measured when the knee was applied with 50 N and 100 N anterior-posterior forces, respectively. During level gait [82], internal rotation of the femur relative to the tibia of less than 5 degrees was observed during the stance phase. External rotation of 9.4 degrees of the femur with respect to the tibia was measured during the swing phase. *In vitro* tests showed different values of internal-external rotation. At 90 degrees of knee flexion, by applying 100 N of anterior-posterior force to a cadaver knee, an average of 20 degrees of total tibial rotation was possible [49]. The rotation decreased to 8 degrees when the knee was at full extension. Rotation motion is vital to athletes, gymnasts and sportsmen as allowing them to perform physical activity such as ice skating, gymnastic, football and others.

2.5.3 Adduction/Abduction

The rolling motion, which predominates in early flexion, 0°-20°, produces posterior translation of the point of tibial-femoral contact [37,70]. As the flexion proceeds and at angles greater than 30°, sliding becomes dominant [4]. The knee also shows adduction of approximately 13° during the stance phase of gait but the abduction/adduction motion of the knee during the swing phase was measured to be less than 10° [4]. Motion (frontal plane) during walking was also measured with an electrogoniometer by Kettelkamp's group [74]. In their finding, nearly all of the 22 subjects, maximal abduction of the tibia was observed during extension at heel strike and at the beginning of the stance phase, and maximal adduction occurred as the knee was flexed during the swing phase. The total amount of abduction and adduction averaged 11°.

2.5.4 Anterior/Posterior Translation

Translation of the knee in the anterior-posterior direction has been measured by several researchers, either *in vitro* or *in vivo*. Fukubayashi et al. [49] have tested the anterior-posterior motion of nine normal cadaver knees in 0° to 90° of flexion, by applying A-P forces up to 125 N. They found that the greatest total A-P displacement of the tibial occurred with the knee at 30° of flexion, being 10 mm and 13 mm for the 50 N and 100 N force, respectively. The peak anterior displacement, approximately 7 mm, occurred at 30° of flexion, while the peak posterior displacement, approximately 6 mm, occurred at 75° and 90° of flexion. Minimum displacement occurred with the knee at full extension.

By means of *in vivo* biomechanical testing, Torzolli et al. [143] applied anterior and posterior forces with the knee at 90° of flexion while the resulting A-P displacement was measured. A roentgenographic technique was used to measure this displacement and other knee kinematics parameters. Total anterior-posterior displacement measured approximately 4 mm to 7 mm with forces of 50 N and 100 N, respectively. Lafortune et al. [82], using shin markers based technique to measure the A-P displacement of the tibia while walking. When the knee was flexed, the tibia experienced a posterior translation and when the knee extended, the tibia moved anteriorly. Posterior displacement of 3.6 mm (S.D. 1.8 mm) during stance phase, and 14.3 mm (S.D. 3.7 mm) during the swing phase, were recorded. Differences in technique and type of knee (cadaver or living human) used were the main factors influenced the differences in measured displacement by different authors.

2.6 KINETICS WITHIN THE KNEE JOINT

The forces acting in the knee during activity were calculated as early as the 1930s [38]. The only method of predicting forces within the knee joint is by ***inverse dynamics*** calculations. Using this method, the ground reaction force on the foot is first recorded using a force plate, along with the kinematics of the lower limb and then calculations are required to convert this force into the joint reaction force. Axial/compression force (vertical force), internal-external torque, adduction-abduction moment, varus-valgus torque and anterior-posterior force are the most significant forces sustained by the knee joint while undergoing an activity. Forces acting across the articulating surfaces of joints have received much attention due to their importance in the design of total joint replacement and in the understanding of joint lubrication problems. Although many studies [31,102,104,150,151] have been carried out in the field of knee joint biomechanics, most of the investigations are limited to the analysis of joint movement and very few have examined joint forces. It is because there is not direct way to measure these joint forces.

Level gait:

Morrison [103] performed a detailed study to calculate the forces transmitted across the knee, on 12 subjects. The ground reaction force during one step was measured using a force plate. Accelerations of limb segments were calculated from measurements taken from the cine film records. The external force system acting at the knee joint was then calculated by summing ground force and acceleration forces acting on the limb. In order to calculate the forces transmitted by the joint articulations and the connective tissues under dynamic conditions from the ground reaction force obtained, a set of reference axes (Figure 2-8) had been adopted. The directions of all forces acting across the knee joint were defined in terms of this system of tibial axes. The femoral condyles were assumed to

rotate relative to the tibia about a fixed centre line parallel to the Z_s axis and intersecting the Y_s axis of the tibia (Figure 2-8). This centre line was taken to be coincident with the axis of rotation of the knee joint in the position of 180° extension (full extension). The Y_f axis represented the mechanical axis of the femur and the Z_f axis was coincident with the centre line of the condyles. The movements of the knee were controlled by the muscles and ligaments. In order to track the period of which muscle groups were active during flexion-extension, an electromyographic (EMG) data were recorded.

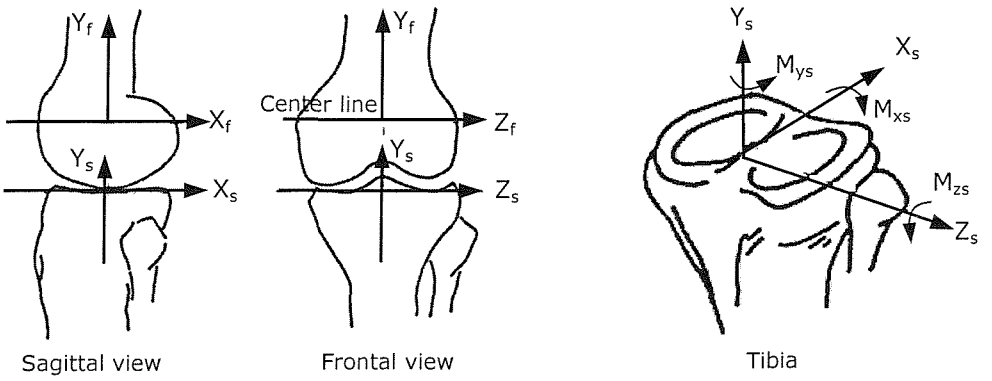

Figure 2-8: Reference axes on the joint articulation, expressed in terms of tibial reference axes [103].

Two forces transmitted by the joint articulations were: compressive force R_y acting in the direction of the Y_s axis of the joint, and a side or shear force R_z acting in the medio-lateral direction. Force R_z was assumed to be transmitted partly as a friction force acting between the faces of the opposing condyles. The effect of friction in the joint in the anterior-posterior direction was neglected. It was therefore assumed that an anteriorly directed force on the tibia was resisted by the anterior cruciate ligament whilst a posteriorly directed force was resisted by the posterior cruciate ligament. The direction of the force imposed on the joint by a ligament was defined in terms of the positions of the ligament's attachments relative to the tibial axes. Markers were placed on skin of the subjects during recording of cine film. For each frame of film data co-ordinate systems were calculated representing the position of the pelvis, femur and tibia. The position of muscle and ligaments were also determined. After these were obtained, the accelerations of each limb segment were calculated by means of numerical differentiation from displacement-time graphs generated for each marker. By summing ground reaction force and acceleration effects, the complete external force system acting on the knee joint was obtained in terms of three orthogonal forces and moments (Figure 2-8). The function of the muscle and ligament groups was then included. Sets of equations were developed and according to the period of muscle actions, anterior-posterior force, compressive force and shear force could then be calculated (by applying *Newton's Law of Motion* to each limb segment). By considering the knee joint to operate according to the mechanical principles described

earlier and applying experimental results to the joint model, a complete force analysis of the joint under dynamic conditions could be achieved.

In Morrison's study, the maximum joint force calculated at the knee (together with the muscle forces) during normal walking, was in the range of 2 to 4 times BW (Figure 2-9). The subjects' knee joint, all sustained an internal torque of the femur relative to the tibia during the stance phase of walking gait cycle with peak internal torque values as high as 8.34 N m and as low as 5.65 N m being predicted (Figure 2-10). After the stance phase, the subjects' knee joint was subjected to external torque. Morrison found that greater portion of the load was transmitted by the medial condyles when the joint was highly loaded. Morrison found that there was no significant difference in the joint forces calculated for male and female subjects in this study.

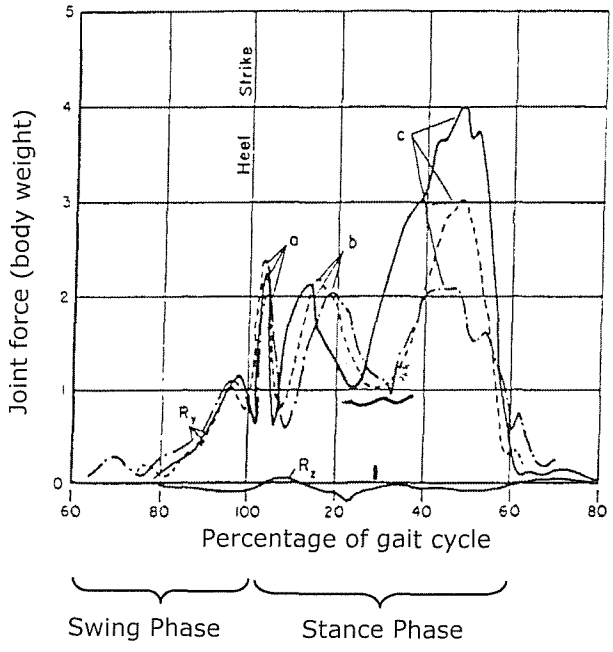

Results show the greatest, average and smallest values of maximum joint forces, R_y. The average values of peaks *a, b* and *c* were 2.43, 2.23 and 2.74 times body weight, respectively

Figure 2-9: Joint force at the knee joint during level walking [103].

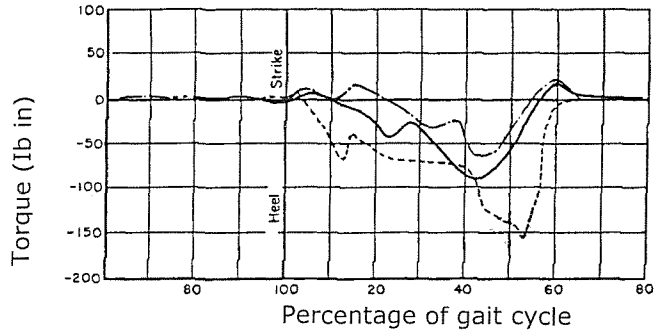

Results show the greatest, average and smallest values of maximum torque. The peak torque was approximately 8.34 N m

Figure 2-10: Torque acting at the knee joint during level walking [103].

Knee kinetics during walking has also been investigated by Patrick Costigan and co-workers [31]. Costigan et al. also adopts a similar method to Morrison [102,103] in predicting the knee joint forces. Basically, motion of subjects is recorded using an optoelectric motion tracking system. Ground reaction force during the motion is measured by a force plate. Markers are fixed at the leg and are used to define local segment coordinate systems. Standardized radiographs with additional scaled radiographic measurements were used to help construct a subject specific knee model; helping to estimate the forces that generated the knee joint moments. The forces and moments are calculated using the inverse dynamics approach. The predicted muscle force is also added to the net external force and then partitioned into components along the tibial shaft; this alters the net compressive and anterior-posterior shear forces.

Figure 2-11 shows the forces transmitted by the articular surfaces of the knee. Four peaks were observed in the axial force results. The first peak being at the heel strike, 2nd peak being during the mid-stance phase, the 3rd peak being at the end of stance phase and the 4th peak occurred at the end of the swing phase. Comparing these to the Morrison [102,103], all four peaks during the stance and swing phases were also seen in Morrison's results. The instant of these peaks occurred were also similar. During the swing phase, the foot is not in contact with the ground and hence, no vertical force transmitted through the joint. The axial or vertical forces seen in the Costigan and Morrison results, between 80% and 100% of the gait cycle were due to the muscles action. It was postulated that the muscles tried to reposition the joint during this period of swing phase (80% to 100%), to get ready for the next heel strike. The values of these axial forces were noticed to be less than those during the stance phase.

The greatest axial force measured was approximately 3.8 times body weight (BW). From the axial force plots, a range of compression force was observed. Majority of the subjects' axial force occurred within a range of 0.7 BW to 2.9 BW (500 N to 2000 N), during the stance phase of gait cycle. A range of anterior-posterior force was observed. The greatest posterior force measured was approximately 0.55 BW (385 N). The greatest peak torque measured from the seven subjects was 7.5 N m. This value is close to the prediction of Morrison [103].

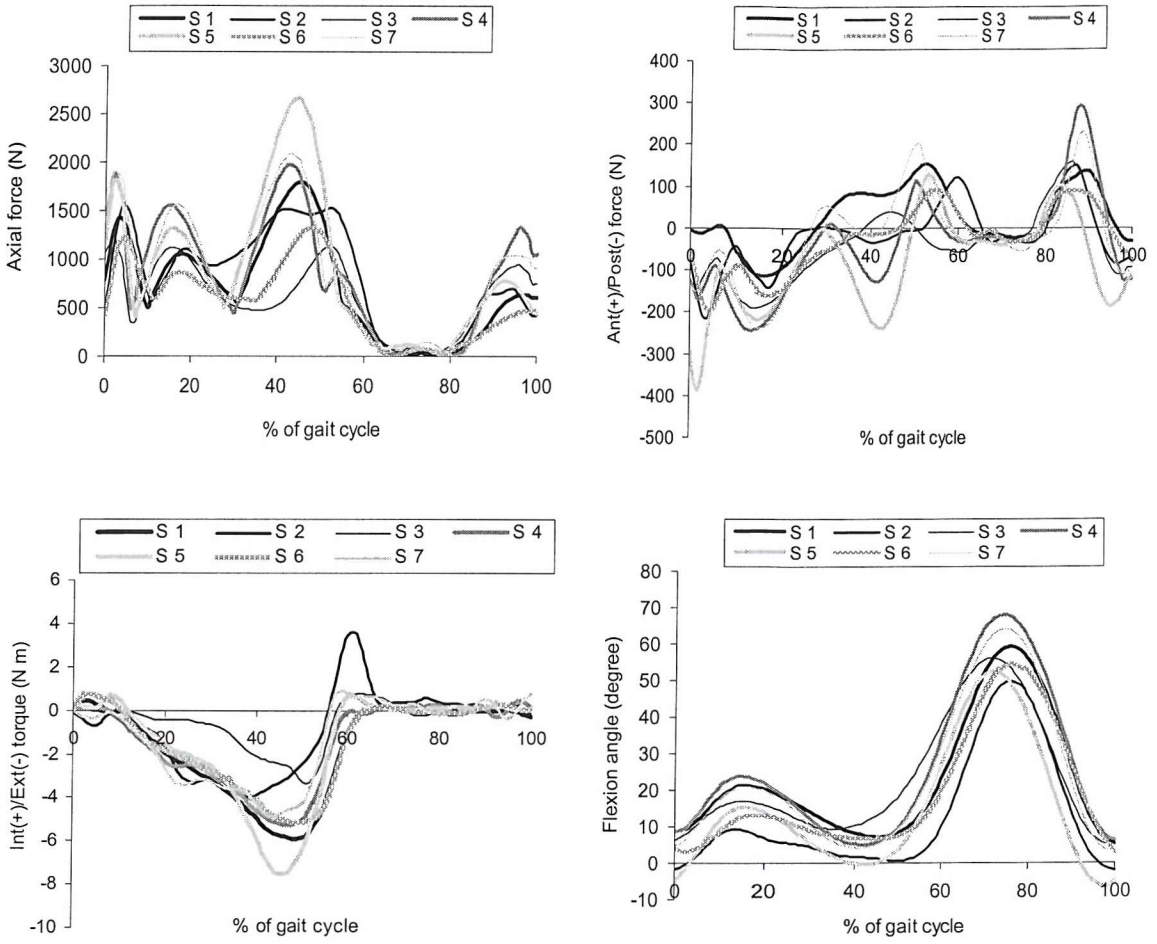

Figure 2-11: Knee joint forces for level gait measured and calculated by Patrick Costigan. S : Subject

Stairs Ascend:

Stair climbing is of particular interest since stairs are frequently encountered in daily living. From mechanical viewpoint, stair climbing is different from level walking. The differences are reflected by changes in the ranges of motion of the different joints during gait, and changes in the phasic muscle activities and in the maximum joint forces and moments [3,4,31]. Several studies had been carried out to investigate and predict the forces encountered by lower extremities during stair climbing and descending.

Costigan et al. [31], examined hip and knee joint kinetics during stair climbing in 35 young healthy subjects using a subject-specific knee model to estimate bone-on-bone tibiofemoral and patello-femoral joint contact forces. The subjects were 15 males and 20 females, with average age, height and mass of 24.6, 1.7 m and 65.4 kg, respectively. Their results were that the average peak value of axial/compression knee force was 33.87 N/kg, S.D. 10.95 (approximately 2215 N or 3.2 BW). The average peak anterior-posterior (AP) contact force was 11.68 N/kg, S.D. 4.09 (approximately 763.9 N or 1.1 BW) and the average peak internal-external moment was calculated to be 6.54 N m, S.D. 0.04. These forces were the internal forces at the knee joint which taking into account the forces of muscle contraction. Figure 2-12 shows the measured knee angles and the estimated knee contact forces. First 40% of the stair ascent cycle was known as the swing phase as there was hardly any vertical loading at the knee joint (Figure 2-12 B). The stance phase was from 40% to 100% of the activity cycle with increasing vertical loading. During the loading phase, the maximum knee angle was approximately 75° (Figure 2-12 A). Anterior-posterior force at the knee acted throughout the activity cycle (Figure 2-12 C), whereas internal-external moment was observed only during the stance phase (Figure 2-12 D).

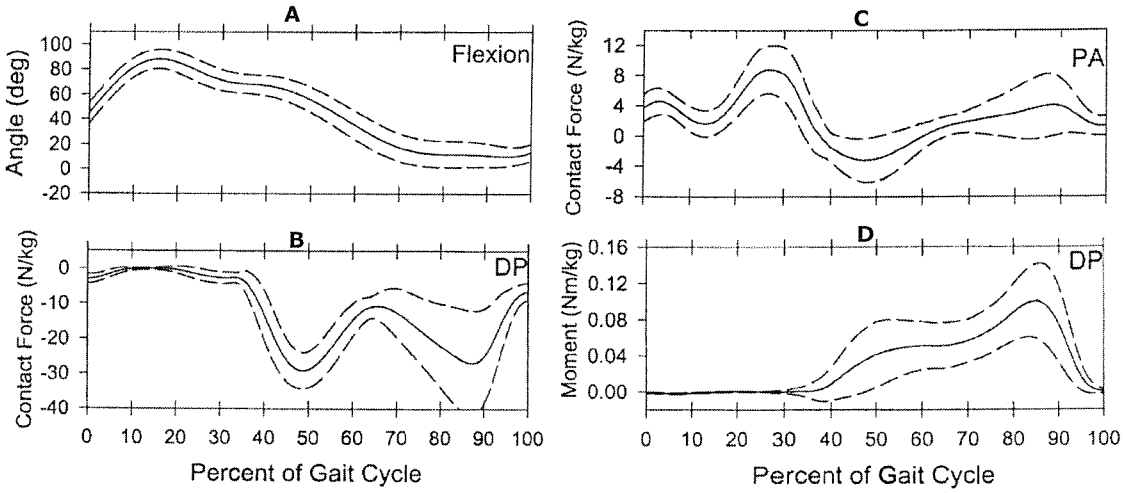

Figure 2-12: Knee angles and estimated knee contact forces during stair ascent [31]. The solid line represents the group mean while the dashed line represents ± one standard deviation.

2.6.1 Summary of Knee Joint Forces: Axial/Compression load, Anterior/Posterior Shear Forces, Internal/External Moment

The maximum tibiofemoral joint compressive forces for various activities have been reported (Table 2-3). These values vary with activity, knee joint angle, and analysing technique. For patients with total knee arthroplasty, it is most important to detect the compressive forces during daily activities such as level walking, rising from a chair, ascending or descending stairs. These activities create the compressive force ranging from 3 to 7 times body weight.

Author	Activity	Knee angle (degrees)	Force (× BW)
Morrison [104]	Walking	15	3.0
Harrington [77]	Walking		3.5
Costigan (personal contact)	Walking	68	2.8
Morrison [103]	Stair descent	60	3.8
	Stair ascent	45	4.3
Ellis et al. [77]	Rising from chair		3 - 7
Dahlkvist et al. [32]	Squat-rise	140	5.0
	Squat-descent	140	5.6
Costigan et al. [31]	Stair ascent	85 - 90	3.2

Table 2-3: Tibiofemoral joint forces: Compression.

The maximum tibiofemoral joint posterior shear forces for various activities are shown in Table 2-4. In walking down or up stairs these forces are in the range of 0.4 to 1.7 times body weight.

Author	Activity	Knee angle (degrees)	Force (× BW)
Ericson and Nisell [77]	Cycling	105	0.05
Costigan (personal contact)	Walking	68	0.35
Costigan et al. [31]	Stair ascent	85	0.37

Table 2-4: Tibiofemoral joint forces: Posterior shear.

On the other hand, the maximum tibiofemoral joint anterior shear forces are about 0.04 to 0.7 times body weight (Table 2-5). This value is bigger than posterior shear forces.

Author	Activity	Knee angle (degrees)	Force (× BW)
Ericson and Nisell [77]	Cycling	65	0.05
Morrison [103]	Stair ascent	30	0.04
	Stair descent	15	0.1
Morrison [104]	Walking	15	0.2
Costigan et al. [31]	Stair ascent	85	0.74
Costigan (personal contact)	Walking	68	0.42

Table 2-5: Tibiofemoral joint forces: anterior shear.

Authors	Activity	Internal/external torque(N m)
Morrison [104]	Walking	Peak: 16.65
		Low: 5.65
Costigan (personal contact)	Walking	Peak: 5.87
Costigan et al. [31]	Stair ascent	Average: 6.54
Andriacchi et al [3]	Stair ascent	6.8 (S.D. 3)
	Stair descent	15.1 (S.D. 9.1)

Table 2-6: Tibiofemoral internal/external torque, in N m, for walking, stair ascent and descent.

There are significant axial torques occurring during walking and other activities. The torques act at the foot as a consequence of the twisting of the body as it swings over the planted foot. The direction of the torque is internal, such that the lateral tibial plateau tends to move anteriorly. Taylor et al. [140] measured the torque in walking and found it to be around 8 Nm.

Chapter 3

TOTAL KNEE JOINT REPLACEMENT

Total knee replacement (TKR) employs specially designed components, or prostheses, made of high strength, biocompatible metals and plastics, to replace the worn out cartilage and affected bones in the knee joint. The metal that is most commonly used is an alloy of cobalt, chromium and molybdenum. The plastic is ultra-high molecular weight polyethylene (UHMWPE). These materials have been used in the joint replacement for about 30 years. The aim of TKR is to restore function to the knee so that the patient could perform daily activities in a pain free condition.

3.1 TOTAL KNEE REPLACEMENT AND ITS EVOLUTION

In modern total knee replacement surgery, only the worn-out cartilage surfaces of the joint are replaced (Figure 3-1). The entire knee is not actually replaced. The operation is basically a 're-surfacing' procedure.

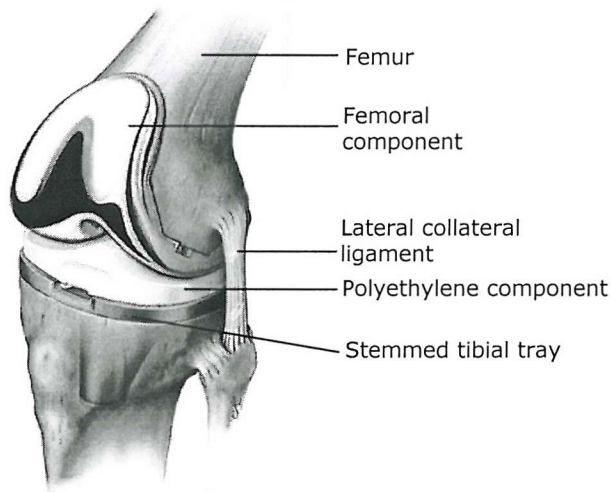

Special jigs are used to accurately trim the damaged surfaces at the end of the distal femur. The devices shape the end of the distal femur so it conforms to the inside of the prosthesis. The proximal end of the tibia is cut flat across the bone and a portion of the bone's centre is drilled out.

Figure 3-1: Total knee joint replacement with the ligaments intact.
[http://www.hipnknee.org/index.htm]

The surgeon removes just enough of the bone and the prosthesis is inserted to the bone, with or without bone cement depending on the type of prosthesis. Bone cement is a type

of polymer, famously known as PMMA. The cement is a mixture of PMMA particles, the liquid monomer MMA (methyl-methacrylate), a radio-opaque barium salt and initiator to start the polymerisation reaction of the MMA to PMMA. Implant bonding to bone takes time to develop especially in the old patient. As the bone cement helps in providing better gripping between bone and metal (implant), cemented prosthesis is mostly popular in the old patient. The collateral ligaments, muscles and tendons are left intact. Alignment abnormalities can usually be corrected during the operation by adjusting the direction of bone cuts, removing bone spurs (osteophytes), and releasing tight ligaments. The prostheses are inserted and tested; and the soft tissues were balanced. The surgeon wants to be sure that the joint line (alignment of prosthesis in the lower limb) is in the right place and the kneecap is accurately aligned for proper joint movement. If it is necessary to resurface the kneecap, the surgeon will apply a shaped piece of polyethylene that maintains the original width of the kneecap.

TKR is one of the most successful of all surgical procedures. Prior to the development of TKR technology, patients with advanced arthritis of the knee suffered from chronic pain and loss of functional independence. Following total knee replacement, more than 90% of patients have no pain, or only slight pain. Most patients can live a full and independent life [39].

The goals of total knee replacement are:

- Pain relief
- Improved knee motion (enable patients to stand and walk, i.e. daily activities, that are not limited by the knee)
- Improved knee strength

Total knee replacement is an elective surgery. Disabling and painful diseases involving the knee joint can be treated conservatively, without having knee replacement surgery. The following is a list of alternatives to total knee replacement surgery. They are:

- Specialized braces
- Arthroscopy
- Cartilage transplantation
- Osteotomy
- Uni-compartmental arthroplasty
- Arthrodesis or knee fusion

3.2 DESIGN FORMS OF TKR

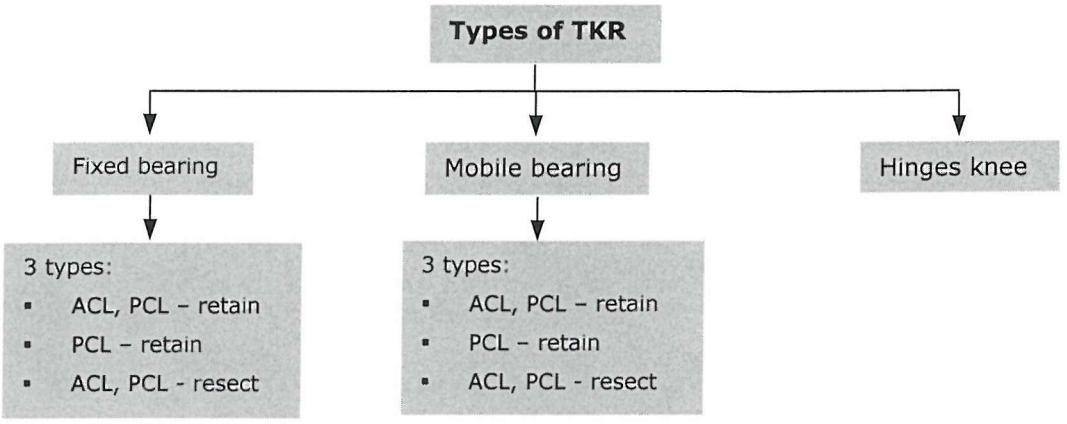

Figure 3-2: Types of total knee joint replacement.

There are numerous designs of total knee replacement (TKR) available in the market today, but only a limited number of design forms and types. The three main types of TKRs: fixed bearing, mobile bearing and hinges knees (Figure 3-2). Fixed bearing TKRs are used most commonly. In a fixed bearing knee as the polyethylene insert is rigidly attached to the tibial tray, there is no desirable movement present between them. In a mobile bearing design, the polyethylene insert is allowed to rotate on the tibial tray. Fixed bearing knees and mobile bearing knees can be further classified into three types – (i), preservation of both posterior cruciate (PCL) and anterior cruciate (ACL) ligaments; (ii), preservation of only the PCL and, (iii), without retaining either of the cruciate ligaments. Figure 3-3, Figure 3-4 and Figure 3-5 show three different types of fixed bearing knee available in the market.

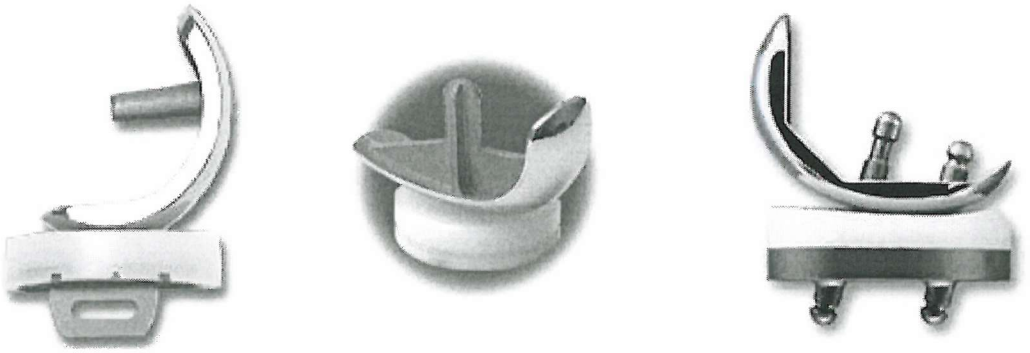

(a) (b) (c)

Figure 3-3: Fixed unicompartmental knees. (a) Oxford Phase 3 Unicompartmental Knee [www.biomet.com], (b) Repicci II ® Unicondylar knee [http://biometmerck.co.uk], (c) PFC Sigma Unicompartmental (DePuy). These types of unicondylar prostheses allow the retention of the anterior and posterior cruciate ligaments.

(a) (b) (c)

Figure 3-4: Posterior cruciate retaining, fixed bearing knee. (a) AGC knee [http://biometmerck.co.uk], (b) PFC Sigma Cruciate Retaining (DePuy) [http://biometmerck.co.uk], (c) NexGen ® CRA (Zimmer) [http://www.zimmer.com].

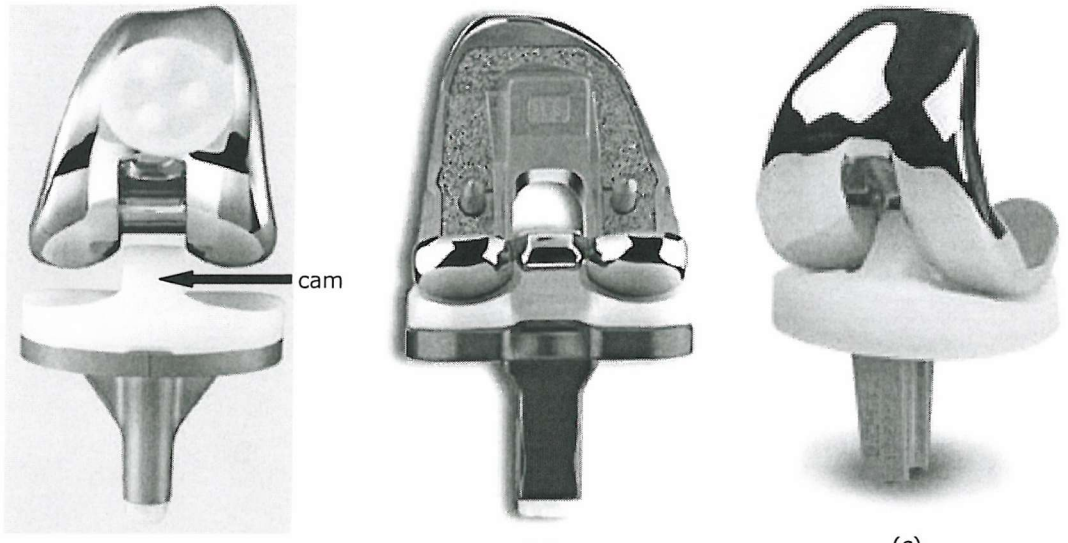

(a) (b) (c)

Figure 3-5: Posterior cruciate substituting total knee systems (or posterior stabilized knee). (a) PFC Sigma Knee System Cruciate-Substituting [www.famet.com.tr], (b) NexGen Posterior Stabilized Knee (LPS) (Zimmer) [http://www.zimmer.com], (c) AGC High Post Posterior Stabilised (HPPS) Knee [http://biometmerck.co.uk]. Both cruciate ligaments are resected. Posterior stabilized design knee has more posterior polyethylene dish and also the anterior upsweep of the poly is higher. In most designs, an intercondylar cam (some with spine, such as the PFC Sigma knee) is added to control the anterior position of the femur on the tibia.

For the knee design where both the cruciate ligaments are resected (i.e. the posterior cruciate substituting knee), there is an intercondylar cam which is added to control the anterior position of the femur on the tibia (Figure 3-5). Another feature of this design is that the polyethylene dished more posteriorly and the anterior lip is higher. These features are not seen in the PCL retaining type. The translation of the femur is mostly controlled by the posterior cruciate ligament. Preserving the PCL prevents excessive anterior contact point and aids the rollback of the femur [151].

Durable long-term fixation has been documented for many designs of fixed-bearing total knee replacement. However, in the late 1970s and the early 1980s, implant fixation and polyethylene wear was recognized as a factor in the late failure of TKR [25,65]. Conventional fixed-bearing knee prostheses have been proved to be clinically successful but with some reservations. In a study of 101 knees with fixed-bearing knee prosthesis [28], 96 percent had good-to-excellent clinical results, and the rate of survival of the prosthesis, with revision as the end point, was 96.4 percent after ten to fifteen years of follow-up. Most of the patients involved in these follow-up studies have been elderly individuals with low activity levels, and thus low demands have been placed on the prosthesis. With a few exceptions [35], there is little evidence that the same results could be duplicated in more active people. Also, even allowing for the preceding reservation, polyethylene wear and osteolysis remain important problems with current fixed-bearing knee prostheses.

Implant conformity and constraint are interrelated with regard to polyethylene wear and aseptic loosening. The push for lower conformity designs in the 1980s was in an attempt to decrease constraint [96]. Less constraint allows greater range of motion, less stress on the implant-bone or implant-cement interface and theoretically a lower chance of aseptic loosening [45,129]. However, as conformity decreases, smaller areas of joint contact caused greater contact stresses. Increased contact stresses along with greater translation and shear stress may lead to accelerated polyethylene wear and premature failure of the TKA. Conversely, greater conformity leads to greater stability as the contact area of the articulating surfaces of the prosthesis increased. This, in turn, enabled the forces in the knee joint to spread over a large surface and hence, decreased the contact stresses. As the contact stresses decreased, this would reduce the chances of polyethylene wear particularly delamination wear. However, the increased constraints can elevate the forces transmitted across the bone-implant interface, increasing the risk fixation failure.

Mobile bearing knee designs promote load sharing through the femoral-polyethylene and polyethylene-tibial tray components. This concept of dual-surface articulation by eliminating the rotation at the tibiofemoral articulation but allowing the rotation of polyethylene-tibial tray instead, can greatly increases the contact area between the femoral and tibial components from approximately 200 mm^2 in a good fixed bearing

design, to 1000 mm^2 or more for the mobile bearing design [25]. This reduces the contact stresses from approximately 25 MPa to 5 MPa or less in the mobile bearing [25], which is sufficiently low that it should not cause polyethylene damage even in active use.

According to Bert et al. [18], there are some disadvantages with mobile-bearing knees, i.e. dislocation due to 'spin-out' may occur in designs without a mechanical stop, and when a stop is present, wear may occur as the polyethylene bearing strikes against it. Mobile bearing knee designs are not a new concept, in fact it was designed almost 25 years ago, with the first prosthesis used was the Oxford unicondylar device (Biomet, Bridgend, South Wales) and has become a very successful knee implant. The second was the Low-Contact Stress (LCS) prosthesis (LCS, DePuy, Warsaw, Indiana), which was based on similar concepts. There are numerous companies with their own versions of mobile bearing knee replacement, examples of these are: Genesis II (Smith & Nephew), MBK (Zimmer), ISA (Stryker Howmedica Osteonics), Rotaglide (Corin), Trac II (Biomet) and many more (Figure 3-6). Mobile bearing knee is also known as meniscal bearing knee and this type of implant offers motion in two directions, both internal-external rotation and anterior-posterior motion.

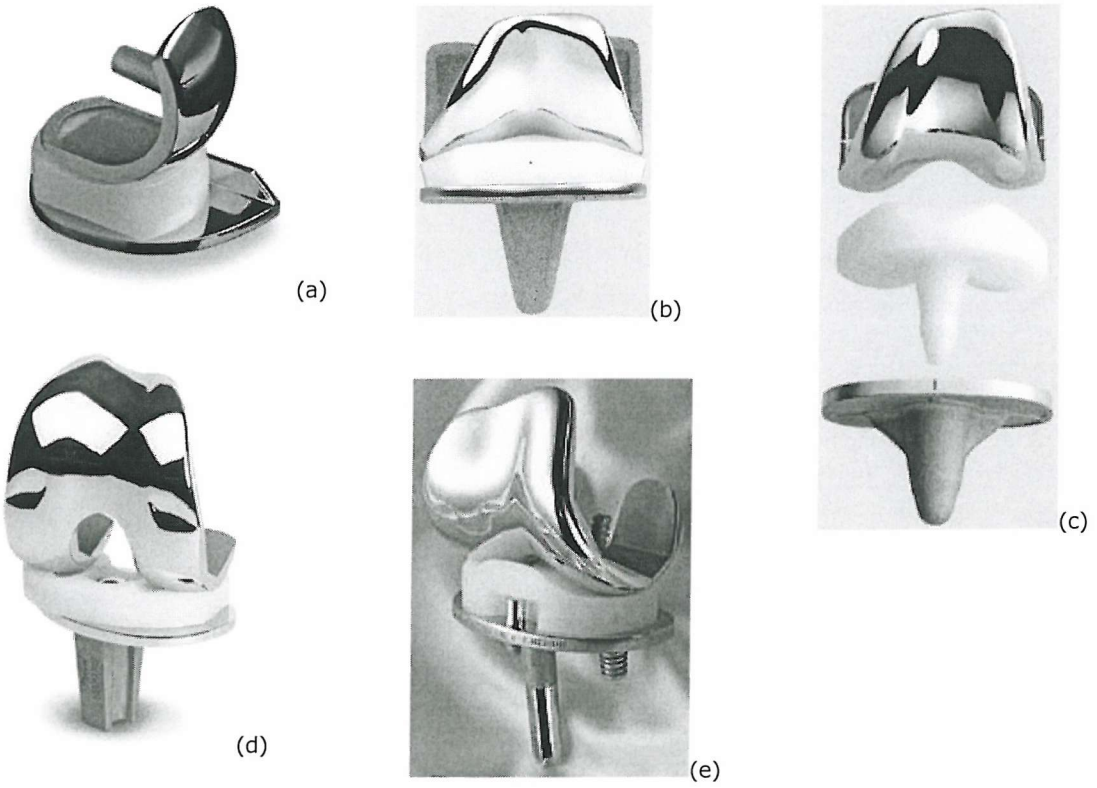

Figure 3-6: Different mobile bearing knee designs. (a) Oxford (Biomet) [http://biometmerck.co.uk], (b) LCS rotating platform (DePuy) [www.famet.com.tr], (c) PFC rotating platform (DePuy) [www.famet.com.tr], (d) Oxford Total Meniscal Knee (TMK) (Oxford) [http://biometmerck.co.uk], (e) Rotaglide (Corin) [http://www.corin.co.uk].

Besides the two types of TKR designs mentioned above, there is another type of total knee, known as 'linked' or hinge design. The characteristics of a linked or hinge design are [151]:

i. Stability is provided in all degrees of freedom. Varus-valgus and hyperextension being particularly important, although there can be some laxity, for example rotational, in one or more degrees of freedom.
ii. A linkage, such as a hinge, to provide stability and prevent subluxation or dislocation.
iii. Intramedullary stems are required to provide adequate fixation.

Figure 3-7 shows several types of linked hinge total knee. These prostheses are specially designed for patients who have significant bone loss, ligamentous deficiencies, bone tumors and multiple knee revision arthroplasties [151]. The long stems in these designs are useful for filling large bone defects and also for protecting against fractures.

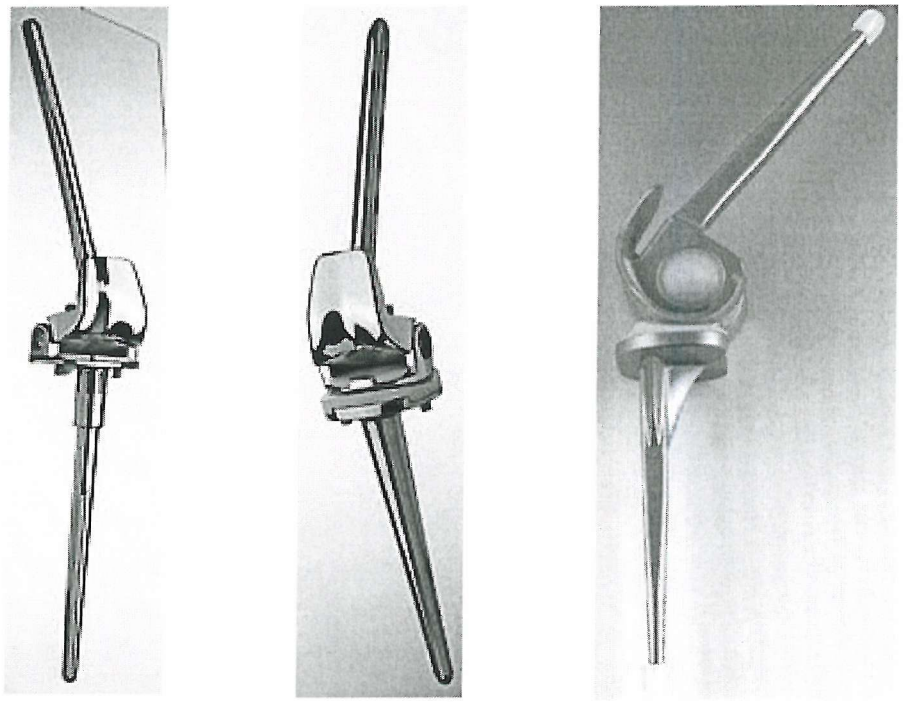

(a) (b) (c)

Figure 3-7: Designs of hinge total knee. (a) SMILES Fixed Knee Hinge (Stanmore) [http://www.stanmoreimplants.co.uk], (b) SMILES Rotating Knee Hinge (Stanmore) [http://www.stanmoreimplants.co.uk], (c) Link-Endo model (Waldemar-Link) [http://www.linkorthopaedics.com].

3.3 FAILURE MODES IN TKR

Loosening, infection and polyethylene wear are well-recognized complications of total knee arthroplasty. Loosening of knee implant is linked to the tibial tray and femoral component-bone interfaces. From the Swedish knee arthroplasty register report (2001), loosening of knee implant was the major limiting factor in the longetivity of knee systems. A total of 35% of the total knee revisions was due to loosening. The report accounted knee implants between 1990 and 1999. Loosening is probably a result of poor initial fixation, for example poor cementing technique by surgeons [79]. Infection sometimes occurred in patients after the implant surgery, causing postoperative wound healing complications and bacterial infections and as a result the body may reject the components [79]. For the purpose of this study, only the failure mode of the polyethylene component will be discussed in detail. Failure due to polyethylene wear has been demonstrated in both hip and knee implants [40,45,71,117,119,136,146]. A number of factors have been shown to affect polyethylene wear, including patient related factor (size, sex and level of activity) [13], material property of the PE and physiological loading of the knee joint. Besides these, the accuracy of the alignment of the components, the design of the prosthesis and the implant materials are also important to the durability of the polyethylene component. The wear problems associate with the polyethylene insert can be classified into several types, according to what has been seen from clinical retrievals during knee revision surgery. There are three main types of degradation of polyethylene: delamination, abrasive wear and third body wear [41,117]. Delamination and abrasive wear can then be classified into several modes depending on the degree of polyethylene degradation, for example: scratching, pitting and burnishing.

Delamination was defined as areas where a layer or sheet of polyethylene had separated or peeled away from the bulk of the tibial insert [41]. The surface where the layer of the polyethylene has been lost will leave the new surface rough and pitted and in some cases polyethylene is also peeled away from the surrounding edges [40,41,45,71,75,117,136,146,161] (Figure 3-8).

(a) (b)

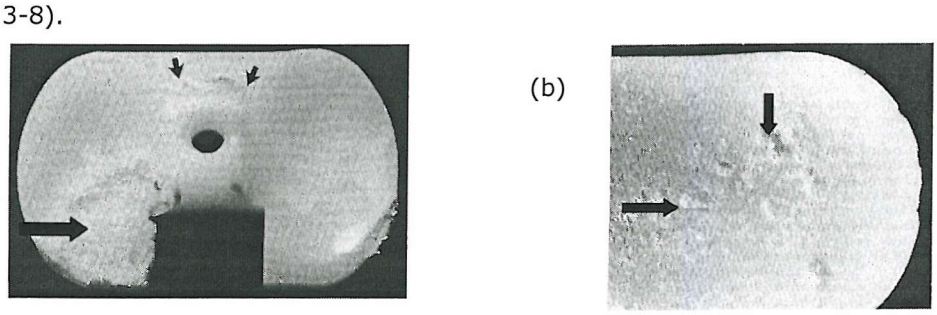

Figure 3-8: (a) Delamination: areas in which large, thin, surface sheets of polyethylene have separated from the bulk of the polyethylene component [117]. (b) Pitting: shallow, irregular voids in the articulating surface, often with one or more straight edges and typically measuring 2 to 3 mm across and about 1 mm deep [161].

Delamination wear was commonly seen as a major problem in the 1980s. The reason being in the way the polyethylene component was manufactured and sterilized [13,46,163]. The use of gamma irradiation in air resulted in high oxidation during the sterilization of the PE component which caused the polyethylene to be more susceptible to delamination wear. Sterilization using gamma radiation has led to oxidative degradation, which occurs in some but not all PE resins at 1 mm below the articulating surface, that is, within the area of maximal shear stress [13,163]. This subsurface oxidation is considered to be the cause of delamination, leading to catastrophic failure of the PE insert [13]. Due to this disadvantage in gamma irradiation in air method, significant effort has been made to improve the wear properties of PE. Polyethylene is currently stabilized against oxidative degradation either by sterilization without irradiation or by irradiation sterilization in an inert atmosphere, such as argon, nitrogen or vacuum. Polyethylene that is sterilized using this current new method is very unlikely to show substantial degradation [46]; hence, delamination is less prone to occur in the future.

Abrasive wear or surface wear of PE (Figure 3-9) is becoming the predominant concern of long-term failure in knee prostheses after improvement in the sterilization method of PE was introduced [46]. The wear particles produced from abrasive wear are generally at the micron (range from 2-20 μm) and sub micron level [46]. These extremely small particles can lead to osteolysis and these foreign bodies (wear debris) can cause great pain and inflammation. From a biological point of view, small debris particles (2 micrometer or less) are more dangerous to our body as these small particles can travel from the knee to the other part of the body through the lymphatic system [75,117].

Wear debris, which is mostly polyethylene, migrates to the surrounding soft tissue, where it eventually triggers a biological reaction. When the body deals with the debris it also releases agents that attack the bone, generally near the interface with the implant. As result, the joint becomes more susceptible to infection and bone resorption, which loosens the prosthetic components. This is how osteolysis takes place [2]. This process can potentially occur in any implant system (for example in hip replacement) regardless of implant design or fixation mode [2].

Polyethylene wear debris may be generated at the articulating surfaces between the femoral component and the PE insert and also between the surfaces of PE insert and the tibial tray in the mobile bearing knee designs. The kinematics and stresses of the knee have a large effect on the abrasive wear of the PE insert. In general, the amount of wear (of polyethylene) has been shown to be a direct function of the applied load, sliding distance (kinematics) and wear factor. This is also known as Archard's law [6], and was developed in the early 50's. Several studies [8,152] using hip wear simulator have shown that as the applied load and sliding distance increased, the wear volume of the

polyethylene would also increase proportionally. Although these studies were conducted in the total hip prostheses, the theory could also be applied in total knee replacement. Wear factor is dependent on the test configuration and the final wear volume. The amount of wear may also be influenced by TKR design (which governs the kinematics), polymer degradation, time-dependent loading, patient activity as well as the test configuration (with or without lubrication) [8].

Wear rates produced in one of the knee simulator studies [46], which only flexion-extension and anterior-posterior motions of the knee were tested, were generally smaller than the tests done which included the internal-external rotation. The flexion-extension and the anterior-posterior translation of the knee produced a simple linear motion in the anterior-posterior direction. Under this uni-directional condition, the polyethylene became strain hardened and hence, increased the PE wear resistance in anterior-posterior direction [46]. At the same time, the PE wear resistance in the transverse direction became much weaker [46]. If internal-external rotation was simulated, whereby causing transverse translation in the knee, this would increase the PE wear rate. Abrasive wear rate also increases with the sliding distance. The more translations and rotations experienced by a knee prosthesis, the higher the wear rate. Increasing the forces magnitude in the knee joint is also a major contributor to the increase polyethylene wear rate. In the study carried out by Fisher et al. [46], the PE wear rate for low force and kinematics input conditions (maximum axial force 1250 N, maximum anterior translation 5 mm and maximum external rotation 2°) was 7.7 ± 2 mm^3 per million cycles but the wear rate increased to 41 ± 14 mm^3 per million cycles with high kinematic and force input conditions (maximum axial force 2500 N, maximum anterior translation 10 mm and maximum external rotation 4°). Figure 3-9 shows burnishing (a less severe of abrasive wear) and compare with a more severe form of abrasive wear.

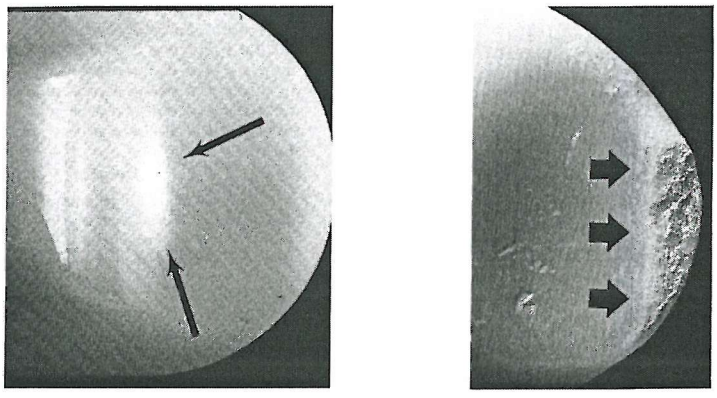

(a) (b)

Figure 3-9: (a) Burnishing: highly polished areas (arrows) [161]. (b) Abrasion: areas which the polyethylene has a shredded or tufted appearance (as shown in the arrows) [161].

Surface deformation in the polyethylene has also been reported [41,161]. This was a reshaping process of the polyethylene component due to cold flow of the material (Figure 3-10). Usually, the curvature of the articular surface changed due to pressure from the femoral component. However, the pressure from this component was not large enough to cause any material removal. Cold flow was seen on some polyethylene components in several designs [41,161], such as the Synatomic prosthesis (Depuy) and the Arizona prosthesis (Depuy). Cold flow usually occurred on the undersurface of the polyethylene, in contact with the metal tray and evidence of cold flow was normally located above screw holes in the metal tray.

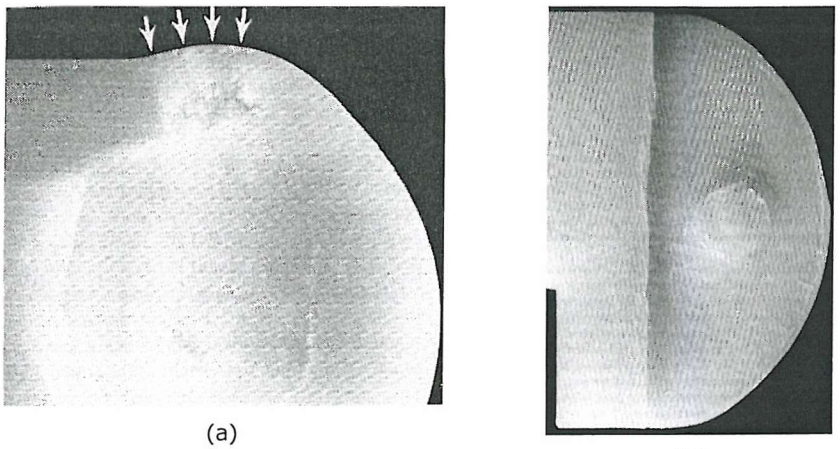

(a) (b)

Figure 3-10: (a) Surface deformation: evidence of permanent plastic deformation causing changes in the curvature of articulating surfaces [161]. (b) Evidence of subsurface cold flow of polyethylene into the screw hole of a tibial base plate [117].

Polyethylene wear debris from the delamination wear process and also bone-cement debris have been documented in the retrieval studies [161] being pressed inside into the polyethylene component (Figure 3-11). These wear debris could cause more damage and accelerated the wear rate of the polyethylene. This is the so-called third body wear.

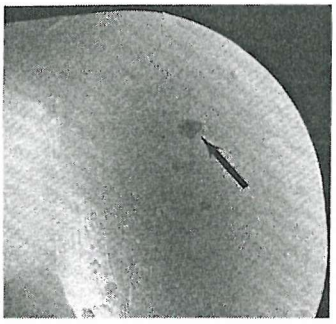

Figure 3-11: Bone-cement debris pressed into the articulating surface. This could be recognised by a difference from the surrounding polyethylene (arrow) in colour or texture, or both [117].

Undersurface wear [114] may also occur between the polyethylene bearing and the tibial baseplate in both mobile bearing and fixed bearing knees. Initially, tibial components had a monoblock construction; that is, the polyethylene was moulded onto the tibia baseplate during manufacture. This type of design has yielded successful and durable long-term results. Unfortunately, increased sizing options have made modularity a virtual necessity so that at present, in most cases, the polyethylene is no longer attached to the tibial baseplate by the manufacturer but is fixed to the baseplate with some kind of locking mechanism by the surgeon during the operation. No currently used locking mechanism is entirely reliable, and varying degrees of motion occur between the polyethylene and the baseplate. This motion can, of course, result in undersurface wear and the production of polyethylene particles. The problem is compounded because, for manufacturing reasons, the baseplate often is made of titanium and the surface is usually unpolished.

3.4 FACTORS AFFECTING PERFORMANCE OF TKR

The performance of TKR is influenced by three main factors: 1) patient related factor such as the mass of patient, ligament and bone quality, and the activity level of patient; 2) TKR design, and 3) surgery related factor such as the orientation of the knee prosthesis in the lower limb, soft tissues balancing and surgical approach. These three factors will influence the kinematics of the knee prosthesis. As a result, this will also have an effect on the stresses in the polyethylene component and the fixation. Here, further discussions will focus on these three factors.

3.4.1 Influence of Ligaments

Ligament balancing is an integral part of TKR and is highly dependent on correct alignment of the knee in flexion and extension [157]. According to Whiteside [157], since the mid-1970s, the rudimentary concepts of releasing the medial collateral ligaments in knees with varus deformity and the lateral ligaments in knees with valgus deformity have been widely taught and practiced. If the collateral ligaments were not balanced properly, varus-valgus instability was likely to occur [27]. Cameron and Hunter [26] reported on 4 cases of acquired valgus instability and noted that in 3 cases falls in the early recovery period had produced traumatic rupture of the medial collateral ligament (MCL) and medial capsule. Failure to achieve adequate medial-lateral soft tissue balance intraoperatively is probably the most common cause for early failure.

For a knee joint with the medial or lateral collateral ligament that are too tight at either side after total knee replacement, may cause varus or valgus instability. The tighter and stiffer collateral ligament will cause the other collateral ligament to stretch more and

hence, it will become more slack compared to its original state. A slack collateral ligament (at either medial or lateral side) may cause subluxation to the knee component and in some cases dislocation of the knee prosthesis have also been reported [50,67].

3.4.1.1 Preservation of ACL and PCL

The closest scheme for restoring normal constraint is to retain the cruciate ligaments and to resurface the femoral condyles in combination with shallow plastic tibial surfaces. This scheme is based on preserving as many of the anatomical structures as possible, thus minimizing the shear forces in the plastic surface and on the fixation and maintaining the proprioceptive effects of the ligaments. Preservation of both cruciate ligaments was used in early unicompartmental designs (Marmor and Unicondylar), where one or both sides of the joint were replaced, and in designs with connected components (Townley, Duocondylar, Duopatella, Geomedic and Cloutier). The ideal indications for preserving both cruciates are in the younger and more active patients where the bone geometry and the surrounding ligaments are not severely compromised. However, certain factors have limited the practise of preserving both cruciates:

- Many designs have used close-to-flat plastic surfaces, which have a high sensitivity to geometric placement, tightness and slope of the tibial components in the sagittal plane, resulting in an incidence of instability.
- The plastic components have often been thin, resulting in excessive wear and deformation. However, in the Marmor design, which used net-shape-moulded polyethylene, the destructive delamination type of wear was not reported [19].
- The surface area and the fixation methods of many of the unicompartmental components were inadequate, leading to a much higher rate of loosening than in total condylar types of TKR.
- The surgical procedure was difficult, partly due to the limited exposure when both cruciates were preserved, and to the lack of adequate bony landmarks for instrument alignment.

In recent years, efforts have been made to overcome these disadvantages, such as by improved surface designs, more accurate instrumentation and techniques, more wear-resistant polyethylene, better fixation and more vigorous selection of patients. The possibility of using small incisions with more rapid recovery has also led to a resurgence of interest in unicompartmental replacement [106,142].

3.4.1.2 Preservation of PCL

In the conventional bicompartmental total knee replacement, the ACL has to be resected and the PCL is retained or resected is depending on the prosthesis design. Posterior cruciate retaining (PCR) total knee arthroplasty has been indicated as a means of preserving anatomic femoral rollback, providing posterior stability and potentially increasing patients' range of motion [91,135]. Studies using cadaveric knees have demonstrated [72] that preserving the PCL prevented an excessive anterior contact point and the shear force was shared between the ligaments and the polyethylene surfaces. In the absence of the PCL, the contact points were too anterior for both flat and curved surfaces polyethylene components. Rollback of femoral component after preservation of the PCL had been shown by several authors [4,7,77], using anatomical and theoretical models. Roll back is believed to prevent impingement of the femur on the posterior portion of the tibia during flexion and, thereby increases the available range of knee flexion. The combination of external rotation and roll back of the lateral femoral condyle permits flexion angles up to 140°. Without the rollback mechanism, impingement of the soft tissues of the knee between the posterior rim of the tibia and the posterior aspect of the femur would limit flexion to between 90° and 105° [72].

Stiehl et al. [135], using the fluoroscopy method, studied the kinematics (follow-up study) of 5 different PCL retaining prosthetic designs: Porous Coated Anatomic (Howmedica), Ortholoc (Wright Medical Technology), Genesis (Richards), Anatomic Modular Knee (DePuy) and Miller-Galante 2 (Zimmer). Examinations were also made on normal knees to determine normal kinematics. The authors found that in the normal knee at full extension, the femoral component was in contact with the tibia at 6 ± 1 mm anterior to the midline in the sagittal plane of the tibial joint surface. In the intact knee, during flexion, the femoral component translated to 2 ± 1 mm posteriorly. Throughout most of the flexion cycles, the tibiofemoral contact points remained relatively close to the midline. In comparison to the PCR total knee prostheses started at 10 ± 5 mm posterior to the midsagittal line during extension. Unlike the normal knee which translated posteriorly during flexion, all PCR total knees translated to a point 5 ± 3 mm anterior to the midsagittal point. Stiehl et al. [135] calculated the average normal knee flexion angle to be 118° (range 110° to 137°). For the PCR total knees studied the average maximum weight bearing knee flexion angle achieved was 98°.

From the Stiehl et al. [135] study, the PCR TKAs had shown different kinematics from the normal knee and less range of movement. This less range of motion might be related to the loss of femoral roll back. Preservation of PCL had limited the anterior translation but had caused too much posterior displacement. Loss of the anterior cruciate ligament may be an important factor, which may explain these abnormalities. Besides Stiehl et al. 1995,

several investigators had also demonstrated relatively little femoral roll back in PCL retaining designs [76].

From what has been reported, rollback of femoral component does not occur in a consistent manner, depending on the type of prosthesis used in patient and other factors. Attention must still be given to PCL retaining TKAs especially those that had achieved *proper knee balance and degree of movement.*

3.4.1.3 Resection of PCL

Retention of the posterior cruciate ligament is based on the assumption that the PCL is biomechanically and histologically normal. The PCL in osteoarthritic knees may show pathological degeneration [78] and be less stiff than the normal posterior cruciate ligament. Due to this PCL quality problem, surgeons had opted for PCL-sacrifies TKR designs for some patients. If the PCL is resected, then usually some mechanism is required to substitute for its function in the implant design. For example, a posterior stabilizing post on the tibial component is designed to enforce posterior rollback of the femoral component on the tibial surface and to prevent posterior subluxation [39,94,148]. However, dislocation and extra bone resection make this option less than ideal. One possible mechanism for improving posterior stability is to deeply dish the tibial polyethylene and apply a high anterior tibial lip [148]. Both the factors: ligament retention or resection and prosthesis design are interrelated.

Resection of the PCL had significantly increased the anterior-posterior translation as compare to the normal knee, as reported by Matsuda et al. [94]. Femoral rollback is important to improve knee extension strength and to increase range of motion [94]. Insall et al. [67] reported that fewer than 25% of patients with a deeply dished implant and resected posterior cruciate ligament could climb stairs and the average range of knee angle was 90°. Patients with the PCL resected have smaller flexion angles when compare to the normal knee and PCL retaining designs, with average flexion angle of 118° and 98°, respectively [135].

3.4.2 Prosthetic Design

The outcome of arthroplasty can be influenced by the choice of prosthesis. Some of the earliest implants were simple hinges. These designs had the advantage of being easily aligned and inserted, and frequently, the short-term relief of symptoms was excellent. *Long term follow up, however, has shown a high incidence of aseptic and septic loosening*

[67]. Using a Walldius prosthesis, Young et al. [163] reported that no prosthesis survived 10 years. Hui and Fitzgerald [66] reported a 23% incidence of major complications in hinged total knee arthroplasty and an 11.7% incidence of infection. The highly constrained nature of the design is a prominent factor in the high complication rate in these series. The fixed-axis hinge results in both high rates of metallic wear and the transmission of large stresses to the prosthetic stem and the bone-cement interface. These factors are assumed to be responsible for the high rate of aseptic and septic loosening and component breakage [66].

Cadaveric studies before and after posterior cruciate-retaining TKR reveal that the degree conformity is the primary stabilizer after TKR [134]. In the intact knee, the cruciate and the collateral ligaments are the primary restraints to translation and rotation in the loaded and unloaded states [48,49,150]. After total knee replacement, rotational stability is coupled to coronal stability, which is maintained in part by the collateral ligaments, provided that the joint line is restored to its proper level [157,159]. Under physiological loading levels, the stabilizing effect of surface geometry and contact forces can exceed contributions of the posterior cruciate and collateral ligaments [96,134]. More conforming implants provide greater rotational and anteroposterior stability at all flexion angles [96,141].

Studies of polyethylene retrievals reveal greater wear in inserts that are flatter or less conforming in the coronal and sagittal planes [45,84]. It is postulated that a lack of conformity between the femoral and tibial components chronically stresses ligamentous supports, which eventually weaken and allow clinical or sub clinical laxity. Abnormal translation then leads to abnormal polyethylene stresses and accelerated polyethylene wear with premature failure of the TKR [45,96]. Late instability can present as a direct result of asymmetric or progressive polyethylene wear [19,20,26].

Conformity is not the only factor affecting the performance of the TKR [12]; the thickness of the polyethylene component also plays an important role. Bartel et al. [12] conducted a study on the effect of thickness of polyethylene insert on the contact stresses within the articulating surfaces. He found that the stresses within the contact surfaces of TKR generally increase as the thickness of polyethylene decreased. The thickest component was always the least stressed or had the least strain.

Prosthetic design changes have been made to help to reduce the incidence of dislocation in specific systems. Modifications to the Insall-Burstein II posterior stabilized prosthesis (Zimmer, Warsaw, IN), including elevation and anterior translation of the polyethylene post by 2 mm, significantly reduced the rate of dislocation in the series reported by Lombardi et al. [86] from 2.5% (5 of 252) to only 0.2% (1 of 656). Similar improvements have been noted by Ranawat et al. [122] with changes in the PFC prosthesis (Johnson &

Johnson, Raynham, MA); an increase in the height of the post from 8 to 14 mm eliminated the occurrence of dislocation.

3.4.3 Alignment of Prosthesis

Alignment of the prosthesis with respect to the lower extremity has been identified as one of the major factors that influence the success of knee arthroplasty [27,67,126,129,157]. In the frontal plane, the normal alignment of the lower extremity is approximately 0° of mechanical alignment or 7° to 9° of tibiofemoral anatomic valgus. There have been different opinions from various researchers. Townley [144] believes the alignment in the lower extremity with a total knee replacement (TKR) should have the mechanical axis medial to the centre of the knee. Whereas Insall et al. [68] believes it should be laterally aligned.

Several studies have been carried to investigate the axial alignment of knee prosthesis and in which position the components give the best stability to the patients. Lotke and Ecker [87] emphasized the need for achieving a normal alignment (0° of mechanical alignment) in total knee replacements if they are to endure. Different tibiofemoral angles had been reported to which a TKR is best tolerated with and they are summarised in Table 3-1.

Authors	Alignment angle (degree) and direction
Clarke and Scott [27]	5° - 8° valgus
Whiteside [157]	5° - 7° valgus
Hvid and Nielsen	7° ± 5° valgus
Ritter et al. [126]	7° - 9° valgus
Yoshioka et al. [162]	5° ± 2° valgus
Ranawat and Rodriguez [122]	3° - 8° valgus

Table 3-1: Range of tibiofemoral angle and direction of alignment reported by various researchers.

These are the axial alignment angles that the researchers found to provide the best clinical performance in total knee arthroplasty. However, this is just one of the factors that influenced the clinical success. Other factors which affect the performance and success of TKA are ligament and soft tissues balancing within the joint in TKR, the load applied in the joint and kinematics after post-op.

According to the study of Ranawat et al. [122], malalignment in the sagittal plane of the normal knee joint usually affects range of motion, with resultant tightness or laxity of the soft tissues. They used radiography method to assess the effect of malalignment of the

joint. A tibial component in excessive extension (anterior slope) could produce a flexion block due to tightness or impingement in the posterior aspect of the joint. A tibial component in excessive flexion (posterior slope), could produce instability in flexion, or a flexion contracture, depending on the level of resection.

The malalignment in the frontal or anteroposterior plane affects the distribution of the load between the medial and lateral condyle of the tibia. The goal should be to equalize load distribution between the two tibial condyles to prevent mechanical overload of the cancellous bone with resulting aseptic failure. In a review of 124 total knee replacements by Ewald et al. [43], a consistent association was found between varus alignment and medial tibial radiolucency, whereby the radiolucency indicated that there was loosening of the implant. They suggested that varus alignment overloads the medial tibial condyle may result in eventual fixation failure. In another revision study of 421 total knees (posterior cruciate condylar type) conducted by Ritter et al. [126], there were a total of 8 failures, with 5 failures aligned in varus and 3 aligned neutrally. There were no failures in the valgus group. In their study, patients were classified into a normal group that was 5° to 8° anatomic valgus, a varus group that was from 4° anatomic valgus to any degree of varus and a valgus group that was more than 9° anatomic valgus. The authors suggested that surgeons should align a total knee prosthesis in neutral group or a slight amount of anatomic valgus to give the patient the best chance for long-term survival.

In a study by Hsu et al. [64], the load distribution between the tibial condyles was examined by changing the alignment of the knee replacement in synthetic bones. The advantage of this method, by altering the alignment of the joint, produced a predictable alteration in load distribution that was notable in the polyethylene tibial component of a total condylar prosthesis. A femorotibial alignment of 7° valgus best equalized the forces between the tibial condyles. The effect of valgus malalignment has been studied by Grace and Rand [55], showing that 10 out of 25 knees with patellar instability had greater than 10° of valgus deformity.

Femoral malrotation has been studied in cadaver specimens by Anouchi et al. [5] by altering the femoral component rotation and assessing the effect on stability and patellofemoral tracking. The authors found that internal rotation of the femoral component produced a construct that was tight medially and gapped open laterally in flexion. In addition, the patellofemoral tracking was close to normal, and the contact pressures most evenly distributed on the patella, with a component externally rotated 5°. In a similar cadaveric study, Rhoades et al. [125] noted that a femoral component placed 5 mm lateral to the centre on the distal femur produced patellofemoral tracking closes to normal.

In the latest study by Romero et al. [128], they performed total knee replacements on 10 cadaveric knees, to investigate the influence of total knee alignment and femoral component malrotation (at 3° and 6° internal and external malrotation degrees) on femorotibial laxity. The mean varus and valgus displacement of the tibia for a given knee flexion angle (0°, 30°, 60° and 90°) was compared among tests with femoral components at neutral, at 3° and 6° internal rotation, and at 3° and 6° external rotation. These comparisons were done with tests with the tibial component perpendicular to the mechanical axis and at 3° varus inclination to the mechanical axis. All the total knees were vertically loaded at 150 N and the tibial component was subjected to a 10 N m torque. The result showed that there were no statistically significant differences in varus or valgus laxity between different malrotations of the femoral components during full extension. The largest mean varus laxity (7.3° ± 1.0°) was measured at 60° knee flexion with the tibial component perpendicular to the tibial shaft and the femoral component in 6° internal rotation. At the same tibiofemoral alignment, the mean varus laxity (3.6° ± 1.0°) was observed in the 6° external rotation. With the tibia at 3° varus inclination to the mechanical axis, the mean varus laxity (6.4° ± 1.3°) for the femoral component at 6° internal rotation was statistically significantly larger than for the femoral component at 6° external rotation (2.9° ± 0.9°). The valgus test at 60° did not show large difference among different femoral component positions. The valgus laxity remained under 3°. At 90° knee flexion, the varus and valgus laxities were small (range 1.8° ± 0.3° to 2.6° ± 1.2° for varus laxity and 1.4° ± 0.6° to 1.9° ± 0.8° for valgus laxity) and showed no significant differences between the component positions.

Malrotation of the femoral component may lead to patellofemoral instability, wear or loosening of the femoral component and patellar fracture [128]. Internal rotation of the femoral component also may increase stresses on the tibial component leading to wear or loosening. As the study of Romero et al. [128] showed that most knees exhibited varus laxity with internal rotation of the knee, therefore, internal rotation of the femoral component should be avoided.

3.5 EVALUATION OF TKR

With the increasing number of total knee replacements, the number of revisions of total knee also increases. From literature review, it can be concluded that polyethylene wear is a major contributor to revision surgery. Several studies [10,12,36,51,92] have been carried out to investigate the stresses and wear of polyethylene component, either using finite element analysis or *in vitro* experiment (knee wear simulator). All these methods share the same basic principle – trying to simulate the *in vivo* condition in a replaced knee as closely

as possible. Several methods have been used to evaluate the performances of total knee joint replacement and they will be discussed in this chapter.

3.5.1 Knee Wear Simulators

Knee simulating machines have been developed for the evaluation of the performance of TKR and are reported in the literature. There are two main types of knee simulators; those that are force-controlled and those that are displacement-controlled. There are also other categories of knee simulators, which are defined according to the freedom of movements of each simulator.

Walker et al. [150] developed a knee wear simulator (Figure 3-12) which aimed to reproduce the kinematics of TKR in patients and to assess the long-term wear of the polyethylene component. The simulator was based on the input of forces and moments rather than on displacements and rotations. Soft tissues restraints were included in this simulator by using a set of 4 springs and bumpers. The force data used in this simulator are based on the Morrison's force predictions [88,102,103]. The Stanmore knee simulator has been proven as a suitable testing machine for the evaluation of knee joint kinematics and the wear in different types of total knee replacement. Soft tissues constraint in the machine was required to maintain the displacements within physiological limits. Due to the ability of the simulator to reproduce the kinematics seen in clinical studies, the test configuration of this simulator has since been used by several authors [13,15] to perform various studies on the TKR. The resultant displacements of the force-controlled simulating machine are dependent on the input forces. Without the soft tissue restraints, Walker [150] noted that for the low constraint TKR designs moved unrealistically and in some cases, dislocation of the femoral component was seen.

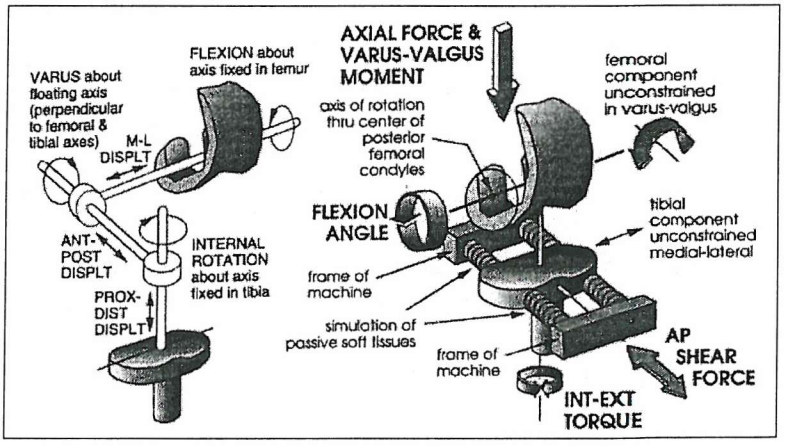

Figure 3-12: A schematic of the Stanmore knee wear simulator, developed by Walker [150]. It is a force-driven simulator. The directions of input forces are shown above. The bumpers at the anterior and posterior are used as representation of soft tissues at the knee joint.

The Stanmore knee simulator is not the only available knee simulating machine, there are others with different experimental configurations. For example, Burgess et al. [24] used a six-station knee wear simulator to assess the wear performance of Kinemax (Howmedica, U.K.) TKR. The simulator applied a representative flexion-extension motion, ranged from 0 to 65°; axial load of maximum value 3000 N and anterior-posterior translation of up to 15 mm. Internal-external rotation or torque were ignored in the study. The wear test was conducted over eight million cycles. From the *in vitro* test, Burgess et al. concluded that the wear rate and burnished appearance of the bearing surfaces was similar to retrieval study performed by Wasieleski et al. [153]. Burgess et al. did not see any delamination of the PE insert.

Barnett et al. [10] developed the method of mixed displacement and force-controlled using a knee simulating machine and in this study the A-P displacement and allow I-E rotation profiles were input and defined prior testing. This machine used the ISO standards 14243-1 for axial load and flexion-extension as input parameters. In Barnett et al. study [10], the performance of the displacement-force-controlled knee simulator was evaluated by comparison of the wear seen in the PFC Sigma knee prosthesis. Twelve PFC knees were subjected to a wear test of 2 millions cycles using this simulator and at the end of the test, this study showed no significant differences in wear rate and wear scar area among the prostheses. The wear scars seen, including burnishing (predominant), uni-directional scratching and pitting, were a good physiological representation of those observed in a clinical study.

In one recent study, Beaule et al. [13] carried out an experiment to investigate the polyethylene wear characteristics produced in Stanmore knee simulator and compared the results to the ex *vivo* data. His study was to assess the validity of the knee wear simulator whether it is capable of producing a similar type and amount of wear and particles as occurs in clinical practice (or ex *vivo*). Six posterior stabilised total knees (5 Insall-Burstein II, Zimmer, Warsaw, IN and 1 PFC, Johnson & Johnson, Raynham, MA) were used in the Stanmore knee simulator. Loadings such as the axial force (the largest force, 2 to 4 times body weight), anterior-posterior force and internal-external torque were applied to the simulator. 1, 5 and 11 millions cycles were carried at the knee simulator and this would most closely approximate time *in vivo* at 1, 5 and 11 years post knee replacement. Polyethylene wear particles were recovered and this was compared to the clinical results of 6 patients. The authors found that in both the knee simulator and ex *vivo*, the polyethylene components exhibited burnishing (predominant wear type) and scratching of the surface.

Beaule's finding was consistent with the study of Barnett et al. [10], whereby the burnishing was the main damage mode. The backside (of polyethylene-tibial tray) wear was minimal and showed some zones to have a light abrasive wear. Other than surface damage, the particles produced in the Stanmore knee simulator were of comparable size but had less variability in their form compared to the particles produced *in vivo*. A total of 2272 ex *vivo* and 2284 knee simulator particles were analyzed. The average distribution of wear particle type for the *in vivo* and knee simulator, respectively was 73% and 64% for rounded and, 27% and 36% for elongated. The differences in these results were that wear conditions *in vivo* were strongly affected by patient factors, such as gait, weight and limb alignment. In order to achieve that, the knee simulator model must be sufficiently close to the clinical situations. In this study, the Stanmore knee wear simulator was undergoing a comparable wear mechanism to that *in vivo* and had proven to provide useful and reliable information.

All the wear studies discussed above applied the loading patterns during walking cycle. Benson et al. [15] addressed the importance of assessing the wear performance of TKR during other activities and instead of applying load during walking cycle, they applied loading patterns during stair descent to Natural Knee I (Sulzer Orthopaedics). The mechanical test configurations were those used in the Stanmore simulator. The axial loading during stair descent was significantly higher than level gait. The maximum axial loading during stair descent was approximately 4200 N; whereas during level gait, the value peaked at 2500 N. Larger knee flexion angle and internal-external torque were also applied during stair descent. The anterior-posterior load was slightly less during stair descent when compared to level gait. This wear test [15] showed that there was significantly more weight loss seen in the TKR design during stair descent than during level gait.

The literature review has shown the extensive interest among researchers to evaluate the performance of TKRs, in order to gain better understanding wear mechanisms occurring in total knee joint. The knee simulators, for example, have proved to be very reliable and able to reproduce the wear seen in clinical studies. In order to achieve this, it is largely dependent on the input parameters that to be used in the simulating machine. The displacement-controlled simulating machine [10] is useful in a way that 'realistic' motion or displacement of knee prosthesis is guaranteed as the kinematics are used as the parameters that drive the machine. The simulator is programmed to give a particular displacement waveform, so it is also assumed that the simulator will only deliver a maximum force to achieve the wave form. In the total knee joint, the kinematics pattern of a knee prosthesis are dependent on the loading in the joint and also on the geometric design. A more constrained design would have less movement compared to the less constrained design. Due to these reasons, the force-controlled simulating machine has the advantage over displacement-controlled machine. The kinematics patterns of a knee

prosthesis are dependent on the forces input data. Force driven simulator is able to show the differences between geometric designs and their kinematics. On the other hand, in order to examine the relation between prosthesis design and its kinematics using a displacement-controlled simulator, a unique displacement for each different design needs to be assigned. In this way, the relation between the geometric design and kinematics could be achieved.

There are several limitations with the current experimental wear testing. Wear studies are unable to directly measure the contact pressures in the TKR. There is simply no way to measure the contact pressures in the contact surface in parallel with the wear testing. Using a knee wear simulator can be very costly. Furthermore, there is also need for an actual TKR component, which can be very costly. Wear testing can also be extremely time consuming. A simple wear test of up to 5 million cycles can sometimes take up to 3 months [13]. Moreover, if mistakes occur, wear testing cannot be repeated using the same component. It will not only expensive but also waste of time. Most of the wear studies only simulate walking cycle and have not accounted for patient-to-patient variability. All the experimental studies have yet to examine the performance of TKR at malalignment or malorientation. The mechanical set-up to test TKR design under malorientation, although possible, is somehow complicated as highlighted by Haider et al. [59].

3.5.2 Numerical Simulation of TKR

Sathasivam et al. [130,131] developed knee computer models with different bearing surface geometries, and analysed the effect of these differences on the contact stresses and kinematics of TKR. The first knee model [130] only predicted the kinematics (A-P displacements, I-E rotations) of the femur relative to the tibia for a set of input forces and moments. This model used mathematical equations to calculate the new equilibrium position of the knee model after sets of forces and moments were applied to it. This was a static simulation. An A-P force test and an internal-external rotation test were carried with an oscillating A-P force and I-E torque, at 10° and 60° of flexion. The knee model was under a constant compression force of 1500 N. The Kinemax Condylar with the standard tibial insert (CONDYLAR) and the 'high stability' insert (LOWSTRESS) of higher constraint was used. The kinematics results showed good agreement with the data obtained from Stanmore knee simulator, for the same prosthesis design. The mathematical knee model also carried out studies to predict the effect of coefficient of friction at the articulating surfaces and soft tissue restraint forces, on the A-P translation and I-E rotation of the model. Both of these restraints were shown to have effect on the kinematics predicted and there were good agreements between this theoretical (mathematical) model and the experimental one.

Godest et al. [53] also developed a computational knee model by using a computer-aided engineering (CAE) package in order to predict a total knee replacement TKR kinematics in the sagittal plane. The knee model was developed based on the mechanical arrangement used in the Stanmore knee simulator [150] and in the model developed by Sathasivam and Walker [130] discussed above. Solid femoral and tibial components were built to represent the Stanmore simulator and the model only simulated two-dimensional motions. Both the femoral and tibial components were constrained to stay in contact throughout the simulation in the sagittal plane. Two non-linear springs were used to define explicitly the forces exerted by the springs allocated at the Stanmore knee simulator. These anterior and posterior springs represent the action of the soft tissues at the joint. Godest's knee model also took into account of friction forces. The computational knee model was subjected to four external forces, the vertical compression load F_c applied to the femoral component (constant value 1500 N), the anterior-posterior force F_{ap} applied to the tibial tray (ranging from −300N to +300 N), the forces of both non-linear springs (represents soft tissues) and the friction forces (coefficient of friction 0.07). A constant velocity translational motion was applied to the tibial tray. ADAMS^{TM} kinematic solver calculates the motions of the mechanism and the reaction forces within the mechanism as a function of time and at each time step, the solver displays positions of the TKR components. Simulations were done at flexion angles of 10° and 60° for two TKR designs, the Kinemax Lowstress and the Kinemax Condylar TKR from Howmedica. The output of this study, i.e. the anterior-posterior displacement of the two TKR designs was validated by comparing kinematics data obtained from Stanmore knee simulator.

Both the TKR designs showed good correlation in terms of A-P displacements with the knee simulator. The models were also compared to Sathasivam model [130], which was a computational model and also showed good agreement in the kinematics performance. Godest also simulated the models by changing the stiffness of the springs (i.e. varying the soft tissues restraint) with flexion angle. The reason being that in the intact knee, soft tissue restraints vary significantly with flexion angles [49]. The results for both designs, modelling the soft tissue restraints using constant stiffness leads to the underestimation of less than 10% of both the A-P laxity of the TKR joint. Although the results showed only small percentage of difference, varying the soft tissues restraint was essential. This is because soft tissues (ligaments and capsule) constraint the movements of the intact knee [49].

The use of this computer model is very limited to only predicting the kinematics of the knee prosthesis. It is unable to predict either the contact pressures or the stresses within the articulating surfaces of the prosthesis. Due to this reason, a more sophisticated method - finite element analysis has been introduced which is capable in predicting the kinematics as well as the stresses and contact pressures within the prosthesis.

3.5.3 Finite Element Analyses

General Theory

The basic principles underlying the finite element methods are simple. For example, a body in which the distribution of an unknown variable (such as the temperature or displacement) is required. Firstly, the region of the body is divided into an assembly of subdivisions called elements, which are considered to be interconnected at joints, known as nodes (Figure 3-13).

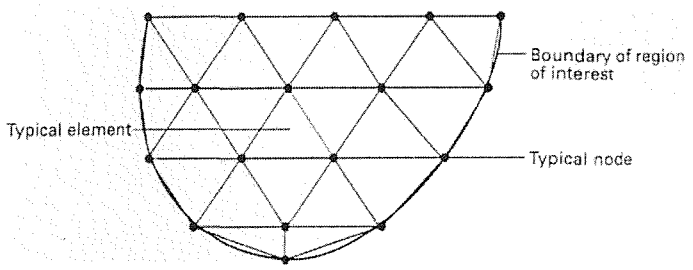

Figure 3-13: Discretization of a region of a body into a number of finite elements [44].

The variable is assumed to act over each element in a predefined manner, with the number and type of elements chosen so that the variable distribute through the whole body is adequately approximated by the combined elemental representations. The distribution across each element may be defined by a polynomial (for example, linear or quadratic) or a trigonometric function. After the problem has been well identified, the governing equations for each element are calculated and then assembled to give the system equations. The element equations may be found in a variety of ways and that the equations of a particular type of element for a specific problem area (for example, stress or displacement) have a constant format. Thus, once the general format of the equations of an element type is derived, the calculation of the equations for each occurrence of that element in the body is straightforward – i.e. substituting the nodal coordinates, material properties and loading conditions of the element into the general format. The individual element equations are assembled to obtain the system equations, which describe the behaviour of the body as a whole. These generally take the form:

$$[k]\{U\} = \{F\}$$

where $[k]$ is a square matrix, known as the stiffness matrix; $\{U\}$ is the vector of an unknown nodal displacements or temperatures; and $\{F\}$ is the vector of applied nodal forces. Before this, equation is solved for $\{U\}$, the unknown, some form of *boundary condition* must be applied. There may be several hundred or several thousand such equations, which means that computer implementation is mandatory.

Preprocessing and Postprocessing

The theory of FE includes matrix manipulations, numerical integration, equation solving and other procedures carried out automatically by commercial software. We (the user) may see only hints of these procedures as the software processes data. We mainly deal with *preprocessing* (describing loads, supports, boundary conditions, materials and generating FE meshes) and *postprocessing* (sorting output, listing and plotting of results). In a large software package the analysis portion is accompanied by the preprocessor and postprocessor

3.5.3.1 Static FE Analyses of TKR

Sathasivam et al. [131] performed a static FE analysis examining the polyethylene stresses during level gait. The forces (compression force, A-P force and I-E torque) and flexion angle applied to this model were those used in the Stanmore simulator. Kinematics predicted from earlier rigid body analysis [130] were used by taking relative positions and applied to the static FE model at 1% intervals of stance phase of gait. From this study, the different condylar geometries of knee prostheses showed differences in kinematics and contact stresses. The more conforming knee model showed lower stress because larger contact areas distributed the load on the articulating surfaces. The femoral and tibial components of the more conforming design had higher degree of conformity in the frontal plane as compared to the other model. The less conforming model recorded higher contact shear stresses than the more conforming one. Based on this study, Sathasivam suggested that different designs would have different durability.

The effect of conformity of TKR designs and the thickness of the polyethylene insert on the contact stresses within knee prosthesis was further studied by Bartel et al. [11,12]. Finite element models of eight different designs knee prostheses models were developed. Bartel et al. [12] only developed half of each of the knee systems (the models have symmetric articulating surfaces) and they simulated a worst case loading condition, by loading the medial side of the TKR. 3000 N load was used as this high force was recorded exerted to the knee joint during activities of daily living. The axial force used in Bartel's model was 2 times larger than Sathasivam's model [130]. The knee models were meshed with eight noded solid brick elements, and consisted of a femoral component and a polyethylene insert. The polyethylene component was modelled as a non-linear material (elastic-plastic) with a yield stress of 14.5 MPa. The thickness used in polyethylene insert for each of the design was obtained from manufacturer's data or some from measurements. The thickest polyethylene was 8.5 mm and the thinness was 4.0 mm.

From the results, Bartel et al. [12] found that high contact stress (highest approximately 60 MPa) was seen in the non-conforming designs. The more conforming design, for example the HSS 913 knee showed the lowest contact stress, 40 MPa. Bartel et al. also reported the von Mises stress and strain and once again, the more non-conforming designs showed the highest values. The models (for example, the AMK prosthesis), which showed the highest von Mises stresses also had the thinnest polyethylene insert thickness (4 mm). The HSS 913 knee model had the thickest polyethylene insert (8.5 mm), hence had lower von Mises stresses. This study showed the advantages of designs that have more conforming articulating surfaces and thicker polyethylene components. The more conforming articulating surfaces enable the load to transfer over a large contact area and this results in smaller stresses.

Liau et al. [85] conducted a study on the effect of malalignment on stresses in polyethylene component of total knee prostheses. They developed three-dimensional finite element models of the tibiofemoral joint of knee prostheses for three different designs. These were the high conformity flat-on-flat (HFF), high conformity curve-on-curve (HCC) and the medium conformity curve-on-curve (MCC). The femoral component was modeled as rigid body elements. The ultra high molecular weight polyethylene (UHMWPE) tibial component was assumed as an elastic-plastic material, with elastic modulus of 1016 MPa, yield stress was 14.07 MPa and Poisson's ratio was 0.46. The thickness of the UHMWPE tibial component in these three models was all 6 mm. Three malalignment conditions including the medial translation (0.25, 0.5 and 1.0 mm), internal rotation (1°, 3° and 5°), and varus tilt (1°, 3° and 5°) of the femoral component relative to the tibial component were simulated. A compression load of 3000 N (approximately 4.4 BW) was applied to the tibiofemoral joint at 0° flexion. The finite element code ABAQUS 5.8-10 was used to carry out the contact analysis.

Liau et al. [85] managed to show the importance of malalignment effect on stresses in tibial polyethylene component. The rotational line between the femoral and tibial components has the least effect on polyethylene wear but varus/valgus malalignment, even with the best designed prosthesis elevated the stress and therefore would be likely to accelerate wear. They concluded that the greatest increase of contact stress and von Mises stress was occurred in the low conformity flat-on-flat design of knee prosthesis under the severest malalignment condition. The high conformity curve-on-curve design of knee prosthesis has the minimal risk of polyethylene wear under malalignment conditions.

Liau et al. [85] and Bartel et al. [12], both applied the same amount of axial force and only uni-directional loading simulations were carried out. Both of these studies only predicted the contact stresses in the articulating surfaces without taking into account the kinematics

and this was the opposite for Sathasivam et al. [131] study, whereby the kinematics were predicted but not the contact stresses.

All the studies mentioned above concentrated on the fixed bearing knee prosthesis and only reported the resulting contact stresses. Otto JK and colleagues [112] modelled a three-dimensional Depuy LCS PS knee and the mechanics at the mobile and bearing interfaces were studied. The model was loaded with vertical axial load (uniaxial loading only) of either 1, 2, 3 or 4 BW (1 BW = 685.5 N) and also, while the model at full extension an equally distributed (50:50) or medially biased load (60:40) was also performed to investigate the contact stress area and the peak von Mises stress changes. From the study, as the vertical axial load increased, the peak von Mises stress in the polyethylene component also increased, but not proportionally to the load. The highest peak von Mises stress was 31.41 MPa when 4x BW of axial load was applied to the joint. By altering the loading position towards the medial condyle (60:40 load case), did not change the peak von Mises stresses as compare to the 50:50 loading case. The rotation between the femoral and polyethylene component (bearing interface) was also reported here. The bearing interface relative rotation reached a peak of 2.2° at 30° of flexion.

Most of the FE analyses contact routines were based on either penalty function approach, Lagrange multiplier methods or a combination of these two techniques [105,156]. The penalty function method is a general technique of constraint imposition where extra terms of stiffness matrix are added inside the original finite element stiffness matrix. These extra terms are described as the gap elements connected across the potential contact interface and the stiffness is derived from a specified penalty number. Mottershead et al. [105] studied the modelling of knee prosthesis (Bartel knee [11,12,131]) by using Gauss point contact constraint. The principal feature of the contact algorithm is the use of Lagrange multiplier methods for the application of displacement constraints to surface Gauss points of a contacting body to prevent mesh overlap. This method proved to be very effective in modelling non-linear frictionless static contact between two elastic bodies and particularly pleasing contact stresses results were obtained as compared to the Bartel knee [11,12,131].

The static FE studies discussed here are only able to predict the stresses within the knee model, without considering the kinematics of the replaced joint, i.e. the static FE analyses only predicted stress value at a certain period of gait cycle, depending on the input parameter(s). For example, if force value at 35% of the gait cycle is used, then the predicted stress value is that at 35% of the gait cycle. The kinematics of the knee joint has large effect on the long-term durability. Hence, it is important to include the kinematics of the joint when trying to assess the performance of TKR.

3.5.3.2 Explicit FE Analyses of TKR

The advantage of explicit FE approach is that it is able to predict the stresses in the knee model by taking into account of both the loads applied and kinematics generated within the model. Unlike static FE analyses whereby the stresses generated were only linked to the load applied without considering the kinematics part. The stress distribution generated within the polyethylene component in a TKR is interrelated with the load applied and also the design of the articulating surface of the knee prosthesis. Different design of knee prostheses will influence the kinematics of the knee replaced. The performance of a TKR is also dependent on several other factors as discussed in previous section of this report, such as the surgical alignment and soft tissues balancing.

Using two-dimensional FE knee model, Reeves et al. [124] applied axial force and A-P motion of a cycle walking gait and found that the non-conforming knee prosthesis produced higher stresses than the conforming prosthesis. The non-conforming prosthesis also exhibited higher rates of plastic strain accumulation than conforming prosthesis, if both had similar kinematics. This paper also tried to model the strain accumulation in the polyethylene component over repeated gait cycles, i.e. dynamic cyclic loading tests. A total of 7200 walking gait cycles were performed. This was equivalent to about 3 days of normal gait. Reeves et al. [124] confirmed from their study that the anatomical rollback motion initially produced lower strain rates, but as simulations were carried on for longer repeated cycles, it was found that designs, which allow rollback might produce higher strains. The results suggested that the non-conforming model with rollback was the most damaging and the conforming model without rollback was the least damaging. In other words, the conforming model that without the anterior-posterior motion of the femoral component over the tibial component produced the lowest long-term rate of plastic strain accumulation and hence, have longer lifetime. Without the rollback, the motion of the knee allows the polyethylene component to deform with time, increasing the contact surface area (the geometry becomes more conforming) and eventually reduces the contact stresses. From this study, Reeves and colleagues indicated that mobile bearing knee type is the best performance prosthesis because the femoral component conformity is maximized with minimal constraint at the tibial interface. Reeves et al. model has many limitations. Only one directional force was applied to the 2-D knee model. There is a need to improve this model, such as using 3-D knee model and applying A-P force, axial force and torque to the model, which are encountered by the *in vivo* knee joint.

Giddings et al. [51] is the first paper to develop a force driven FE knee model, which predicts the kinematics and stresses of TKR simultaneously. Then using this model they predicted the polyethylene stresses and the A-P translations for a commercially available cruciate retaining TKR (Scorpio, Stryker Howmedica Osteonic) by varied the stiffness of the

soft tissue, which was represented by a pair of linear springs. In the analysis run by Giddings et al. [51], four various spring stiffness (1, 7.3, 100 and 200 N/mm) were used to simulate the spring-loaded bumper system in the Stanmore Knee Simulator. A three dimensional finite element knee model was constructed. The femoral and tibial components were modelled as rigid bodies. The polyethylene was modelled as an elastic-plastic material. The boundary and loading conditions for the knee system were based on the mechanical environment of the Stanmore Knee. Axial force, anterior-posterior load and flexion-extension motion were simulated. Contact between the femoral component and the tibial insert was assigned a coefficient of friction of 0.085.

Overall, Giddings et al. [51] found that the stresses within the polyethylene insert, were comparatively insensitive to the stiffness of the spring. When the stiffness of the spring was increased by two orders of magnitude, i.e. from 1 N/mm to 200 N/mm, the maximum contact stresses, von Mises stresses and the von Mises strains in the polyethylene insert varied by only 15 to 59 percent. For the A-P displacement of the prosthesis, in general, increasing the stiffness of the bumper system decreased the displacements of the tibial tray. The maximum posterior displacement recorded was 3.4 mm, for the lowest spring stiffness 1 N/mm and as the spring stiffness increased up to 200 N/mm, the posterior displacement decreased and the maximum value was 1 mm. This value was 2.4 mm less than the model with 1 N/mm spring stiffness. The authors concluded that by increasing the stiffness of the spring decreased the displacements (anterior-posterior displacements) of the tibial component. Giddings et al. ignored the I-E torque in their study. It is essential to include the I-E torque in the FE model as in *in vivo*, shear forces (torque) have a large influence on the kinematics in the joint.

Godest et al. [52] developed an improved TKR model as compare to Giddings et al. [51]. This model has three-dimensional kinematics motion (six degrees of freedom). This study was to simulate a knee joint replacement during a gait cycle using explicit finite element analysis and the outputs were the kinematics and the internal stresses within the prosthesis in a single analysis. Explicit FE codes are used because of the inherent advantage of avoiding matrix inversions and also generally are superior for problems where non-linear material properties and contact forces must be modelled. Besides that, explicit finite element codes are also computationally advantageous for large and complex simulations like the knee prosthesis as the codes help to save the solution time. Godest et al. [52] modelled the PFC Sigma knee (DePuy International, Leeds UK). The femoral component was modelled as rigid body and the polyethylene insert was modelled using hexahedral solid elements with an elastic-plastic material. This finite element model was developed to have boundary conditions as close as the mechanical environment existing in the Stanmore knee simulator [150].

Additionally, two planar joints were defined at the model to simulate the action of soft tissues. The two planar joints were assigned to have linear fuction, $F = Kx$ (K, stiffness of planar joint; x, displacement occurred) and a linear stiffness of 10.4 N/mm. This paper did not simulate the effect of different spring stiffnesses and was different from Giddings et al. [51]. This model was force-driven and the loading parameters (compression/axial force, anterior-posterior force and internal-external torque) were those defined from the Stanmore knee simulator. The simulation also included the friction force. When comparing Godest knee to Giddings knee, Godest et al. [52] included the torque function into the simulation, whereas Giddings' model did not. One similar thing of both studies was that both groups modelled their knee model as according to the Stanmore knee model.

Two types of output were obtained from this study, the kinematics and the stress distribution. The anterior-posterior displacement of the femoral component and the internal-external rotation of the tibial component were compared to experimental data obtained from the Stanmore knee simulator. The contact stresses within the prosthesis were also reported in Godest et al. [52] study. All the kinematics results showed good correlation with the experimental data, in terms of values and patterns.

In a report by Otto and his group [113], several improvements were carried out to the model used in their static analysis [112]. Axial force, A-P force and torque were used to drive their model. In addition, linear soft tissue constraints of 30 N/mm AP displacement and 0.6 N-m/deg axial rotation were modelled with linear springs. The friction coefficient was also taken into account between contact interfaces. The authors studied the effect of varying the AP constraint, axial rotational constraint and the friction coefficient, while keeping all other variables (all the applied forces) constant. Among all simulations, they found that the friction coefficient had the most significant influence on articulation mechanics when compared to reference model. The mobile interface rotation was the highest, at 7.91° and the peak contact stress dropped from 17.21 MPa to 14.57 MPa, when the friction coefficient was reduced from 0.085 to 0.0425.

3.5.4 Current Evaluations of TKR Using FE

Finite element analysis has great potential in analysing and predicting the performance of total knee replacement. Although there have been many FE studies, to date, there are a numerous limitations with the current methods.

Knee motion is dynamic but most of the FE analyses were static analyses [12,53,85,112,130,131]. This means that load was applied to the stationary prosthesis and the corresponding contact stress was recorded for that period at a particular flexion angle. Bartel et al. [11] proposed that surface damage in tibial component was associated with the stresses in the polyethylene generated at and below the articulating surfaces. *In vitro* experiment by Blunn et al. [21], however showed that stresses alone were insufficient to generate contact fatigue observed *in vivo*. Blunn et al. cyclically loaded a cylindrical indenter on a flat slab of polyethylene. When the indenter was cyclically loaded and translated across the polyethylene surface, subsurface cracks were observed. They were unable to generate subsurface cracking when the indenter was stationary. Hence, this study proved that relative sliding, as well as stress, played an important role in the surface damage modes relevant to total knee replacements.

The studies by Liau et al. [85], Otto et al. [112], Reeves et al. [124] and Bartel et al. [12] have one common limitation in their FE knee models, i.e. the models were loaded only in one direction. An axial force was applied to the tibiofemoral joint of knee prostheses. Their study did not simulate the *in vivo* condition of the knee joint and need improvements. In *in vivo*, the knee joint is not only subjected to the axial force, but is also subjected to the anterior-posterior shear force and torque. These forces are important and need to be included in the FE study as these actually influence the motions of the knee prosthesis *in vivo*. Researchers such as Godest et al. [52] and Otto et al. [113] included these forces in their simulations. These studies predicted the A-P displacements and rotational angle of the prosthesis as a resultant of these forces. Until now, only one gait has been simulated, based on idealized force data from Morrison [102,103] prediction. The knee is subjected to other activities during a normal daily life, such as stair descent, stair ascent, squatting and etc. Wear testing and FE simulation that only concentrate on a single idealized load case do not reflect loads applied during other types of activities, which are thought to apply higher loads at the knee joint as compared to level gait. In addition to this, as previously discussed in section 2.6, the knee joint forces during level gait very between subjects. Subject related factors such as the gait pattern and body mass contribute to the differences observed in the force data. The variations in the predicted forces for an activity suggest that a TKR experiences a range of kinematics and stresses, and testing the TKR using a single idealized load case is too conservative. Therefore, there are needs to

simulate the performance of the TKR using variable patient-to-patient joint forces and as well as other activities, in order to comprehensively assess the performance of the TKR.

Most of the studies assumed that the TKR was perfectly positioned. However, perfect alignment of the knee prosthesis in the joint is difficult to achieve clinically. Errors in surgery occurred [122] while trying to install the implant into the joint. The malalignment study by Liau et al. [85] needs more improvements. The improvements that should be made including using dynamic forces, soft tissue constraints and friction into the FE model. Soft tissue constraints are particularly important because in *in vivo*, soft tissues such as the collateral ligaments provide more constraints in the knee joint. Current experimental wear studies have yet to simulate the effect of misalignment on the wear performance of the TKR. The experimental set-up to simulate the malorientation of the components is complicated [59] and also perhaps some experimental machines do not have freedom of movement for misalignment testing. Using FE analysis, it allows the freedom of changing load profile, boundary condition and TKR orientation easily and repetition of simulations at anytime.

The aim of the project is to further develop and improve FE models of the knee to better account for variations in patient specific loading, different activities loading as well as misalignment of the TKR. Besides level gait, stair descent, stair ascent and squatting activities are simulated. Then, improvements are made to the existing FE model by modelling ligaments to the TKR and their effect on the performance of the TKR is examined. Patient specific loadings during level gait and stair ascent are also simulated. Malorientation of the TKR relative to the ligaments are also being assessed under two different activities: level gait and stair ascent. For all the studies, the performances of the TKR are reported in terms of kinematics and contact pressures.

Chapter 4

FINITE ELEMENT ANALYSIS OF TKR: ASSESSMENT OF MODELLING PARAMETERS

Two different designs of total knee implants have been assessed in this study. Prior to any simulations, mesh refinement tests and sensitivity analyses were carried out for the knee implants for different modelling parameters. The two designs - PFC Sigma Fixed Bearing and PFC PLI are from same manufacturer, DePuy International (UK). Geometry of the implants, pre-processing procedures such as meshing, defining of material properties and setting of boundary conditions are discussed in this chapter.

4.1 TOTAL KNEE DESIGNS AND GEOMETRY

For this study, two different designs of knee implants were developed, namely PFC Σ fixed bearing and PFC PLI knee systems. These models are posterior cruciate retaining type. The same femoral component was used for the two designs (Figure 4-1), but the geometry of the polyethylene inserts used (Figure 4-2 and Figure 4-3) was different. The model of the femoral component was generated from geometry of a size-3 component.

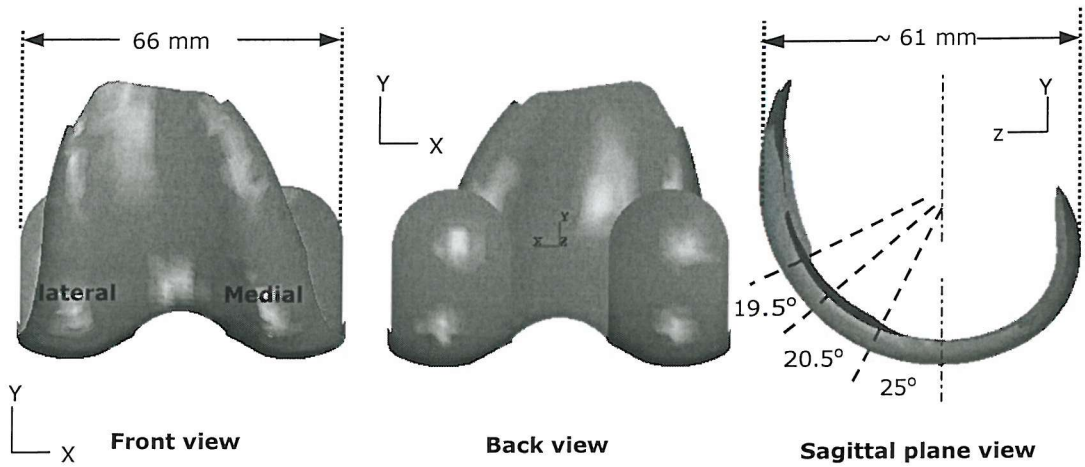

Figure 4-1: Femoral component used in the PFC Σ fixed bearing and PFC PLI designs.

The PFC Sigma model was previously developed by Godest et al. [52]. From the frontal view (Figure 4-1), lateral side of the femoral component front plate is slightly bigger than the

medial part. The femoral condyles, viewed from the back, are symmetrical. The contact surface of the femoral component comprises three circular arcs in the sagittal plane and the biggest radius is the arc that will be at the lowest contact point with the polyethylene insert. To simplify the analysis, only surface that is contact with polyethylene component is constructed. The difference between the PFC Sigma and PLI is in the geometry of the respective polyethylene components.

The geometrical model of the polyethylene insert for the PFC PLI knee was obtained in IGES format. Subsequent geometry manipulations were carried out within I-DEAS (I-deas Master Series 7.0 – SDRC, Hitchin, UK). Complex geometry of the polyethylene insert that was not in the contact simulation was simplified in order to make meshing process easier. The geometry of the articular surface was kept unchanged. The mesh for the PFC Σ polyethylene insert had already been generated by Godest et al. [52]. The geometry of the PFC Σ fixed bearing and PFC PLI polyethylene inserts are shown in Figure 4-2 and Figure 4-3, respectively.

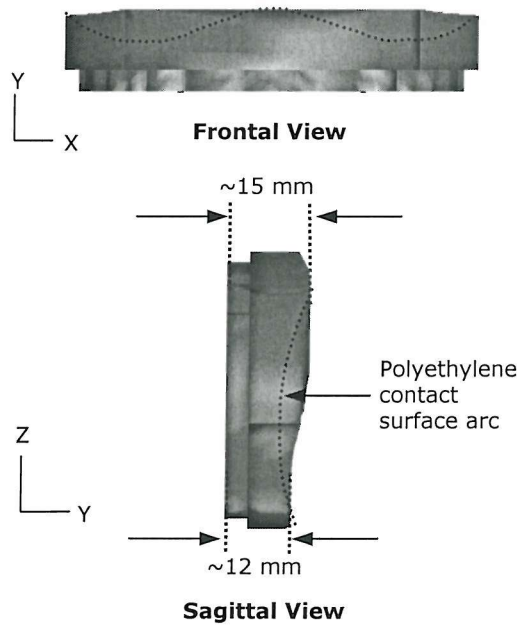

Figure 4-2 shows the polyethylene insert for the PFC Σ fixed bearing knee. The anterior lip of the polyethylene is thicker than the posterior lip, i.e. approximately 15 mm and 12 mm, respectively. The radius of curvature of the polyethylene contact surface is slightly bigger than the femoral condylar curvature radius. The tibial tray is not modelled because in this fixed bearing design, the polyethylene is fixed inside the tray and no movement is allowed between them.

Figure 4-2: PFC Σ fixed bearing polyethylene insert.

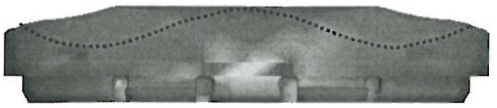

Frontal View

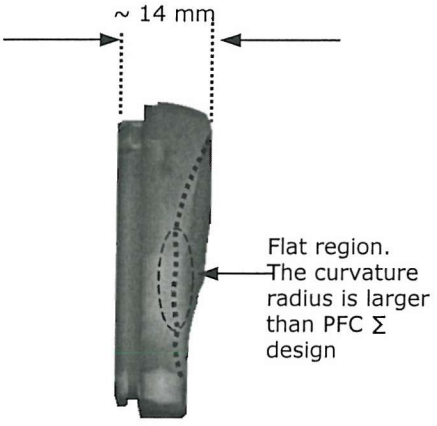

Sagittal View

The PFC PLI polyethylene insert looked similar to the PFC Σ fixed bearing polyethylene. However, the PLI insert has a larger radius of curvature of contact surface compares to PFC Σ fixed bearing, particularly in the sagittal plane. The contact surface of the PLI design is slightly flat in the middle of the insert. Since no desirable movement is allow between the tibial tray and the polyethylene insert, the tibial tray is excluded in the simulation.

Figure 4-3: PFC PLI polyethylene insert.

4.2 MESHING

The mesh for the PFC Σ design already existed [52]. The polyethylene insert used was mapped mashed using hexahedral elements. The polyethylene insert of the PFC PLI was meshed in I-DEAS. Initially, a surface mesh was defined using linear triangular elements. This was done to constrain mesh on the articular surface to the required density. Solid meshes of linear tetrahedral elements were generated from the surface mesh for all the enclosed volume (Figure 4-4).

The resulting tetrahedral elements on the model's surfaces shared the same nodes with the surface elements, which were later deleted. For the PFC PLI insert, an element edge length of 1 mm was fixed for all the contact interfaces and 3 mm for the rest of the surfaces. These values were chosen after a mesh refinement study was performed to assess the mesh (section 4.6 MESH DENSITY).

The femoral component was developed in the previous study [52] and was modelled as a rigid surface and meshed using four noded shell elements with an average edge length of 1.7 mm. The reason linear tetrahedral element mesh was chosen for the PFC PLI polyethylene insert was due to complex curvature geometry of the component.

The final construct meshes of polyethylene were then exported to Pam-Generis (ESI Group, France), the pre-processor of the FE software, Pam-Crash-Safe. The rest of the pre-processing was performed here.

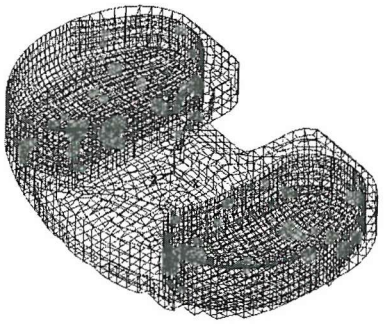

PFC Σ fixed bearing polyethylene mesh
(Developed by Godest et al. [52])

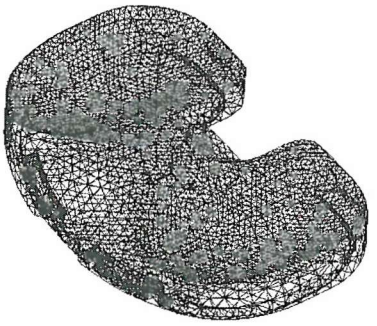

PFC PLI polyethylene mesh

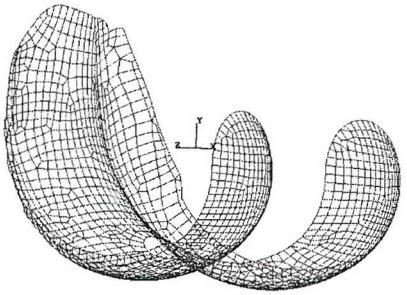

Mesh of femoral component

Figure 4-4: Polyethylene inserts and femoral component meshes for the PFC Σ and PFC PLI designs.

4.3 MATERIAL PROPERTIES

The femoral component was made of cobalt chromium and in this study, it was assigned with an elastic property of 211 GPa and Poisson ratio of 0.3. This is 200 times stiffer than the polyethylene component. The polyethylene was assigned as an elastic-plastic material and its elastic modulus was 580 MPa. The yield stress of the polyethylene is 14.5 MPa. The material property data was supplied by DePuy International Ltd (UK). A plot of plastic stress-strain curve for the polyethylene insert is shown in Figure 4-5. The insert was modelled as a deformable body.

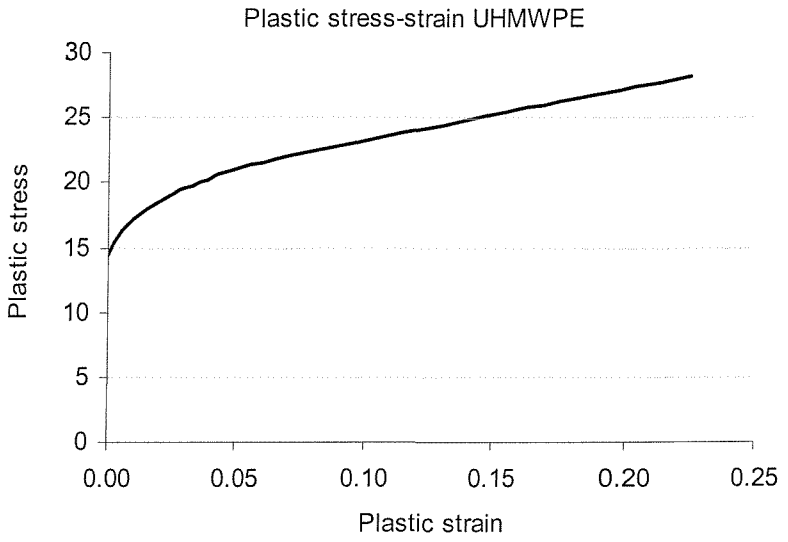

Figure 4-5: Plastic stress-strain curve for the polyethylene insert [52].

4.4 BOUNDARY CONDITIONS

Appropriate boundary conditions were applied to the FE total knee model to replicate the mechanical environment of the Stanmore Knee simulator [150]. A diagram of one of the knee implants is shown to give an idea the boundary conditions applied to the implant (Figure 4-6).

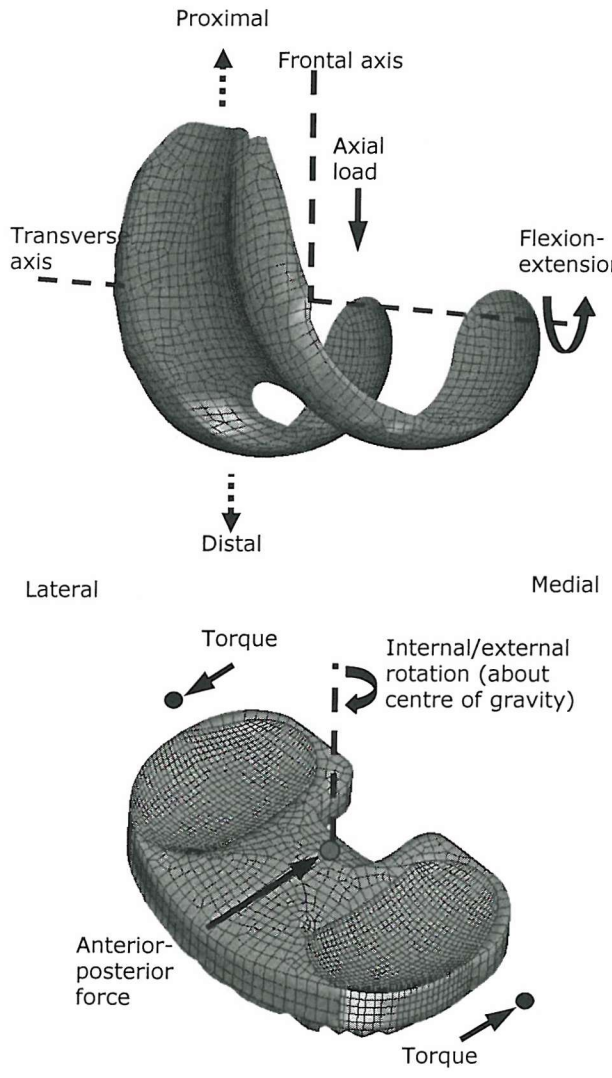

The femoral component was allowed to translate in the proximal-distal direction, to rotate about its transverse axis to simulate flexion-extension and about a frontal axis to simulate varus-valgus rotation. The femur was also centrally located at the flexion-extension axis. The tibial component was allowed to translate in the anterior-posterior and in the medial-lateral directions and to rotate about its longitudinal axis located in the middle of the tibial condyles to simulate internal-external rotation. At equilibrium position, the femoral component and the tibial polyethylene insert were in contact at the deepest point on the tibial polyethylene surface. The bony structures such as the femur, tibia and patella were not included in the study.

Figure 4-6: Meshes of the femoral and polyethylene component. Each shows the respective applied forces and flexion-extension motion.

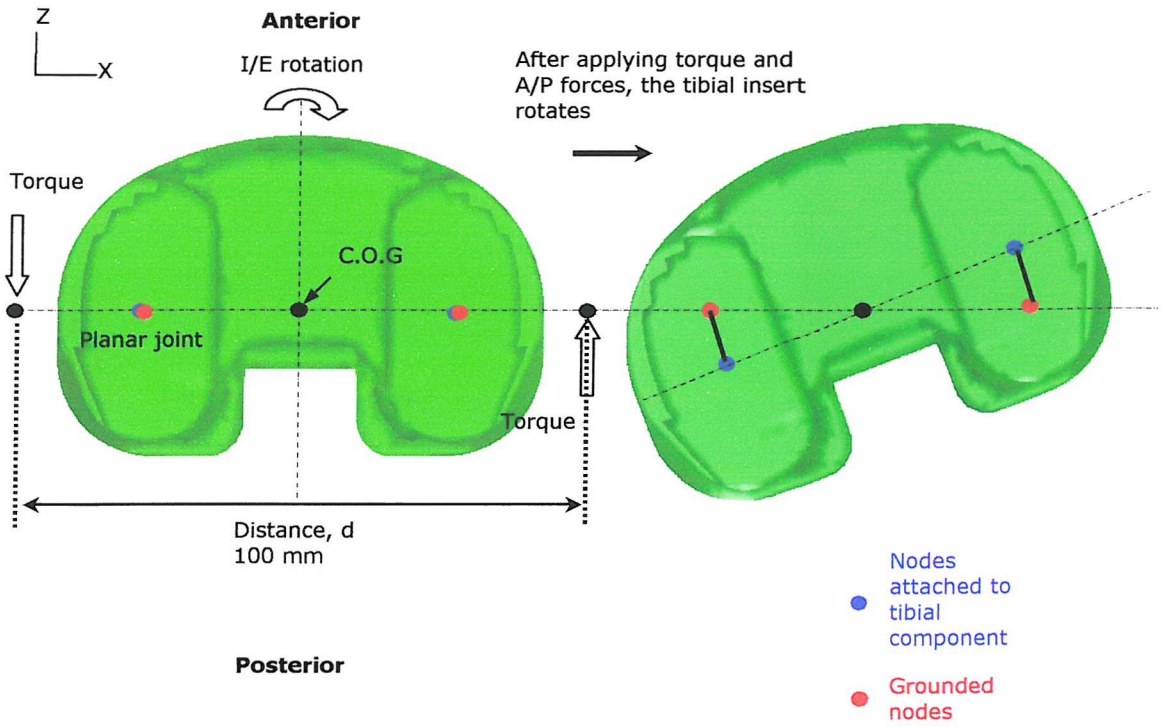

Figure 4-7: View from the back of the tibial component. Medial and lateral planar joints were constructed to represent the soft tissues actions. Each planar joint was constructed from 2 nodes, one was grounded (red) and one was attached to the tibial tray (blue). Internal-external torque was applied to two nodes as shown above. Torque = F x d (unit: N m).

Two planar joints were defined to simulate soft tissues actions. These replicated the spring/bumper configuration present in the Stanmore knee simulator. Each of the planar joint was constructed using two nodes: one grounded and another rigidly attached to the tibial component (Figure 4-7). At the neutral position, the two nodes (the grounded and attachment nodes) were at the same point. After applying torque and A/P forces, the attachment node would displace (Figure 4-7, polyethylene insert on the right).

The planar joints were placed at the medial and lateral sides of the tibial component, to constrain the anterior-posterior translation and internal-external rotation of the TKR (Figure 4-7). Both the planar joints were assigned a linear stiffness function. A stiffness of 10.4 N/mm was used for each planar joint. The corresponding rotational restraint was approximately 0.30 Nm/deg. These values were the same as those in the Stanmore knee simulator.

This was a force-driven model and the boundary condition time histories for the axial force, internal-external torque, anterior-posterior force and flexion-extension angle were defined according to the experimental protocol used in the Stanmore knee simulator. These were the standard walking cycles. Axial force and flexion-extension angle were

applied about the centre of rotation of the femoral condyles. Anterior-posterior (A-P) loads were applied about the centre of gravity of the tibial tray and internal-external (I-E) torque about two nodes tied at medial and lateral sides of tibial component. The distance of medial node or lateral node from the centre of gravity of the tibial component was 50 mm.

ISO standard load case was used. This was the level gait load data used in the Stanmore knee simulator. The axial load, A-P force, I-E torque and flexion-extension angle for the ISO standard load are shown in Figure 4-8.

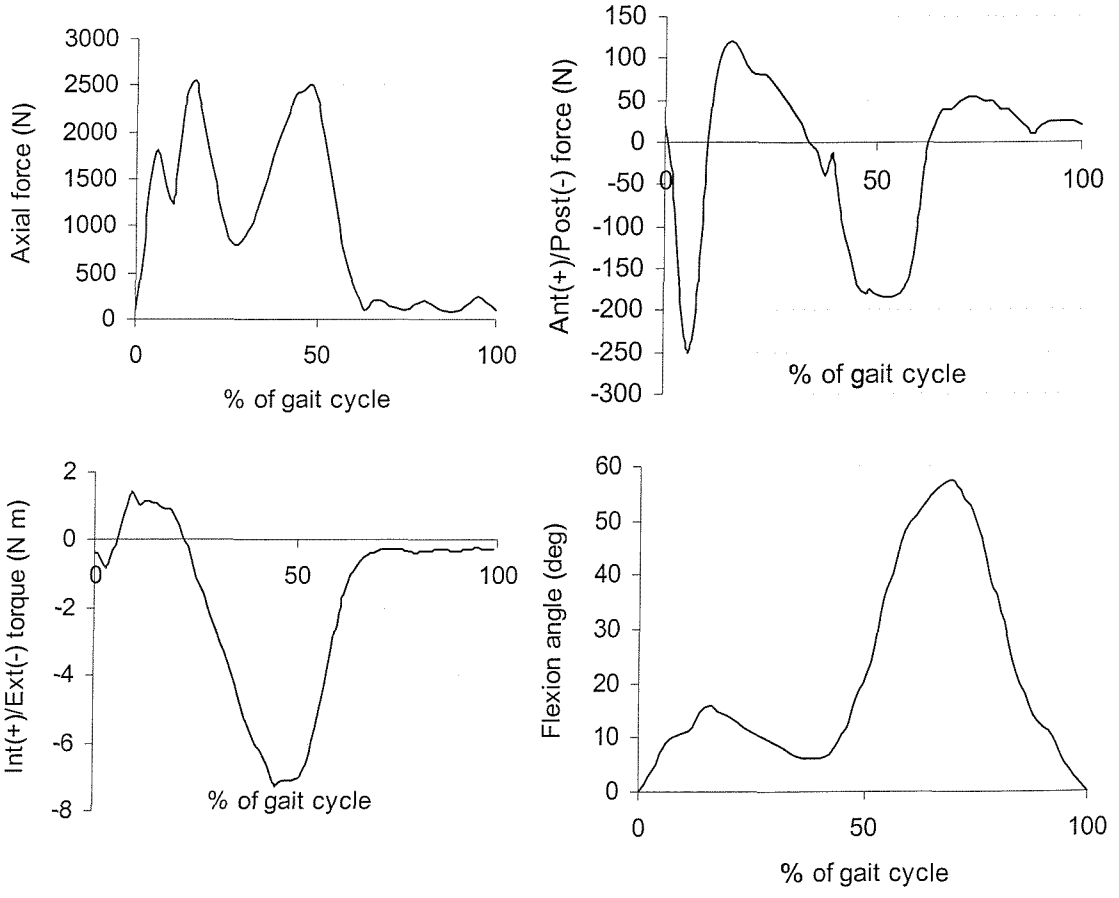

Figure 4-8: ISO standard load case.

4.5 SOLUTIONS

Pam-Crash-Safe (ESI Group, France) was used to solve the non-linear FE problem in this study. For the PFC Sigma fixed bearing knee and PLI knee system, contact between the femoral component (modelled as a rigid body) and the polyethylene insert were of interest. The applied forces were functions of time and the parameters that were examined include the kinematic performances of the total knee and contact stresses between the contact bodies. The solutions obtained were dependent on the way the FE model was constrained and the contact type used in the software.

4.5.1 Contact Analysis in Pam-Crash-Safe

The range of finite element techniques for the treatment of problems in contact mechanics is extensive and varied. A brief description of the way contact is simulated in Pam-Crash is given below. Pam-Crash adopts the 'penalty' contact theory and allows the contact to perform automatically throughout the simulation.

In Pam-Crash, contact bodies are defined in 'sliding interface definition card'. The polyethylene insert was defined as 'slave' (finite nodes) and the femoral component as 'master' (finite segments). The nodes on the outer potential contacting surface of the polyethylene are selected as slave and treated as potential contacting nodes; meanwhile the elements on the potential contacting surface of the femoral component are selected as master and treated as potential contacting surfaces. After this is done, contact events are modelled by first performing contact search operations, to detect possible contact events. If physical contacts are detected, then calculation of contact normal and tangent forces will take place. In order to ensure a successful contact events search, it is suggested that a coarser mesh for the 'master' segments (in this case, the femoral component) and a finer mesh for the 'slave' segments (in this case, the polyethylene insert).

An advanced 'penalty' method based contact algorithm (contact element type 44 in Pam-Crash) is used to model the contact between the two components. For this algorithm, the geometric penetration of the slave nodes is penalised by counteracting forces proportional to the penetration depth and a penalty factor chosen by the user. A second order polynomial approximation of the master surface is used. This approach has been specifically developed to model contact between spherical surfaces and to avoid point contact in the contact surface due to facet effects at the element boundaries.

In this formulation, a contact thickness, h_{cont} is defined. This indicates the distance away from a contact face where physical contact is established. In Pam-Crash, the contact thickness is on both sides of the contact body (Figure 4-9).

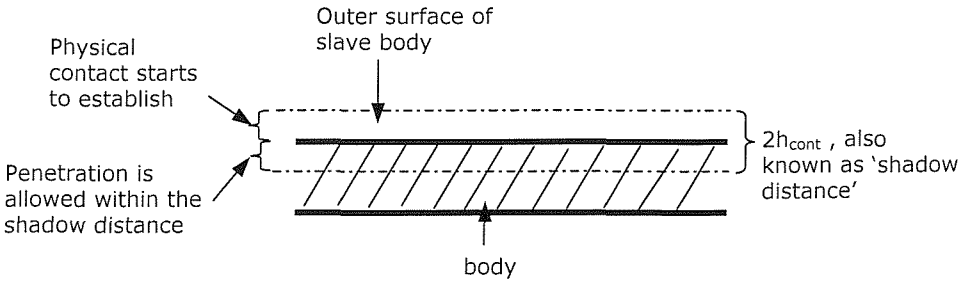

Figure 4-9: Illustration of the contact establishment in Pam-Crash.

The value of contact thickness has a significant impact on the accuracy of the solution and the computational cost. If too small value of h_{cont} is choosen, then this may cause the 'master' surface to bounce back up the 'slave' body. When physical contact is established within the too small h_{cont} thickness, the normal restoring force generated will be large enough to push the 'master' surface off and hence, bounce off the 'slave' body. If the h_{cont} value is too large, the normal restoring will not be large enough to push the 'master' surface back up the 'slave' surface and hence, this may cause penetration. According to Pam-Crash, perforations are penetrations of slave nodes beyond the 'shadow' distance (Figure 4-9). Once beyond this distance, the simulation will be considered to have failed. In this study, contact thickness values of 0.1 and 0.15 are considered.

If a node from the master surface penetrates through the slave body but within the h_{cont} thickness, a restoring or counter-acting force will be generated. This restoring force is proportional to the penetration distance of the node into the solid and acts in the direction normal from the node to the surface of the solid. This process allows contact to be simulated.

4.5.2 Post-processing

4.5.2.1 Kinematic Performance of Knee Implant

The post-processing part of this study was carried out in Pam-View. The animation of dynamic movement of the knee implant is possible in this software. The kinematics performances of the knee implants at the contact interface were calculated. The anterior-

posterior displacement and internal-external rotation are the resultant movement after sets of load being applied to the FE knee model. Two nodes are defined: one as the centre of body of the femoral component and another as the centre of body of the tibial tray or polyethylene insert. These nodes are fixed in their position and are the reference points for the components motions. The anterior-posterior (A-P) displacements and the internal-external (I-E) rotations recorded is the movement of the tibial insert relative to the femoral component. All of these motions use the global coordinate system.

4.5.2.2 Contact Pressures and von Mises Stress

Maximum contact pressures, as a resultant of the forces applied to the contact surfaces were examined. In Pam-View, it is possible to display graphic contour plots on pressures and stresses, as well as area of the contact pressures (size of contact patches) generated by the polyethylene insert. As well as predicting the pressure distribution, the peak contact pressures were also recorded throughout an activity. The contact pressures generated are independent of post yield behaviour and are dependent on the applied load and kinematics generated.

Von Mises stresses in the polyethylene as a result of loading were also examined. In general, von Mises stress is a better indicator for failure criteria. This is because von Mises stress takes into account stresses present in three main directions: X, Y and Z in the global coordinate system and are dependent of material property.
The von Mises stress is defined as the formula below:

Von Mises stress = sqrt {3. *[sqr (Stress_XY) + (Stress_YZ) + sqr (Stress_ZX)] + sqr (Stress_XX) + sqr (Stress_YY) + sqr (Stress_ZZ) – (Stress_XX * Stress_YY) – (Stress_YY * Stress_ZZ) – (Stress_ZZ * Stress_XX)}

A series of finite element simulations were performed to assess the influence of modelling-based parameters on the predicted kinematics and stresses.

4.6 MESH DENSITY

Several mesh refinements were performed to test the convergence of parameters of interest, i.e. the kinematics and the contact pressures. The same femoral component was used in all the simulations. It was modelled as four-noded shell element, with a total 1911 element and 2015 nodes. The polyethylene insert of both designs was meshed with different element sizes and was summarized below.

PFC Σ Fixed Bearing Knee

The mesh density study of this model was previously carried out by Godest et al. [52], a former PhD student working with the group. In brief, two mesh densities of the polyethylene components were considered. The first model had an average element edge length of 2 mm in the contact area and the second model had an average element edge length of 1.2 mm. These models were modelled as hexahedral elements. The mesh density study was compared with the experimental data obtained from the Stanmore knee simulator.

PFC PLI Knee

Four PFC PLI FE models (polyethylene insert) were generated, starting with an initial element edge length of 2.0 mm at the contact surfaces of the polyethylene insert, and decreasing the element size down to 1.0 mm. The rest of the volume of these four models was meshed with 3.0 mm element edge length tetrahedral elements. Table 4-1 shows the four models generated by varying the element edge length at the contact surfaces, and the total number of elements and nodes in the polyethylene insert.

Model	Element size (mm)	Number of elements	Number of nodes
1	2.0	19415	4662
2	1.5	22559	5328
3	1.2	30193	6998
4	1.0	38983	8864

Table 4-1: Element edge length at the contact surfaces and total number of elements and nodes generated in the PFC PLI polyethylene insert.

Material properties and boundary conditions were assigned to the models, as reported in the previous sections. The parameters of interest were the A-P displacements, I-E rotations and the contact stresses. These parameters were plotted as a function of a percentage of one full activity cycle. Convergence of these parameters was examined as a result of the different degrees of mesh refinement. All of the simulations were performed with a time step of 0.005 ms (or 0.5 μs).

The plots of convergence study for the PFC Σ fixed bearing knee are not shown, as the results have been previously published [52]. Summary of the results will be discussed. The predicted A-P translations, I-E rotations and the peak contact pressures for PFC PLI design are shown in Figure 4-10.

4.6.1 PFC Σ Fixed Bearing Knee

In general, the predicted kinematics for the coarse mesh and the fine mesh were similar in general trends and the absolute magnitudes [52]. The mesh density appeared to have little effect on the predicted motions of the TKR. Differences were seen in the maximum contact stresses. In general, Godest et al. found that the predicted peak contact stress followed the same general trend. The coarse mesh predicted a peak contact stress of 22 MPa; while the fine mesh showed a value of 17 MPa. Godest et al. further studied mesh refinement for the PFC Σ fixed bearing knee and reported that there was no differences as compared to previous fine mesh. Therefore, the fine mesh with an element edge length of 1.2 mm at the contact surfaces was used in further analyses in this study.

4.6.2 PFC PLI Knee

In general, all meshes predicted similar trend of A-P displacements, I-E rotations, maximum contact pressures and maximum von Mises stresses (Figure 4-10). During the stance phase of gait, the peak posterior displacement of the tibial insert relative to the femoral component for all the meshes was approximately 7.7 mm (Figure 4-10 a). Between 12.5% and 25% of the gait cycle, the tibial insert of mesh 1 and mesh 2 returned to near neutral position. However, mesh 3 and mesh 4 predicted an average anterior translation of approximately 0.7 mm. No significant changes were observed during the swing phase, i.e. between 60% and 100% of the gait cycle, in the A-P displacements between the four meshes (Figure 4-10 a).

There were no significant differences in the I-E rotations throughout the gait cycle (Figure 4-10 b). Overall, the average peak external rotation of tibia relative to the femur of all the models was approximately 13.5°, at about 50% of the gait cycle. The tibia insert rotated externally during the swing phase. Mesh 1 predicted slightly less peak internal tibia rotation relative to the femur as compared to mesh 4, between 70% and 80% of the gait cycle. The peak internal tibia rotation for mesh 1 was 3.8° against 5.9° for mesh 4. The difference was 2.1°.

The predicted maximum contact pressures for mesh 1 exhibited the highest pressure compared to the other three meshes (Figure 4-10 c). Large transients were observed throughout the gait cycle. Similarly, mesh 2 and mesh 3 also showed large oscillations but slightly less than mesh 1. In mesh 4, the maximum contact pressures were more stable and large transients such as those seen in the previous three meshes were not observed in mesh 4. There were slight oscillations typically at the first 10% of the gait cycle and during the swing phase of the gait cycle.

Transients were observed in the maximum von Mises stress, especially mesh 1 and mesh 2 (Figure 4-10 d). Mesh 1 is the coarsest mesh and tended to exhibit big oscillations. The peak maximum von Mises stress was 25 MPa, predicted by all the meshes. From the contact area observation, edge contact occurred in all the models and hence, peak von Mises stress of 25 MPa was observed. Since the maximum von Mises stress was larger than the yield stress of the polyethylene (14.5 MPa), plastic deformation would occur in all the polyethylene inserts.

Further simulations on finer meshes (smaller than element edge length of 1 mm) did not show any significant differences in the kinematics and stresses. Hence, PFC PLI polyethylene insert mesh 4, which was meshed with element edge length of 1 mm, was selected as the final PLI FE model for further simulations.

Figure 4-10(a)

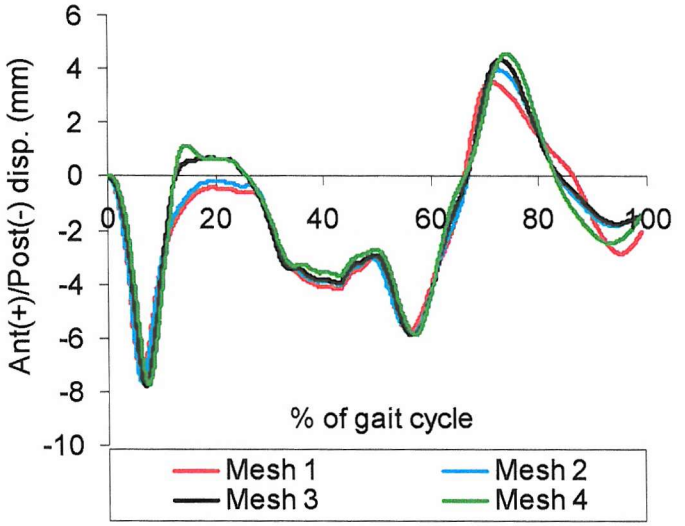

Figure 4-10(b)

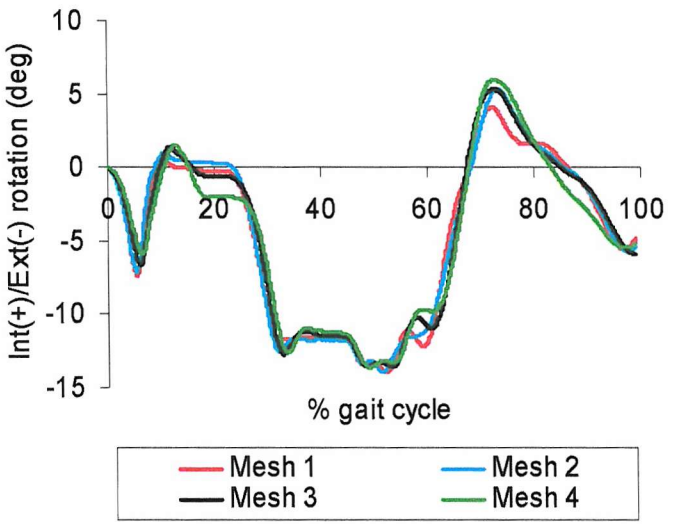

Figure 4-10(c)

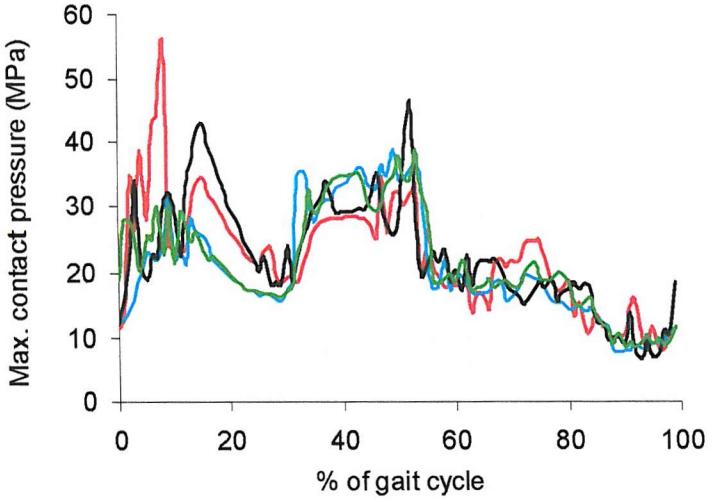

Figure 4-10(d)

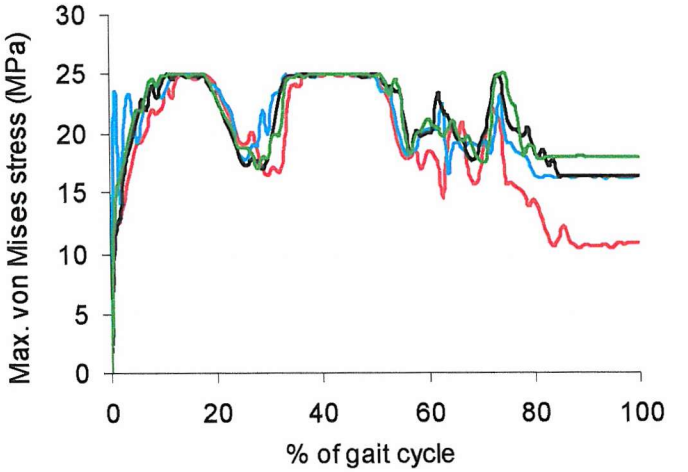

Figure 4-10: Predicted (a) A-P translations; (b) I-E rotations; (c) maximum contact pressures and (d) maximum von Mises stresses for the PLI knee convergence mesh refinement studies. Details of mesh 1 to mesh 4 could be obtained in Table 4-1.

4.7 TIME STEP

The FE analyses in this report were simulated over 1 s (1000 ms), representing one full cycle for an activity. In some analyses, extra few seconds were added at the beginning of an activity cycle in order to avoid sudden loading of the model. Loading the model too quickly at high value will cause penetration at the contact surface or the bounce back of the model as a result of impact. In Pam-Crash, the numerical calculations are done according to the time step defined over the one full activity cycle. For example, if 0.005 ms was chosen as the time step, then in every 0.005 ms of time interval, numerical calculations would be carried out. In Pam-Crash, at each increment of time step, the latest numerical calculations will base on the previous time step calculations. In general, the time step needs to be adjusted during the analysis. The CPU time required is dependent on the size of the time step. The smaller the time step, the more time is required to complete a simulation as the numerical calculations need to be updated more often. With the smaller time step, more CPU storing spaces are needed at the same time.

4.7.1 Influence of Time Step

Time step sensitivity was examined using the PLI designs. Time step study for the PFC Σ knee is not discussed here, as it had been previously published [52]. Four different time steps were chosen, starting with 0.007 ms, 0.005 ms, 0.003 ms and down to 0.001 ms. The predicted kinematics and the stresses using these four time steps were shown in Figure 4-11. The size of time step has big effect on the A-P displacements, as seen in Figure 4-11 a. Using the time step size of 0.007 ms and 0.005 ms showed completely different peak anterior displacement and peak posterior displacement of the tibia relative to the femur. A general trend of A-P displacement was observed in the four time steps. Simulations using time step size of 0.003 ms and 0.001 ms exhibited similar A-P displacements values. In terms of the predicted I-E rotations, the time steps size of 0.007 ms and 0.005 ms predicted significantly different value of peak internal-external rotations. However, in the smaller time steps of 0.003 ms and 0.001 ms, both predicted fairly similar I-E rotations. Using larger time step produced larger oscillations in the predicted maximum contact pressures (Figure 4-11 c). Fewer changes were observed in the maximum von Mises stress (Figure 4-11 d) as the polyethylene insert started to yield.
Since time steps of 0.003ms and 0.001 ms exhibited fairly similar results, the smallest time step, 0.001 ms was chosen and used in most of the simulations in further studies.

Figure 4-11(a)

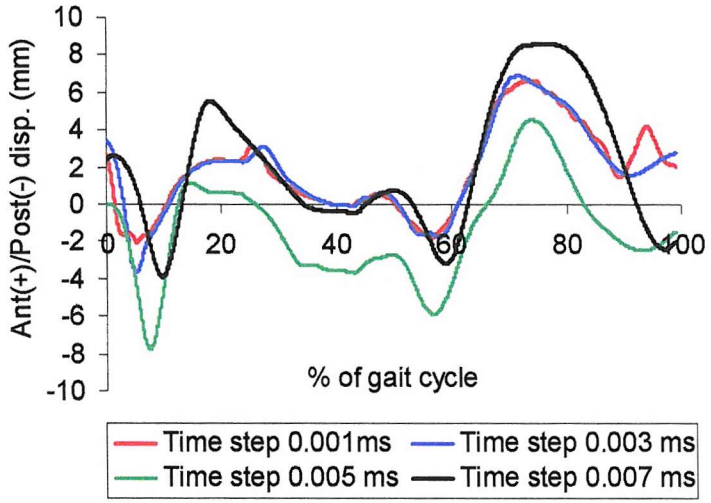

Figure 4-11(b)

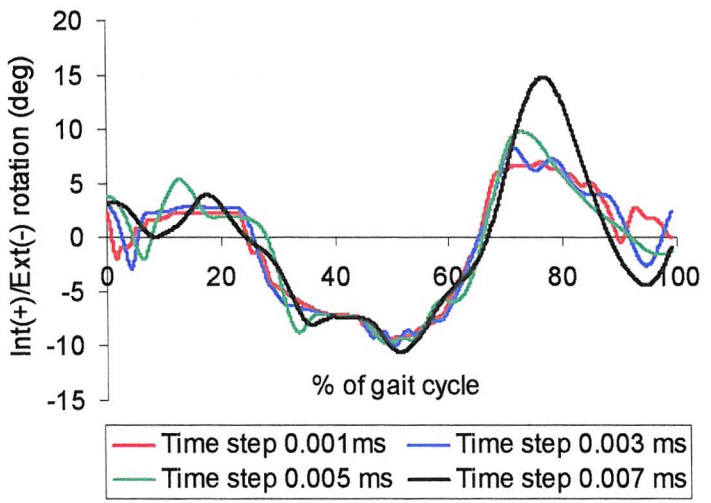

Figure 4-11(c)

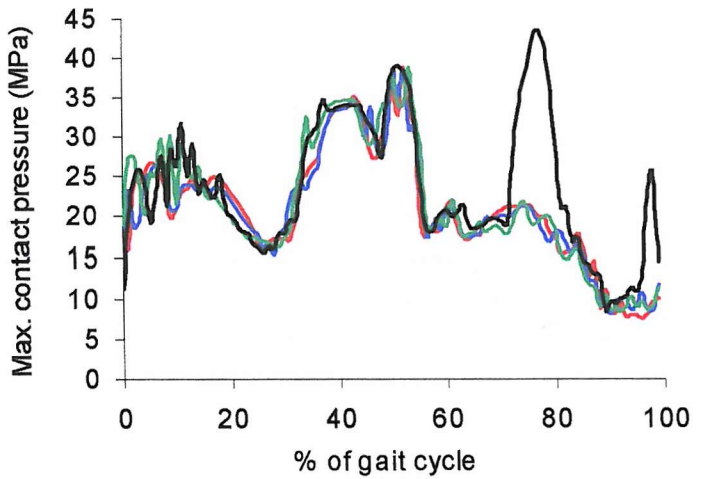

Figure 4-11(d)

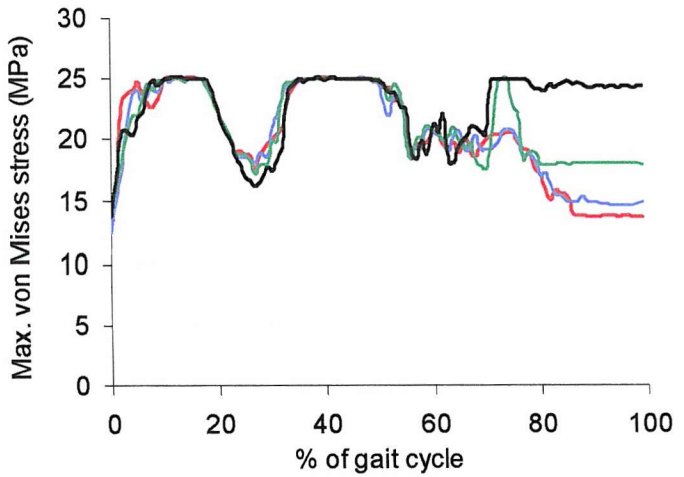

Figure 4-11: The influence of time step on the predicted: a) A-P displacements; b) I-E rotations; c) maximum contact pressures and d) maximum von Mises stresses.

4.8 FRICTION

The relative motion of the femoral component made of cobalt-chrome and the polyethylene insert made of polymer had shown to be affected by friction [42,52,130]. The influence of friction on the contact analysis had been published by Godest et al. [52]. In their report, a frictional value of 0.04 predicted the closest kinematics as compared with the experimental data. Hence, for all the simulations, friction coefficient of 0.04 was used.

4.9 SUMMARY

The influence of various solution-dependent parameters was examined to observe their effect on the predicted kinematics and internal stresses of TKR. Firstly, the mesh density appeared to have little influence on the kinematics of the TKR. The internal stresses of the polyethylene insert were found to be largely affected by the mesh density (Figure 4-10 c). The maximum contact pressure values fluctuated from one mesh to another and were difficult to analyse. The maximum von Mises stresses plot showed less oscillations when compared to the maximum contact stresses plot. Examining the von Mises stresses (Figure 4-10 d), the polyethylene insert started to yield, hence; the stresses value did not increase higher than 25 MPa. From both the maximum contact pressures and maximum von Mises stresses plots, the smallest mesh density exhibited the least transients and the most stable results. Linear tetrahedral element was used to model the PFC PLI polyethylene insert. In stress analysis, tetrahedral element shows a constant stress with an element, whereas hexahedral element (in PFC Σ fixed bearing polyethylene insert) shows stress gradients in each element. This is a disadvantage of using tetrahedral element as slightly high contact stresses are predicted. The reason PFC PLI polyethylene insert was meshed with tetrahedral elements was due to the lack of software efficiency to mesh the curvature surfaces with hexahedral elements. Attempts were made to mesh the inserts with hexahedral elements in I-DEAS but failed due to too many distorted elements. In general, it is easier to fit tetrahedral elements into complex geometry, for example the polyethylene component, than cube elements (hexahedral). As a result, the polyethylene insert for PFC PLI design was meshed with tetrahedral elements. There were less oscillations in the finest mesh and from further simulations on finer meshes (finer than mesh 4), showed no significant differences in kinematics and stresses. Hence, mesh 4 with element edge length of 1 mm was selected as the final PLI model for further simulations.

The predicted kinematics was significantly affected by the time step but the contact pressures and stresses were not being affected too much compared to the kinematics. The predicted trends were independent of this parameter. A large time step such as 0.007 ms and 0.005 ms tended to over and under estimate the kinematics, respectively.

Convergence in the kinematics was reached when smaller time step such as 0.003 ms and 0.001 ms was used. When large time step size was chosen, oscillations were observed especially at the swing phase of gait cycle, i.e. between 60% and 100% of the gait cycle (Figure 4-11 c). Some oscillations were also seen in the first 10% of the gait cycle. Although small time step requires high CPU times and memory requirements, it will still be used as solution time step due to smaller transients observed.

Summary

- PFC Σ fixed bearing and PFC PLI total knee designs were examined. These were posterior cruciate retaining type of TKR.
- Sensitivity analyses such as mesh densities, time steps and frictions, were carried out for both designs. Influence of these parameters on the kinematics and contact pressures for the PFC Σ fixed bearing knee was published in Godest et al. [52]. From the sensitivity tests, for PFC PLI knee, the polyethylene insert was meshed with tetrahedral element edge length of 1 mm. Time step of 0.001 ms and friction coefficient of 0.04 were selected to be used in further simulations.

Chapter 5

EXAMINATION OF TKR PERFORMANCE FOR A VARIETY OF ACTIVITIES

A total of four activities will be studied. These include level gait, stair descent, stair ascent and squatting. Details on the differences between these loadings and method of simulations will be discussed in this chapter.

5.1 INTRODUCTION

The stress distribution within the polyethylene insert of a total knee replacement is dependent on the kinematics of the joint. The kinematics is in turn relying on the load applied at the knee joint as well as the geometrical design of the contact surface. Knee kinematics have been studied in numerous activities such as level walking, walking up and down a ramp, climbing and descending stairs. Although many gait studies that have been performed, the force data at the knee joint is limited and not easily obtained. The first attempt to predict the kinematics and the stresses of the TKR was by applying the ISO standard load case. These forces were those applied to the Stanmore knee simulator [150]. The ISO standard loads were based on the gait measurements performed by Morrison J.B [102,104].

At present, TKR performance especially in terms of kinematics and wear of the polyethylene component are only evaluated under a limited range of kinematics conditions, such as a standard gait cycle [150,151]. This does not reflect loads applied during other types of activities performed during daily living. Morlock et al. [101] performed a study to measure the duration and frequency of daily activities in patients after total hip replacement (THR). It was found from 31 patients that the most frequent daily activity was sitting, whereby an average of 44.3% of the total 12 hours measurement time (day time only) was spent on this activity. The second most frequent activity was standing (24.5% of the time), followed by walking (10.2%), lying (5.8%) and stair climbing/descending (0.4%). The patient's average age in Morlock et al. study was 62.5 years. In younger patients, more demanding activities such as jogging and squatting are expected and these activities require bigger range of motions than those reported by Morlock et al.

Stairs ascent and descent, running and other activities, are thought to apply higher loads at the knee joint as compare to level walking [15,31]. For example, forces as high as 5.5 times of body weight (approximately 4000 N) [15,31] have been predicted at the knee while a subject performs stair descent or walking down a slope. This force value will either increase or decrease depending on several factors. If the subject had abnormal gait and/or over weight, then the forces within the joint were likely to increase. The polyethylene wear rate is directly dependent on the contact stress distribution over the articulating surfaces and the sliding distance (kinematics) [19,20,36,117,136,137]. In order to understand a TKR performance, a wider range of activities needs to be analyzed.

In this study, as well as considering level gait 3 alternative activities were also considered. For stair descent, the axial loads and flexion angles are reportedly higher compared to other activities [89,102,103]. Loading patterns that have been reported during stair descent were used to establish loading patterns for input into the FE simulation. As no single study in the literature reported all four loading input parameters, inputs were based on results from three separate studies as summarised by DesJardins et al. [33]. The four input loads were: flexion-extension angle [95], axial or compression force [115] anterior-posterior force [95] and internal-external torque [3].

Stair ascent activity was also examined. The loads during stair ascent were obtained from Patrick Costigan, Queens University, Canada (Personal Communication). A total of nine healthy elderly subjects were asked to perform a step-up task and the ground reaction force was recorded via force plate. Then, using the inverse dynamic method, the knee joint reaction force was calculated. For this study, the average of knee joint loadings from the nine subjects were calculated and applied to the simulation. Stair ascent involves a bigger range of flexion angle compared to the level gait. The highest flexion angle was 88° (from the averaged data).

During squatting, the knee flexes up to 135° [32]. Squatting or rising from a deep squat is important as this activity involves great flexion angle as compared to level gait, stair descent and ascent. The measurements of the kinematics and calculations of the knee joint forces during squatting was performed by Dahlkvist et al. [32] using an indirect approach – inverse dynamic method. The axial forces and the A-P forces calculated were the average of six subjects. Since this was a two-dimensional analysis, torque at the knee joint was not obtained.

The study of simulating various activities not only benefits in the area of the performance of the TKR, but also important in the design of prostheses. Different total knee replacements are catered for different patients' needs. The understanding of how different implants would perform under different activities would help in the selection of the most

suitable implants for patients with different demands. As a result, this could help in optimising the knee joint movement after surgery. The aim of this section was to examine the kinematics and contact stresses of the PFC Σ fixed bearing knee under four different loading conditions.

5.2 METHOD

The ISO standard 14243-1 walking cycle (level gait), stair descent and ascent, and squatting cycles loading patterns were applied to the force-controlled FE knee model as described in previous chapter. Comparisons of loading data for these activities are shown in Figure 5-1.

From Figure 5-1 (a), the stance phase or loading phase for level gait and stair descent activities were between 0% and 60% of the activity cycle. The swing phase or unloading phase was from 60% to 100% of the activity cycle. The peak axial force during stair descent was approximately 4100 N (approx. 6 times of bodyweight, BW). Level gait exhibited less axial force with the peak value of approximately 2550 N (3.6 times BW) when compared to the stair descent activity. The stance phase for stair ascent was from 40% to 100% of the activity cycle. This activity was observed to have the lowest axial force as compared to the other three activities. The peak axial force for stair ascent was approximately 1330 N (approx. 1.9 times BW). The large difference in the peak axial force between stair ascent and the other activities could be due to the way the forces being obtained. Stair ascent data were the averaged from nine subjects. Also, the 4 sets of force data came from 4 different sources using different methods to calculate the joint reaction force. During the swing phase of level gait, stair ascent and descent, only small forces were estimated at the knee joint. Squatting exhibited totally different loading pattern. The axial force during squatting increases continually throughout the activity cycle. The peak axial force was approximately 5250 N (approx. 7.5 times BW).

Figure 5-1 (b) shows the A-P forces for the four activities. The squatting activity exhibited the highest posterior force among the four activities. The peak posterior force was 2900 N (4.1 times BW). Figure 5-1 (c) is the plot without the A-P forces of squatting activity and using different force scale, the difference of A-P forces between level gait, stair descent and ascent can be shown clearly. In general, there was no consistent pattern of A-P force among the four activities. The A-P force during level gait ranged from + 110 N to – 250 N and during stair descent, the A-P force ranged from + 110 N to – 120 N. During the swing phase of stair ascent cycle, i.e. between 0% and 40% of the activity cycle, a high A-P force at the knee joint was observed. The low axial force during the swing phase of stair ascent cycle was not able to restrain the femoral component in place and caused the femoral

component to sublux. Hence, simulation was performed only for the stance phase of stair ascent. During the stance phase of stair ascent cycle, only posterior force was observed and ranged from 0 N up to approximately – 140 N. Torque function, Figure 5-1 (d), was ignored in the squatting activity as explained in section 6.1. Stair descent exhibited the highest I-E torque, with the peak external torque of 15.5 N m. The peak external torque during level gait was approximately half the value of stair descent, i.e. 7.2 N m. Both level gait and stair descent showed fairly similar I-E torque pattern. Stair ascent exhibited fairly low I-E torque value. The torque ranged from + 0.6 N m to –2.7 N m. During stair descent and stair ascent, the knee joint starts at 20° and 29.5°, respectively. Due to this, the femoral component in the simulation was positioned at the respective flexion angle at the beginning of the cycle. During level gait, the knee starts at full extension. The time step used was set at 0.002 ms.

Figure 5-1(a)

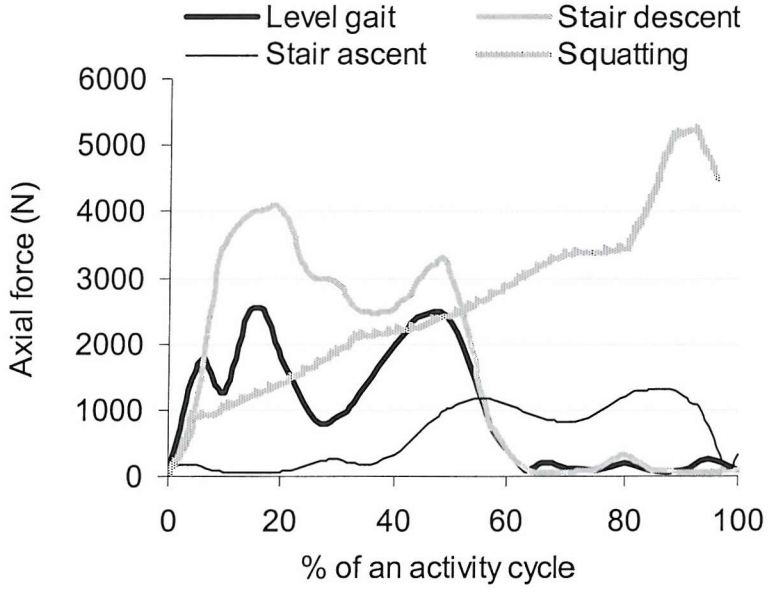

Figure 5-1(b)

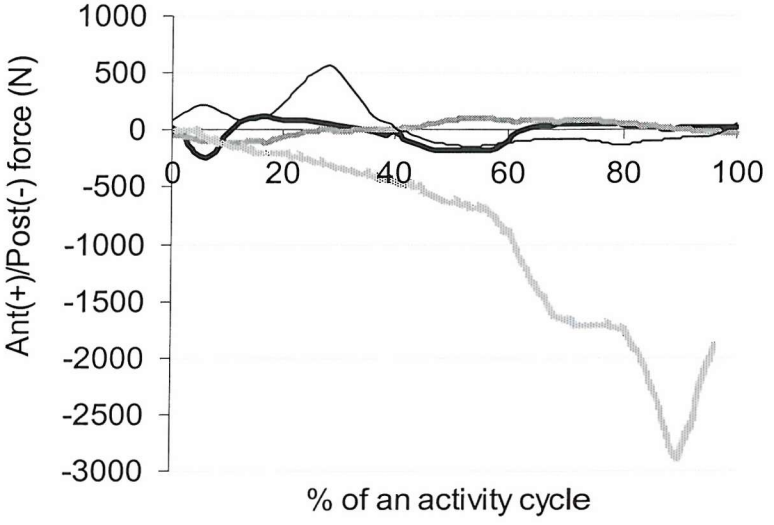

Figure 5-1(c)

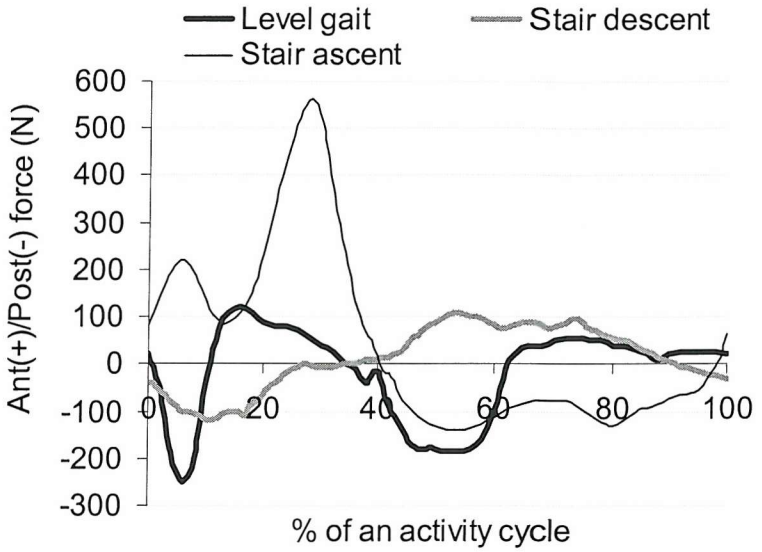

Figure 5-1(d)

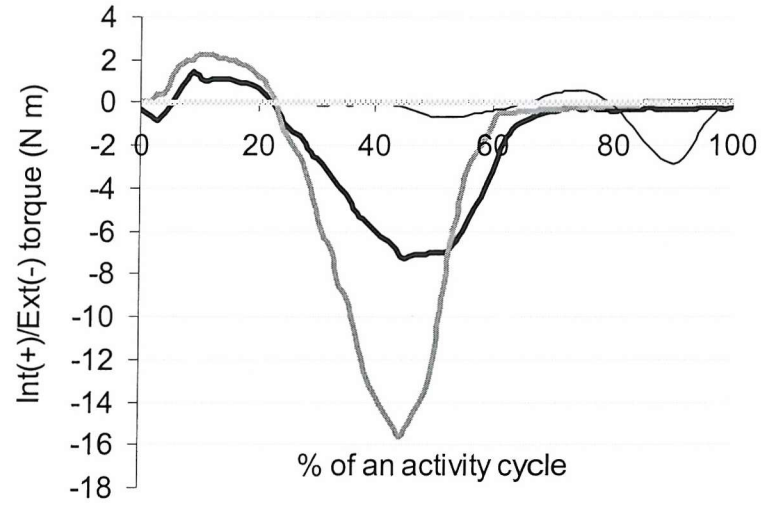

Figure 5-1(e)

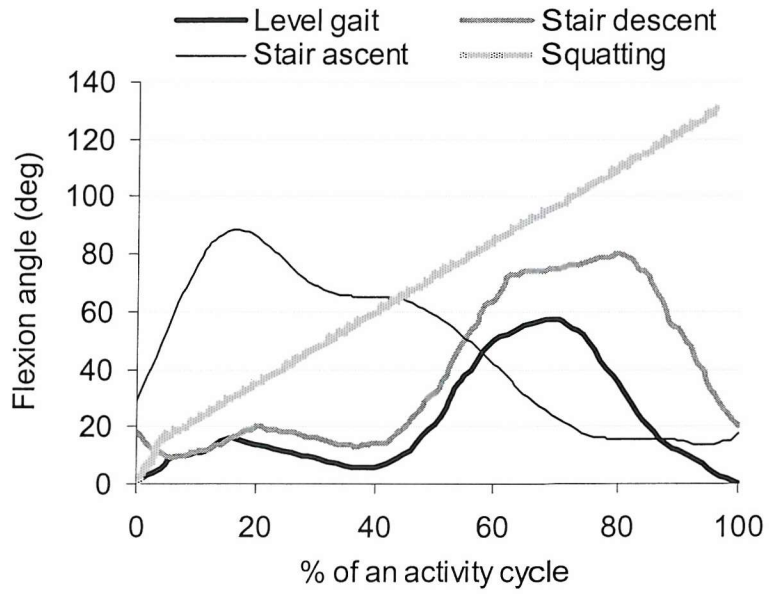

Figure 5-1: The variations of: (a) axial forces; (b) anterior-posterior forces with squatting activity; (c) anterior-posterior forces without squatting activity; (d) internal-external torques and (e) flexion-extension angles for level gait, stair descent, stair ascent and squatting activities.

5.3 RESULTS

The predicted anterior-posterior displacements, internal-external rotations of the TKR are shown in Figure 5-2. Contact pressures between the contact surfaces of the components and von Mises stresses in the polyethylene insert were also reported. Comparisons were made between the four activities for the predicted kinematics and stresses.

There was no consistent pattern of A-P displacement among the four activities (Figure 5-2 a). During level gait, the tibia translated posteriorly with respect to the femur at the first 5% of the gait cycle. Then, it moved anteriorly from 5% to 10% of the gait cycle. The tibia translated posteriorly relative to the femur between 10% and 60% of the gait cycle. The peak posterior displacement was approximately 4 mm, occurring at 60% of the gait cycle. Then, the tibia displaced anteriorly towards the initial starting position. For stair descent activity, the tibia exhibited posterior translation from the beginning of the activity cycle. The tibia tended to stay posteriorly till 50% of the activity cycle. The peak posterior displacement of the tibia relative to the femur was approximately 9.3 mm, occurring at 25% of the activity cycle. From 50% of the stair descent cycle, the tibia moved anteriorly and passed the initial starting position at 60% of the activity cycle. It continued to move anteriorly and reached peak anterior displacement of 4 mm at 66% of the activity cycle. After this, the tibia displaced posteriorly towards the initial starting position. At the end of the activity cycle, the tibia was at posterior position from the neutral position. Only the stance phase was simulated for stair ascent. Throughout the stair ascent loading cycle, i.e. between 40% and 100% of the activity cycle, the tibia displaced posteriorly. The peak posterior displacement of the tibia with respect to the femur was 4.6 mm, occurring at 65 % of the activity cycle. Then the tibia anteriorly translated towards the initial starting position. In squatting activity, the total knee system failed at 84% of the activity cycle, when the knee flexion reached approximately 115°. During squatting, the tibial insert displaced posteriorly relative to the femur. The maximum posterior displacement was 10.0 mm.

Stair descent showed the largest external rotation of the tibial insert relative to the femur among the four activities (Figure 5-2 b). The tibial insert started with a slight internal rotation and when reaching about 23% of activity cycle, the tibial insert started to rotate externally. The maximum external rotation was approximately 7.5°, at 50% of the stair descent cycle. The tibial insert then rotated in the opposite direction and reached its neutral position, 0° at the end of the activity cycle. When compared to the level gait, the tibial insert internally rotated at the beginning of gait cycle and at 10% of the gait cycle, the tibial insert externally rotated. It reached peak external rotation of approximately 4.9°, at 59% of the gait cycle. The tibia insert then internally rotated and remained at slightly external 1° throughout the swing phase of gait cycle. During stair descent, the tibia insert

rotated externally 2.6° more than to the level gait. At the starting of the stair ascent cycle, the tibia insert rotated externally with respect to the femur and at 50% of the activity cycle, the tibia rotated internally and reached peak internal rotation of 0.7° at 73% of the activity cycle. The tibia then rotated externally passing the initial starting position. The peak external rotation of the tibial relative to the femur was 3°, occurring at 92% of the stair ascent cycle. After that, the tibia rotated internally back to the neutral position. No I-E rotation was observed during squatting activity as the torque at the knee joint was ignored.

Generally, there were two peaks of contact pressures occurring during the stance phase of gait cycle and stair descent cycle (Figure 5-2 c). The first peak for the two activities was smaller than the 2nd peak. The peak maximum contact pressure during level gait was approximately 22.3 MPa, occurred at 46% of the gait cycle. Stair descent showed twice as high the peak maximum contact pressure value compared to level gait, with peak value of nearly 45 MPa. Two peaks were observed during the stance phase of stair ascent cycle. The first peak was greater than the 2nd peak. The peak maximum contact pressure for stair ascent was approximately 20 MPa, occurring at 55% of the stair ascent cycle. Generally, contact pressures within the articulating surfaces during squatting increased gradually and reached the peak maximum contact pressures of 35 MPa, at 84% of the activity cycle before the model failed. The femoral component rode up the anterior lip of the tibial insert and subluxed as the tibial insert continued to translate posteriorly.

From Figure 5-2 (d), the peak maximum von Mises stress for level gait was 17.8 MPa, observed at 46% of the gait cycle. From the figure, it showed that the maximum von Mises stress for the squatting activity increased gradually throughout the activity. Both stair descent and squatting activities resulted in the peak maximum von Mises stress of 25 MPa. The peak maximum von Mises stress for stair descent occurred at 21% of the activity cycle and between 43% and 53% of the activity cycle; while for squatting, this occurred from 30% of the activity cycle till the model failed. The maximum von Mises stress remained at constant value of 10 MPa from 60% to 100% of the stair descent cycle. Two peaks were observed during stair ascent activity. The peak maximum von Mises stress was approximately 20 MPa, occurring at 55% of the activity cycle. The second peak exhibited smaller peak value than the first peak.

Figure 5-2(a)

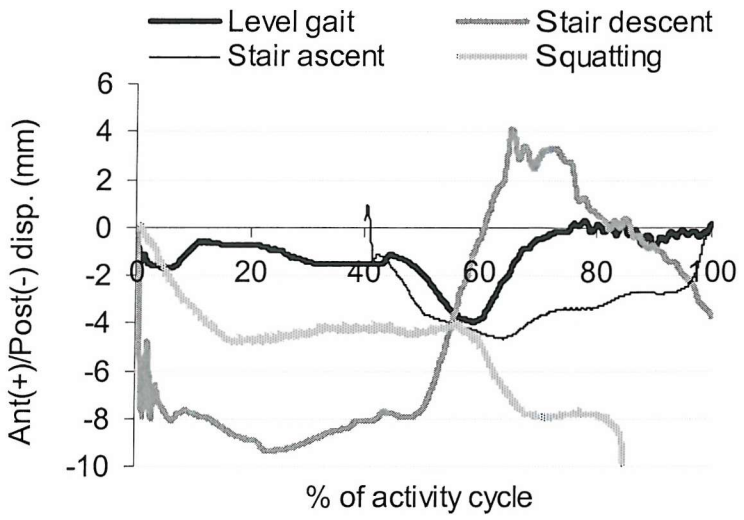

Figure 5-2(b)

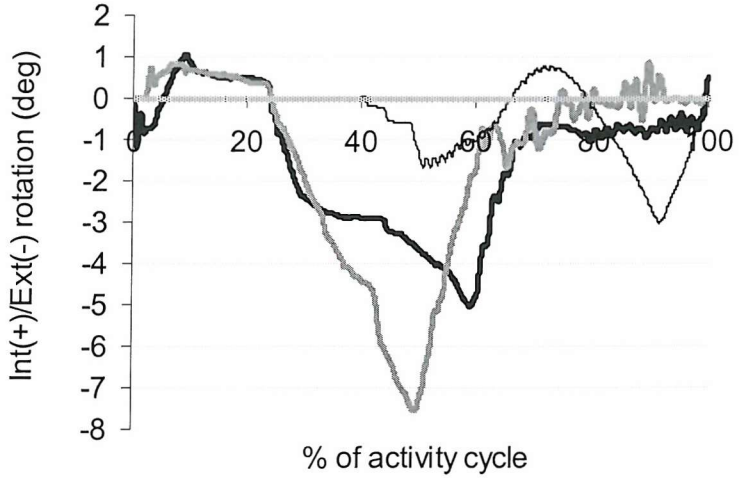

Figure 5-2(c)

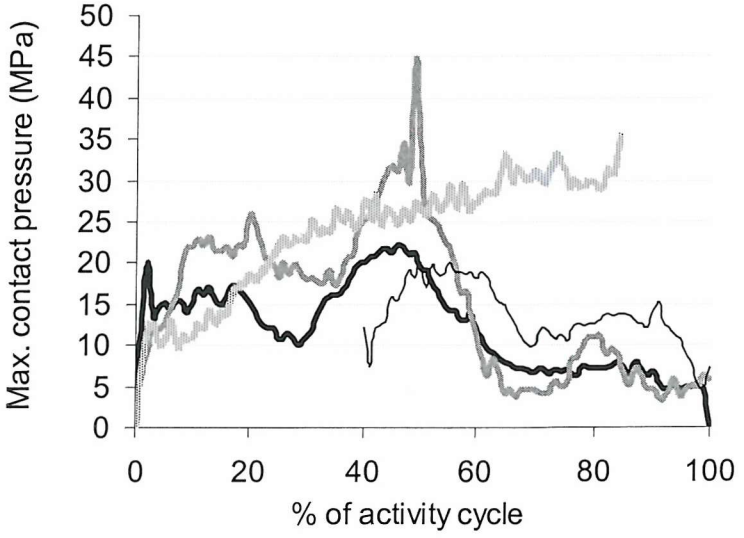

Figure 5-2(d)

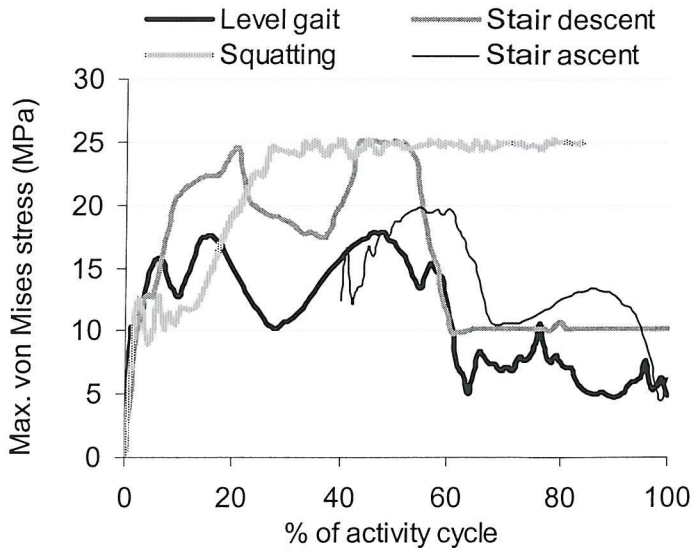

Figure 5-2: The predicted: (a) A-P displacements; (b) I-E rotations; (c) maximum contact pressures and (d) maximum von Mises stresses for level gait, stair descent, stair ascent and squatting activities.

Figure 5-3 shows the maximum contact pressure distributions for the four activities. At the beginning of the level gait cycle, both condyles started at a slightly anterior position and displaced 2 mm posteriorly when the gait cycle reached 15%. At 5% of the gait cycle, the maximum contact pressure recorded was less than 10 MPa. The contact pressure increased to approximately 15 MPa at 15% of the gait cycle. As the gait cycle proceeded from 15% to 45% of the gait cycle, the lateral condyle tracked to a maximum of 4 mm (from the starting position) at the anterior direction but the medial condyle remained at similar position. The tibial insert externally rotated at these periods of the gait cycle. The contact pressures decreased slightly between 15% and 35% of the gait cycle but increased to the peak when reaching 45% of the gait cycle. The peak maximum contact pressure was approximately 22.3 MPa. This was shown in the maximum contact pressure plot in Figure 5-2 c. After 45% of the gait cycle, the amount of pressure at both of the condyles reduced and the lateral condyle moved to a slight posterior position when reached 65% of the gait cycle. At 85% of the gait cycle (swing phase), only very little amount of pressure was observed in the tibial insert and both of the condyles were at slightly posterior part of the insert. Throughout the swing phase, the contact pressures recorded were not exceeding 7 MPa, as shown in Figure 5-2 c.

At the beginning of stair descent cycle, both the medial and lateral condyles were at a posterior position. As the activity cycle proceeded to 15%, the two condyles still remained at the same posterior position, but the contact surfaces were under higher contact pressures as compared to level gait. The contact pressures increased from the beginning

to 20% of the stair descent cycle (Figure 5-2 c). At 5% and 15% of the stair descent cycle, the peak maximum contact pressure was 12.5 MPa and 21.4 MPa, respectively. Between 15% and 45% of the stair descent cycle, the lateral condyle started to move anteriorly while the medial condyle moved to the posterior edge of the tibial insert. The joint was under high contact pressure of value 32 MPa. At this stage, the knee flexed at a higher angle compared to the earlier stair descent cycle. From 65% to the end of the stair descent activity, both the condyles were at slightly posterior position from the centre of the condyles. Little pressure was subjected to the knee joint at end of the stair descent activity. The recorded contact pressures during the swing phase of stair descent cycle, ranged from 5 MPa to 10 MPa, as observed in Figure 5-2 c.

For squatting activity, both the condyles were at slight posterior part of the tibial insert at the beginning of the activity cycle. As the squatting cycle proceeded, the femoral component flexed, the condyles moved anteriorly and remained at the same position throughout the activity cycle. When examining the A-P displacement plot, Figure 5-2 a, the tibial insert translated posteriorly throughout the squatting activity. The contact pressures increased gradually from 0 MPa up to 35 MPa, from the beginning till the end of the squatting activity (i.e, 84% of the activity cycle). As the squatting activity proceeded from 45% to 84% of the activity cycle, the condyles translated anteriorly and come into contact at the very anterior lip of the tibial insert. The model failed as the polyethylene completely damaged and the femoral component subluxed anteriorly as the knee tried to flex further. The contact pressure area during squatting is smaller than level gait and stair descent activities. The shape of the contact pressure for level gait and stair descent is rounder and bigger.

The stance phase for stair ascent was between 40% and 100% of the activity cycle. The selected percentage: 45%, 55%, 65%, 75%, 85% and 95% are shown in Figure 5-3. At the beginning of the stair ascent cycle, both medial and lateral condyles started at slightly posterior position from the neutral position. The femur was flexed at approximately 65°. When the stair ascent cycle proceeded from 45% to 55%, the contact pressures increased. The peak contact pressure was 20 MPa at 55% of the stair ascent cycle (Figure 5-2 c). At this stage the flexion angle was 55° and the axial load was at the peak, 1172 N. The condyles remained at similar position. From 55% to 65% of the stair ascent cycle, the condyles moved slightly posteriorly and the contact pressures decreased from 20 MPa to approximately 15 MPa. Further extension of the knee till 75% of the stair ascent cycle showed further decreased of the contact pressures to approximately 11 MPa. The condyles translated slightly in the anterior direction. At 85% of the stair ascent cycle, the medial condyle displaced slightly in the posterior direction and the lateral condyle moved slightly in the anterior direction. There was a slight increased (increment of 2 MPa) in the contact pressures. The increased in the contact pressures correspond to the increased in the axial

load (Figure 5-2 c). From 85% till the end of the stair ascent cycle, the medial condyle and the lateral condyle further displaced in the posterior and anterior directions, respectively. The axial load decreased gradually and hence, the contact pressures also reduced. The knee was extended and remained at approximately 15° between 80% and 100% of the stair ascent cycle. From Figure 5-3, the contact pressure area was smaller between 45% and 65% of the stair ascent cycle. The contact area became rounder and bigger when the stair ascent cycle proceeded from 65% to the end of the activity cycle.

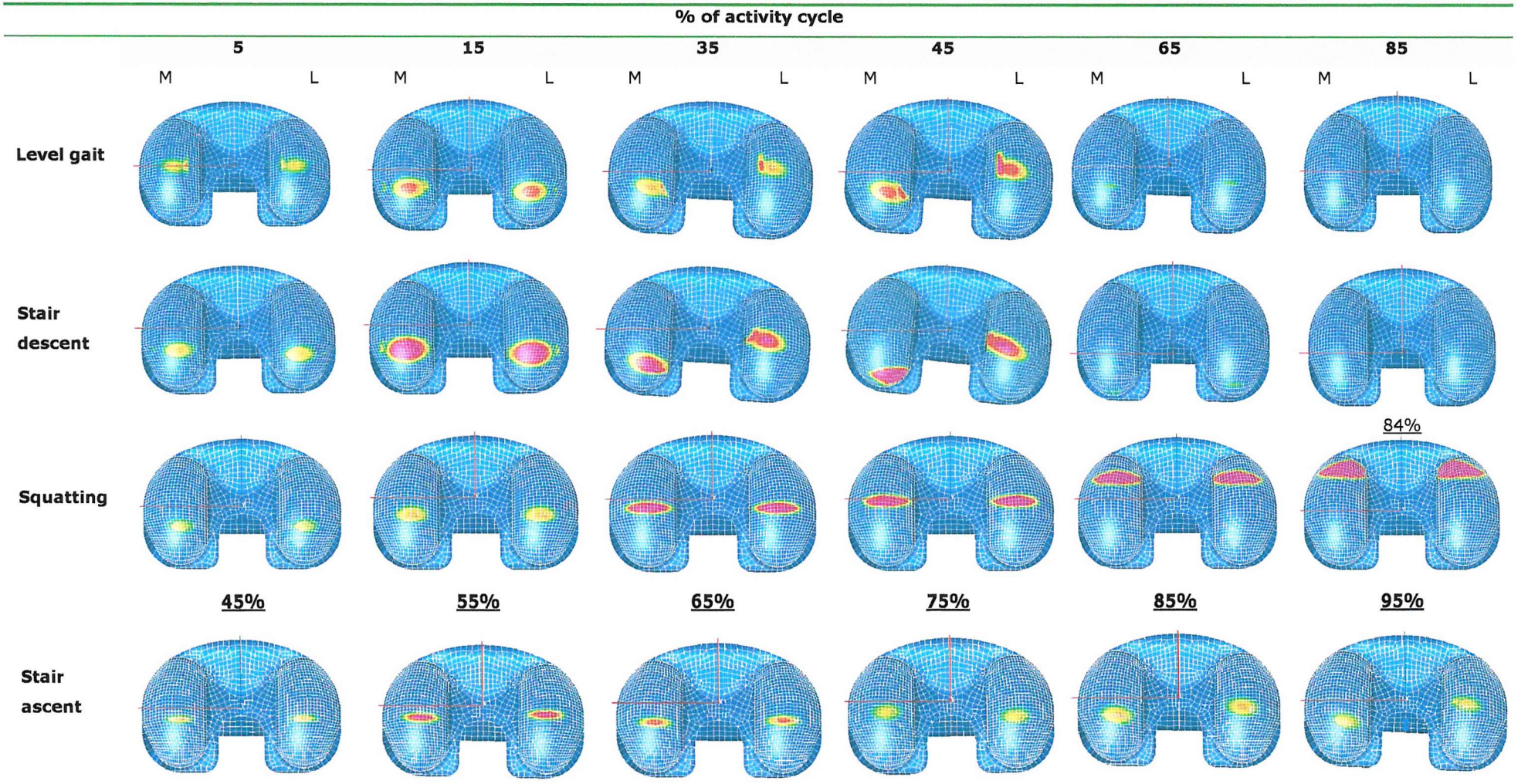

Figure 5-3: Maximum contact pressure distributions between the femoral component and the tibial insert for level gait, stair descent, squatting and stair ascent activities. M: medial; L: lateral

5.4 DISCUSSIONS

The kinematics produced was very dependent on the loadings at the joint. The kinematics trend varied from one activity to another. For the squatting activity, the posterior displacement of the tibial insert relative to the femoral component increased consistently as the posterior force (Figure 5-1 b) applied at the tibia also increased gradually. The simulation failed at 84% of the squatting cycle. At this stage, the flexion angle recorded was 115°. As the femoral component continued to flex, the tibial insert continued moving in the posterior direction relative to the femur. High axial force of approximately 5.85 times BW being applied at the model at that time and in addition to the reduction in contact area as a result of high flexion angle, this produced a very high contact pressure. The tibial insert was compressed at high force and started to yield. Further simulation showed that the femoral component rode up the anterior edge of the tibial insert and subluxed. The tibial insert was deformed. Figure 5-4 shows the model when flexed till 84% of the squatting activity and the plastic strain at tibial insert. The polyethylene plastically deformed with plastic stress of approximately 21.43 MPa (refer to Figure 4-5, plastic stress-strain curve for polyethylene insert).

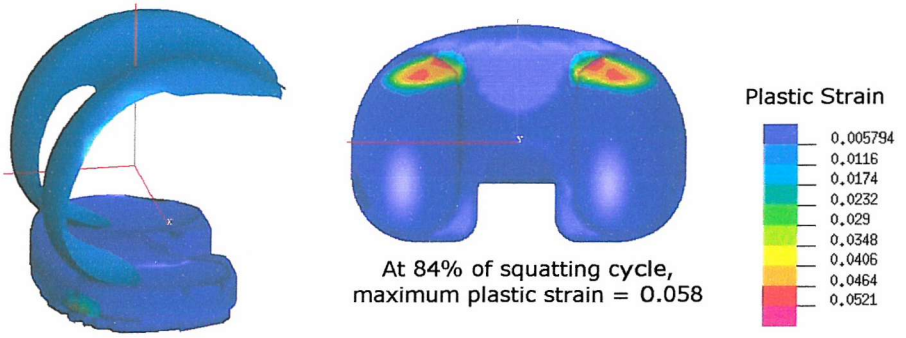

Figure 5-4: The position of the femoral component at 84% of the squatting cycle. The equivalent plastic strain = 0.058

For stair descent, although the applied A-P force was smaller than for level gait, with approximately 120 N in both anterior and posterior direction, however a higher A-P movement at the tibial insert relative to the femur was observed. During stair descent, a torque of 15.5 N m was applied to the model and this was approximately twice the value applied during walking. As a result, larger external rotation at the tibial insert with respect to the femur was predicted. At the end of the stair descent cycle, the tibial insert translated back to near the original starting position and as did the I-E rotation. Similarly, the kinematics during level gait was dependent on the loads applied. The maximum posterior displacement and the maximum external rotation of the tibia with respect to the femur was produced just before toe-off, as a result of maximum posterior force and high external torque applied to the tibia. For stair ascent, posterior force was applied to the

tibia throughout the activity cycle and hence, posterior displacement of the tibia relative to the femur was observed. The I-E rotations were influenced by the torque applied and slightly on the A-P force.

The maximum contact pressures and maximum von Mises stresses were influenced by the axial force applied and the degree of flexion angle during activities. In some activities, the contact pressures were also affected by the kinematics produced. During level gait, two peaks of contact pressures, one occurred at approximately 16% of the gait cycle and a second at approximately 48% of the gait cycle, occurring at a similar time as the peak axial load. When examining the contact pressures plot during level gait, the first peak contact pressure was smaller than the 2nd peak contact pressure. Although both had similar peak axial load, the 2nd peak had a greater contact pressure as the knee was flexed at a slightly higher flexion angle and exhibited the biggest external rotation at that time. For stair descent activity, the 2nd peak of the contact pressure was greater than the first peak even though the axial force applied during the 2nd peak was less than the first peak. High contact pressures at the 2nd peak was due to the change in direction of the tibial insert with respect to the femur in the A-P displacement and I-E rotation. For stair ascent, two fairly similar values of peak axial force were applied at the model. The first peak of contact pressure was greater than the 2nd peak and the main reason for this was that the knee was at a higher flexion angle as compared to during the 2nd peak. At the first peak of contact pressure during stair ascent, the flexion angle was approximately 60° and at the 2nd peak of contact pressure, the flexion angle was approximately 15°. When the knee was flexed to a higher flexion angle, smaller contact area was created and hence, increased the contact pressure. This was observed in Figure 5-3 during stair ascent. For squatting activity, the contact pressures gradually increased as a result of consistent increased in the axial force applied and increased in the flexion angle. At the starting of the squatting activity, the contact area was bigger and the contact pressure was less. This was shown in the first 15% of squatting activity in Figure 5-3.

The von Mises stresses within the model were directly dependent on the contact pressures. When the contact pressures increased, the von Mises stresses also increased. The axial force during stair descent was about 2.4 times bodyweight more than level gait and this significant difference had caused the polyethylene insert to plastically deform. The permanent plastic strain occurred in the inner posteromedial condyle. At the end of stair descent cycle when the axial force at the knee joint reduced to less than 50 N, the maximum von Mises stress still remained at a constant value of approximately 10 N. This indicates that the polymer had yielded and plastically deformed as shown in Figure 5-5.

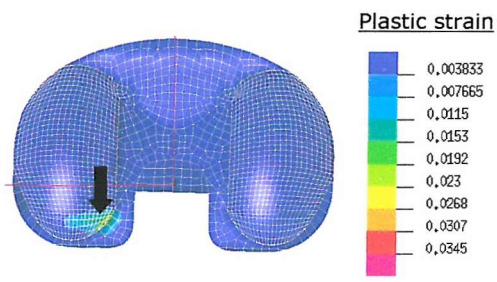

Figure 5-5: The polyethylene insert showed permanent plastic strain (arrow), from 40% to the end of the stair descent cycle. As a result of the permanent plastic strain, the maximum von Mises stresses remained at a constant value of approximately 10 MPa during the swing phase. This permanent stress was known as residual stress.

The level gait results obtained in this study are those of Godest et al. [52]. Their results have been validated and compared to a knee wear simulator and therefore we know the kinematics for level gait are representative. The kinematics during stair descent were reported in Benson et al. [15,16] study. To our knowledge, this is the only report available that simulated the wear performance of a TKR using stair descent loading. Direct comparisons of results from this study to Benson et al. were not possible as different TKR design was simulated. Benson et al. [15,16] predicted the maximum posterior displacement and the maximum anterior displacement of the tibial component relative to the femoral component to be approximately 1.5 mm and 4 mm, respectively. The peak external rotation of the tibial component relative to the femoral component was approximately 7°. The A-P translations of PFC Σ design predicted from this study was observed to exhibit larger translation as compared to NK I TKR (Sulzer Orthopaedics) [15,16], but fairly similar external rotation of the tibial insert was observed between the two studies. Kinematics differences occurred as different prosthetic designs have different conformity of articulating surfaces. No studies have yet to simulate the performance of TKR using stair ascent and squatting activities; and hence, the kinematics and contact stresses for both activities obtained in this study are not comparable to the others.

There are several limitations in this study that need to be considered while examining the results. The forces during stair descent were obtained from different studies and did not represent the knee joint forces for a specific individual. If the knee joint forces for a specific individual during stair descent were able to obtain, then perhaps different kinematics pattern or value would be produced. Costigan's stair ascent data appeared lower than level gait. The main reason was that Costigan's stair ascent load data were the average of nine subjects; whereas Morrison's level gait load data were the average of three subjects. Further limitation was the torque was ignored during squatting activity due to the analysis method, i.e. it was a 2-dimensional analysis. The collateral ligaments and posterior cruciate ligament (PCL) were not modelled in this study. The function of PCL is to avoid excessive posterior displacement of the tibia. If the PCL were modelled, the posterior displacement during these activities might be less. On the other hand, the function of collateral ligaments is to provide rotational constraint as well as displacement

constraint to the knee joint. If these ligaments were modelled, different rotational degree might be observed.

This study showed that the TKR is subjected to different types of daily activities and produced different kinematics trends and values. More demanding activities such as stair descent, squatting and stair ascent, as compared to level gait activity had resulted in higher contact pressures. This indicated that higher wear rates for the polyethylene insert, particularly for this TKR design typically at these activities.

Summary

- The knee joint undergoes a variety of daily activities. Standing and walking are the most common ones. Experimental (knee simulator) and FE studies should also examine that performance of TKR for a variety of activities and not just limit to level gait that is very conservative. By doing so, the performance of the TKR could be tested optimally.
- Stair descent and squatting activities from this study were observed to be more demanding activities than level gait, in terms of kinematics and contact pressures.
- The kinematics trend observed in this study varied from one activity to another and is dependent on the loads applied. The contact pressures were dependent on the axial load applied, the knee flexion angle and also the resultant kinematics.
- The contact pressures for level gait were more dependent on the axial load and the flexion angle of the knee joint. For stair descent activity, the contact pressures were influenced by the applied axial load and the resultant kinematics. Meanwhile, for stair ascent and squatting, the contact pressures were affected by the applied axial load and the high flexion angle.
- Plastic yielding was observed in the polyethylene insert for stair descent and squatting activities.

Chapter 6

INFLUENCE OF ECCENTRIC LOADING ON TKR PERFORMANCE

6.1 INTRODUCTION

Normal alignment of the lower extremity is approximately 0 degree of mechanical alignment or 7 degree to 9 degree of tibiofemoral anatomic valgus [100,126,157,158]. The main objectives of total knee replacement surgery are to restore function by lower extremity re-alignment as well as balancing soft tissues. However, perfect knee alignment is not always obtained. Varus-valgus malalignment has been shown to cause high contact stresses within the polyethylene insert [85] and in some cases may cause severe damage of the component. Varus or valgus malalignment can occur during surgery when alignment of the prosthesis and extremity are not restored correctly. As a result, one side of the component will be over loaded [9]. These changes can alter the stress distributions on the contact surface and the soft tissue tension at the knee joint. An *in vitro* study of varus-valgus malaligment in the TKR was performed by Haider et al. [59]. This was done by shifting the compression load from the centre towards the medial side of the prosthesis. The experimental setup applied the ISO standard load case to the Stanmore knee simulator and the effect of malalignment on the kinematics of TKR was examined. The soft tissues actions were represented by a pair of springs with stiffness of 7.24 N/mm each. They found that offsetting the compression load 5 mm and 10 mm away from the centre to the medial side changed the A-P displacements and I-E rotations of the TKR when compared to the neutrally positioned axial force. However, the amount of changes was not mentioned in their report.

Polyethylene wear is the predominant concern in total knee replacements. In many retrieval analyses, an asymmetric wear beginning at the posteromedial part of tibial insert was the common pattern [153]. The progressive femoral-tibial subluxation, which resulted in polyethylene failure, was demonstrated to be associated with post-operative extremity malalignment and excessive varus positioning of the tibial component [45]. Therefore, the role of extremity and implant alignment in wear of the polyethylene insert is an issue. The majority of biomechanics studies, which investigated the contact stress in the polyethylene insert have only assumed the ideal alignment between the total knee components [51,52] and ignored the potential influence of malalignment included the eccentric loading.

Haider et al. [59] simulated the effect of medial eccentric loading on the kinematics during walking for PFC Σ knee on a Stanmore knee simulator. The axial loading was offset from 0 mm to 5 mm and 10 mm, towards the medial side. They reported that the effect of medial eccentric loading on the kinematics was small, but postulated larger effect on the contact pressures. However, they did not provide any kinematics values. According to Haider et al. [59], the offsets of axial loading complicated the test setups of the knee simulator. In a static FE study, Liau et al. [85] reported that by tilting the femoral component with respect to the tibial component at varus 1°, 3° and 5°, gradually increased the contact stresses at the medial side of the contact surface for all the three different conformity designs. The limitations of the two studies are that: no kinematics value was reported by Haider et al. and the kinematics were not assessed by Liau et al. Furthermore, Liau et al. used a static FE analysis by applying a constant axial force. The knee's movement is a dynamic process and was not considered in Liau et al. [85] study.

To date, there are only a few dynamic finite element knee model studies that simulate full activities like level gait [51,52,113]. In these simulations, the soft tissues are normally represented by linear spring with various stiffness and only represent the horizontal constraints provide by the soft tissues. Godest et al. [52] modelled the horizontal soft tissue with spring stiffness of 10 N/mm and applied the ISO standard load cycle to the FE knee model. In another study, Giddings et al [51] studied the various spring stiffness with values of 1, 7.3, 100 and 200 N/mm and assessed the effect of various spring stiffness has on the kinematics and contact stresses in the prosthesis. Taylor and Barrett [139] used the model developed by Godest et al. [52] to examine the effects of medial eccentric loading on the kinematics and stresses generated by a TKR. Eccentric loading was modelled by moving the point of application of the axial force medially. They found that as the distance of point of application of the axial force moved away from the centre of the femoral component by up to 15 mm, which corresponds to a medial:lateral load ratio of 85:15, the A-P translations and the I-E rotations of the prosthesis increased steadily. However, there were significant increased in the A-P displacements and I-E rotations when the offset of the axial force increased to a further 5 mm. At this point, the axial force was applied through the centre of the medial femoral condyle. They observed significant internal rotation, with the femoral component tending to ride up the anterior lip of the lateral condyle. The limitation of this study was that the soft tissues were represented by horizontal linear springs with stiffness of 10 N/mm. No vertical constraint of ligament was included in their study. In the knee joint, the soft tissues particularly collateral ligaments are positioned in the vertical direction and hence, are likely to resist any abnormal vertical motions that may occur, for example during unicondylar loading, and may act to limit excessive rotations by limiting the degree the femoral component can ride up the anterior slope of the polyethylene insert.

Since there is lack of information on the medial and lateral eccentric loading study, the main objective of this study is to assess the kinematics and contact stresses of the TKR under eccentric loading. In this study, simple structures of medial and lateral collateral ligaments are modelled to the existing FE knee model. Then, medial and lateral eccentric loading are performed. The predicted kinematics and contact pressures are compared with the FE model without the collateral ligaments. This is the first time such study has been carried out using the collateral ligaments FE model. Taylor and Barrett [139] had performed the simulations of medial eccentric loading, but they did not look at the influence of lateral eccentric loading as well as the influence of collateral ligament in the eccentric loading. Therefore, there is a need for this kind of analysis.

6.2 METHOD

Using the PFC Σ model described in Chapter 4, the effects of eccentric loading were simulated by displacing the point of application of the axial load medially or laterally, each time by an increment of 5 mm, along the flexion-extension axis of the femoral component, as in Figure 6-1.

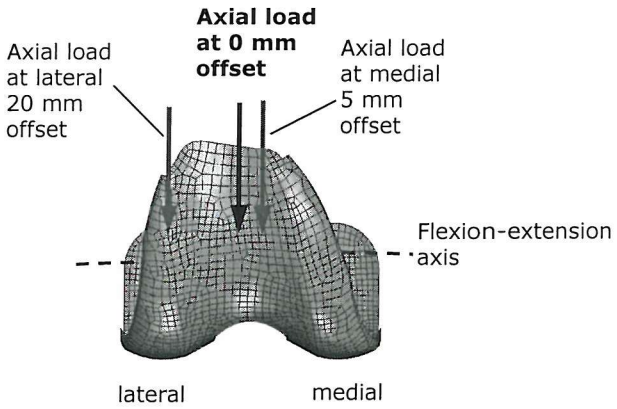

Figure 6-1: Lateral and medial eccentric loading study.

As the point of loading was moved away, the centre of rotation for varus-valgus rotations also moved. The direction of A-P force and torque remained the same. The ligamentous constraints were simulated in one of two ways:

In the first instance, the ISO standard wear test configuration was simulated, with the ligaments being represented as horizontal springs. A stiffness of 10 N/mm was assigned to each of these springs. This model will be referred to as the **horizontal linear spring (HLS)** model.

In the second case, the medial and lateral collateral ligaments were explicitly represented and were modelled using membrane elements. The ligaments were able to take tensile load, but were allowed to buckle if subjected to compressive loads. The medial collateral ligament (MCL) and lateral collateral ligament (LCL) had stiffness of 130 N/mm and 110 N/mm, respectively [98]. The MCL was longer than the LCL. The cross-section of the MCL was 10 mm in width by 80 mm in length (view in the sagittal plane). The cross-section of the LCL was 10 mm by 55 mm. The proximal ends of both ligaments were attached rigidly to the femoral component and the distal ends were attached to the tibial component. The origins (the proximal insertion point) of these collateral ligaments were assumed to be approximately parallel to the femoral component. The ligaments were modelled vertically in all viewing planes, as shown in Figure 6-2. This model will be referred to as the **collateral ligaments** model.

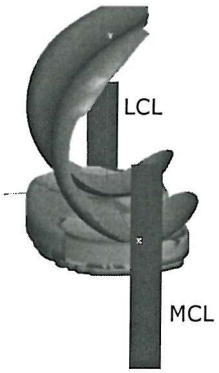

Figure 6-2: PFC Sigma knee with medial collateral (MCL) and lateral collateral (LCL) ligaments.

Load and kinematic data used in this study were defined according to the ISO standard 14243-1 walking cycle (level gait), experimental protocol used in the Stanmore knee simulator, as reported in Chapter 4 (Figure 4-8). A total of 18 cases was simulated: 0 mm offset replicating a bi-condylar load cases, 5 mm, 10 mm, 15 mm and 20 mm offsets medially and laterally representing eccentric loading, for both HLS and collateral ligaments models.

6.3 RESULTS

The force distributions in the medial and lateral condyles were calculated. The resulting A-P displacements and the I-E rotations of the tibial insert relative to the femoral component were recorded for both models. Contact pressures and von Mises stresses generated within the contact surfaces of the prosthesis were also reported in this study. Comparisons were made between HLS model and collateral ligaments model.

6.3.1 Medial Eccentric Loading Study

The force distributions for both the HLS and the collateral ligaments models were fairly similar (Table 6-1). For bi-condylar load case (0 mm offset), both medial and lateral condyles sustained a 50:50 ratio of axial force. Increasing the medial offset, increased the load on the medial condyle. For uni-condylar load case, i.e. at 20 mm offset, only a small percentage of load was transmitted to the lateral condyle. The lateral condyle for the model with collateral ligaments sustained 10% of the axial loading, while the HLS model sustained only 5% of the loading.

Medial loading (mm) away from centre of femoral component	Distribution of forces (%) in the HLS model		Distribution of forces (%) in the collateral ligaments model	
	Medial	**Lateral**	**Medial**	**Lateral**
0 (centre)	50.0	50.0	50.0	50.0
5	61.5	38.5	60.0	40.0
10	72.5	27.5	72.3	27.7
15	83.5	16.5	80.5	19.5
20	95.0	5.0	90.0	10.0

Table 6-1: Loading ratios of medial:lateral condyles in %, for HLS model and collateral ligaments model in the medial eccentric loading study.

The study of medial eccentric loading using the HLS model has been published in Taylor and Barrett [139]. A description of the kinematics, contact pressures and contact stresses results were included in this study for clarity when making comparisons between the HLS model and collateral ligaments model.

Overview of Medial Eccentric Loading Kinematics

From the kinematics results, the HLS model showed significant differences in the A-P displacements and I-E rotations as the medial offset increased from 0 mm to 20 mm. The contact pressure distributions within the articulation surfaces of the HLS model are presented in Figure 6-3. The collateral ligaments model showed less changes in the kinematics as compared to the HLS model. As a result, contact pressures distributions for the worst case, i.e. the medial 20 mm offset load case will be shown and compared between the collateral ligaments model and HLS model, in Figure 6-8.

The pressure distributions for medial 5 mm and 10 mm offset load cases are not shown here because these two cases do not show significant changes in the kinematics and contact pressures when compare to the centrally loading case. Comparisons of pressure distributions are only shown for medial 0 mm, medial 15 mm and medial 20 mm offset load cases, in Figure 6-3.

For the 0 mm offset load case, which was also referred to as the bi-condylar load case, at the beginning of the gait cycle (5%) both medial and lateral condyles were at their neutral position, which was slightly anterior. As the gait cycle proceeded to 15%, the medial and lateral condyles moved posteriorly. The peak maximum contact pressure increased from 0 to approximately 17 MPa, from 0% to 15% of the gait cycle. Between 15% and 45% of the gait cycle, the lateral condyle moved 1.2 mm anteriorly while the medial condyle remained largely at the same position as it was at 15% of the gait. The maximum contact pressures decreased from 15% to 35% of the gait and then increased gradually and reached peak maximum contact pressure value of 22 MPa at 47% of the gait cycle. Then, from 45% to 65%, the lateral condyle returned to the posterior position on the tibial component. Both condyles remained in a slightly posterior position during the swing phase of gait, i.e. between 60% and 100% of the gait cycle. Throughout the whole gait cycle, the pressure distributions on both condyles was even as the compression load was shared of ratio 50:50 between the two condyles. During the swing phase, the contact pressures were recorded at approximately 7 MPa.

At the beginning of the gait cycle of the medial 15 mm offset load case, most of the contact occurred at the medial condyle, meanwhile the lateral condyle tracked to the anterior inner edge of the tibial insert. Between 5% and 15% of the gait cycle, the medial condyle moved slight posterior and contact pressure increased to peak value of 20 MPa. The lateral condyle also tracked from initial anterior position to a posterior position. When examining the maximum contact pressures plot, Figure 6-6 a, the first peak contact pressures occurred between 15% and 20% of the gait cycle. The lateral condyle then moved to the anterior edge at approximately 35% of the gait cycle. The medial condyle remained largely at the same position. The contact pressures decreased from 17% to 35%

of the gait as the axial load applied also decreased (Figure 4-8 a, Chapter 4). Between 35% and 45% of the gait cycle, both condyles remained stationary. When examining the contact pressures plot, Figure 6-6 a, the contact pressures increased to a peak value of 36 MPa at 45% of the gait cycle. Both condyles then moved slightly posteriorly during swing phase, i.e. at 65% of the gait cycle. Not much contact pressures (approximately 9 MPa) were seen at the swing phase.

For the uni-condylar load case, it showed completely different kinematics and contact pressure distributions as compared to the other load cases. The medial condyle sustained most of the axial load (approximately 95%, from Table 6-1) and little load was transferred to the lateral condyle. The first peak contact pressures occurred between 15% and 20% of the gait cycle and the 2nd peak occurred at approximately 50% of the gait (Figure 6-6 b). At the beginning of the gait cycle, the medial condyle was centrally located and then moved to a slightly posterior position at about 15% of the gait cycle. The lateral condyle translated from the anterior edge to the posterior edge of the tibial component from the beginning to 15% of the gait cycle. The contact pressures increased gradually to a peak value of approximately 21 MPa at 15% of the gait cycle. As the gait cycle proceeded till 45%, the position of the medial condyle still remained largely at the same, not much displacement had taken place. However, the lateral condyle rode up the anterior lip of the tibial insert, nearly subluxing, between 45 and 50% of the gait cycle. The lateral condyle then moved back towards the centre position at about 60 % of gait cycle. When examining the maximum contact pressures plot, Figure 6-6 b, the contact pressures decreased from 20% to 30% of the gait cycle and increased again from 30% to 50% of the gait cycle. The 2nd peak contact pressure was the greater than the 1st peak contact pressure. The 2nd peak contact pressure recorded was 42.4 MPa. During the swing phase, both the condyles remained in a slightly posterior position. The contact pressure distributions during the swing phase were low (approximately 9 MPa).

Contact pressures distributions for medial eccentric loading study: HLS model

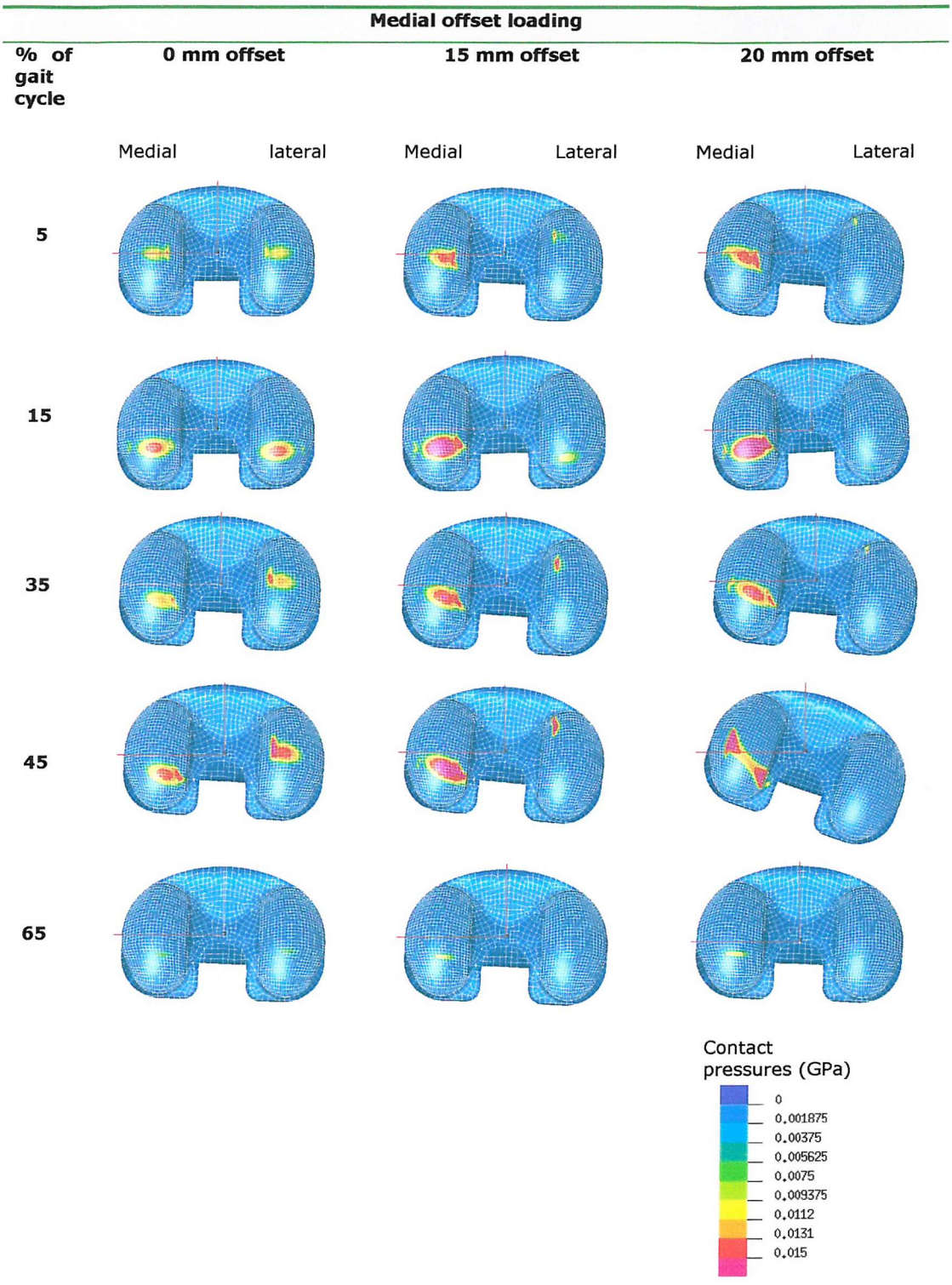

Figure 6-3: Contact pressure distributions in the polyethylene insert for the medial eccentric loading study for HLS model. Only 0 mm (bi-condylar), medial 15 mm offset and medial 20 mm (uni-condylar) offset load cases are shown here.

In general, medial eccentric loading produced a consistent pattern of A-P displacement. At the first 5% of the gait cycle, the tibia translated posteriorly with respect to the femur and then anteriorly till 15% of the gait cycle. Then, the tibia moved posteriorly and reached peak posterior displacement just before toe-off. After toe-off, the tibia translated anteriorly, back to the initial starting position.

Figure 6-4 (a) shows the A-P displacements for the HLS model as previously reported by Taylor and Barrett [139]. Increasing the medial offset of the axial force, by up to 15 mm, produced a steady increase in the maximum posterior displacement of the tibial component relative to the femoral component. The value increased from approximately 4.0 mm to 5.2 mm, at about 58% of the gait cycle. Increasing the medial offset from 15 mm to 20 mm produced a significant increase in the maximum posterior displacement. The displacement increased sharply from approximately 5.2 mm up to 8.2 mm.

For the 0 mm offset, the A-P displacements of HLS model and the collateral ligaments model showed no significant differences during the stance phase of gait cycle, from 0% to 60% of gait (Figure 6-4 b), although there were some small differences during the swing phase. The maximum posterior displacements of the tibial component for the HLS and collateral ligaments models were 4.0 mm and 4.5 mm, respectively. As the distance of the medial offset increased up to 20 mm, the posterior displacement of the tibial component increased consistently for the collateral ligaments model. The maximum posterior displacement for the collateral ligaments model for uni-condylar load case, i.e. at medial 20 mm offset was approximately 5.1 mm, occurring at 59% of the gait cycle. When compared between the HLS and the collateral ligaments models, the HLS model displaced 3.1 mm more than the collateral ligaments model for the medial 20 mm offset load case.

Figure 6-4(a)

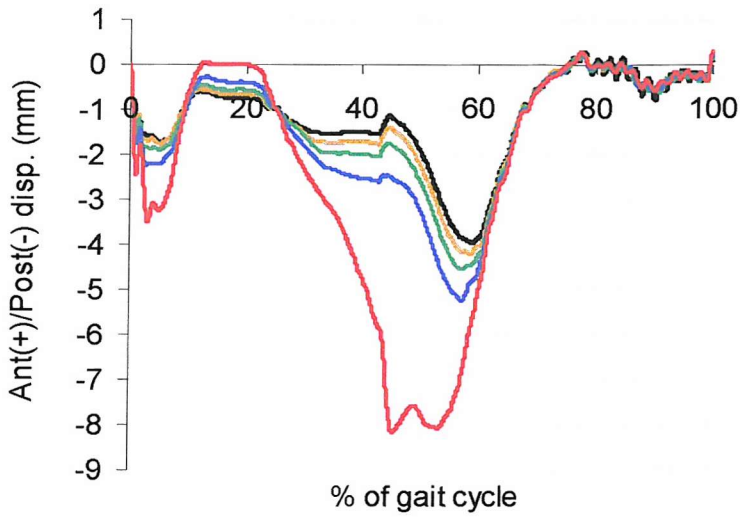

Figure 6-4(b)

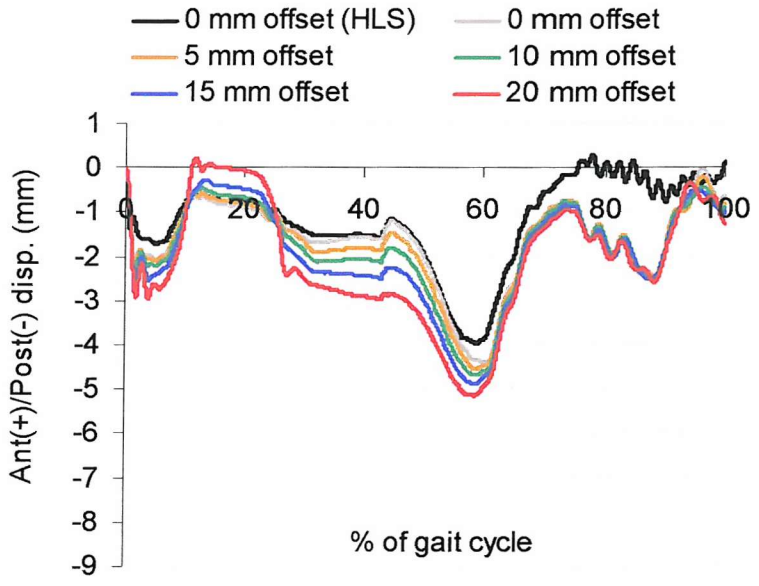

Figure 6-4: The predicted A-P displacements for: a) HLS model [139], and b) collateral ligaments model for medial eccentric loading study.

Both models exhibited a similar trend of I-E rotations (Figure 6-5). The tibia rotated internally with respect to the femur and just passed the initial position at 10% of the gait cycle. It remained at internal rotation and then rotated externally from 25% to 60% of the gait cycle. After toe-off, the tibia once again internally rotated and returned to the initial starting position.

A general trend was observed in the predicted I-E rotations for the medial eccentric loading study for the HLS model, as in Figure 6-5 (a). The maximum external rotation of the tibial component relative to the femoral component, which occurred at about 60% of the gait cycle, increased steadily from 4.9° to 6.8° when the offset was increased from 0 mm to 15 mm. When the medial offset increased from 15 mm to 20 mm, there was a significant difference in the external tibial rotation. The value increased from 6.8° to 19.2°. The tibial component externally rotated 12.4° more with an increment of only 5 mm in the medial eccentric loading, i.e. from medial 15 mm to 20 mm offset.

From Figure 6-5 (b), for 0 mm offset load case, there were no significant differences in the I-E rotations for both the HLS model and the collateral ligaments model. The maximum external tibial rotation relative to the femoral component for both models was approximately 4.9°. For the collateral ligaments model, as the medial offset increased from 0 mm up to 20 mm, the tibial external rotation also increased steadily. The maximum external tibial rotation was 6.5° at 46% of the gait cycle, when the medial offset was at 20 mm away from the centre of the body of the femoral component. The maximum external tibial rotation for 5 mm, 10 mm and 15 mm offset load cases for the collateral ligaments model fell in the range of 4.9° to 6.5°. The collateral ligaments model externally rotated 12.7° less than the HLS model.

Figure 6-5(a)

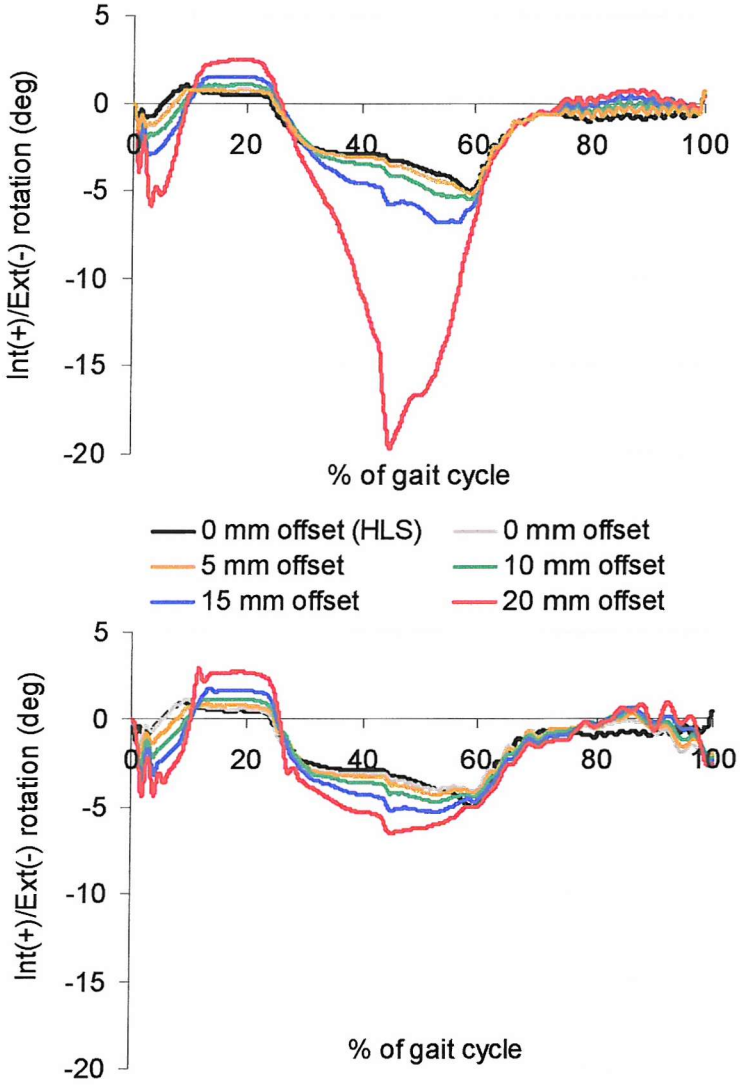

Figure 6-5(b)

Figure 6-5: The predicted I-E rotations for: a) HLS model [139] and b) collateral ligament model for medial eccentric loading study.

The maximum contact pressures for the HLS model increased steadily as the medial offset increased from 0 mm to 20 mm (Figure 6-6 a). The peak maximum contact pressure generally occurred between 40% and 60% of the gait cycle.

For the 0 mm offset load case, the peak maximum contact pressure was 22 MPa and occurred at 47% of the gait cycle. For the 20 mm offset load case, the peak maximum contact pressure increased to 42.4 MPa. From Figure 6-6 (b), the maximum contact pressures for the HLS model were generally less than the collateral ligaments model for 0 mm offset load case. The peak maximum contact pressure for the collateral ligaments model was 27 MPa, i.e. 5 MPa higher than the HLS model. As the medial offset increased from 0 mm to 20 mm, the maximum contact pressures for the collateral ligaments model

did not change extensively. The pressures value stayed quite consistent for all the models. The highest maximum contact pressure was 30 MPa for 20 mm offset load case for the collateral ligaments model. Compared to the HLS model for medial 20 mm offset load case, the collateral ligaments model were 12.4 MPa lower. The collateral ligaments tended to hold the tibial insert and femoral component tighter and hence, during the swing phase of gait cycle, higher maximum contact pressures were observed for medial eccentric loadings as compared to the HLS model. In general, contact pressures of 15 MPa were recorded throughout the swing phase of gait for all the eccentric loading models.

Figure 6-6(a)

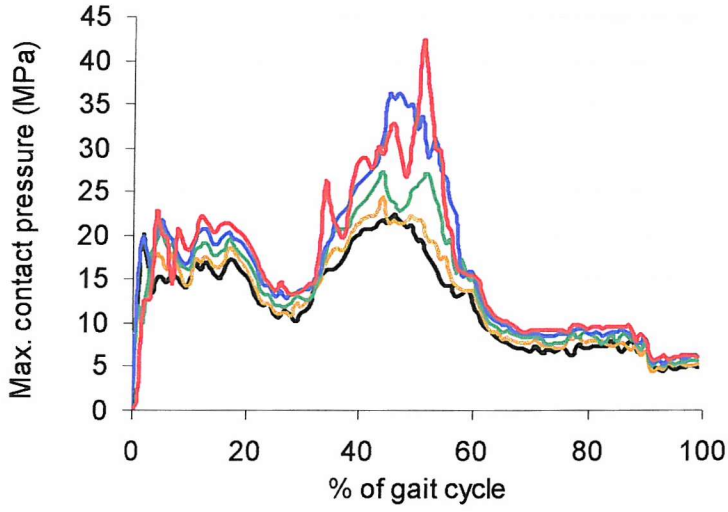

Figure 6-6(b)

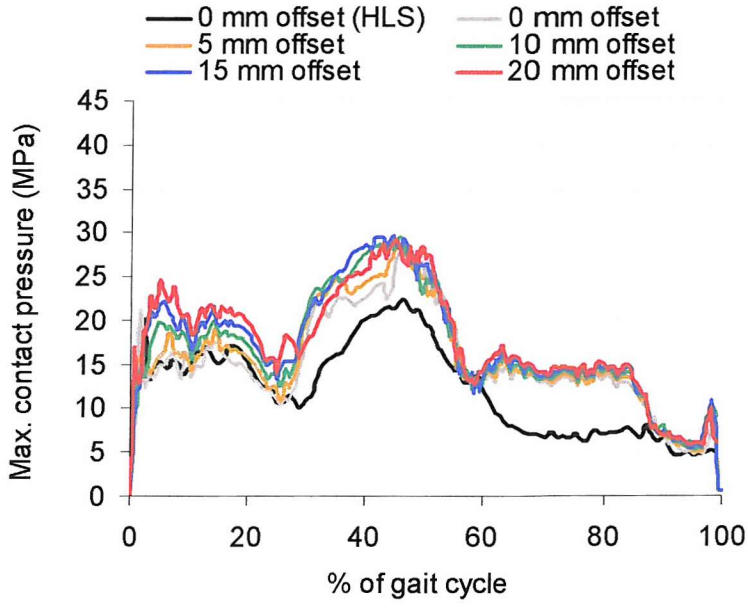

Figure 6-6: The predicted maximum contact pressures for: a) HLS model [139] and b) collateral ligaments model for medial eccentric loading study.

A steady increase in the maximum von Mises stresses was observed in the HLS model as the medial offset increased from 0 mm to 20 mm, Figure 6-7 (a) next page. The stress plots followed similar trend and there was an average of 1 MPa to 2 MPa increment when the offset increased from 0 mm to 15 mm. An offset of 20 mm further increased the peak von Mises stresses by up to 3 MPa. Although this seems only a small increase in the stresses, due to the elastic-plastic material property of the polyethylene, this means that generation of significant amounts of plastic strain. Medial 20 mm offset showed the highest maximum von Mises stress among the other offset load cases, with the peak maximum von Mises stress of 24.1 MPa, occurring at 45% of the gait cycle. The residual plastic strain caused the maximum von Mises stress to remain at 10 MPa during the swing phase of gait for the HLS model, for the medial 20 mm offset. This effect was not seen in the four other offset load cases.

The maximum von Mises stresses for the collateral ligaments model were slightly higher than the HLS model for 0 mm offset load case, Figure 6-7 (b). Larger differences were observed especially at the swing phase of gait cycle not just for 0 mm offset load case but also for all other offset load cases. The collateral ligaments model tended to sustain higher stresses during the swing phase, with an average value of 15 MPa. As the medial offset increased from 0 mm to 20 mm, the maximum von Mises stresses also increased gradually. Comparing the collateral ligaments model and the HLS model for the medial 20 mm offset load case, the collateral ligaments model showed smaller value of peak maximum von Mises stress. The peak value recorded was approximately 22 MPa. This was 2 MPa less than the HLS model. As expected, during the swing phase of gait cycle, the maximum von Mises stresses were higher in the collateral ligaments model than in the HLS model, for all the medial offset load cases. Between 60% and 85% of the gait cycle, the maximum von Mises stresses recorded ranged from 13 MPa to 17 MPa. After 85% of the gait cycle, the value decreased.

Figure 6-7(a)

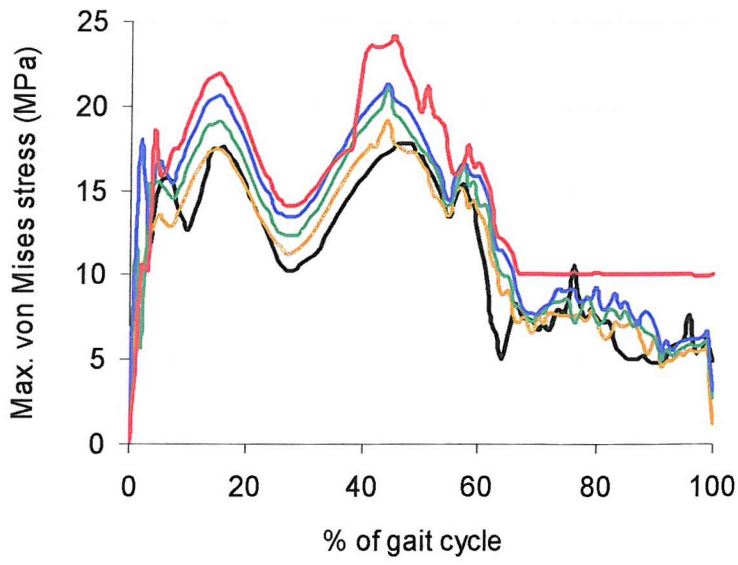

Figure 6-7(b)

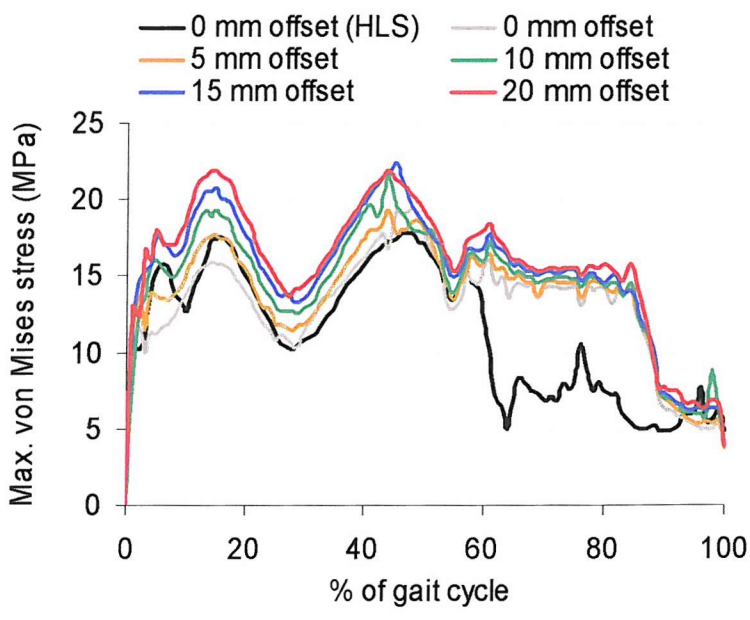

Figure 6-7: The predicted maximum von Mises stress for: a) HLS model [139] and b) collateral ligaments model for medial eccentric loading study.

Comparison of contact pressures distributions between the HLS model and collateral ligaments model are shown in Figure 6-8, next page. The selected results are only for the medial 20 mm off load case.

For uni-condylar load case, the medial condyle for the HLS model sustained most of the axial load, approximately 95% and little load was transferred to the lateral condyle (Figure 6-8). Similar result was observed for the collateral ligaments model with the medial condyle sustained about 90% of the axial load. The peak contact pressure at the first 5% of the gait cycle for HLS model and collateral ligaments model was 21 MPa and 24.5 MPa, respectively. For both models, at the beginning of the gait cycle, the medial condyle was centrally located and then moved to a slightly posterior position, at about 15 % of the gait cycle. The lateral condyle translated from the anterior edge to the posterior edge of the tibial component from the beginning to 15 % of the gait cycle. The axial load applied increased from the beginning to 15% of the gait cycle and had resulted the contact pressures to increase as well. As the gait cycle proceeded till 45 %, the position of the medial condyle for the two models still remained largely in the same place. However, the HLS model externally rotated 12.7° more compared to the collateral ligament model. The lateral condyle of the HLS model rode up the anterior lip of the tibial insert, nearly subluxing, between 45 % and 50 % of the gait cycle. The lateral condyle of the HLS model then moved back towards the centre position at about 60% of the gait cycle. During the swing phase, i.e. from 60% to 100% of the gait cycle, both condyles for this model remained at a slight posterior position. The contact pressure distributions during the swing phase were low as not much load was applied to the knee joint.

For the collateral ligaments model, the lateral condyle moved to the anterior lip of the tibial insert but still remained in close contact with the tibial insert. There was still a small amount of load transferred through the lateral condyle as the collateral ligaments tended to hold the two condyles together. For medial 20 mm offset load case, the contact pressures for the collateral ligaments model during the swing phase were observed to be approximately 15 MPa; whereas for HLS model, the contact pressures were approximately 9 MPa. During the swing phase, the lateral condyles for the collateral ligament model returned to a slight posterior position.

Contact pressures distributions for medial 20 mm offset load case: Comparisons between HLS model and collateral ligaments model

Medial offset loading at 20 mm		
% of gait cycle	**Horizontal linear spring (HLS) model**	**Collateral ligaments model**
5	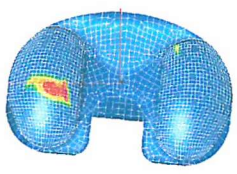	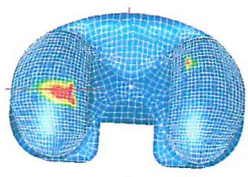
15	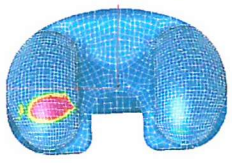	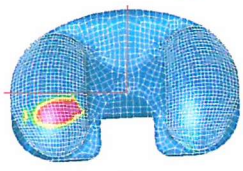
35	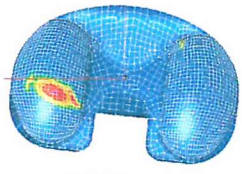	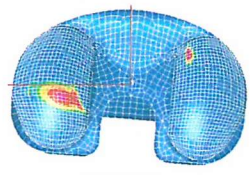
45	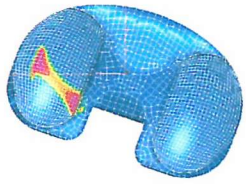	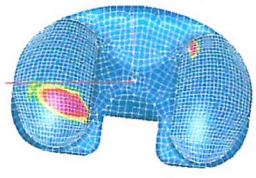
65		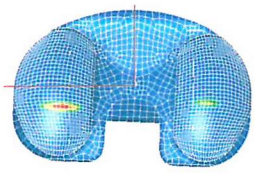
80	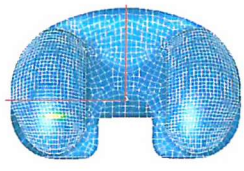	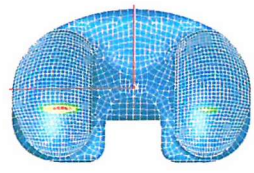
90	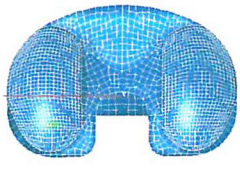	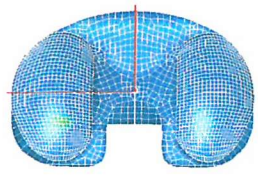

Figure 6-8: Contact pressure distributions for medial 20 mm offset loading case, for HLS model and collateral ligaments model.

6.3.2 Lateral Eccentric Loading Study

From Table 6-2, both the HLS model and collateral ligaments model showed no significant difference in the force distributions within the medial and lateral condyles for the lateral eccentric loading study. For bi-condylar load case, both medial and lateral condyles shared 50 per cent of the axial load. For uni-condylar load case (20 mm offset), the lateral condyle for the collateral ligaments model received slightly less axial load compared with the HLS model. The collateral ligaments model sustained 92% of the axial load, while the HLS model had 95.5% of the axial load applied to the lateral condyle.

Lateral loading (mm) away from the centre of femoral component	Distribution of forces (%) in the HLS model		Distribution of forces (%) in the collateral ligaments model	
	Medial	**Lateral**	**Medial**	**Lateral**
0 (centre)	50.0	50.0	50.0	50.0
5	38.7	61.3	38.3	61.7
10	27.5	72.5	27.3	72.7
15	16.0	84.0	16.5	83.5
20	4.5	95.5	8.0	92.0

Table 6-2: Loading ratios of medial:lateral condyles in %, for HLS model and collateral ligaments model in the lateral eccentric loading study.

Overview of Lateral Eccentric Loading Kinematics

Contact pressures distributions for three loading conditions, i.e. the centrally loaded, lateral 15 mm offset and lateral 20 mm offset load cases will be described in detail in Figure 6-9. The lateral 5 mm and 10 mm offset load cases are not shown as these two cases do not show significant changes in kinematics when compare to the 0 mm offset load case.

The 0 mm offset model will not be discussed as it is the same as reported in Figure 6-3. For the 15 mm lateral offset, both the condyles were not at neutral position as compared to 0 mm offset load case at the beginning of the gait cycle. The medial condyle tracked to the anterior inner edge of the tibial component while most of the contact occurred at the lateral condyle, which was slightly anterior at the neutral position. As the gait cycle progressed, at about 15% of the gait cycle, the medial condyle moved posteriorly and so did the lateral condyle. More contact at the medial condyle occurred at this stage as compared to the beginning of the simulation. The contact pressures on the lateral condyle increased as the axial load applied also increased. The peak contact pressures increased

from 15 to 20.5 MPa, from 0% to 15% of the gait cycle. Between 15% and 35% of the gait cycle, the medial condyle moved slightly to the posterior inner edge of the tibial component and the lateral condyle tracked from posterior to anterior, returned to the position from which it started. At this stage, the contact pressures slightly decreased as the applied axial load also decreased. Between 35% and 45% of the gait cycle, both the medial and lateral condyles remained largely at the same position. From Figure 6-12 a, the highest contact pressure for lateral 15 mm offset was approximately 25.6 MPa, occurring at 43% of the gait cycle. During the swing phase, i.e. from 60% of gait cycle onwards, both the medial and lateral condyles were at posterior positions of the tibial insert with little contact pressure. The contact pressure for lateral 15 mm offset during the swing phase was recorded to be no more than 10 MPa.

The lateral 20 mm offset load case, which will be referred to as the lateral uni-condylar load case. The lateral condyle started in a slightly posterior position. The lateral femoral condyle moved posteriorly on the tibial insert with only little contact on the medial side, at 15% of the gait cycle. The first peak maximum contact pressure was 23.5 MPa, occurring at 16% of the gait cycle and then the value decreased until 30% of the gait cycle. Between 15% and 35% of the gait cycle, the lateral condyle moved slightly anteriorly. The medial condyle remained at the posterior position. The contact pressures slightly decreased. As the gait cycle proceeded, at 45% of the simulation, the lateral condyle did not move significantly. Throughout the stance phase, the medial condyle stayed in contact with the tibial component at posterior position. This was unlike the medial 20 mm offset case, whereby the lateral condyle rode up the tibial component. For lateral 20 mm offset load case, the highest maximum contact pressure was 30.3 MPa and occurred at 43% of the gait cycle. During the swing phase, both the condyles remain in a slightly posterior position. The contact pressure distribution during swing phase was observed to be no more than 10 MPa.

Contact pressures distributions for lateral eccentric loading study: HLS model

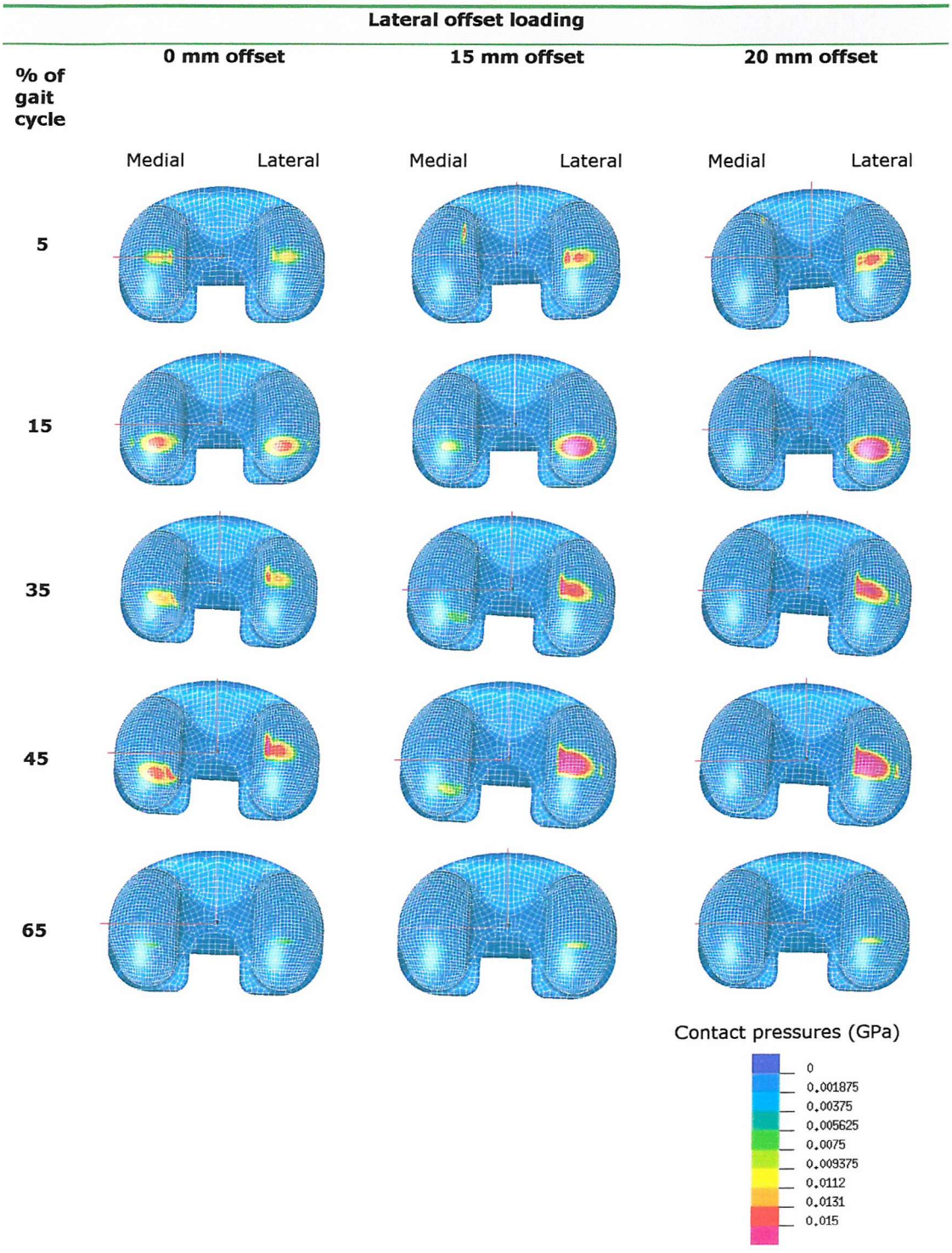

Figure 6-9: Contact pressures distributions in the polyethylene insert for the lateral eccentric loading study for HLS model. Only 0 mm (bi-condylar), lateral 15 mm offset and lateral 20 mm (uni-condylar) offset load cases are shown here.

In general, a consistent pattern of A-P displacement was obtained for HLS and collateral ligaments models. The model translated posteriorly at the first 5% of the gait cycle and then displaced anteriorly until 13% of the gait cycle. After 13% of the gait cycle, the model moved in the posterior direction. From 40% to 60% of the gait cycle, the model further displaced posteriorly. After toe-off, i.e. 60% of the gait cycle, the model translated anteriorly towards the initial starting position.

Increasing the lateral offset of the axial load by up to 20 mm in the HLS model produced a steady decrease in the maximum posterior translations of the tibial component relative to the femoral component, from approximately 4.0 mm to 3.2 mm, at approximately 60% of the gait cycle (Figure 6-10 a). For lateral offsets loading, bigger changes in the A-P displacements were observed between 20% and 50% of the gait cycle, while for medial offset loading (Figure 6-4 a), significant changes occurred between 30% and 60% of gait cycle. Increasing the lateral offset, decreased the posterior displacement of the tibial component, especially between 20% and 50% of the gait cycle.

From Figure 6-10 (b), for 0 mm offset, the A-P displacements for HLS model and collateral ligaments model were fairly similar during the stance phase of gait cycle. Increasing the lateral offset from 0 mm to 20 mm only decreased the maximum posterior displacement of the tibial component relative to the femoral component by small fraction. This maximum posterior displacement usually occurred at about 60% of the gait cycle. Larger changes in the posterior displacements were in between 0% and 50% of the gait cycle. Differences were observed during the swing phase of gait between these two models for all the lateral offset load cases. The collateral ligaments model generally exhibited higher tibia posterior displacement relative to the femur. The peak posterior tibia displacement for all lateral offset load cases was 2.5 mm, occurring at approximately 90% of the gait cycle.

Figure 6-10(a)

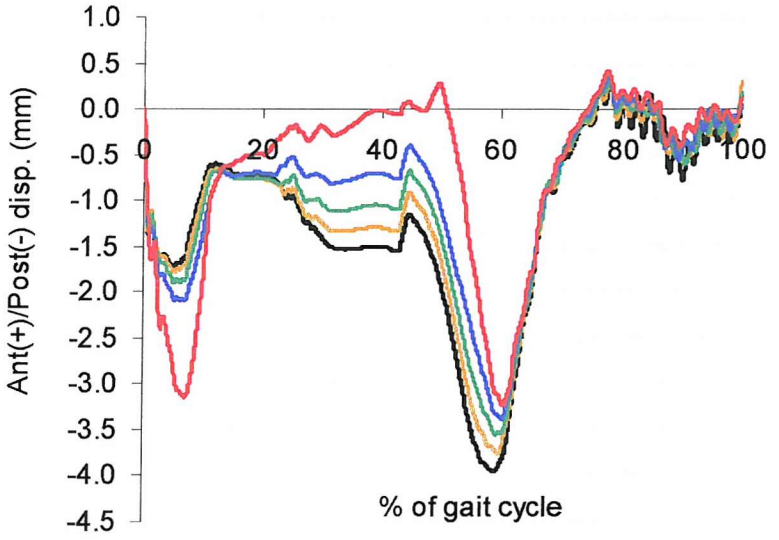

Figure 6-10(b)

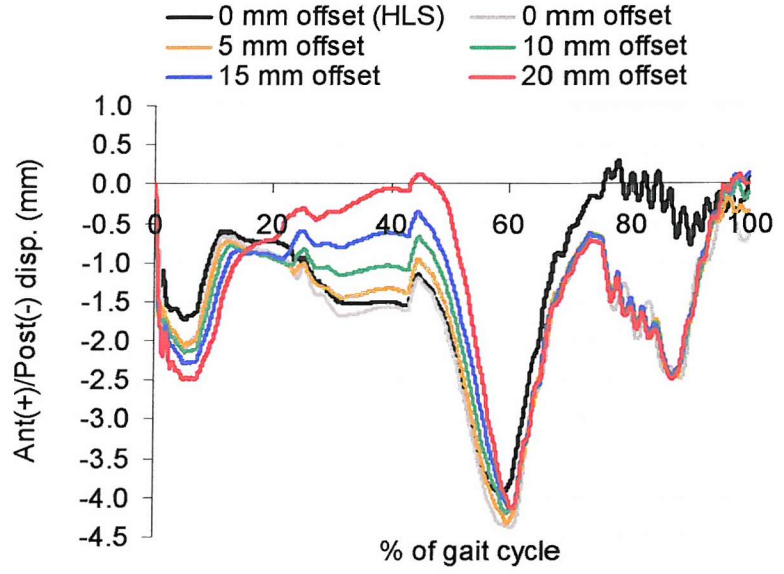

Figure 6-10: The predicted A-P displacements for: a) HLS model and b) collateral ligaments model for lateral eccentric loading study.

From Figure 6-11 (a) and (b), both models exhibited a similar trend of I-E rotations for all the lateral eccentric load cases. For the first 10% of the gait cycle, the tibial insert rotated internally with respect to the femur. Then, the tibial insert rotated in the external direction, passed the initial rotation position and reached peak external tibial rotation just before toe-off (i.e. just before 60% of the gait cycle). After that, the tibia internally rotated towards the initial starting position.

Increasing the lateral offset from 0 mm to 15 mm did not significantly change the external rotation of the HLS model, as in Figure 6-11 (a). The uni-condylar loading at the lateral side had more effect in the external rotation of the tibial insert relative to the femoral component. The peak external rotation which occurred at approximately 58% of the gait cycle, increased from 4.9° to 6.8° when the lateral offset increased from 0 mm to 20 mm. A sharp increased in the internal tibia rotation relative to the femur was observed between 0% and 10% of the gait, when lateral offset loading increased from 15 mm to 20 mm. The tibial insert of the HLS model internally rotated 5.2° at 7.6% of the gait cycle for lateral 20 mm offset, as compared to 1.1° at 0 mm offset.

For the collateral ligaments model (Figure 6-11 b), similar effect was observed whereby increasing the lateral offset from 0 mm up to 15 mm did not significantly influence the external rotation of the tibial insert relative to the femoral component. For 0 mm offset, both the HLS and collateral ligaments models showed similar trend. Only when the offset increased to 20 mm, the external tibial rotation was higher for the collateral ligaments model. The maximum external rotation reached was 5.5°. As compared to the HLS model for lateral 20 mm offset, the collateral ligaments model rotated 1.3° less. An average of 0.4° to 0.6° of consistent increment in the tibial internal rotation was observed at the first 10% of the gait cycle as the lateral offset increased from 0 mm to 20 mm.

Figure 6-11(a)

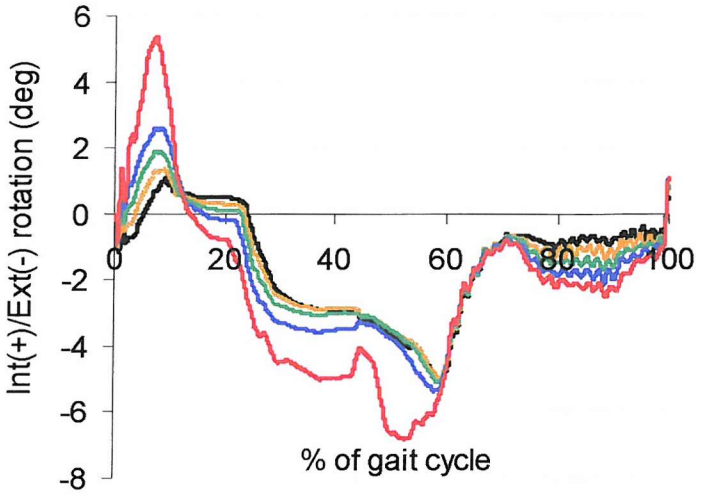

Figure 6-11(b)

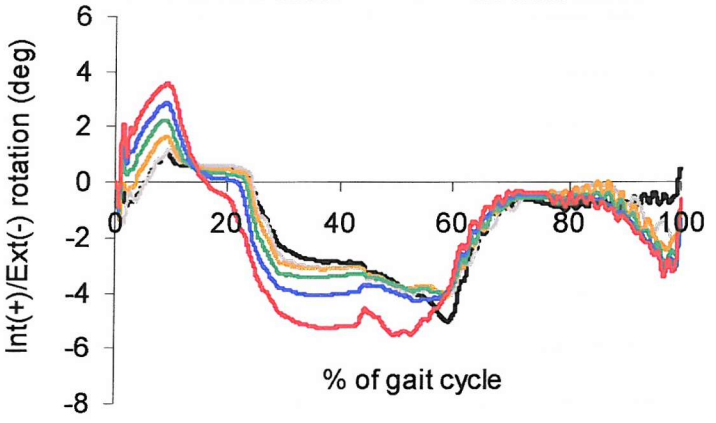

Figure 6-11: The predicted I-E rotations for: a) HLS model and b) collateral ligaments model for lateral eccentric loading study.

In general, there were two peaks in the maximum contact pressures with the peak occurring between 15% and 20% of the gait cycle and a second occurring between 40% and 50% of the gait cycle (Figure 6-12 a and b). The 2nd peak in general was greater than the first peak.

From Figure 6-12 (a), the maximum contact pressures for the HLS model were fairly similar for the bi-condylar and lateral 5 mm offset load cases. The peak maximum contact pressure for 0 mm offset for the HLS model was 22 MPa. Small increase in the maximum contact pressures was observed when the offset increased from 5 mm to 10 mm. For lateral 15 mm offset, the peak maximum contact pressure for the HLS model was approximately 26 MPa, at 45 % of the gait cycle. The peak maximum contact pressure increased 4.4 MPa and reached 30.4 MPa when the axial loading was at the middle of lateral condyle.

There was a consistent increase in the maximum contact pressures for the collateral ligaments model when the offset increased from 0 mm to 20 mm, Figure 6-12 (b). For 0 mm offset, both the HLS and collateral ligaments models had similar maximum contact pressures. The peak maximum contact pressure for the collateral ligaments model at 0 mm offset was 24.3 MPa and as the offset increased to lateral 20 mm, the peak maximum contact pressure increased 24.3% and the peak value was 30.2 MPa. Lower contact pressures were observed in the HLS model during the swing phase of gait as compared to the collateral ligaments model. The higher contact pressures during the swing phase for collateral ligaments model as the ligaments tended to hold the insert and femoral component tighter together during simulations.

Figure 6-12(a)

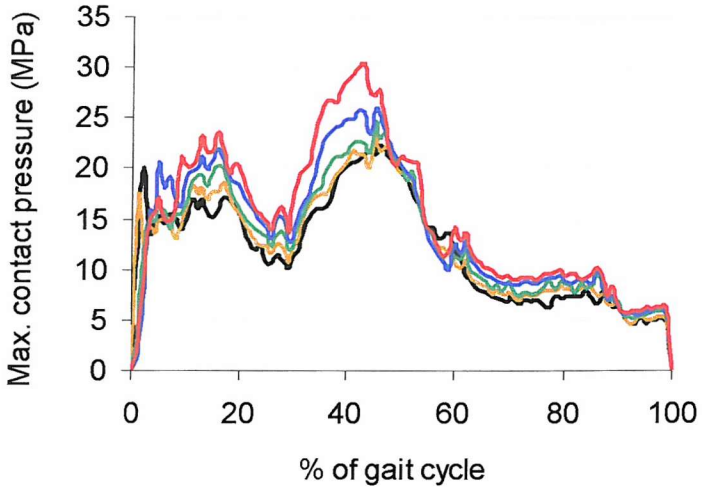

Figure 6-12(b)

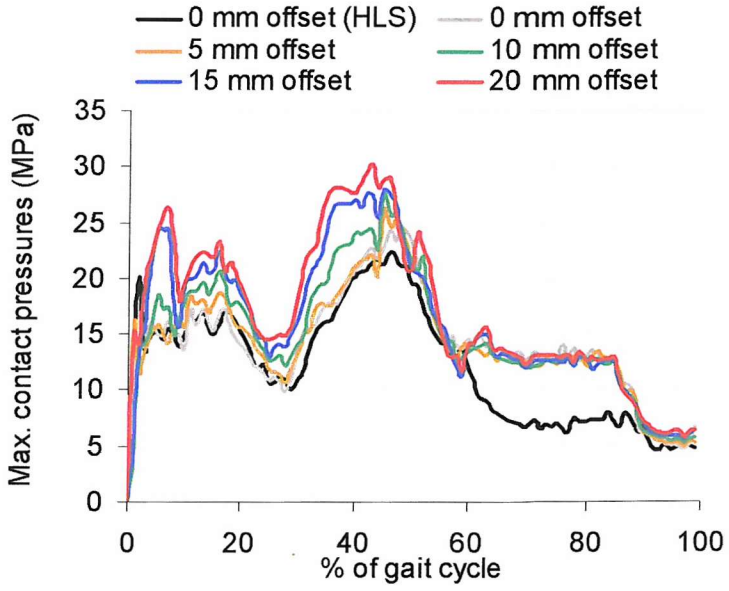

Figure 6-12: The predicted maximum contact pressures for: a) HLS model and b) collateral ligaments model for the lateral eccentric loading study.

As expected, the maximum von Mises stresses were observed to concentrate at the lateral condyle. The peak von Mises stress increased by approximately 3 MPa throughout the stance phase of gait when the axial load was offset up to 15 mm (Figure 6-13 a). The peak maximum von Mises stress for lateral 20 mm offset was 23.7 MPa.

From Figure 6-13 (b), a similar increment in the peak von Mises stress was observed for the collateral ligaments model. An increased of 3 MPa throughout the stance phase of gait was recorded as the lateral offset moved from 0 mm to 15 mm. The peak von Mises stress was at lateral uni-condylar load case, with the peak value of 23.7 MPa. Differences were observed during the swing phase of gait in the HLS model (Figure 6-13 a) and collateral ligaments model (Figure 6-13 b). The collateral ligaments model had higher maximum von Mises stress of between 13.5 MPa and 14.5 MPa during the swing phase.

Figure 6-13(a)

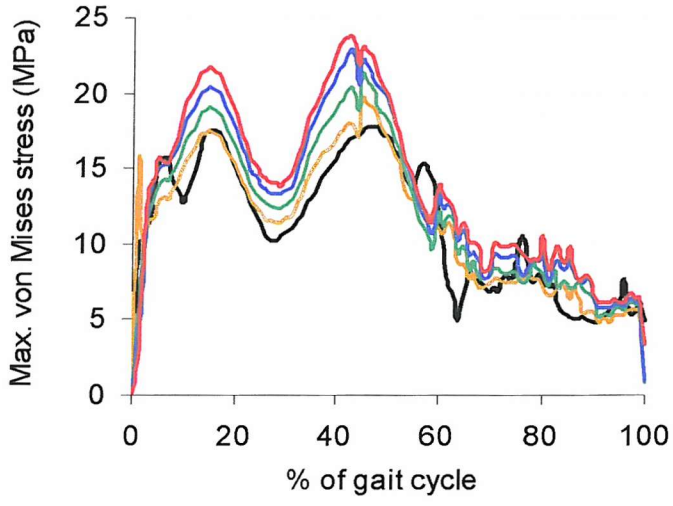

Figure 6-13(b)

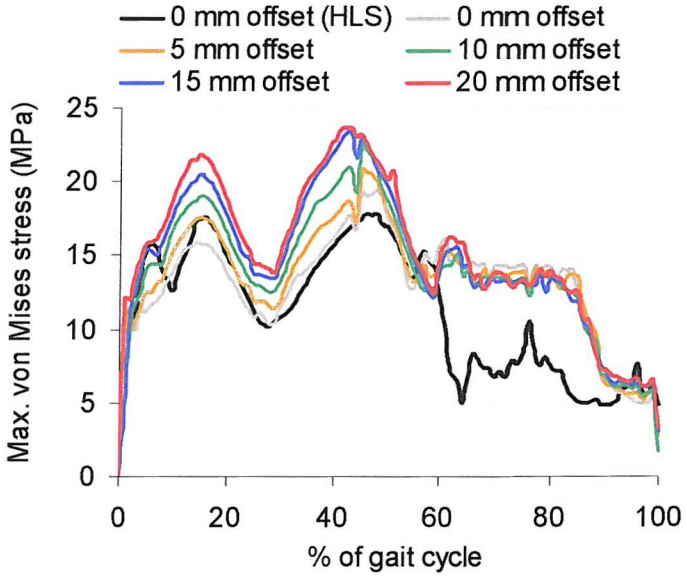

Figure 6-13: The predicted maximum von Mises stress for: a) HLS model and b) collateral ligaments model for lateral eccentric loading study.

The contact pressure distributions are compared between HLS model and collateral ligaments model for lateral 20 mm offset load case, in Figure 6-14.

From Figure 6-14, both HLS and collateral ligaments models had similar starting position occurring at the early stage of the gait cycle. The lateral condyles sustained most of the pressures and only very little pressures were observed in the medial side. At 5% of the gait cycle, the lateral condyles for both models were slightly anterior at the neutral position. The medial condyles were at the anterior inner edge of the tibial component. Only 8% of the axial load was transferred to the medial side of collateral ligaments model. As the gait cycle proceeded, at 15% of the gait cycle, the lateral condyles tracked to a slight posterior position, while the medial condyles moved to a similar position as the lateral side. The contact pressures increased to the first peak when reaching 15% of the gait cycle. The peak contact pressure for collateral ligaments model was 21.5 MPa. From 15% to 45% of the gait cycle, both HLS and collateral ligaments models externally rotated. The lateral condyles moved from a posterior position to a slightly anterior position. Very little axial load was transferred to the medial side. When examining the contact pressure plot, the highest maximum contact pressure for collateral ligaments model was approximately 24 MPa, occurring at 43% of the gait cycle. This value was 5.7 MPa less than HLS model. Then at the swing phase, both lateral and medial condyles of the HLS and collateral ligaments models returned to the neutral position. Compared both the models, the medial condyle of the collateral ligaments model had more pressures than the HLS model. In general, the contact pressures during the swing phase were recorded to be an average of 14 MPa. This was slightly higher than HLS model, which showed value of no more than 10 MPa.

Contact pressures distributions for lateral 20 mm offset: Comparisons between HLS model and collateral ligaments model

Lateral offset loading at 20 mm		
% of gait cycle	Horizontal linear spring (HLS) model	Collateral ligaments model
5		
15	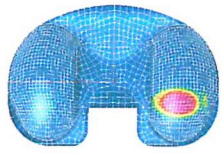	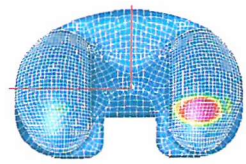
35	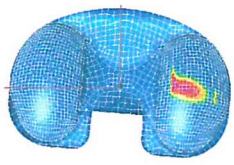	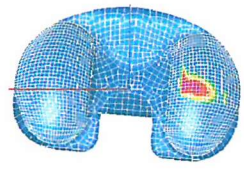
45	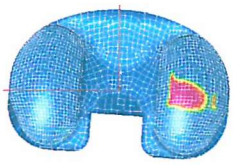	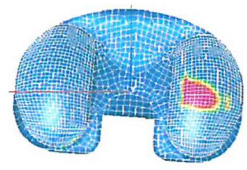
65	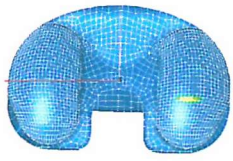	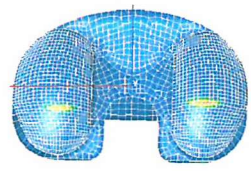
80		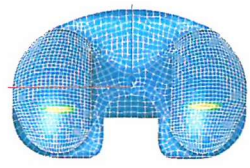
90		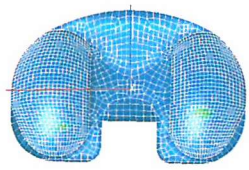

Figure 6-14: Contact pressures distributions for lateral 20 mm offset loading case, comparisons between HLS model and collateral ligaments model.

6.4 DISCUSSIONS

By offsetting the point of application of the axial force, eccentric loading could be simulated. From Table 6-1 and Table 6-2, in general, the axial force distributions in the medial and lateral condyles for both HLS model and collateral ligaments model, for both medial and lateral eccentric loading studies did not show any significant differences. The 0 mm offset model known as bi-condylar load case simulated as even distribution of load (50:50) through the medial and lateral condyle. The 20 mm offset model known as the uni-condylar load case (at either medial or lateral sides). Although the axial load was applied primarily through one condyle, there were still some loads applied to the opposite condyle. These conditions were observed in the HLS model and the collateral ligaments model. For example, the loading ratios of medial:lateral condyles for the HLS lateral 20 mm offset load case were 4.5:95 percent.

The kinematics (A-P displacements, Figure 6-4 and I-E rotations, Figure 6-5) and contact pressures (Figure 6-6) for the 0 mm offset load cases between the HLS model and the collateral ligaments model did not show any significant differences during the stance phase of gait cycle. The peak maximum contact pressures and the peak maximum von Mises stress for the HLS model was slightly lower than the collateral ligament model during the swing phase of the gait. This might due to the collateral ligaments tending to constrain the vertical movement of the components and a slightly more axial load could be transferred through both the condyles, typically during the swing phase. Since the axial load during the stance phase was so much higher than during the swing phase, the collateral ligaments did not have any significant effect on the kinematics and contact pressures.

For the medial 20 mm offset load case, for the HLS model, the model translated and rotated more on the lateral side. This was simply because at the lateral condyle, there was not enough axial load (only 5% of the axial load) to resist the coupled effects of the A-P force and I-E torque applied on it. The horizontal springs with 10 N/mm of stiffness, which acted as representative of the soft tissues were not able to withstand these forces and as a result, high A-P translations and I-E rotations were predicted. This resulted in the lateral condyle riding, up the anterior lip of the tibial insert and nearly subluxing.

For the collateral ligament model, for medial 20 mm offset loading, the lateral condyle moved to the anterior lip of the tibial insert but still remained in close contact with the tibial insert. The femoral tracking on the tibial insert was smooth. The amount of axial load transferred to the lateral condyle was 10% of the total axial load, twice the value in the HLS model. The higher load on the lateral side as well as more vertical constraints from the collateral ligaments had hindered the lateral femoral condyle to continuously track up

the anterior edge of PE insert. This then produced a smooth kinematics at medial uni-condylar loading.

For the HLS model, there were significant increases in the maximum contact pressures when the medial offset increased from 0 mm to 20 mm. For medial 20 mm offset load case, the peak maximum contact pressure was 20.4 MPa higher than the bi-condyar load case. Since extremely high contact pressures were observed for the medial uni-condyar load case, the model also generated the highest maximum von Mises stresses. Residual stress was observed for the HLS medial 20 mm offset model and indicated that the polyethylene had permanently plastic deformed. For the collateral ligament model, the increase in the maximum contact pressures was not as significantly as the HLS model, for all the medial eccentric loading models. The peak maximum contact pressure for the collateral ligaments model for the medial 20 mm offset load case was 12.4 MPa lower than the HLS model.

In the lateral eccentric load case, the A-P displacements gradually decreased and the I-E rotations gradually increased as the offset distance increased. The changes of the A-P displacements and the I-E rotations at lateral 20 mm offset, for both HLS and collateral ligament models were not large as compared to the medial 20 mm offset load case. It is more likely that the A-P displacements and the I-E rotations are coupled to where the axial load is positioned. So, by putting more axial load through the lateral condyle, the prosthesis was unable to exhibit large displacements and rotations at the medial condyle. This also explained the reason that 'ride-up' effect was not seen in the medial condyle, for both HLS and collateral ligaments model.

The maximum contact pressures for the lateral eccentric loading for both HLS and collateral ligaments models were generally smaller than the medial eccentric loading. One explanation for this could be that the lower displacements and rotations exhibited by the model, causes the load to stay at approximately the same position in the polyethylene insert. This allowed the lateral articulating surfaces to become more conforming and hence, increased the contact area. As a result, the contact stresses decreased.

From the A-P displacements and I-E rotations results for both the medial and lateral eccentric loading studies, they showed that if a prosthesis was implanted in mild valgus, it might still performed with reasonable kinematics. For instance, in the worst valgus condition for the HLS model, i.e. at lateral uni-condylar loading, the maximum posterior displacement was 0.8 mm less and the maximum external rotation was only 1.9° more, than the bi-condylar load case. The patient will still exhibit quite similar kinematics as compared to the neutrally aligned implant. The collateral ligaments model also showed similar effect of kinematics. Although the lateral uni-condylar loading condition showed

reasonable kinematics, this loading condition may still be harmful for the polyethylene insert. This was due to the concentration of more than 90% of the axial load on the lateral condyle, which then produced high maximum contact pressures and maximum von Mises stress. For the lateral uni-condylar loading, the peak maximum contact pressure for the HLS model and collateral ligaments model were 30.4 MPa and 30.2 MPa, respectively, representing a 38.2% and 24.3% increase in the peak maximum contact pressures for the HLS and collateral ligaments model respectively, as compared to the neutrally loading condition. Meanwhile, the peak maximum von Mises stress was 23.7 MPa for both models at lateral uni-condylar loading. The peak maximum von Mises stress increased by 33.1% and 22.1% respectively for the HLS and collateral ligaments model when compared to the neutrally loaded model. Higher contact pressures on the polyethylene component would accelerate its wear rate.

On the other hand, if prosthesis was implanted in varus, it would not only increase the kinematics but also significantly increase the contact pressures within the components, as shown in the HLS medial eccentric load case. Although with the collateral ligaments seemed to exhibit reasonable kinematics even at the worst loading condition, this would only be true if the ligaments were perfectly balanced and no laxity. A lax or absent of LCL could result in extreme kinematics, as represented by HLS model at medial uni-condylar loading. Hence, for varus knee the kinematics could be in between HLS model and ligament model. In any cases, medial uni-condylar loading should be avoided as it not only increased the contact pressures, but the kinematics get worse. This would eventually accelerate the wear volume.

It is difficult to make direct comparison of these results with others available in the literature. The predicted kinematics are not able to compare to those reported by Haider et al. [59], as they did not report the exact kinematics value for the eccentric loading study that performed. They only reported that the effect of varus loading obtained by different offsets of the compressive force from the centre was small (up to 10 mm offset). Liau et al. [85] examined various malalignment conditions using static FE. The minimum value of peak von Mises stress recorded was 13.4 MPa for neutrally positioned model (i.e. equally loaded model) and the maximum von Mises stress was 39.5 MPa for model with 5° varus tilt. There are bound to be differences in the stresses reported in this study and from the studies in the literature because different prostheses designs were used and difference in the simulation set-up. Liau et al. [85] conducted varus malalignment study by tilting the femoral component to the varus side of 1°, 3° and 5°. They found that the contact stress increased sharply as the varus tilt angle increased. The highest contact stress was at varus 5° tilt whereby the stress values double the value of the contact stress as compared to the neutral position. Liau et al. did not model any soft tissue constraint in their model.

From this study, it could be concluded that without soft tissue constraint and with horizontal constraint to represent the soft tissue actions, both models showed that for a knee prosthesis would have sustain greater contact stress, especially at uni-condylar loading case. However, in the collateral ligaments model, less variation in the kinematics and contact stresses were recorded for the medial eccentric loading study. Also, the femoral tracking on the tibial insert was smoother for the medial uni-condylar loading when the collateral ligaments were added. This study has shown the importance of modelling the collateral ligaments in the simulation of kinematics and contact stresses of a TKR, particularly when considering abnormal load cases, typically at uni-condylar loading.

Based on the medial and lateral eccentric loading study, it is suggested that placing the prosthesis in neutral or just a slight amount of valgus alignment can still provide satisfactory range of kinematics. This observation is well correlated with clinical findings [9,126]. From clinical follow-up study (4 years), Bargren et al. [9] observed the highest failure rate was when the TKR was aligned in neutral or varus (up to 10°). A total of 12 out of 14 knees failed. Valgus alignment knee showed the highest successful rate, with 16 out of 18 knees performed satisfactorily. Similarly, Ritter et al. [126] found that of the 421 total knee replacements, 244 (56%) knees that revision were in varus. They concluded that surgeons should strive to align the prosthesis in neutral or just a slight valgus.

There are several limitations in this study should be considered when examining the results. Firstly, the collateral ligaments were simplified representative of the real ligaments. The collateral ligaments were crudely modelled as membrane element and the insertion points were ignored. Furthermore, the modelled collateral ligaments were assumed to be tight in full extension and remained the same even at eccentric loading. No variation of soft tissue balance was considered. Posterior cruciate ligament (PCL) was ignored for the PCL-retaining PFC Σ design. It was assumed that constant eccentric load occurred in all the analyses and in addition to that, the A-P force and I-E torque remained the same (in magnitude and point of application) despite variation in eccentricity. In the actual knee, these forces may vary. Improvement to the FE model needs to be done and the effect of eccentric loading on the performance of TKR needs to be re-examined.

Summary

- Medial eccentric loading was the most destructive and dangerous for the TKR when the collateral ligaments were not included. Large increase in the kinematics and contact stresses were obtained from medial uni-condylar loading. The kinematics of the femoral component was not desirable as it rode up the anterior lip of the tibial insert, nearly subluxing. As a result, the polyethylene insert underwent yielding and plastically deformed.
- The predicted kinematics using the collateral ligaments model for the medial uni-condylar load case, showed consistent increases in A-P displacements and I-E rotations. The collateral ligaments acted to resist abnormal vertical motion and produced desirable femoral component tracking on the tibial insert.
- The contact pressures showed consistent increase as medial eccentric loading increased from 0 to 20 mm. The major difference was during the swing phase as higher contact pressures were noticed in the collateral ligaments model when compared to the HLS model. As expected, the von Mises stresses during the swing phase also increased. This might be harmful for the polyethylene insert.
- Lateral eccentric loading did not show significant kinematics variations as compared to the medial eccentric loading even at the worst case loading condition, i.e. uni-condylar loading, for both HLS and collateral ligaments model. However, lateral uni-condylar loading did still increase the contact stresses, which would lead to accelerated wear of this condyle.

Chapter 7

SUBJECT SPECIFIC LOADING STUDY

The aim of this chapter is to assess the performance envelope of TKR using subject specific loading. The study will concentrate on two different activities, i.e. level gait (walking) and stair ascent, performed by two subject groups. In the first attempt, simulations were performed using the PFC Sigma knee with the soft tissues represented by a pair of horizontal linear springs (also known as HLS model). The kinematics and contact stresses were examined under subject specific level gait loading and stair ascent loading. Then, improvements were made to the PFC Sigma knee model. Collateral ligaments and cruciate ligament were modelled and appropriate material properties of these ligaments were assigned, in order to create a more realistic finite element model of the replaced knee. Simulations of subject specific loadings during level gait and stair ascent were repeated in the PFC Sigma knee with these appropriate ligaments. This chapter will also examine the kinematics of the PFC PLI knee system. Collateral ligaments and cruciate ligament were also included. Comparisons of the results obtained were made between the PFC Sigma and the PFC PLI designs.

7.1 INTRODUCTION

The initial function and the long-term performance of total knee joint replacements (TKR) will be dependent on the initial mechanical environment. In particular, abnormal loading and the resulting kinematics are likely to produce excessive polyethylene stresses and accelerated wear. Video-fluoroscopy and radiostereometric analysis (RSA) have shown that a significant proportion of implanted knees exhibit abnormal kinematics [7,30,67,135,148]. Uvehammer et al. [148] assessed the kinematics of 22 knees implanted in 20 patients using RSA. The patients were asked to ascend a platform of 8 cm high. Rotational and translational movements of the tibial and femoral components when flexed at 45° were obtained from their study. They found that the tibial component externally rotated up to 7.3° and also internally rotated up to 7.3° (total range of 14.6°). The minimum and maximum anterior femoral component translations were 2.3 mm and 10 mm, respectively. In a fluoroscopy study, Stiehl et al. [135] has shown highly variable kinematics for the same prosthesis design implanted into eight patients. For example, they reported differences of up to 12 mm in the anterior-posterior displacements during level gait. Similar reports of variable and abnormal kinematics have been reported by other authors [7,73]. A wide range

of kinematics performance of knee prosthesis was observed and suggested that these ranges of movements depend on factors such as patients' gait (wide variety between patients), loading conditions and prosthetic design. The choice of prosthesis will influence the outcome of a knee replacement. Retrieval studies have shown that, unlike hips, the wear of TKR is highly variable [19,20,40,41] and this is probably due to the diverse kinematics, which occurs *in vivo*. These clinical studies are only able to investigate the kinematics without knowing the magnitude and direction of the load applied in the total knee system. Due to this reason, the resultant contact pressures in the polyethylene component are unknown.

Although a wide range of kinematics for a given design of TKR suggests differences in the knee joint contact forces between patients, relatively little is known about the magnitude and distribution of the forces in the knee. No direct measurement of the joint contact force has been reported and we rely on predicted values from inverse dynamics studies. Several studies have measured the force experienced by healthy subjects. In 1969 Morrison [103] presented the joint contact force at the knee for level walking, walking up and down a ramp, and walking up and down stairs. The estimated knee joint axial force of two males walking up stairs was 4.25 times body weight (BW). Costigan et al. [31] examined knee joint kinetics during stair climbing in 35 young healthy subjects. The calculated axial force was on average 3 times BW and could be as high as 6 times BW. They also reported the anterior-posterior force to be ranged from 1 BW up to 1.5 times BW. Such studies have shown variations in the magnitude of the joint contact force *in vivo* due to differences in gait pattern. The differences may be larger in TKR patient population, due to changes in the mechanics of the knee related to the implant design and surgery related parameters (orientation of the implant and soft tissue balancing).

Although it is well understood that a TKR design will experience a range of loading conditions *in vivo*, at present they are typically evaluated using a single load case and the potential influence of patient-to-patient variability ignored. Currently, the main methods of assessment are experimental wear studies [10,13,150] and finite element analysis [12,51,52,113,124]. The majority of the experimental knee wear studies have been performed using an idealised level gait cycle, which is either force [150] or kinematically driven [10]. All studies to date have only compared designs for a single idealised gait cycle.

Most of the FE analyses available are static analyses [11,12,85]. This means that the load was applied to the stationary prosthesis and the corresponding translation or contact stress was recorded for that period at a particular flexion angle. In the finite element (FE) studies, only a few models are available that can predict the kinematics and stresses simultaneously [51,52,61,113,123]. These FE studies are limited in that they only examined the kinematics and polyethylene stresses for a single idealised gait cycle. Although these

studies allow for direct comparison of implant designs, under well-controlled loading conditions, they give no indication of the sensitivity of a design to patient or for that matter, surgery related parameters. However, given that suitable joint contact force data can be found, FE models have the potential to assess the kinematics and stresses as a result of multiple, subject specific load cases and by doing so a performance envelope can be defined. In principle, it should then be possible to assess the sensitivity of TKR design to patient or surgery related variables, by examining the performance envelope. The aim of this study was to apply joint contact force data for a number of individuals for two activities, level gait and stair ascent, to an existing explicit FE model of a commercially available total knee replacement. The predicted kinematics and stresses for each individual were averaged together in order to define a performance envelope for each activity.

7.2 METHOD

Knee joint forces for subject specific loading during level walking and stair ascent were applied to the PFC Sigma HLS model (as discussed in Chapter 7). The boundary conditions of the FE knee model were maintained as previously described in Chapter 4. The time step was set at 0.002 ms. Knee joint contact forces for these two activities are discussed below.

Joint Contact Forces – Subject Specific Load During Level Gait

The knee joint contact forces during level gait were calculated using inverse dynamic method, which has been described briefly in section 2.6, Chapter 2 and in Costigan et al. 2002 [31], for seven healthy, elderly subjects consist of 1 male and 6 females. A summary of the relevant subject related data (height, weight and age) is given in Table 7-1. The forces data were kindly provided by Dr. Patrick Costigan, Queen's University, Canada (personal communication).

Subject	Weight (kg)	Height (cm)	Age (years)	Sex (F: Female; M: Male)
1	68.5	164.5	69	F
2	99.8	171.5	51	F
3	47.8	161.3	71	F
4	60.4	165.0	46	F
5	71.0	182.0	70	M
6	64.0	162.0	72	F
7	70.1	165.0	62	F

Table 7-1: Subjects' characteristics for level gait activity.

The measured axial forces, anterior-posterior forces, internal-external torques and flexion angles from these seven subjects are shown in Figure 7-1 (a) – (d). These values were used as input to the FE model.

From Figure 7-1 (a), a range of axial force values was observed. In general, the axial force curve had three peaks during the stance phase of gait cycle (0% to 60% of the gait cycle) and a fourth during the swing phase just prior to heel strike. The first peak typically occurred during the first 5% of the gait cycle and ranged from 1200 N to 1800 N. The second occurred between 10% and 20% and ranged from 750 N to 1600 N. The third peak typically occurred at 45% - 50% of the gait cycle and was the largest, with values ranging from 1000 N to 2800 N. One particular subject's knee was subjected to axial force of approximately 2800 N or 4 times body weight (BW). Compared to ISO standard data (Figure 4-8, Chapter 4), a near zero value of axial force was observed during the swing phase of gait. The peak forces during the swing phase, which ranged from approximately 500 N up to 1400 N as observed in the axial force curve (Figure 7-1 a) could be the action of knee muscles during that period. As the forces are higher during the stance phase, simulations will only be performed over this period of the gait cycle.

The pattern of the A-P forces (Figure 7-1 b) was less well defined, but at the beginning of the stance phase, the A-P force tends to act posteriorly, ranging from 0 N to 380 N, but then steadily decrease towards zero at 20% of the gait cycle. There is then a steadily increasing anteriorly directed force, which peaks at approximately 50% of the gait cycle, with magnitude ranging from 70 N to 200 N. This then decreases towards zero just prior to toe off (Figure 7-1 b). There was a consistent pattern in the I-E torque data (Figure 7-1 c). From heel strike, the external torque of the tibia relative to the femur increases to a peak at approximately 50% of the gait cycle, with a magnitude ranging from - 3 N m to - 8 N m. The external torque then decreases to near zero at toe off.

From Figure 7-1 (d), it can be seen that not all the subjects started at 0° of flexion angle. Two subjects started with a slightly hyperextended knee at approximately 1.6° and 5°, respectively. The other subjects began between 4° and 8.5° of flexion. The femoral component was flexed according to specific subjects knee flexion angles at the start of the gait cycle. The anterior-posterior displacements, internal-external rotations and contact stresses distributions of the knee prosthesis were reported for each of the subjects in results section.

Figure 7-1(a)

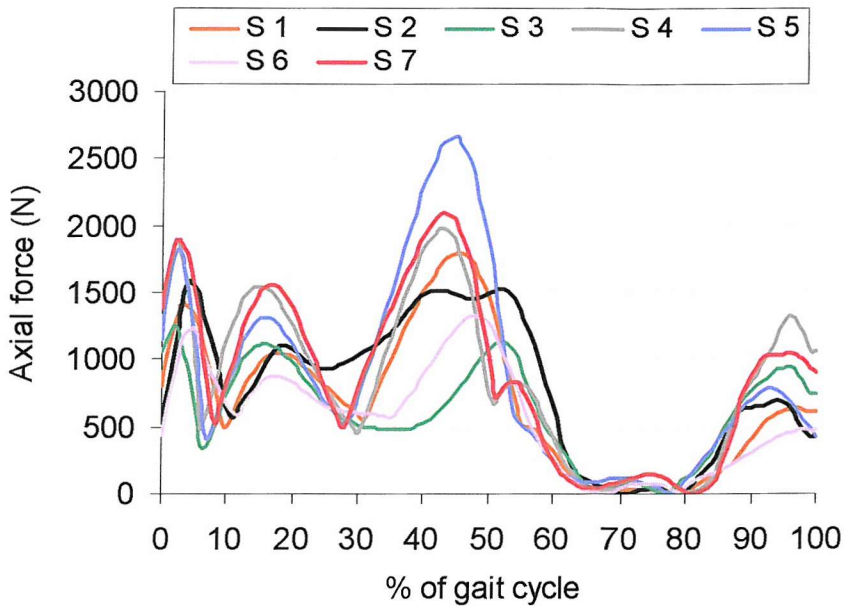

Figure 7-1(b)

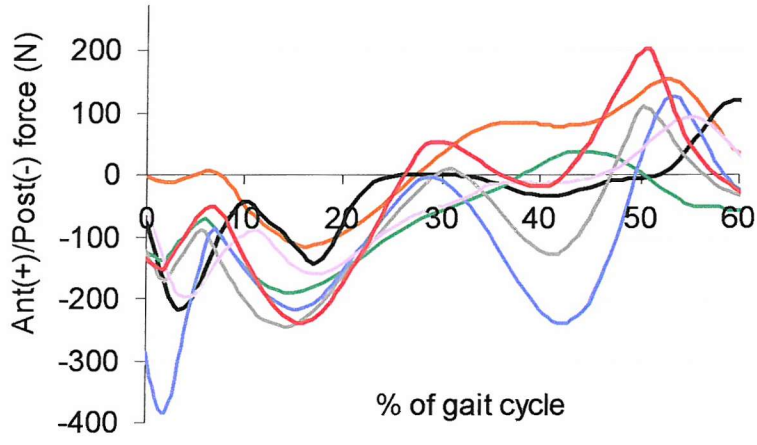

Figure 7-1(c)

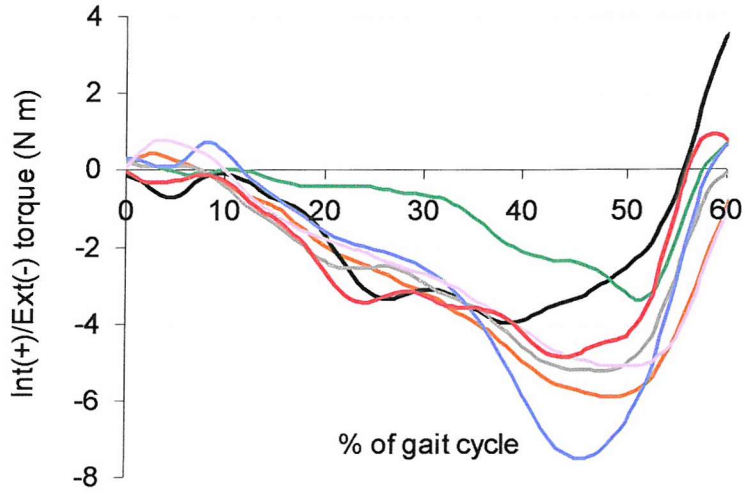

Figure 7-1(d)

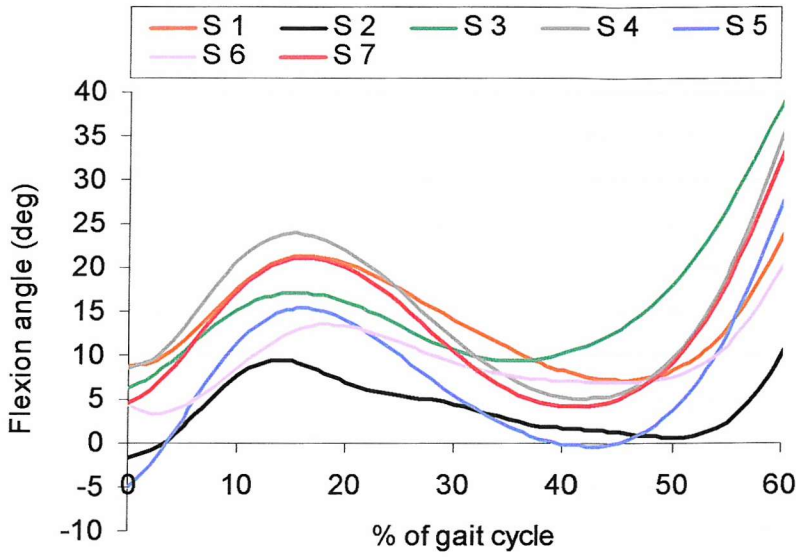

Figure 7-1: The variations of: (a) axial forces; (b) A-P forces; (c) I-E torques and (d) flexion angles for 7 healthy elderly subjects during level gait. S: subject

Joint Contact Forces – Subject Specific Load During Stair Ascent

Again, using the inverse dynamic approach, the knee flexion angle was measured and the various components of the joint contact force were predicted for nine subjects during a stair ascent exercise. The subject related information is summarised in Table 7-2. Again, these force data were kindly provided by Dr. Patrick Costigan (personal communication). Only the stance phase of stair ascent activity, i.e. from 40% to 100% of the activity cycle was simulated in this study.

Subject	Weight (kg)	Height (cm)	Age (years)	Sex (F: Female; M: Male)
1	93	178	66	M
2	71	182	70	M
3	76	178	73	M
4	75	169	70	M
5	64	162	72	F
6	69	165	69	F
7	55	150	66	F
8	78	172	69	M
9	67	169	66	M

Table 7-2: Subjects' characteristics for stair ascent activity.

The axial forces, A-P forces, I-E torques and flexion angles during stair ascent activity are shown in Figure 7-2 (a) – (d). From Figure 7-2 (a), there was quite a consistent pattern in the axial force data. In general, the axial force curve had two peaks at the stance phase. The first peak typically occurred around 50% of the stair ascent activity and ranged from 700 N to 1800 N. The second peak typically occurred between 75% and 85% of the stair ascent activity and ranged from 1000 N to 2500 N.

Figure 7-2 (b) shows the A-P forces for 9 healthy subjects while performing stair ascent activity. Due to the sensitivity in planar measurements taken from the radiograph and any malrotation while imaging the joint reduced the accuracy of the predicted forces. As a consequence, the resulting A-P forces were quite variable, especially during the swing phase, whereby extreme A-P forces were observed (Figure 7-3), with peak anterior force of more than 1500 N, simulations will only be performed at the stance phase. During the stance phase of stair ascent, Figure 7-2 (b), the A-P force of the tibia relative to the femur tends to act posteriorly, ranging from 0 N to 300 N. The I-E torque data is less well defined (Figure 7-2 c), with some subjects experiencing an external torque (majority) and some experiencing an internal torque of the tibia relative to the femur. During the whole period of stair ascent stance phase, the I-E torque data ranged from internal torque 4.0 N m up to external torque 9.4 N m. The peak external torque usually occurred between 85% and 95% of the stair ascent activity. The variation in I-E torque during stair ascent activity is slightly larger than seen in level gait.

A consistent pattern was observed in the flexion angle data, Figure 7-2 (d). All subjects started with a knee flexion angle between 59° and 70° and then extended towards the end of the stance phase.

Figure 7-2(a)

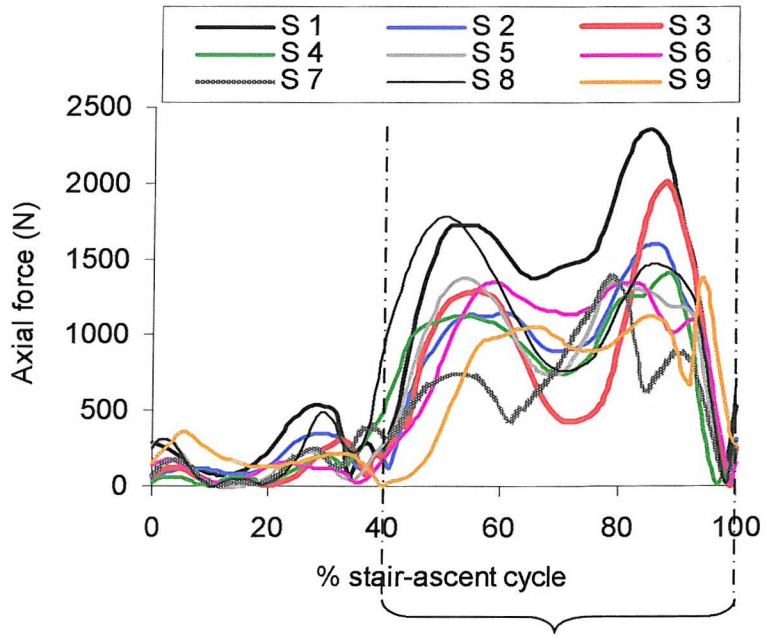

Stance phase/loading phase during stair ascent. Only this phase was interested in the simulations.

Figure 7-2(b)

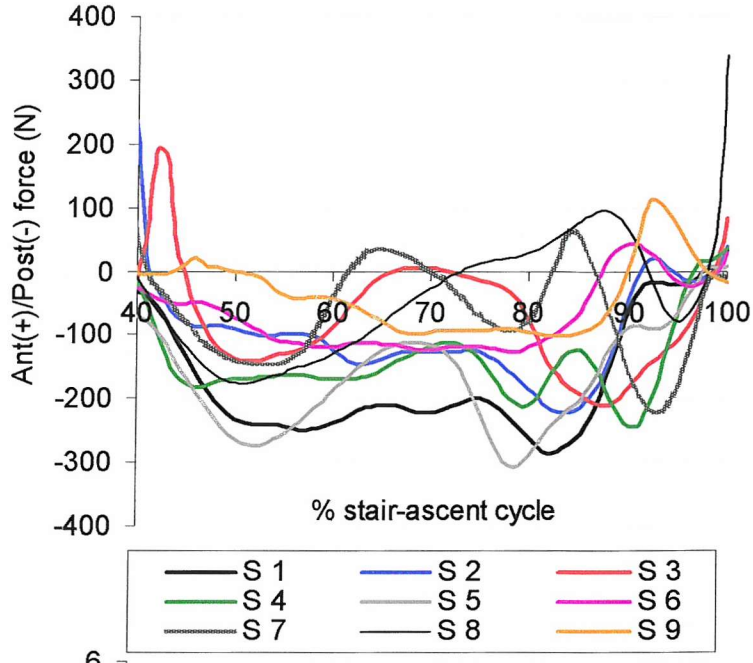

Figure 7-2(c)

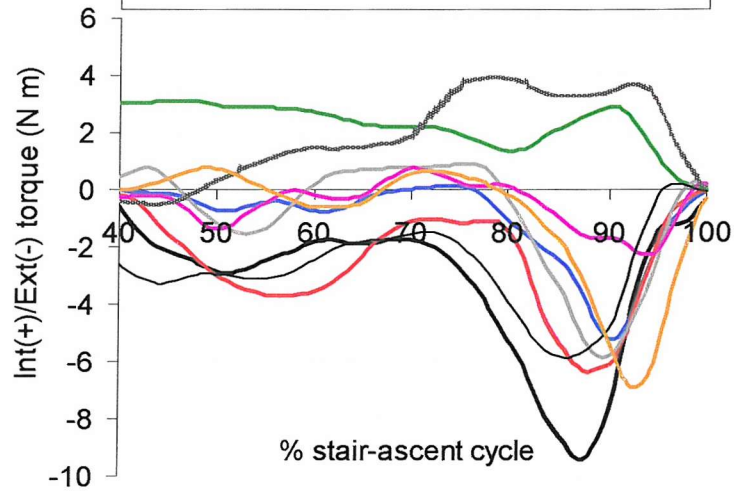

Figure 7-2(d)

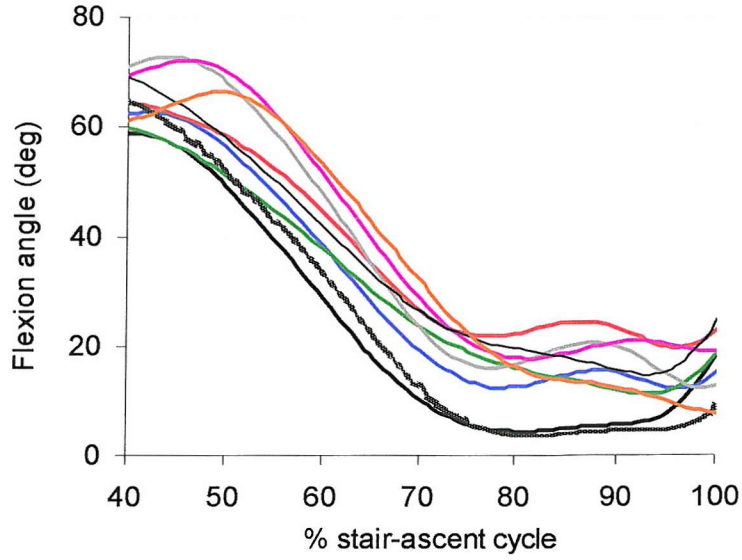

Figure 7-2: The variations of :(a) axial forces; (b) A-P forces; (c) I-E torques and (d) flexion-extension angles for 9 healthy elderly subjects during stair ascent activity. Simulations were concentrated during the stance phase of stair ascent cycle. S: subject

Figure 7-3

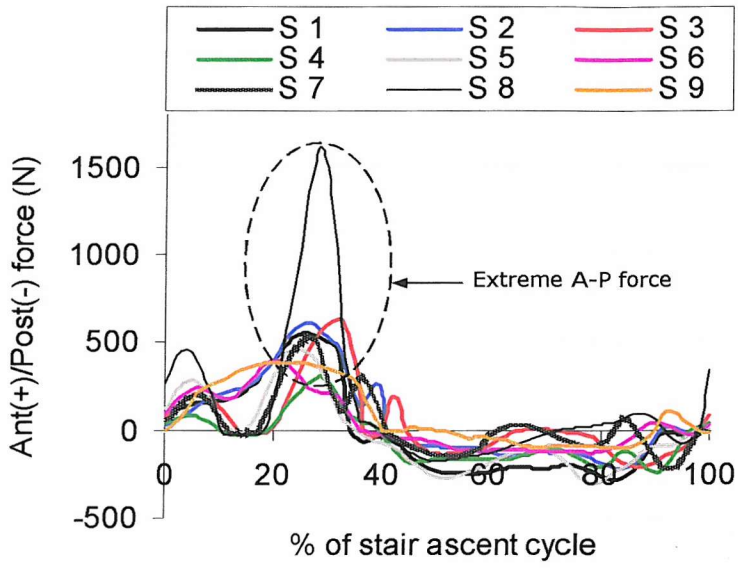

Figure 7-3: A-P forces for 9 subjects during a full stair ascent cycle.

Equilibrium Position of the FE Knee Model

As some of the models were not at the equilibrium position (0° of flexion) anymore, for a given load case, the femoral component was moved to find its equilibrium position for each of the subjects. To find the equilibrium position, the femoral component was first flexed to the specific flexion angle. The femoral component was only allowed to translate in the proximal-distal and anterior-posterior directions. All other directions were constrained. The tibial component was constrained in all directions. Then, an axial force of 100 N was applied to the femoral component and was held for a period of time under this load. The femoral component translated and came in contact at the new deepest point at the bearing surface of polyethylene. Hence, the new equilibrium position was obtained. All kinematics data was then reported with respect to the equilibrium position.

Averaging Simulations Data

For each subject specific load case time histories of the anterior-posterior (A-P) displacements and the internal-external (I-E) rotations were calculated, as well as a time history of the maximum contact pressure and the maximum von Mises stress. For each load case of level gait and stair ascent, the average time history for each parameter has also been calculated, plus and minus one standard deviation, in order to determine the performance envelope.

7.3 RESULTS

7.3.1 Subject Specific Level Gait

The predicted kinematics and the average data for subject specific level gait simulations are shown in Figure 7-4 and Figure 7-5. The contact pressures and stresses are shown in Figure 7-6 and Figure 7-7.

All subjects exhibited a consistent pattern of A-P displacement as seen in Figure 7-4 (a). At the beginning of the gait cycle, the tibial component tended to translate posteriorly with respect to the femur and reached peak posterior displacement at approximately 20% of the gait cycle. Then, the tibial insert tended to move anteriorly, towards the initial starting position, as the stance phase progressed. Just prior to toe off (approximately 50% to 55% of the gait cycle), six out of the seven subjects had moved just anterior of the initial starting position, ranging from 0.5 mm to 2 mm. Overall, the A-P displacement ranged from + 2 mm to – 3.6 mm. When the A-P displacement data was averaged, Figure 7-4 (b), a standard deviation from the mean of 0.5 mm – 1 mm for the A-P displacement was estimated.

Figure 7-4(a)

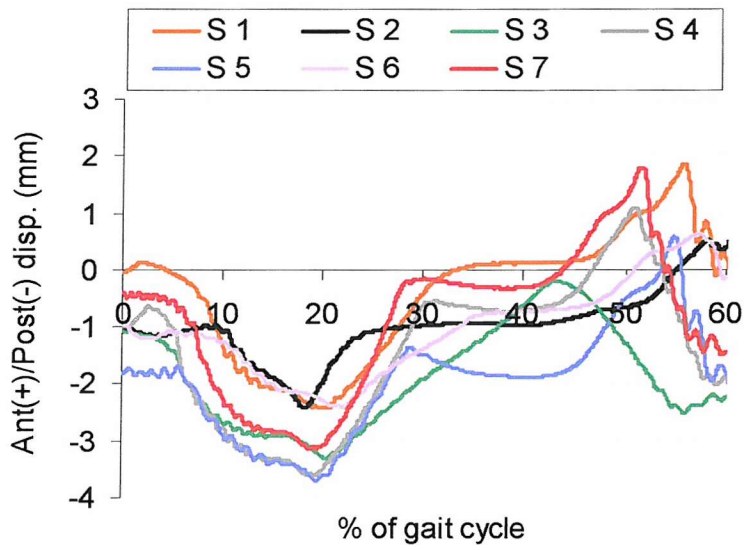

Figure 7-4(b)

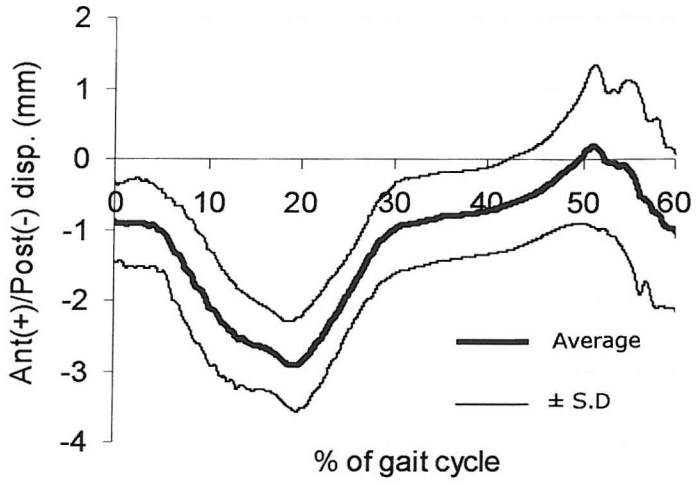

Figure 7-4: a) the predicted A-P displacements, and b) the calculated averages and the standard deviations for subject specific level gait study, for HLS model.

There was a consistent pattern of I-E rotations and ranged from external 5.7º to internal 3º during the stance phase of level gait (Figure 7-5 a). From the predicted I-E rotations, the tibial insert tended to externally rotate with respect to the femoral component from the beginning to approximately 57% of the gait cycle. Then, the tibial component tended to rotate internally, towards the initial starting position. Six subjects, except subject 2, exhibited peak external rotation between 50% and 57% of the gait cycle. Subject 2 exhibited the peak external rotation of 2.9° at about 26% of the gait cycle. When examining the averaged I-E rotation data (Figure 7-5 b), there is little variation in the I-E rotation within the group. A typical standard deviation from the mean ranged from 0.4º to 2.3º was estimated

Figure 7-5(a)

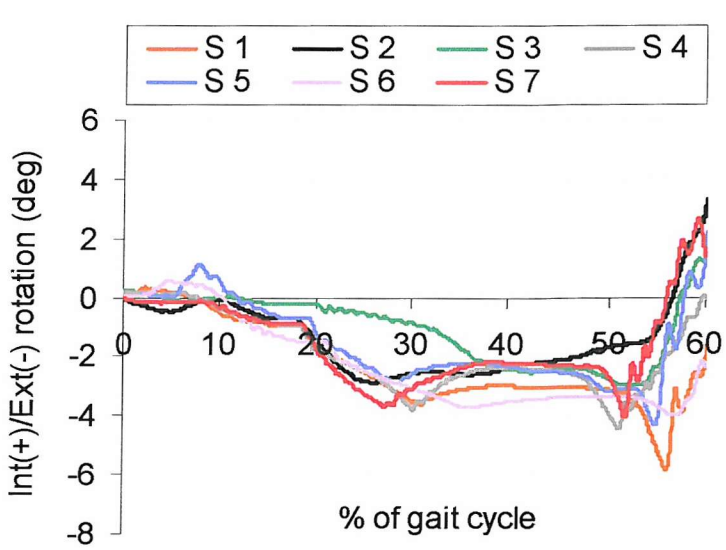

Figure 7-5(b)

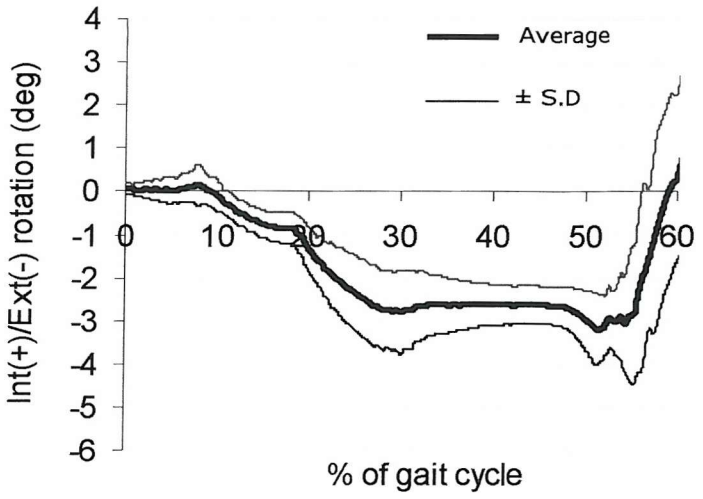

Figure 7-5: a) the predicted I-E rotations, and b) the calculated averages and the standard deviations for subject specific level gait study, for HLS model.

In general, the contact pressures showed consistent patterns (Figure 7-6 a), with three peaks occurring, one just after heel strike (0% to 5% of the gait cycle), a second between 10% and 20% of the gait cycle and the third prior to toe off at 40% and 60% of the gait cycle. In general, the third peak was always the largest, with peak contact pressures varying from 15 MPa to 25 MPa. Overall, the variation of contact pressures ranged from 7 MPa to 25 MPa. When examining the averaged contact pressure data for all subjects (Figure 7-6 b), the standard deviation from the mean varies from 1 MPa to 5 MPa.

Figure 7-6(a)

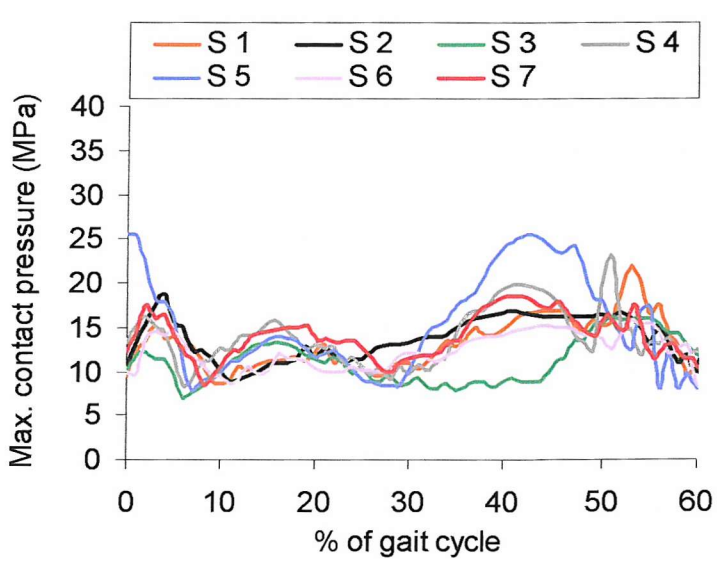

Figure 7-6(b)

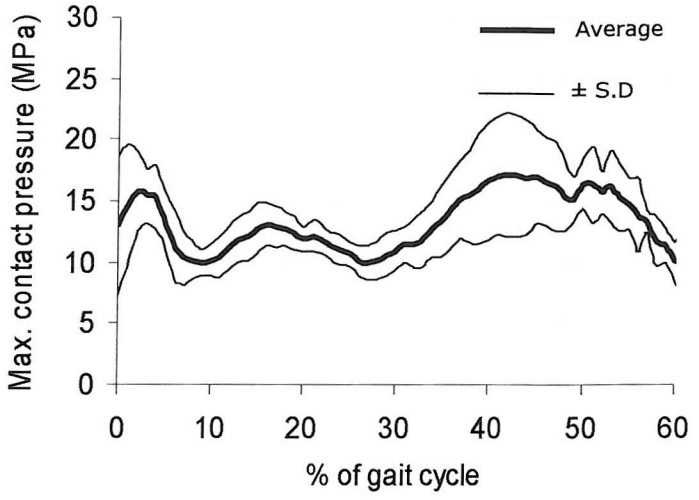

Figure 7-6: a) the resultant maximum contact pressures, and b) the calculated averages and the standard deviations for subject specific level gait study, for HLS model.

There was a general trend in the predicted maximum von Mises stresses and followed the same general trend as observed in the contact pressure prediction (Figure 7-7 a). Three peaks were observed, with the first occurring between 0% to 5% of the gait, the second occurring between 10% and 20% of the gait and the third between 40% and 50% of the level gait cycle. There were some peaks in the von Mises data occurring between 50% and 60% of the gait. These peaks were probably due to the sudden changed in the tibial rotation from external to internal. The variation in the von Mises stresses (between the three main peaks) was estimated to range from 7 MPa to 21 MPa. Averaging the maximum von Mises stresses data produced less variation in the stresses within the group. Overall, during the stance phase, a ± 0.5 MPa – 4 MPa range of von Mises stress was observed.

Figure 7-7(a)

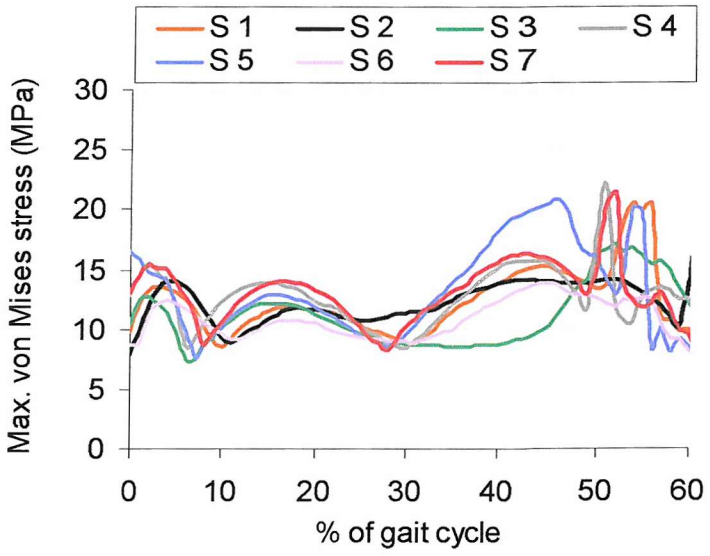

Figure 7-7(b)

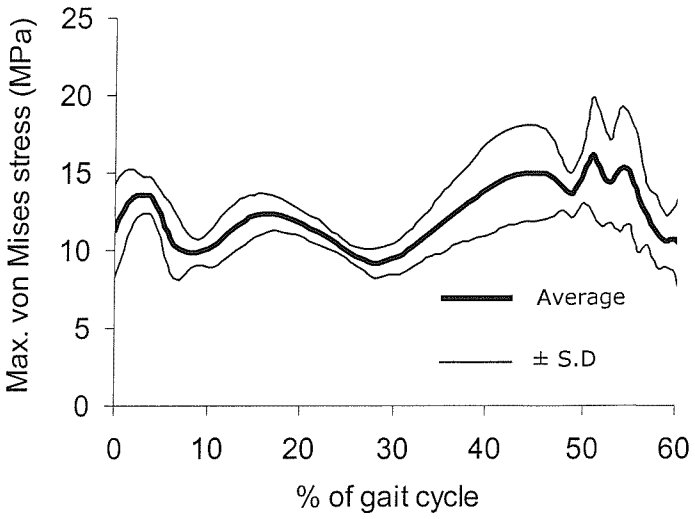

Figure 7-7: a) the predicted maximum von Mises stresses, and b) the calculated averages and the standard deviations for subject specific level gait study, for HLS model.

7.3.2 Subject Specific Stair Ascent

The predicted kinematics and the averaged data are shown in Figure 7-8 and Figure 7-9. The contact pressures and von Mises stress are also reported and are shown in Figure 7-10 and Figure 7-11. For stair ascent activity, only the stance phase of stair ascent cycle, i.e. between 40% and 100% of the activity cycle was simulated.

During the stance phase of stair ascent cycle, all the subjects tended to move posteriorly early in the stance phase, with a posterior displacement varying from 2 mm to 5 mm (Figure 7-8 a). The tibia tended to stay posteriorly during the majority of the stance phase, before moving anteriorly just prior toe-off. Transients were observed at the first 10% of the stair ascent stance phase but tended to settle from 50% of the stair ascent cycle. The analysis for subject 9 did not complete the stance phase. Coupled with the high A-P force (110 N) and I-E torque (7 N m), these forces pushed the tibial component forward and at 90% of the stair ascent cycle, the axial force of subject 9 was too small (approx. 700 N) and not able to hold the femoral component in place. As a result, the femoral component subluxed from the posterior edge of the tibial component. From the averaged data (Figure 7-8 b), a standard deviation from the mean ranged from 0.6 mm to 2.7 mm for the A-P displacements was estimated. It should be noted that Subject 9 was ignored and not included into the averaged data, as it did not complete the stair-climbing activity. In comparison to level gait, stair accent showed significantly higher standard deviations from the mean data for A-P translations.

Figure 7-8(a)

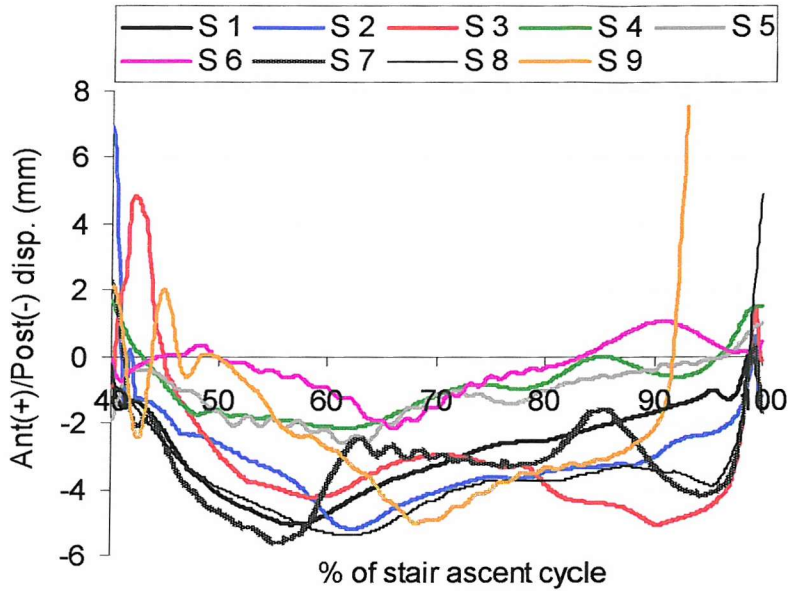

Figure 7-8(b)

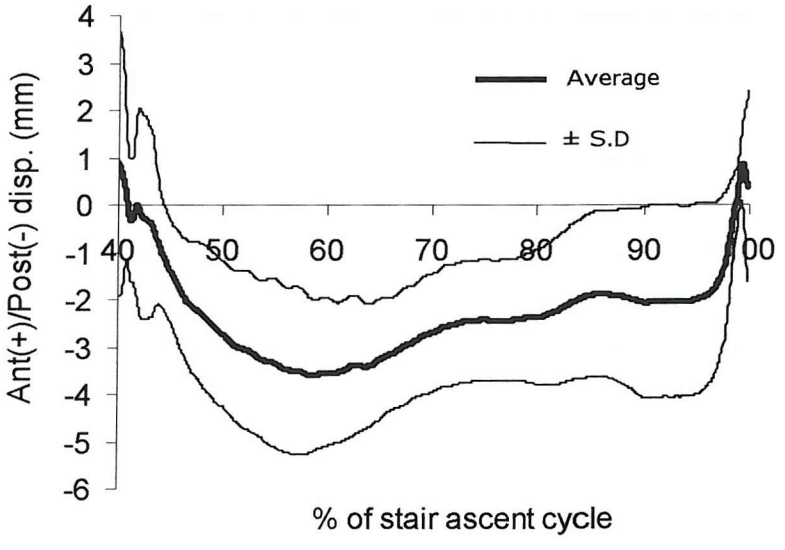

Figure 7-8: a) the predicted A-P displacements, and b) the calculated average and the standard deviations, for subject specific loading during stair ascent activity, for HLS model.

There was no consistent pattern in the predicted I-E rotations (Figure 7-9 a). Seven of the nine subjects showed external rotation of the tibia with respect to the femur and two internally rotated. It should be noted that one subject (subject 9) subluxed due to excessive external rotation at approximately 90% of the stance phase of activity cycle. On average, a 10° variation in the I-E rotations was observed throughout the stair ascent stance phase. Some subjects exhibited an internal tibial rotation with respect to the femur of up to 5°, whilst others externally rotated up to 5°. A few knees showed extreme rotations, for example external rotation of more than 10°. When compared to level gait, stair ascent exhibited higher variation in the I-E rotations. When the I-E rotation data was averaged (8 subjects), Figure 7-9 b, a ± 0.8° - 4.5° range of I-E rotation was observed

between 40% and 90% of the stair ascent cycle. This range double the range observed during level gait.

Figure 7-9(a)

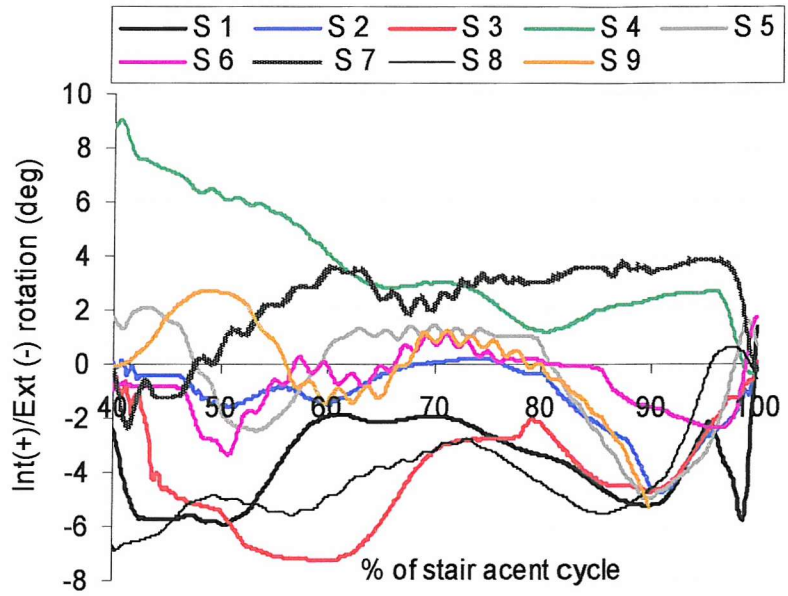

Figure 7-9(b)

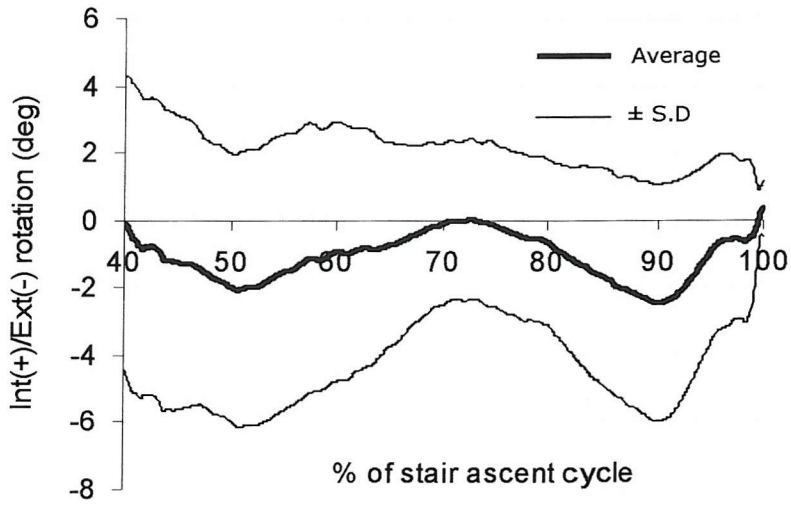

Figure 7-9: a) the predicted I-E rotations, and b) the calculated average and the standard deviations, for subject specific loading during stair ascent activity, for HLS model.

In general, there were two peaks in the contact pressures data during the stance phase (Figure 7-10 a), the first occurring just after heel strike, between 40% and 55% of the stair ascent cycle and the second just prior to toe-off, typically 85% to 90% of the stair ascent cycle. The second peak was generally higher than the first, ranging from 20 MPa to 40 MPa. Subject 1 and subject 9 showed extreme contact pressure values of 41 MPa and over 50 MPa, respectively. Again, as compared to level gait, the averaged contact pressure data has considerable higher standard deviations from the mean, ranging from

1.5 MPa in the early stance phase to 9.4 MPa in the latter stages. Contact pressures from subject 9 were ignored and only contact pressures from subject 1 to subject 8 were taken into account for averaging.

Figure 7-10(a)

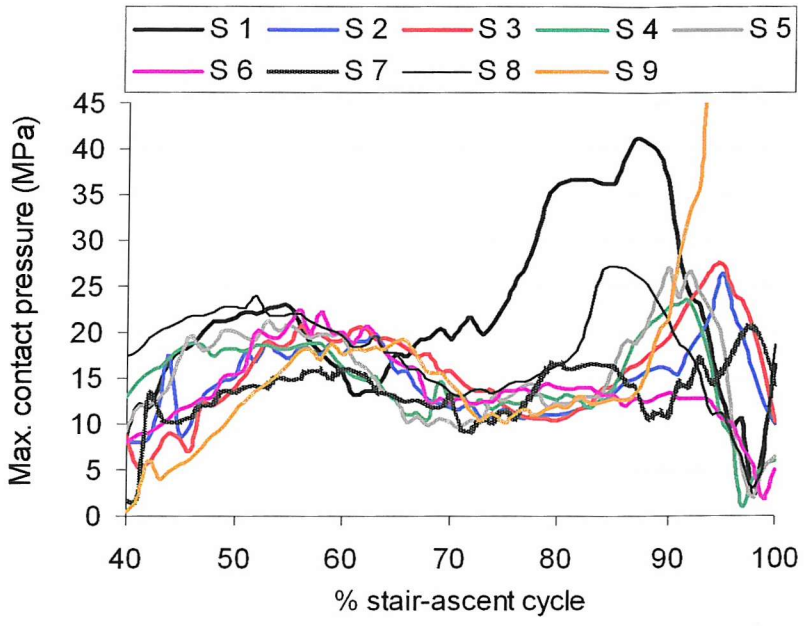

Figure 7-10(b)

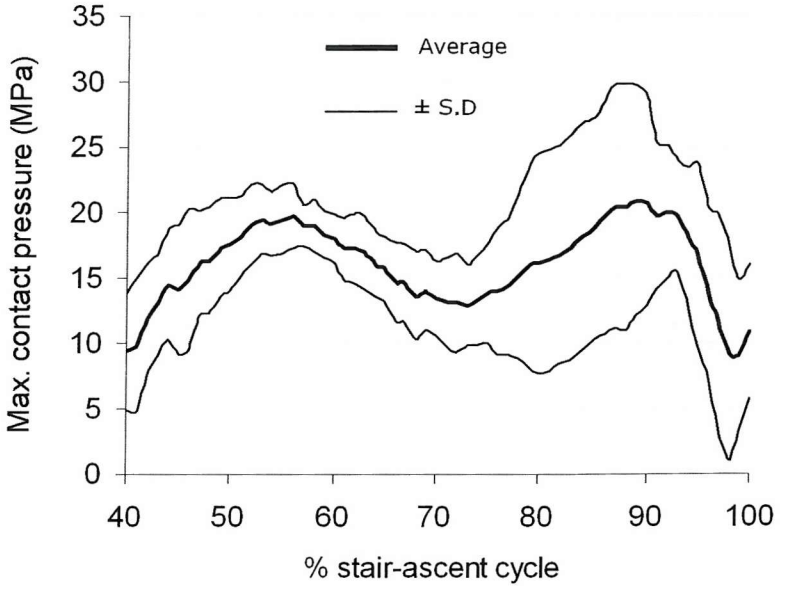

Figure 7-10: a) the predicted maximum contact pressures, and b) the calculated average and standard deviations for subject specific loading during stair ascent activity, for HLS model.

In general, there was consistent pattern in the predicted von Mises stresses again with two peaks occurring, one between 45% and 55% of the stair ascent cycle and a second between 80% and 90% of the stair ascent cycle (Figure 7-11 a). The first peak had peak maximum von Mises stresses varying from 15 MPa to 24 MPa, while the second peak varying from 14.5 MPa to 23 MPa. The von Mises stress does not go higher than 25 MPa due to the material property that was assigned to the polyethylene, i.e. as yielding of the polyethylene is occurring. From the averaged data plot (Figure 7-11 b), a ± 1.6 MPa – 4.6 MPa range of stress value was estimated within the group during stair ascent activity (subject 9 being ignored).

Figure 7-11(a)

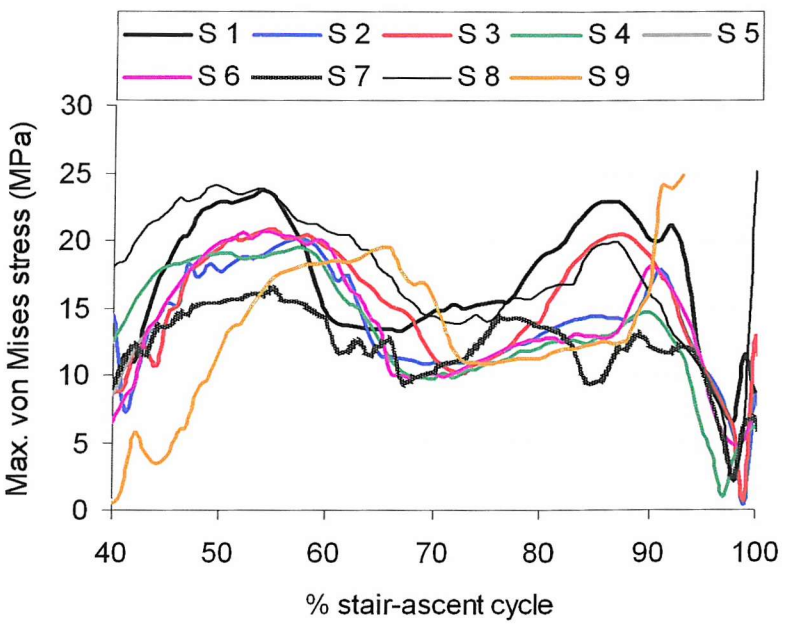

Figure 7-11(b)

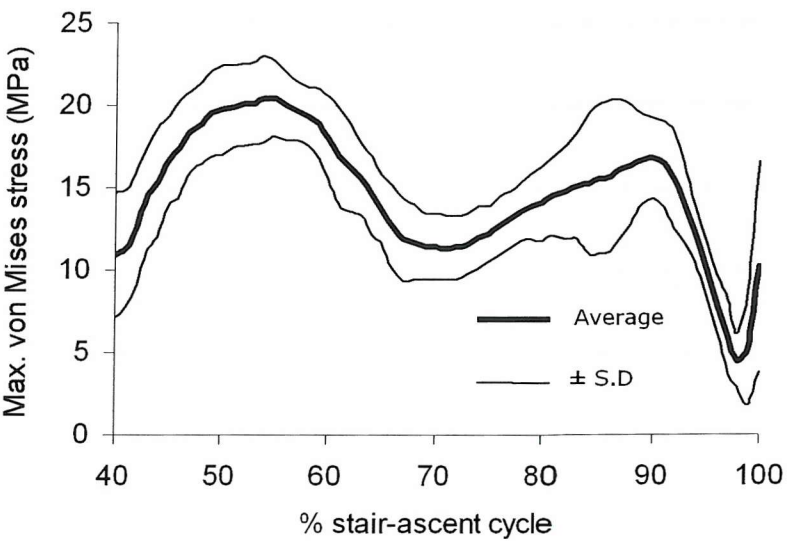

Figure 7-11: a) the predicted maximum von Mises stress, and b) the calculated average and standard deviations, for subject specific loading during stair ascent activity, for HLS model.

7.4 SUBJECT SPECIFIC SIMULATIONS WITH AN IMPROVED LIGAMENT MODEL

In this section, more realistic posterior cruciate ligament (PCL) and collateral ligaments were modelled and added to the PFC Sigma knee model and the PLI knee model. The PLI model is also examined. In section 6.2 of Chapter 6, early improvements had been made to the FE knee model by adding the medial and lateral collateral ligaments. These ligaments were modelled as membrane elements. The femoral origin sites and the tibial insertion sites were positioned in a way that both were parallel and vertical, and the femoral origin sites were co-planar with the femoral component flexion-extension axis. The posterior cruciate ligament was not modelled. In this section, the material properties and origins and insertion locations for the ligaments were adapted from the literature [1,164]. The two knee designs are those that preserve the PCL, hence, the PCL was modelled.

In the present analysis, the ligamentous structures were represented by bar elements extending from the femoral origin to the tibial insertion. The posterior cruciate ligament (PCL) and medial collateral (MCL) were divided into several fibre bundles. The PCL was divided into anterior and posterior fibre bundles, while the MCL was treated as three separate bundles: anterior, oblique and deep. The LCL was represented using a single bundle. Each ligament and each fibre bundle were modelled as a spring with parabolic and linear regions as represented by formulae shown below, where k_1 and k_2 are the stiffness coefficients of the spring element for the parabolic and linear regions, respectively, and, L and L_0 are its current and slack lengths, respectively. The linear range threshold was specified as $\varepsilon_1 = 0.03$.

$$F = \begin{cases} 0 & \varepsilon \le 0 \\ k_1 (L - L_0)^2 & 0 < \varepsilon \le 2\varepsilon_1 \\ k_2[L - (1 + \varepsilon_1) L_0] & 2\varepsilon_1 < \varepsilon \end{cases}$$

The ligament elements were assumed to carry load only when they are in tension, that is when their length is longer than their slack, unstrained length L_0. Ligaments exhibit a region of non-linear force-elongation relationship, the 'toe' region, in the initial stage of ligament strain, and then a linear force-elongation relationship in later stages. An example of force-strain curve for one of the ligament fibre bundles - the MCL-D fibre bundle is shown in Figure 7-12. A force-strain curve for each ligament fibre bundle was created and used as input in Pam–Generis to represent the material property of each ligament. Values of the stiffness coefficients of the spring elements used to model the different ligamentous structures; the origins (x, y, z) and insertions (x', y', z') are shown in Table 7-3. From Table 7-3, when examining the ligaments extension ratio (length of fibre at full extension, L_1 vs. length of fibre at slack, L_0), all fibre bundles except the MCL-A are in 'pre-tensioned' state

(extension ratio more than 1). The MCL-A is slack at full extension (extension ratio smaller than 1).

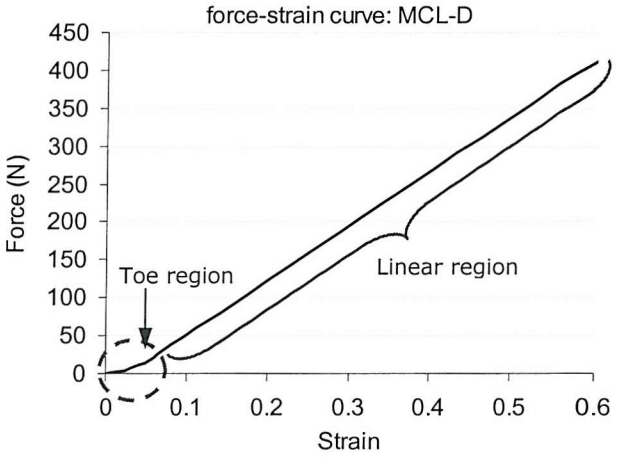

Figure 7-12: Force-strain curve for MCL-D fibre bundle.

The size of the total knee replacement components used in this study is different from those in the literature [164]. Hence, the ligaments position created from the available data in Table 7-3, have been amended by approximation either to slightly anterior or posterior position, proximal or distal direction, to create a more reasonable ligaments position. The PFC PLI knee replacement with bar elements ligaments is shown in the Figure 7-13.

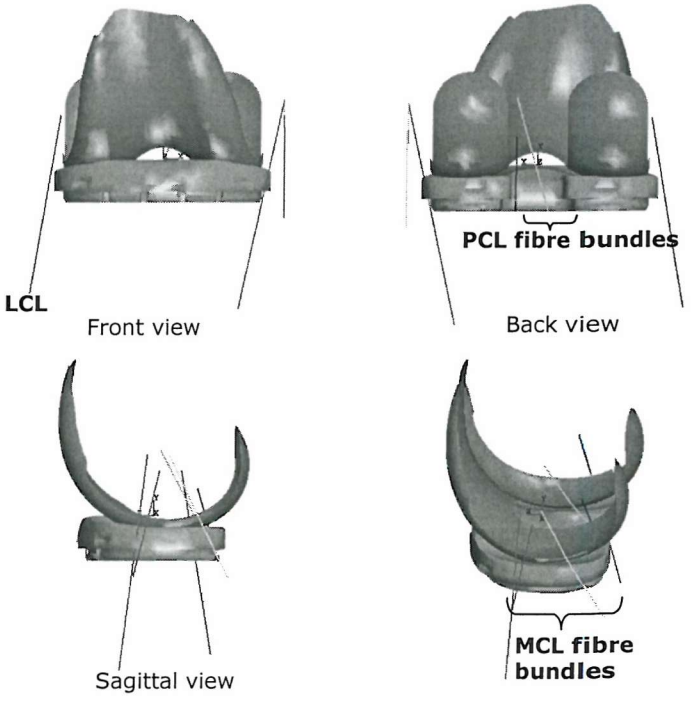

Figure 7-13: PFC PLI knee model with the PCL, MCL and LCL. These ligaments are modelled as bar elements.

Ligament and the fibre bundles	x	y	z	x′	y′	z′	L_1	L_0	k_1	k_2	Extension ratio, e
PCL											
PCL-A	-4.375	22.8	5.8	5.375	1.5	-13	30.037	29.917	31.26	125.00	1.004
PCL-P	-4.375	24.4	-6.2	-4.625	1.5	-13	23.890	22.752	19.29	60.00	1.05
MCL											
MCL-A	-34.375	35	16	-19.625	-33.5	21	70.248	74.732	10.00	91.25	0.94
MCL-O	-34.375	35	9	-34.625	-5.5	-13	44.343	43.010	5.00	27.86	1.031
MCL-D	-34.375	30	12	-34.625	-5.5	17	35.851	34.177	5.00	21.07	1.049
LCL	35.625	30	2	45.375	-28.5	-8	60.144	57.280	10.00	72.22	1.05

Table 7-3: The origins (x, y, z) and insertions (x′, y′, z′) of the ligaments' fibre bundles. L_0 is the ligament slack length; L_1 is the length when the knee is 180° on the lowest contact point (or full extension); k_1 and k_2 are the stiffness of coefficients of the spring elements [164].

7.4.1 ISO Standard Load Case

Before presenting the results of subject specific loading study using the PFC Σ design and PLI design with ligaments, both of these models were tested under ISO standard load case. The purpose of this simulation was to examine the influence of ligaments on the performance of PFC Σ knee by comparing the predicted kinematics and contact pressures with the HLS PFC Σ knee model (with the soft tissues being represented by a pair of horizontal springs). Also, this simulation also examined the validity of the PLI knee model. The predicted kinematics and contact stresses are presented in Figure 7-14.

From Figure 7-14 (a), the PLI knee exhibited posterior tibia translation with respect to the femur at the beginning of the gait cycle and reached peak posterior displacement of 2 mm, at 6 % of gait cycle. Then, the tibia moved anteriorly and at approximately 25% of the gait cycle, the tibia moved posteriorly. At 57.5% of the gait cycle, the model once again translated towards anterior direction and passed through the initial starting position. The peak anterior displacement was 6.6 mm, occurred at 74.5% of the gait cycle. After the peak anterior translation, the model again moved posteriorly.

PFC Sigma ligaments model started with posterior displacement of the tibia relative to the femur at the first 10% of the gait cycle. Then, between 10% and 18% of the gait cycle, the tibia translated anteriorly. From 18% to 60% the gait cycle, the tibia displaced posteriorly and reached peak posterior displacement of 2.9 mm, at 60% of the gait cycle. Then, the tibia moved anteriorly and reached peak anterior displacement of 3.8 mm at 80% of the gait. Between 80% and 100% of the gait cycle, it then translated posteriorly and just passed the initial starting position. The A-P displacements trend between PFC Σ ligaments model and HLS model was fairly similar during the stance phase of gait cycle. Big difference in the A-P displacements during the swing phase, i.e. from 70% onwards was observed. The peak posterior displacement of the PFC Σ HLS model was approximately 3.9 mm, occurring just before toe-off (59% of the gait cycle). There was a 1 mm reduction in posterior translation in PFC Sigma knee with the ligaments. During the swing phase, i.e. from 60% to 100% of the gait cycle, the HLS model moved anteriorly and stayed at the initial starting position. The ligaments model moved anteriorly but did not stay at the initial starting position. It was probably the ligaments tried to pull the tibia in the anterior direction.

From Figure 7-14 (b), the PLI model experienced internal tibia rotation with respect to the femur at the first 10% of the gait cycle. From 23% to 50% of the gait cycle, the tibia rotated externally. The peak external rotation was approximately 9.2°, occurred at 50% of the gait cycle. Then, the PLI knee rotated internally and reached the peak internal rotation of 6.8°, at 77% of the gait cycle. From 77% till the end of the gait cycle, the PLI knee

rotated externally towards the initial starting position. PFC Σ ligaments model and HLS model exhibited fairly similar trend of I-E rotations during the stance phase of gait cycle. The ligaments model first internally rotated and from 15% to 64.5% of the gait cycle, the tibia rotated externally with respect to the femur. The peak external rotation was 5°. Similarly, the HLS model first internally rotated and from 10% to 60% of the gait cycle, the tibia externally rotated relative to the femur. The peak external tibia rotation was fairly similar to the ligaments model, estimated at 4.8°. During the swing phase, HLS model tended to stay at the slightly externally rotation, 0.7° from the initial starting position. However, the ligaments model rotated internally and passed the starting position. The peak internal rotation observed was 3.7°, at 80% of the gait cycle. Then, the tibia of the ligaments model externally rotated and returned to the initial starting position just before heel-strike. From the I-E rotations plot, the PLI knee exhibited larger I-E rotations as compared to the other two models. This is due to lower constraint of the PLI design.

The maximum contact pressures of the PLI knee were generally higher than the PFC Sigma knee models (Figure 7-14 c). The peak maximum contact pressure for the PLI was 38.9 MPa, occurring at 52% of the gait cycle. The contact pressures between PFC Σ ligaments model and HLS model were fairly similar during the stance phase of gait. The peak contact pressure for the ligament model and HLS model was 22.6 MPa and 22.3 MPa, respectively. Significant differences in the contact pressures were observed between the ligaments model and the HLS model during the swing phase. For the ligaments model, the contact pressures were maintained at approximately 15.3 MPa from 60% to 83% of the gait cycle, before decreasing to 6 MPa at the end of the swing phase. For HLS model, the contact pressures were kept at approximately 4.5 to 7 MPa throughout the swing phase. The ligaments tended to hold the femoral condyle and the tibial insert tighter in the ligaments model and created higher contact pressures during the swing phase.

As expected, PLI knee exhibited very high von Mises stresses. The peak von Mises stress recorded was 25 MPa. This indicated that the polyethylene insert yielded and plastically deformed (yielding starts at 15 MPa). The maximum von Mises trend for PFC Σ ligaments model and HLS model was fairly similar during the stance phase of gait. The peak von Mises stress for the ligaments model was 19 MPa, whereas for HLS model was 17.5 MPa. Again, significant differences were observed during the swing phase of gait between these two models. The ligaments model exhibited stress value between 15 MPa and 17.5 MPa, from 60% to 83% of the gait cycle. The von Mises stress then decreased gradually to 7 MPa at the end of the gait cycle. For HLS model, the von Mises stress ranged from 5 to 10 MPa, throughout the swing phase of gait.

This simulation showed that for PFC Σ knee, there were no significant differences in the kinematics and contact pressures when compared between the HLS model and ligaments model, typically during the stance phase of gait cycle.

Figure 7-14(a)

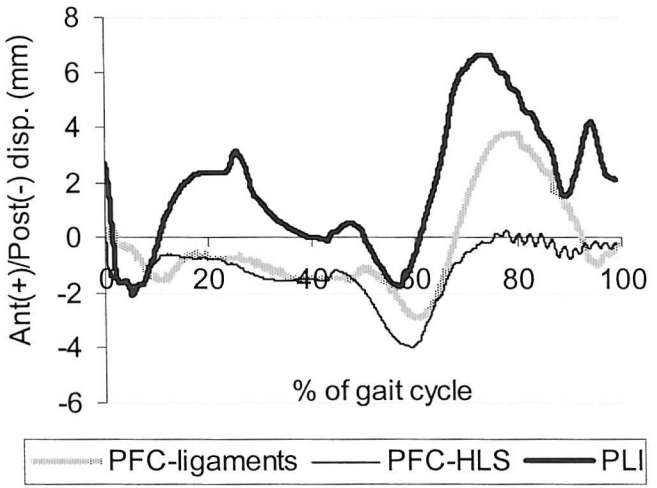

Figure 7-14(b)

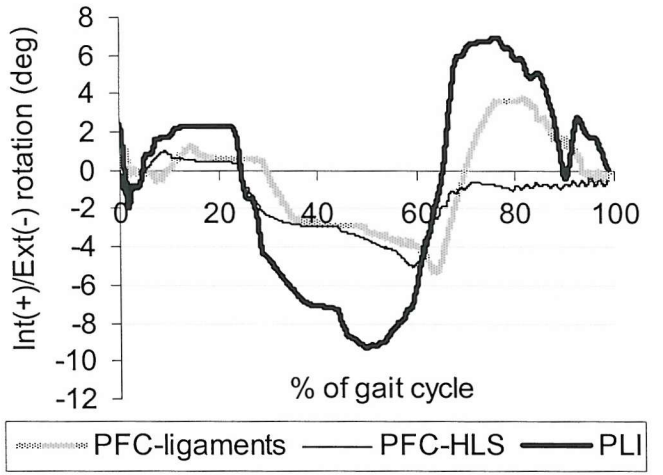

Figure 7-14(c)

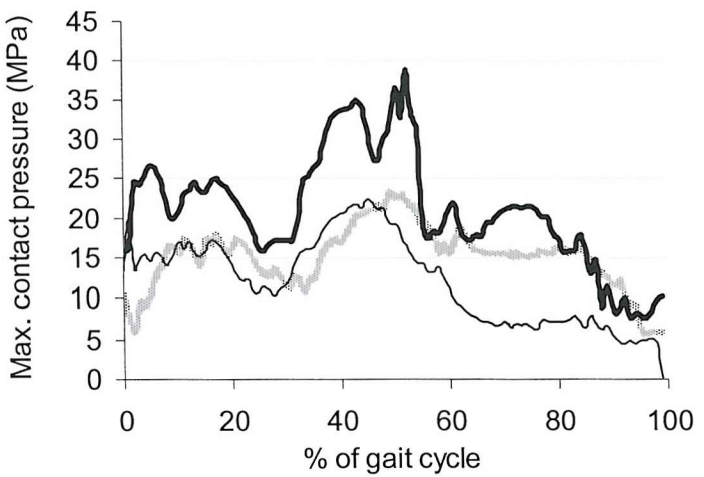

Figure 7-14(d)

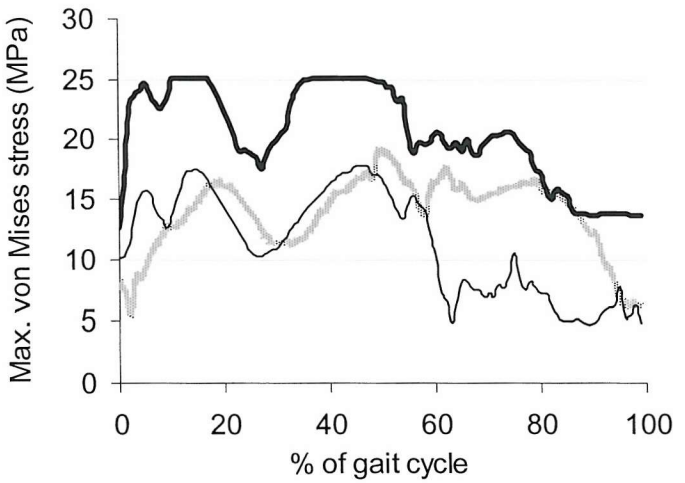

Figure 7-14: The predicted: a) A-P displacements; b) I-E rotations; c) maximum contact pressures; and d) maximum von Mises stresses, for PFC Σ ligaments model, HLS model and PFC PLI model (with ligaments).

Contact Pressure Distributions: Comparisons Between PFC Σ and PLI Models

From Figure 7-14 (c), PLI ligaments model was observed to generate very high contact pressures as compared to the PFC Σ ligaments model. Several instances within of gait cycle for PLI ligaments model and PFC Σ ligaments model are chosen and shown in Figure 7-15. Comparisons are made between the two models.

At the beginning of the gait cycle, both condyles for PFC Σ models (HLS and ligaments) were at slightly posterior position from the middle of the condyles. The peak contact pressure at 5% of the gait cycle was approximately 10 MPa. As the gait cycle proceeded to 15% of the gait cycle, the contact pressures increased. From Figure 7-14 (c), the first peak of the contact pressures occurred between 12% and 20% of the gait cycle. The contact pressure at 15% of the gait cycle increased from 10 MPa to 17.3 MPa. The condyles stayed at similar position as where the starting position was. Then, the medial condyle translated posteriorly and the lateral condyle displaced anteriorly as the gait cycle progressed from 15% to 35 of the gait cycle. The contact pressures decreased at this stage. At 45% of the gait cycle, the medial condyle remained the similar position but the lateral condyle further displaced to anterior edge of the tibial insert. When examining the contact pressures plot, there was an increased in the contact pressure and the 2nd peak occurred at approximately 50% of the gait cycle. At 45% of the gait cycle, the contact pressure was 20.9 MPa. When the gait cycle proceeded to 65% of the gait cycle, the medial condyle translated to posterior edge of the tibial insert and the lateral condyle moved to the position where it started. The contact pressures decreased from 20.9 MPa to 16 MPa. During the swing phase, i.e. 85% of the gait cycle, the medial condyle moved slightly in an anterior direction. The lateral condyle moved to the very posterior edge of the tibial insert. The tibial insert rotated internally. The contact pressures reduced at the end of the swing phase.

For PFC PLI ligaments model, at the beginning of the gait cycle, both condyles were at slightly anterior position from the middle. The contact pressures were significantly higher than PFC Σ ligaments model. At 5% of the gait cycle, the contact pressure was 26.7 MPa. From 5% to 15% of the gait cycle, the medial and lateral condyles moved posteriorly and the contact pressures increased. From Figure 7-14 (c), the contact pressure between 13% and 20% of the gait cycle was 25 MPa. As the gait cycle proceeded from 15% to 35% of the gait cycle, the medial condyle remained at similar position and the lateral condyle displaced to an anterior inner edge of the tibial insert. The contact pressures decreased as the axial force decreased. Then, the contact pressures gradually increased with the axial force as the gait cycle advanced from 35% to 45%. The peak contact pressure recorded for the whole gait cycle was 38.9 MPa, at 52% of the gait cycle. During the swing phase, both condyles translated to a posterior position and the contact pressures decreased consistently till the end of the gait cycle.

PFC Σ knee has higher conformity than PLI knee. The contact pressures for PFC Σ ligaments model were more consistent and the contact areas were larger than PFC PLI ligaments model, as observed from Figure 7-15.

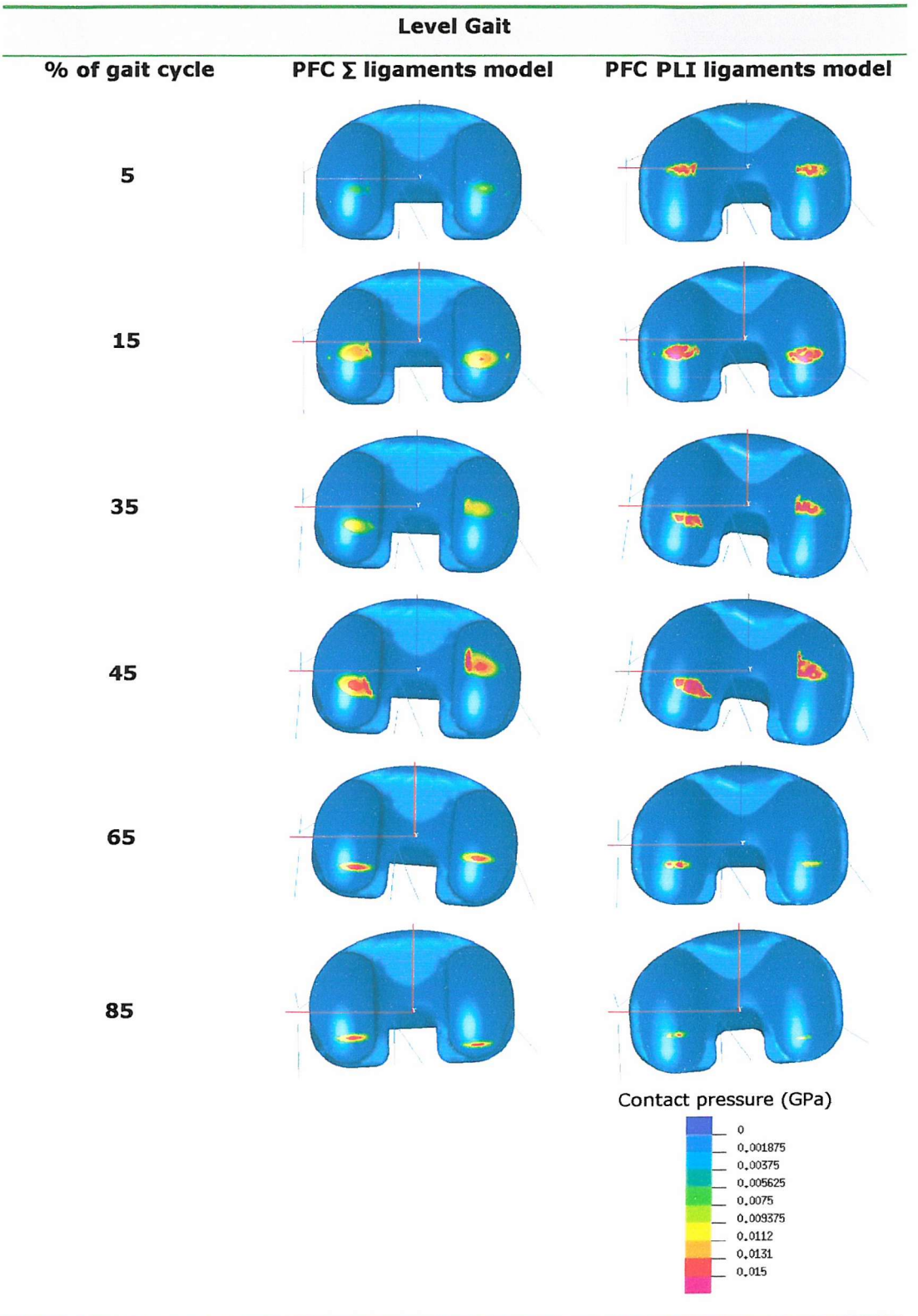

Figure 7-15: Contact pressure distributions for PFC Σ ligaments model and PFC PLI ligaments model.

7.5 RESULTS – SUBJECT SPECIFIC LEVEL GAIT

7.5.1 PFC Σ Ligament Model

The predicted kinematics and the calculated average data are presented in Figure 7-16 and Figure 7-17. The maximum contact pressures and the maximum von Mises stress are shown in Figure 7-18 and Figure 7-19.

From Figure 7-16 (a), a consistent pattern of A-P displacement was observed. At the beginning of the stance phase gait cycle, the tibia tended to translate posteriorly relative to the femur and reached peak posterior displacement at approximately 20% of the gait cycle. Then, the tibia translated in the anterior direction, towards the initial starting position. At approximately between 50% and 60% of the gait cycle, four subjects had just moved anterior of the initial starting position. From Figure 7-16 (a), the peak posterior displacement of the tibia relative to the femur was 3.7 mm (from subject 4) and the peak anterior displacement was just over 2.0 mm (from subject 1). Overall, the A-P displacement ranged from + 2.0 mm to −3.7 mm. In comparison to HLS model, similar range of translations was observed, as discussed and shown in Figure 7-4 a, section 7.3.1. When the A-P displacement data was averaged (Figure 7-16 b), a standard deviation from the mean of 0.3 mm to 1.2 mm was calculated.

Figure 7-16 (a)

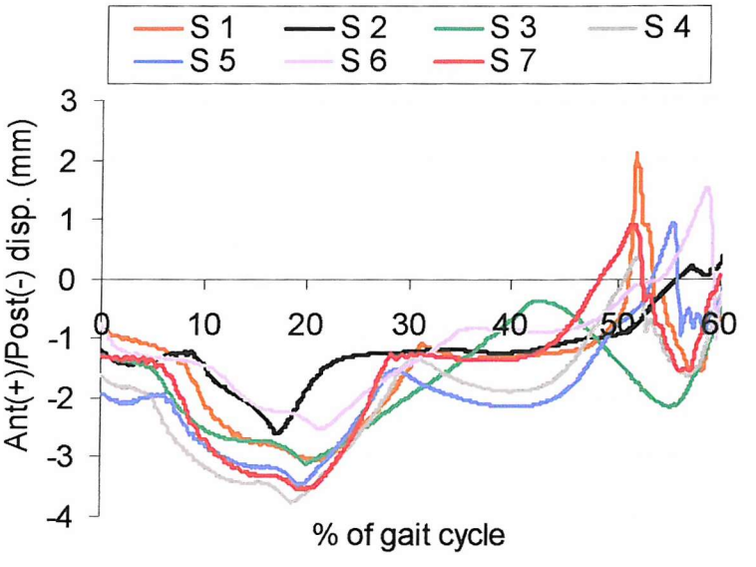

Figure 7-16 (b)

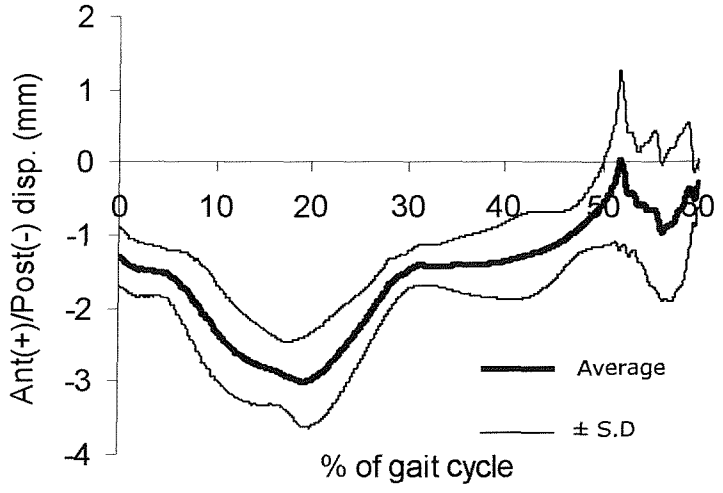

Figure 7-16: The predicted: a) A-P displacements, and b) the calculated average and standard deviations, for subject specific level gait, for PFC Σ knee ligaments model.

In general, a consistent trend of I-E rotation was observed for all the subjects (Figure 7-17 a). During level gait, all subjects experienced external tibia rotation relative to the femur from the beginning of the gait cycle to approximately 50% of the gait cycle. Then, the tibia internally rotated towards the initial starting position. Subject 1 exhibited slightly different I-E rotation pattern, typically between 30% and 50% of the gait cycle. For subject 1, the tibia rotated internally for 2° from the external position, from 30% to 35% of the gait cycle. Then, between 35% and 48% of the gait cycle, the tibia remained at external rotation position before further rotating in the external direction. The peak external rotation occurred just before toe-off, i.e. between 50% and 60% of the gait cycle and ranged from 2° - 6.8°. The overall I-E rotations ranged from - 6.8° to + 4.1° during the stance phase of gait cycle. By averaging the I-E rotation data (Figure 7-17 b), a typical standard deviation from the mean of 0.4° - 3.2° was estimated. This is a large variation as compared to the HLS model (Figure 7-5 b), which had a range of 0.4° - 2.3°. Both HLS model and ligament model exhibited a similar trend for I-E rotations.

Figure 7-17(a)

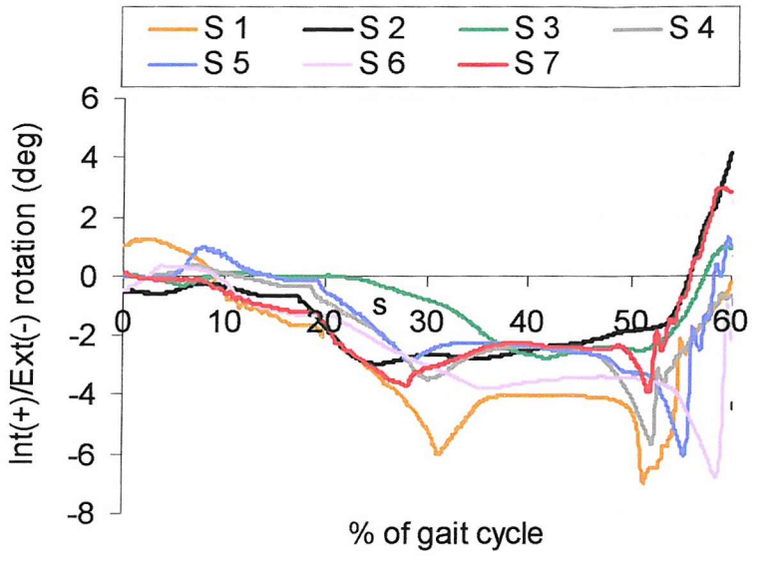

Figure 7-17(b)

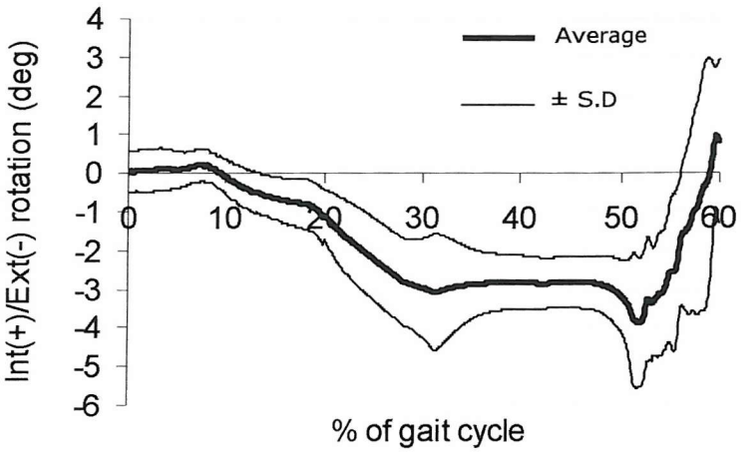

Figure 7-17: The predicted: a) I-E rotations, and b) the calculated average and standard deviations, for subject specific level gait, for PFC Σ ligaments model.

From Figure 7-18 (a), three peaks were observed in the contact pressures during the stance phase of gait cycle; one just after heel strike (0% to 5% of the gait cycle), a second between 10% and 20% of the gait cycle and the third between 35% and 45% of the gait cycle. The third peak was usually the largest. There were some transients in the data, typically between 50% and 60% of the gait cycle. This might be due to the sudden changed in the tibia rotation from external to internal, with respect to the femur. Subject 1 exhibited slightly different trend in the contact pressure. There were two sharp increases in the contact pressures, with the first sudden peak occurred at 32% of the gait cycle and estimated to be 31.8 MPa. The 2nd sudden increased occurred at 52% of the gait cycle and estimated to be 38.6 MPa. These increases were corresponded to the two peaks in the external rotations. Most of the contact pressures ranged from 10 MPa to 28 MPa. As compared to the HLS model (Figure 7-6 a), the maximum contact pressures for

HLS model were more consistent and fewer transients were observed in the data. When examining the averaged maximum contact pressure data (Figure 7-18 b), the standard deviation from the mean varies from 0.8 MPa to 8 MPa. This was significantly higher than the HLS model, which was ranged from 1.0 MPa to 5.0 MPa.

Figure 7-18(a)

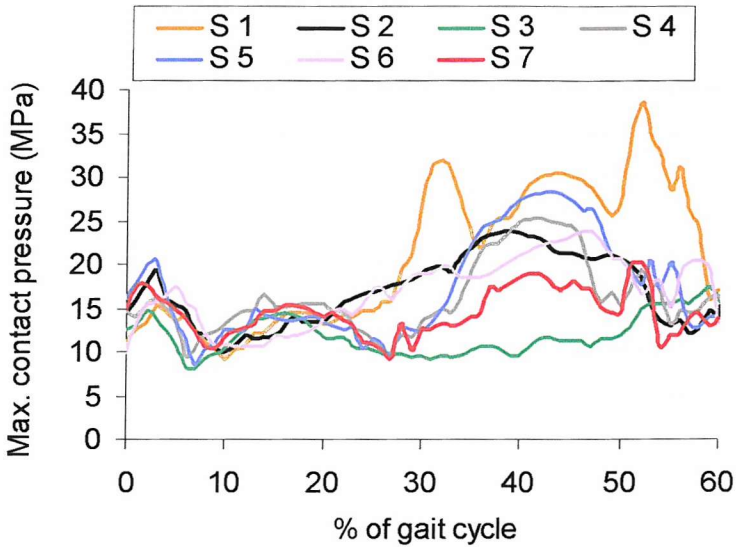

Figure 7-18(b)

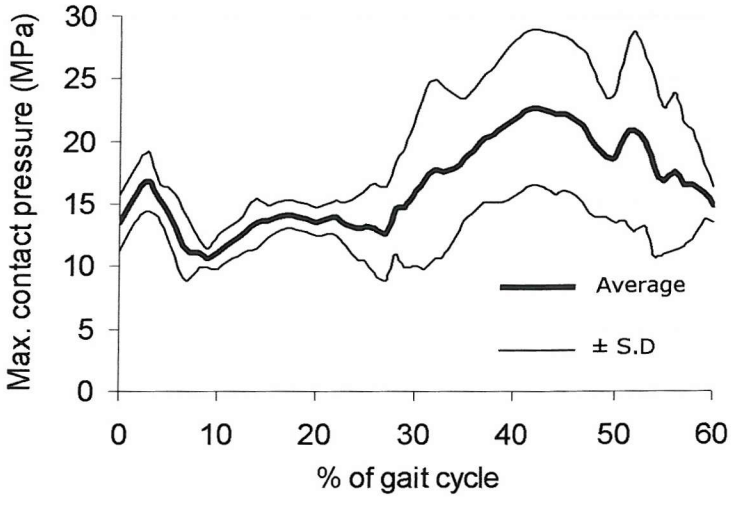

Figure 7-18: The predicted: a) maximum contact pressures, and b) the estimated average and standard deviations, for subject specific level gait, for PFC Σ ligaments model.

From Figure 7-19 (a), subjects 1, 4, 5, 6 and 7 showed the peak maximum von Mises stress of 25 MPa. Sudden increased in the von Mises was observed typically between 50% and 60% of the gait cycle. It was estimated to range from 15 MPa to 25 MPa. The possibility for these transients was the change in tibia rotation from external to internal, with respect to the femur. There is a general trend in the predicted maximum von Mises stress. Overall, the variation in the maximum von Mises stresses was estimated to range from 10 MPa – 25 MPa. The standard deviation from the mean of 0.9 MPa – 5.7 MPa for

the von Mises stress was estimated. In comparison with the HLS model (Figure 7-7 b), the range of von Mises stresses from the ligaments model were larger. The HLS model recorded a ± 0.5 MPa – 4 MPa range of von Mises stress

Figure 7-19(a)

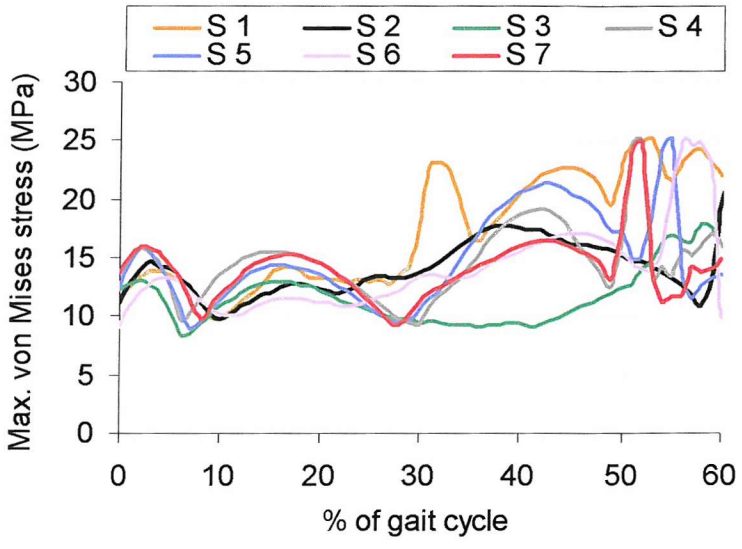

Figure 7-19(b)

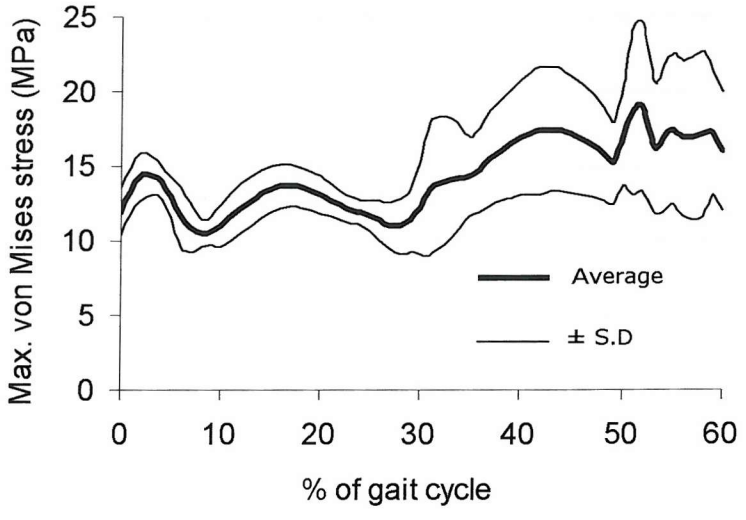

Figure 7-19: The predicted: a) maximum von Mises stresses, and b) the calculated average and standard deviations, for subject specific level gait, for PFC Σ ligaments model.

7.5.2 PFC PLI Ligament Model

The predicted kinematics, contact pressures and stresses are shown in Figure 7-20, Figure 7-21, Figure 7-22 and Figure 7-23. The calculated average and standard deviations for each of the parameters examined are also shown here.

Figure 7-20 (a) shows that with the PLI ligament model, not all subjects started at the same position. At the beginning of the gait cycle, subject 1 started at an anterior position of 2.3 mm. Subject 5 started at a posterior position of 2.9 mm. Five other subjects were observed to start at approximately similar position, near zero. However, a fairly consistent A-P displacement trend was observed for all the subjects. From 0% to 10% of the gait cycle, all subjects exhibited tibia anterior displacement, with respect to the femur. Then, the tibia displaced posteriorly. The peak posterior displacement occurred between 10% and 20% of the gait cycle. Subject 5 and subject 7 exhibited the highest posterior displacement, 3.1 mm, at 20% of the gait cycle. Then, the tibia translated anteriorly and passed the initial starting position (between 25% and 35% of the gait cycle). The tibia tended to stay at anterior position until approximately 50% of the gait cycle, several models further translated in the anterior direction just before toe-off. Subject 7 exhibited the highest anterior tibia translation of 7.4 mm. When examining the A-P forces plot (Figure 7-1 b), subject 7 was subjected to the peak anterior force at that stage. The variation in the A-P displacements was estimated to range from +8 mm to –3 mm (Figure 7-20 a). From the averaged data, a standard deviation from the mean of 0.6 mm – 2.3 mm was estimated (Figure 7-20 b). In comparison with the PFC model (Figure 7-16 b), PLI model exhibited larger range of A-P displacement.

Figure 7-20 (a)

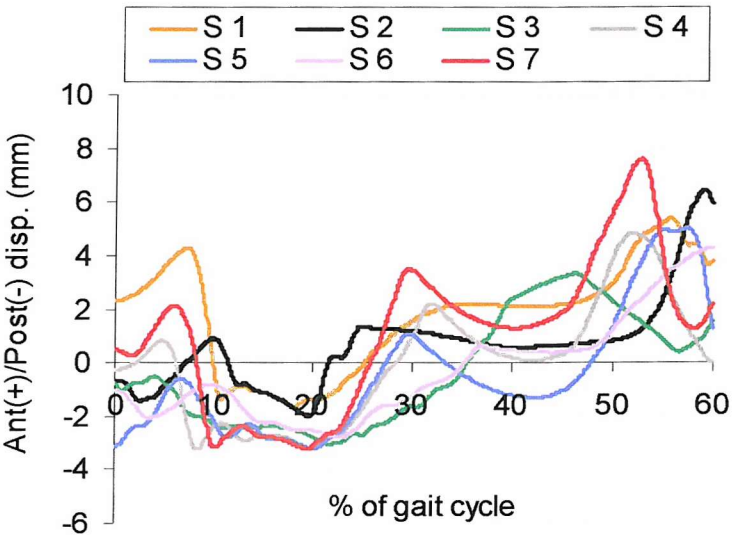

Figure 7-20(b)

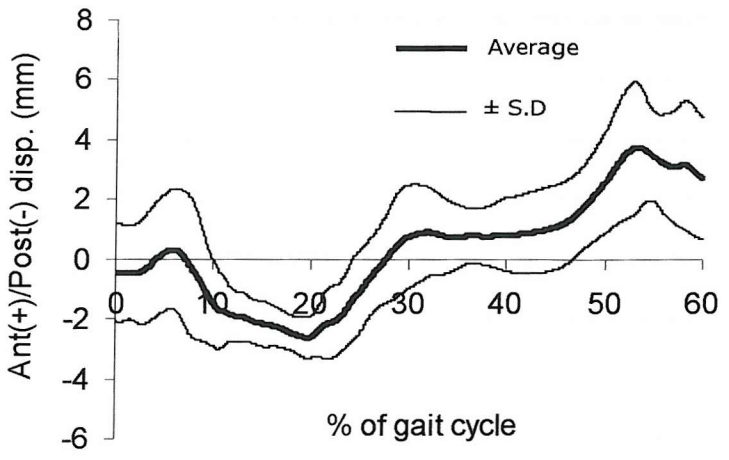

Figure 7-20: The predicted: a) A-P displacements, and b) the averaged data and standard deviations, for subject specific level gait, for PLI ligament model.

There was a similar trend in the I-E rotation data for all subjects (Figure 7-21 b). All subjects exhibited external tibia rotation with respect to the femur and tended to remain at external rotated position. Between 50% and 60% of the gait cycle, all subjects exhibited internal tibia rotation. Subject 1 exhibited a significantly larger external tibia rotation relative to the femur. The peak value predicted was 16.8°, occurring between 50% and 54% of the gait cycle. When examining the A-P forces (Figure 7-1 b) and I-E torques (Figure 7-1 c) plot, Subject 1 experienced an anteriorly directed force from 30% of the gait cycle onwards until 54% of the gait cycle. Couple with the peak external directed torque and high forces produced in the MCL-A and MCL-D fibre bundles, these had resulted in a significant external rotation in Subject 1. The variation of the I-E rotation was estimated to range from - 9° to + 8°. From the averaged I-E rotation data (Figure 7-21 b), a standard deviation from the mean of 1.0° - 5.2° was calculated. This was significantly larger than the range observed for the PFC Σ model (Figure 7-17 b).

Figure 7-21 (a)

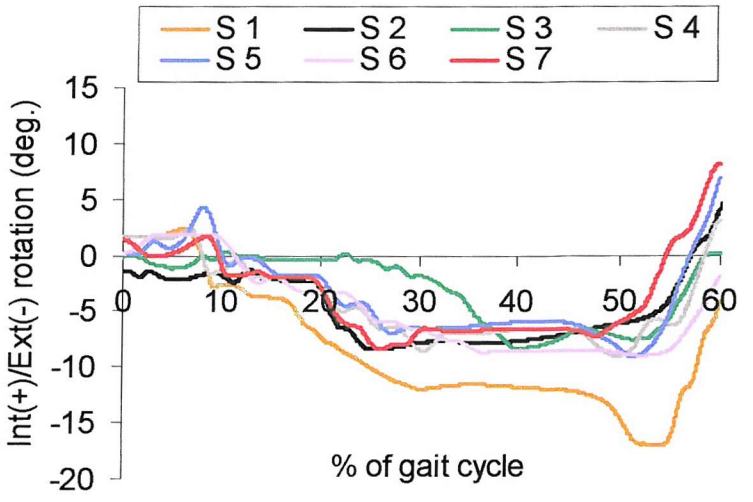

Figure 7-21(b)

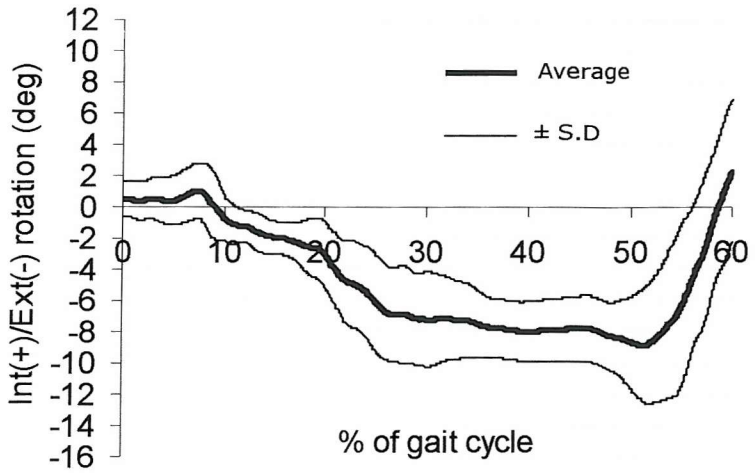

Figure 7-21: The predicted: a) I-E rotations; and b) the averaged I-E data and standard deviations, for subject specific level gait, for PLI ligament model.

From Figure 7-22 (a), transients were observed in the maximum contact pressures data. This was probably due to tetrahedral mesh of PLI model (as discussed in section 4.6, Chapter 4). The variation in the maximum contact pressures was large and ranged from 12 MPa – 41 MPa. The highest maximum contact pressure was 64 MPa and was predicted for subject 1, occurring at 52% of the gait cycle. As the tibia insert externally rotated up to 16°, the medial condyle tracked and rode up to the posterior inner edge of the insert. This created a small contact area and therefore, high contact pressures. By averaging the maximum contact pressures data, a standard deviation from the mean of 1.8 MPa to 15.8 MPa was obtained for the group (Figure 7-22 b).

Figure 7-22(a)

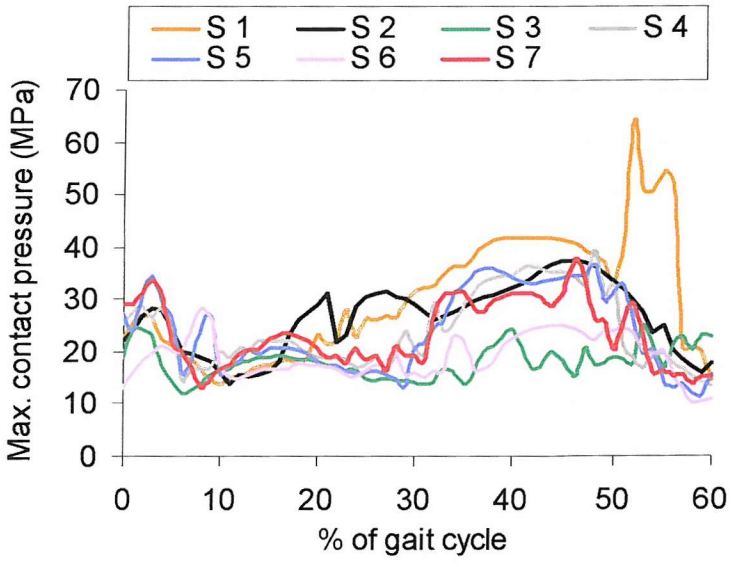

Figure 7-22 (b)

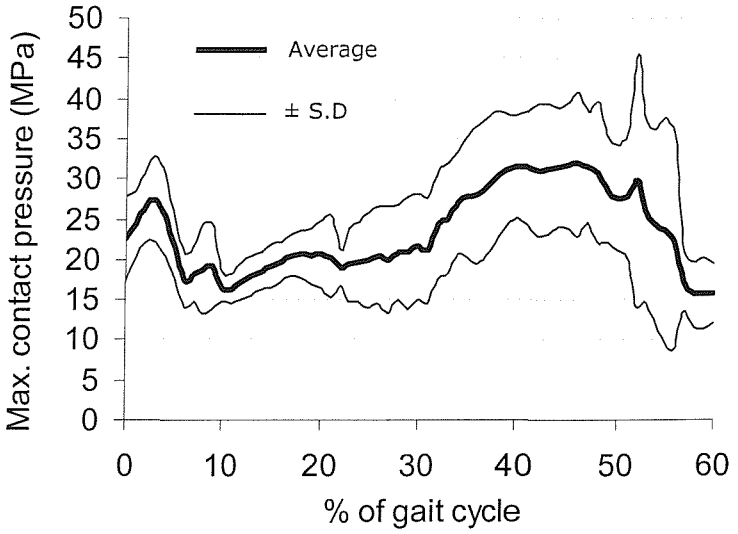

Figure 7-22: The predicted: a) maximum contact pressures, and b) the calculated average and standard deviations, for subject specific level gait, for PLI ligament model.

There was quite a consistent trend in the maximum von Mises stress data, with three peaks occurring (Figure 7-23 a). The first peak occurring after heel strike (between 0% and 5% of the gait cycle), a second between 15% and 25% of the gait cycle and the third usually showed constant stress value. All subjects exhibited peak maximum von Mises stress of 25 MPa. The estimated range of maximum von Mises stress was from 15 MPa – 25 MPa. When the maximum von Mises stress data was averaged (Figure 7-23 b), a ± 1 MPa – 3.9 MPa range of stresses was calculated. Since the maximum von Mises stress was greater than the yield stress of the polyethylene (14.5 MPa), local plastic deformation occurred. For this study, the majority of the maximum von Mises stresses plateau out at 25 MPa and therefore, it is better to refer to the maximum contact pressures data for comparisons between patient-to-patient variability. Figure 7-24 shows the occurrence of plastic strain at postero-medial side of the polyethylene insert when subjected to loading from subject 1 and subject 2.

Figure 7-23 (a)

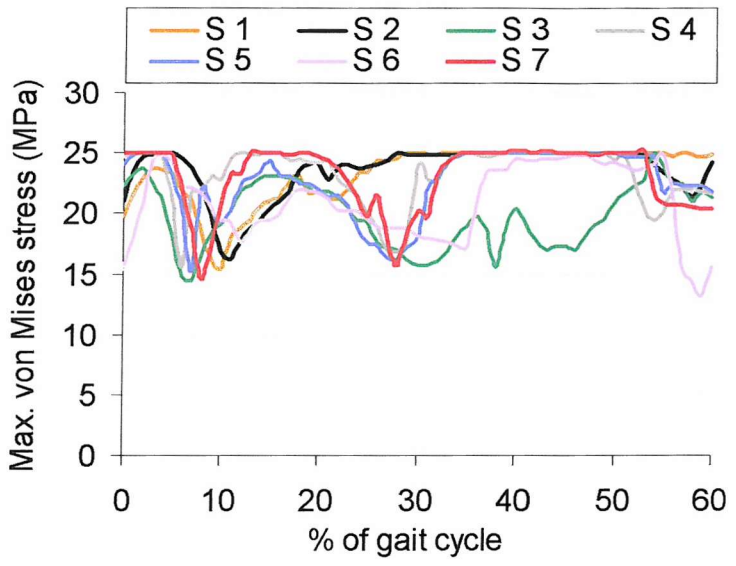

Figure 7-23 (b)

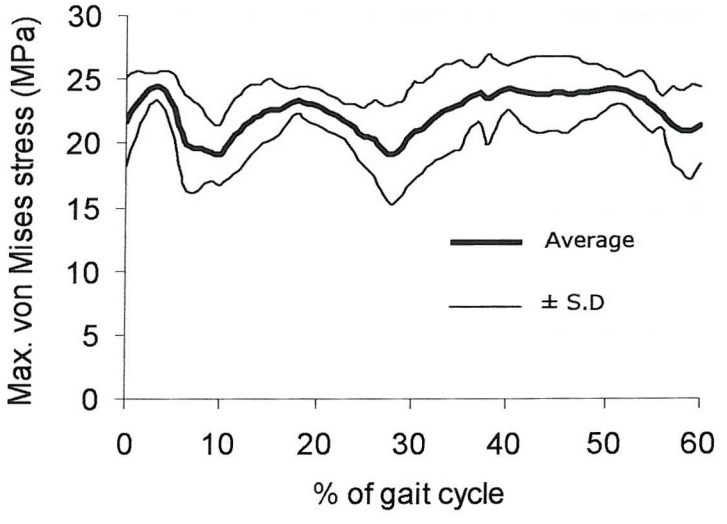

Figure 7-23: The predicted: a) maximum von Mises stresses, and b) the calculated average and standard deviations, for subject specific level gait, for PLI ligament model.

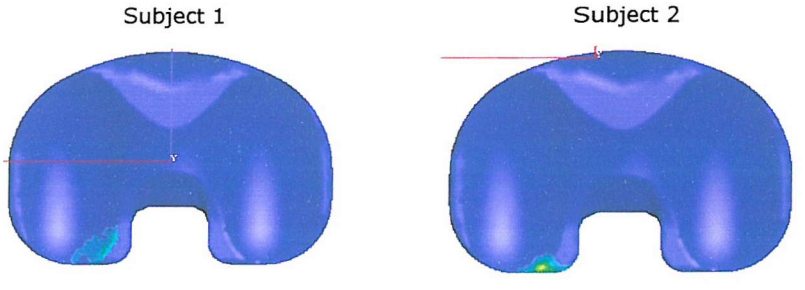

Figure 7-24: The occurrence of plastic strain at postero-medial side of the polyethylene. The maximum plastic strain > 1

7.6 RESULTS – SUBJECT SPECIFIC STAIR ASCENT

7.6.1 PFC Σ Ligament Model

The kinematics, contact pressures and stresses, the calculated average data and standard deviations are shown in Figure 7-25, Figure 7-26, Figure 7-27 and Figure 7-28.

A consistent trend in the A-P displacements was observed from 40% to 100% of the stair ascent activity (Figure 7-25). All the subjects experienced posterior translation at the beginning of the stair ascent activity and stayed posteriorly during the majority of the stance phase before moving anteriorly just prior toe-off. The peak anterior displacement and the peak posterior displacement of the tibia with respect to the femur were approximately 5.3 mm and 4.2 mm, respectively. When compared to the HLS model during stair ascent, the analysis for subject 9 managed to complete the full cycle. From the averaged data (Figure 7-25 b), a standard deviation from the mean of 0.6 mm – 2.5 mm for the A-P displacement was estimated. In comparison to HLS model during stair ascent (Figure 7-8 b), a similar range was observed in the A-P translation.

Figure 7-25 (a)

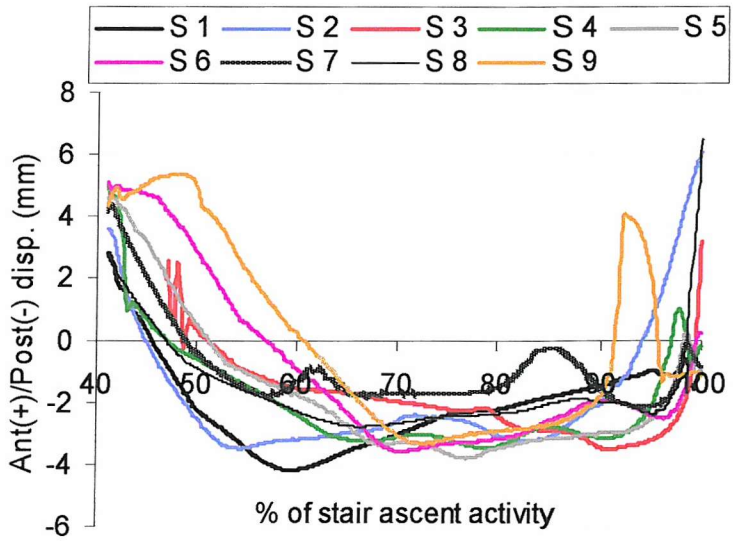

Figure 7-25 (b)

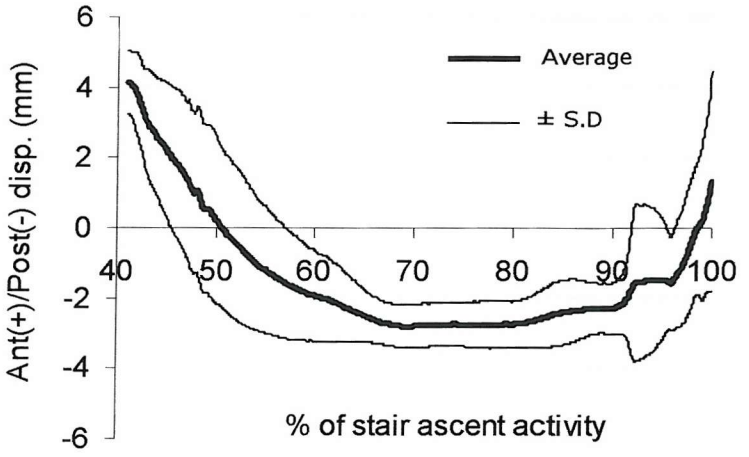

Figure 7-25: The predicted: a), A-P displacements and b), the average and standard deviations, for subject specific stair ascent, for PFC Σ ligament model.

From the predicted I-E rotations (Figure 7-26 a), on average, a 10° variation in the I-E rotations was observed throughout the stance phase of stair ascent activity. There was no consistent pattern of motion. Some subjects exhibited an internal rotation of the tibia relative to the femur of up to 5° and some subjects showed an external rotation of up to 5°. Subject 9 produced a large external tibia rotation with respect to the femur compared to the other subjects. The peak external tibia rotation relative to the femur was 18°. A ± 2° - 6.1° range of I-E rotation was calculated from the group (Figure 7-26 b).

Figure 7-26 (a)

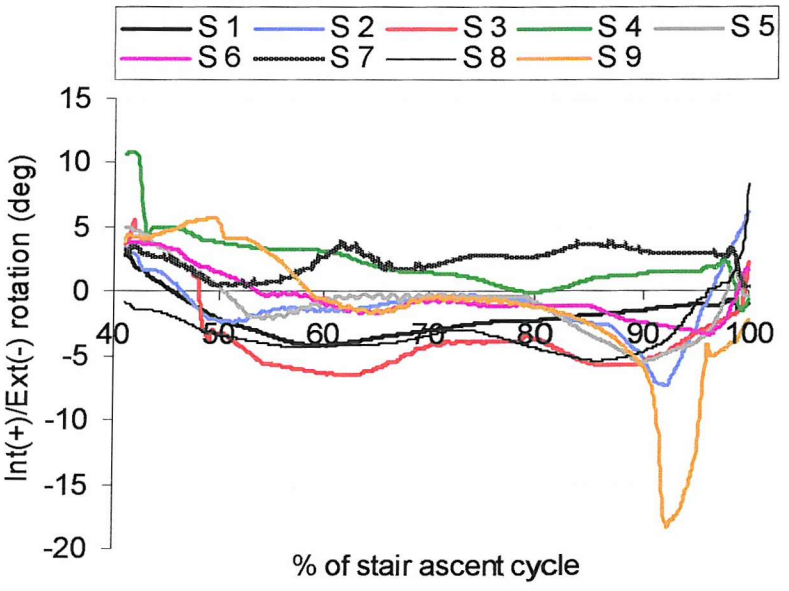

Figure 7-26 (b)

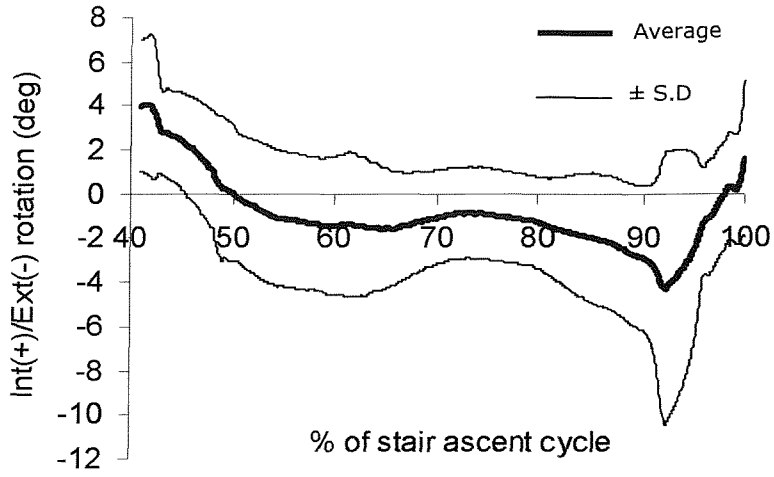

Figure 7-26: The predicted: a) I-E rotations, and b) the calculated average and standard deviations, for subject specific stair ascent, for PFC Σ ligament model.

From Figure 7-27 (a), in general, a consistent trend of contact pressures was observed. There were two peaks in the contact pressure data, the first occurring just after heel strike, between 40% and 50% of the activity cycle and the second just prior to toe-off, typically 85% to 90% of the activity cycle. The first peak ranged from 20 MPa – 30 MPa, whereas the second peak ranged from 20 MPa to 37 MPa. Subject 1 and subject 9 exhibited significantly higher value of peak maximum contact pressures particularly just prior to toe-off. The peak maximum contact pressure for subject 1 and subject 9 was 37.2 MPa and 47.7 MPa, respectively. For subject 1, the high contact pressure occurred as a result of the high axial load at that period (Figure 7-2 a), whereas subject 9 was due to the sudden changed in tibia translation from external to internal. When compared to the HLS model during stair ascent activity (Figure 7-10 a), subjects 1 and 9 also exhibited high peak pressures. Overall, a ± 2.1 MPa – 9.2 MPa range of maximum contact pressure was estimated within the nine subjects during stair ascent activity (Figure 7-27 b).

Figure 7-27 (a)

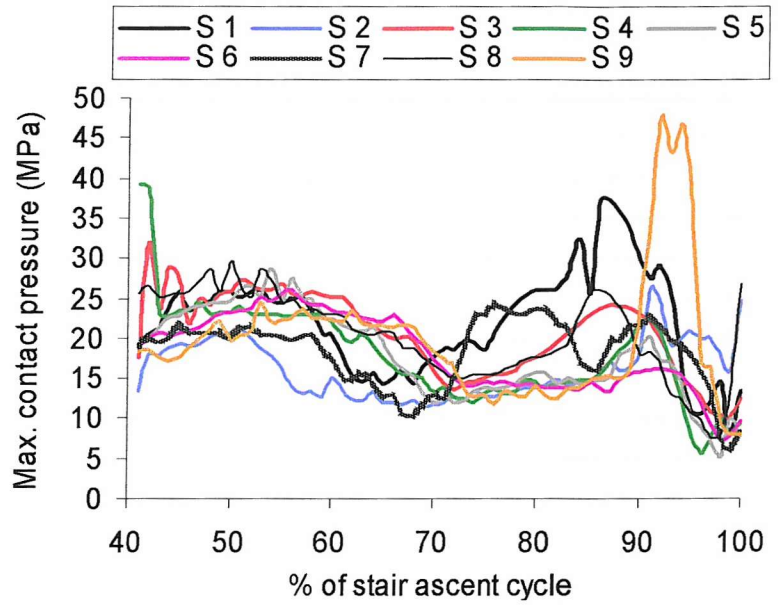

Figure 7-27 (b)

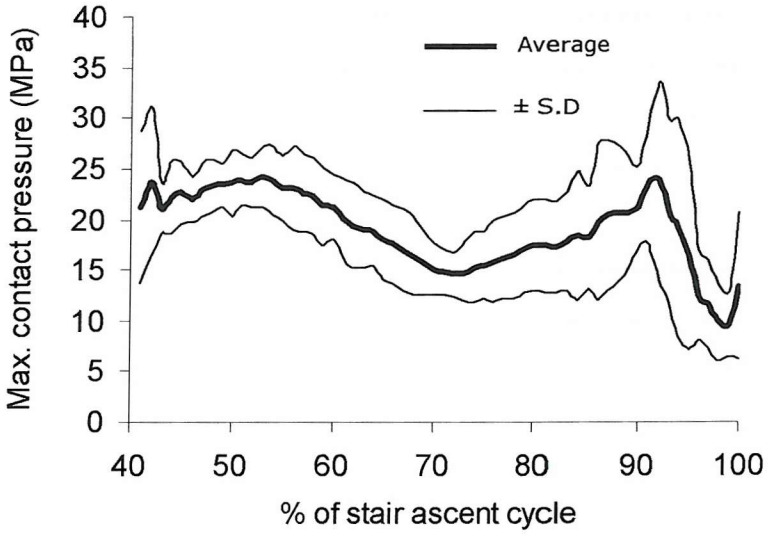

Figure 7-27: The predicted: a) maximum contact pressures, and b) the calculated average and standards deviations, for subject specific stair ascent, for PFC Σ ligament model.

The maximum von Mises stresses from all the subjects were high, with the peak maximum von Mises stress of 25 MPa (Figure 7-28 a). A constant value of von Mises stress was observed in subject 3 and subject 4. Subject 3 recorded a constant value of 19.6 MPa, from 65% - 100% of the stair ascent cycle, while subject 4 recorded a constant value of 17.2 MPa, also from 65% of the activity cycle onwards. Subject 9 also exhibited constant value of von Mises stress typically just before toe-off. In comparison to the HLS model for stair ascent activity (Figure 7-11 a), the trend in the maximum von Mises stress was less well defined (Figure 7-28 a). From the averaged data (Figure 7-28 b), a standard deviation from the mean of 1.1 MPa – 6.4 MPa for the maximum von Mises stress was calculated. Similarly, as the maximum von Mises stresses plateaud out at 25 MPa, a local plastic deformation would occur. For this study, it is probably better to refer to maximum contact pressures to examine patient-to-patient variability. Figure 7-29 shows the plastic

strain in the polyethylene insert for subject 3 and subject 4. The residual plastic strain caused the maximum von Mises stresses for these two subjects to stay at constant value (known as residual stress).

Figure 7-28 (a)

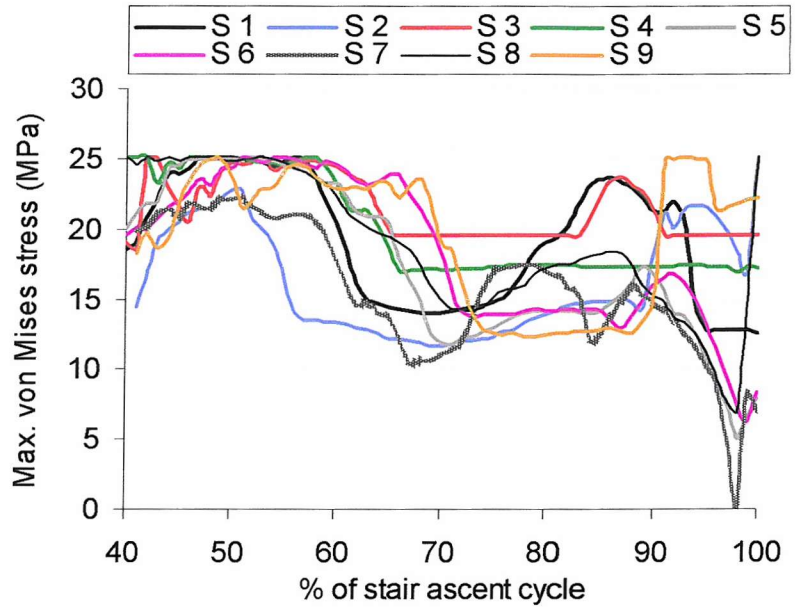

Figure 7-28 (b)

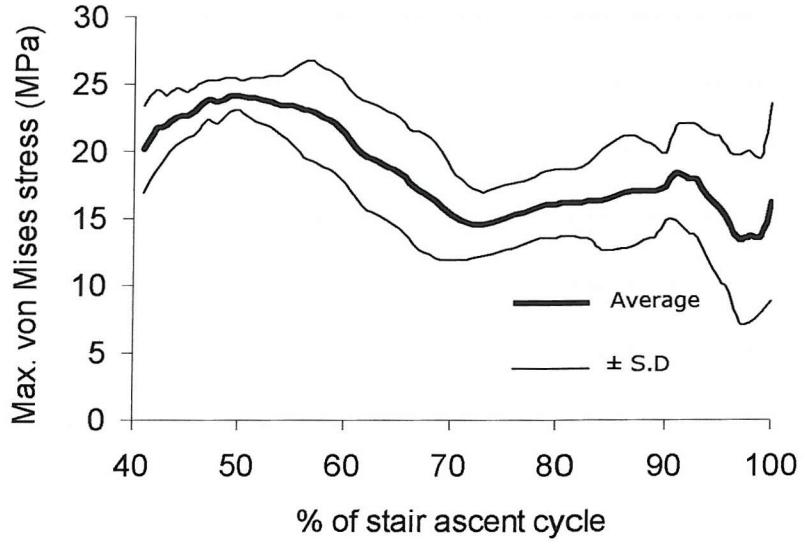

Figure 7-28: The predicted: a) maximum von Mises stresses, and b) the calculated average and standard deviations, for subject specific stair ascent, for PFC Σ ligament model..

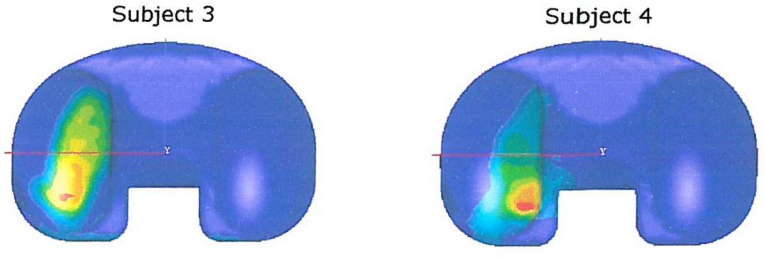

Figure 7-29: Plastic strain in the postero-medial side of the polyethylene insert as observed in subject 3 and subject 4. The maximum plastic strain for both load cases > 10

7.6.2 PFC PLI Ligament Model

The predicted kinematics, contact pressures and stresses are shown in the Figure 7-30, Figure 7-31, Figure 7-32 and Figure 7-33. For PLI knee model, not all the subjects started from 40% of the stair ascent cycle. Attempts had been made to start the simulation from 40% of the activity cycle, but some simulations failed (a few percent after starting of) as a result from the input forces for these subjects. The input data for each of the 9 subjects had to be adjusted to search for the successful starting point. Table 7-4 summarized the starting point of each subject. Subject 4 failed to start off at any point. Hence, the results showed here were for 8 subjects only.

Subject	Starting point (% of stair ascent activity)
1	40
2	41
3	44
5	43
6	41
7	41
8	40
9	47

Table 7-4: Starting position for 8 subjects, in % of stair ascent cycle.

Overall, a consistent trend of A-P displacement was observed (Figure 7-30 a). All subjects started with an anterior position of the tibia relative to the femur, ranging from 6 mm to 9 mm. The tibia component then moved posteriorly towards the initial starting position and tended to stay posteriorly between 60% and 80% of the activity cycle. After 80% of the stair ascent cycle, the tibia translated in the anterior direction, towards the initial position. Just before the end of the stair ascent cycle, i.e. between 90% and 100% of the activity cycle, some subjects have moved just anterior of the initial starting position, ranged from 0 mm – 4 mm. The overall A-P displacement ranged from +9 mm to – 4 mm. The peak posterior displacement of the tibia with respect to the femur was approximately 4 mm, for subject 5. The analyses for subject 8 and subject 9 failed near the end of the activity. In both subjects, the lateral femoral condyle tracked to the posterior edge of the tibial insert and as the LCL continued to pull the lateral condyle posteriorly, the condyle subluxed. The average and standard deviations plot for the A-P displacements, Figure 7-30 (b), was plotted from 47% to 98% of the activity cycle, for 8 subjects. When the A-P displacement data averaged, a standard deviation from the mean of ± 1.0 mm – 3.0 mm was calculated.

Figure 7-30 (a)

Figure 7-30 (b)

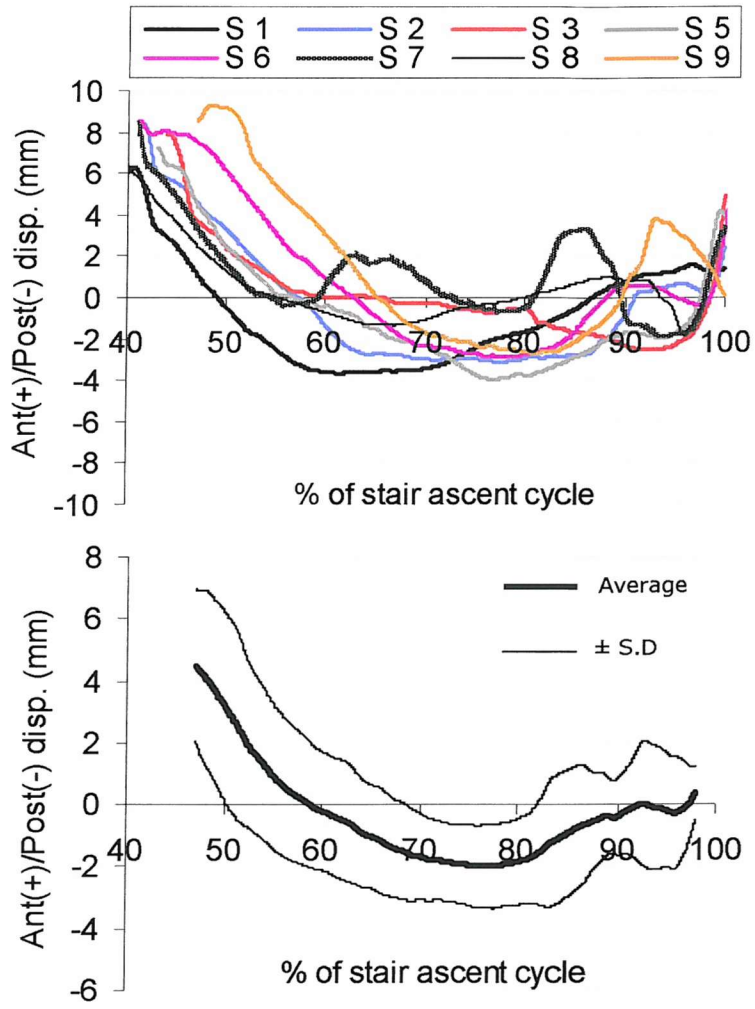

Figure 7-30: The predicted: a) A-P displacements, and b) the calculated average and standard deviations, for subject specific stair ascent, for PLI ligaments model.

Seven subjects (except subject 7) experienced external tibia rotation relative to the femur from the beginning of the stair ascent cycle to approximately 55% of the activity cycle. Then, the tibia rotated internally towards the initial starting position and 20% before the end of the stair ascent cycle, the tibia rotated externally and then internally prior to toe-off (i.e. 90% of the stair ascent cycle). Subject 7 tended to exhibit internal tibia rotation throughout the whole activity cycle. A large variation of I-E rotations, ranging from internal 12° to external 17.5° was observed (Figure 7-31 a). Subject 9 exhibited the highest peak internal rotation of 12° and also the highest peak external rotation of 17.5°. Examining the averaged I-E rotation data (Figure 7-31 b), a standard deviation from the mean of 3.9° - 7.0° for the I-E rotations was calculated.

Figure 7-31(a)

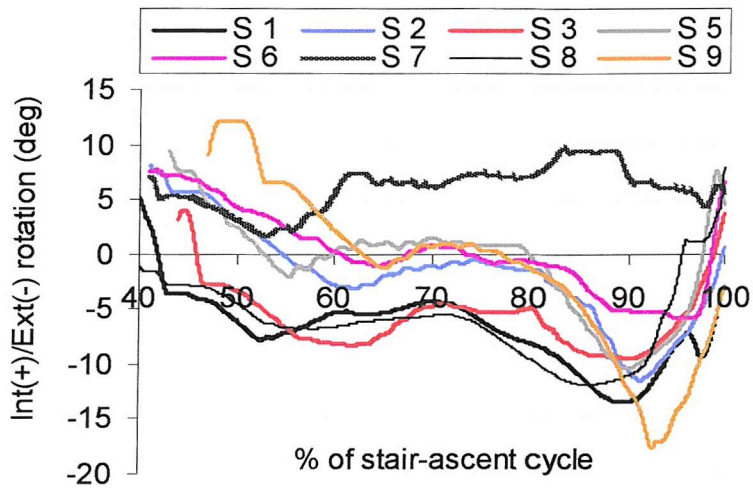

Figure 7-31(b)

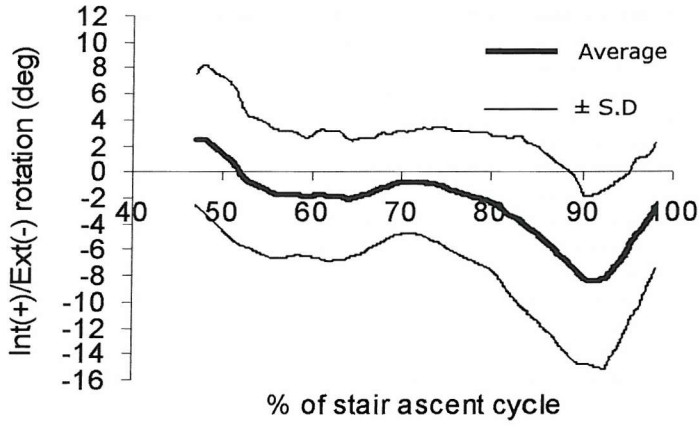

Figure 7-31: The predicted: a) I-E rotations, and b) the average and standard deviations, for subject specific stair ascent, for PLI ligaments model.

The plots (Figure 7-32 a) show a consistent trend of maximum contact pressures with two peaks. The first peak occurred between 45% and 55% of the stair ascent cycle and the second peak, which tended to be larger than the first, occurred between 85% and 95% of the activity cycle. The first peak ranged from 24 MPa – 36 MPa. The second peak showed more oscillations and tended to range from 30 MPa – 50 MPa. Subject 1 and subject 9 showed very high value of peak maximum contact pressure, 49 MPa and 53 MPa, respectively. The results showed there was a wide variation of maximum contact pressure from subject specific stair ascent load data. An estimate of ± 1.0 MPa – 11.5 MPa range of maximum contact pressure was obtained from the averaged maximum contact pressure data (Figure 7-32 b).

Figure 7-32 (a)

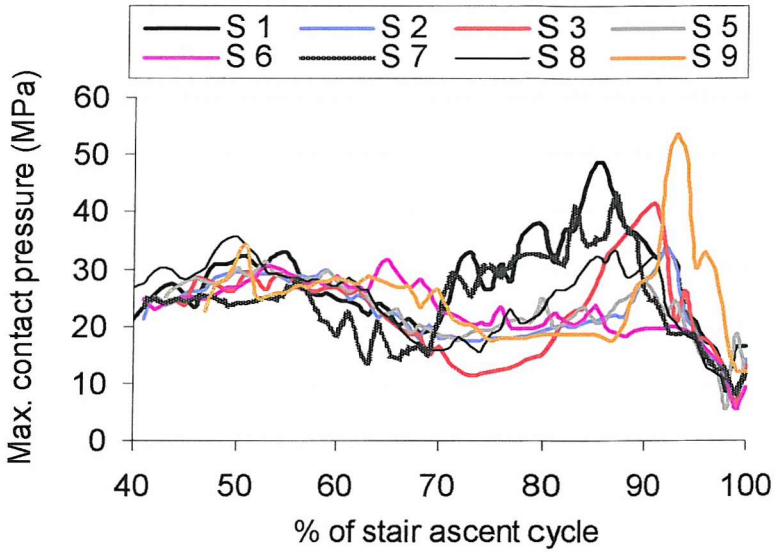

Figure 7-32 (b)

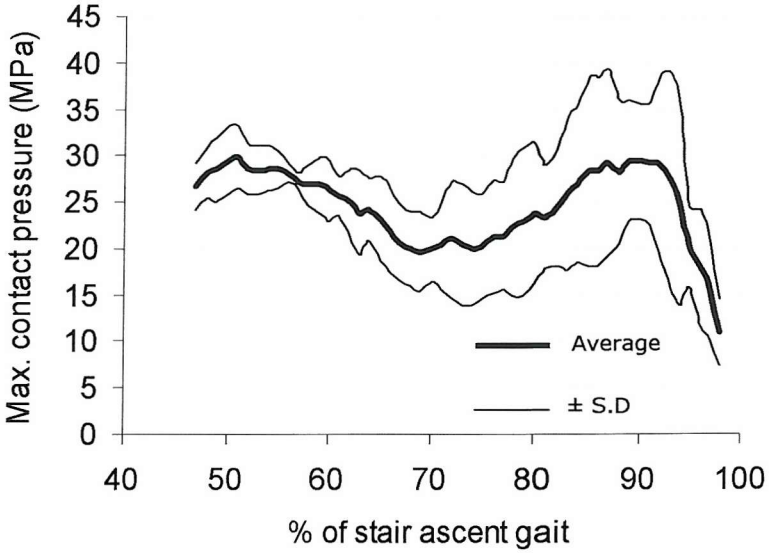

Figure 7-32: The predicted: a) maximum contact pressures, and b) the calculated average and standards deviations, for subject specific stair ascent, for PLI ligaments model.

High contact pressures observed in Figure 7-32 (a) during the stair ascent activity had caused the PLI knee to exhibit high value of maximum von Mises stresses, as in Figure 7-33 (a). Between 47% and 60% of the activity cycle, a constant value of von Mises at 25 MPa was observed. Then, the maximum von Mises stress decreased in the several subjects, occurring between 60% and 80% of the stair ascent cycle. When examining the averaged maximum von Mises stress plot (Figure 7-33 b), it does not mean much, as the polyethylene insert is yielding and no real difference is observed within the subject specific stair ascent von Mises data. Figure 7-34 shows the occurrence of plastic strain in the polyethylene insert for two of the selected subjects.

Figure 7-33 (a)

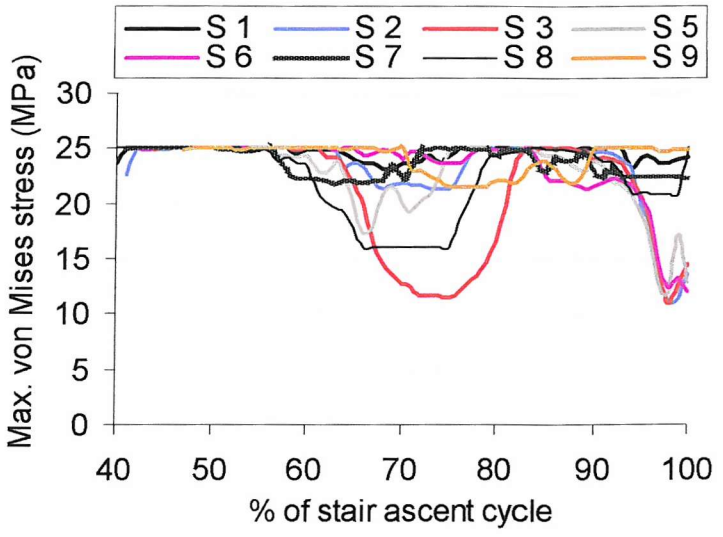

Figure 7-33 (b)

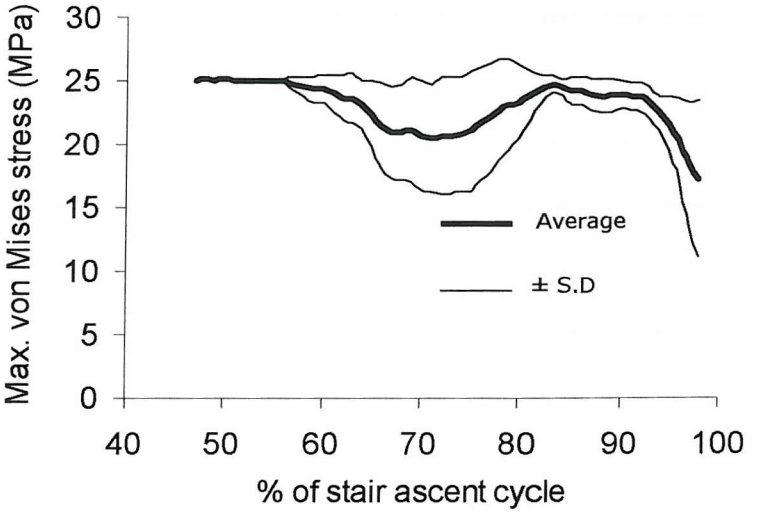

Figure 7-33: The predicted: a) maximum von Mises stress, and b) the calculated average and standard deviations, for subject specific stair ascent, for PLI ligaments model.

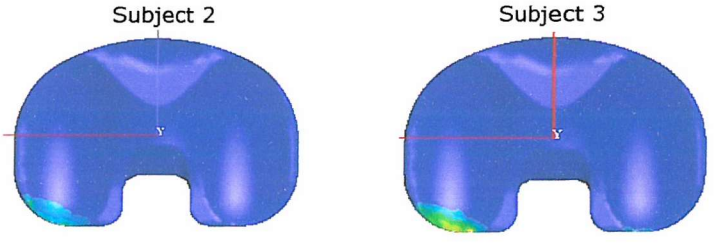

Figure 7-34: Plastic strain at the postero-medial side of the polyethylene for two of the selected load cases. The maximum plastic strain > 10 (very large strain)

7.7 DISCUSSIONS

The stair ascent has been shown to be a more demanding activity as compared to level gait. During stair ascent, more loads are applied at higher flexion angles. Variations in the loads for both activities are influenced by the bony and ligamentous constraints in each subject during specific knee joint functions. Inter and intra variability in motion patterns can be expected for comparable tasks. In other words, subjects can change their walking or stair-ascent patterns at will or walk differently by habit and this produces slight different motion patterns [31]. In general, a wider range of kinematics and contact pressures was obtained during stair ascent for PFC Σ and PLI TKR designs as compared to level gait. This wide range could lead to more uncertainty in performance for a given total knee replacement patient after surgery. The envelope of active knee joint motions from these two activities provide an idea of what performance range of the TKR designs examined would have under condition that the implant is perfectly aligned during the surgery.

The Swedish Knee Arthroplasty Register has reported that current TKR designs can expect to have a survival rate of between 90% and 95% at 10 years. Thus the majority of knees appear to function well. Clinical studies [7,30,69,135,148] have shown a wide range in the kinematics when using the same implant design. The variation in the kinematics may be a result of surgery related, such as implant positioning and soft tissue balancing, and as well as patient related (gait pattern) parameters. Predictions of the joint contact forces for healthy patients have shown significant variations in the relative magnitudes of the axial force, A-P force and I-E torque. It is not difficult to envisage that similar differences may also exist in a population of total knee replacement patients. The 5% to 10% failure at 10 years are likely to be a result of a combination of factors resulting in poor kinematics, abnormal loading which lead to accelerated failure of the prosthesis.

Using current methods for assessing the performance of TKR designs (finite element analysis and knee wear simulators), typically only a single load case is used (ISO standard load). Very few FE studies have applied different loading conditions other than the idealised ISO loading condition. In the FE study performed by Godest et al. [52], the kinematics obtained for PFC Sigma knee showed good agreement with those obtained using experimental knee wear simulator. This load case usually based on an idealised person with a mass approximately 70kg, it is difficult to assess whether the differences observed between TKR designs, in terms of the predicted kinematics and contact pressures, are likely to result in any significant difference in their clinical performance. Failure is unlikely to occur in such cases, as testing under these conditions are close to optimal and predictable. Failure is more likely to be a result of the extremes, for example, the 100 kg patient with poor gait. To date, no study has attempted to look at the potential variation in the predicted kinematics and contact pressures as a result of patient-to-patient

variability in the applied forces. Hence, there is need to apply wider range of knee joint forces for example from different subjects performing different activities, to examine their effect on function of TKR and may be possible to identify designs that are more sensitive to changes in patient related variables and therefore have a higher risk of failure.

The kinematics performance for the level gait and stair ascent activities was seen to vary between subjects. Both activities showed consistent pattern of A-P displacement. Level gait exhibited smaller range of A-P displacement compared to stair-ascent. By modelling realistic ligaments and assigning them with proper material properties did affect the performance of the TKR designs examined. For PFC Σ ligaments model, the variation in the predicted kinematics during level gait activity was not significant as compared to the horizontal linear spring (HLS) model. With the ligaments, the standard deviations from the mean varying from 0.3 mm – 1.2 mm and 0.4° - 3.2° for the A-P displacements and I-E rotations, respectively; whereas for HLS model, the standard deviations from the mean varying from 0.5 mm – 1.0 mm and 0.4° - 2.3° for the A-P displacements and I-E rotations, respectively. A summary of the range of performances for the two prostheses designs, for both activities is shown in Table 7-5 and Table 7-6.

	Standard deviations from the mean for the parameters examined for PFC Σ knee	
	HLS Model	**Ligament Model**
Level Gait		
A-P displacements (mm)	0.5 – 1.0	0.3 – 1.2
I-E rotations (degree)	0.4 – 2.3	0.4 – 3.2
Contact pressures (MPa)	1.0 – 5.0	0.8 – 8.0
Von Mises stresses (MPa)	0.5 – 4.0	0.9 – 5.7
Stair ascent		
A-P displacements (mm)	0.6 – 2.7	0.6 – 2.5
I-E rotations (degree)	0.8 – 4.5	2.0 – 6.1
Contact pressures (MPa)	1.5 – 9.4	2.1 – 9.2
Von Mises stresses (MPa)	1.6 – 4.6	1.1 – 6.4

Table 7-5: Standard deviations from the mean for the kinematics, contact pressures and von Mises stresses using PFC Σ knee, during level gait and stair ascent activities.

	Standard deviations from the mean for the parameters examined for PLI knee
Level Gait	**Ligament Model**
A-P displacements (mm)	0.6 – 2.3
I-E rotations (degree)	1.0 - 5.2
Contact pressures (MPa)	1.8 – 15.8
Von Mises stresses (MPa)	/
Stair ascent	
A-P displacements (mm)	1.0 – 3.0
I-E rotations (degree)	3.9 – 7.0
Contact pressures (MPa)	1.0 – 11.5
Von Mises stresses (MPa)	/

Table 7-6: Standard deviation from the mean for the kinematics, contact pressures and von Mises stresses using PLI knee, during level gait and stair ascent activities.

Both the HLS and ligament models generated similar trend of kinematics, except that in the ligament model, subject 1 exhibited slightly different trend of I-E rotations but similar trend of A-P displacements as compared to the HLS model. The ligament model showed slightly larger range of I-E rotations. This was not expected for the ligament model. It was postulated that the ligaments would provide better constraint to the prosthesis and hence, smaller variation in the kinematics. The difference could be due to the femoral origin sites and the tibial insertion sites of each ligament fibre bundles. During knee motions, the ligaments' fibre bundles are non-uniformly loaded, which depends on the relative orientations of the origin and insertion sites [97,98]. The femoral origin and the tibial insertion were approximately positioned within the FE models in this study. The positioning of these fibre bundles may not be accurate and thus may be unable to represent the actual anatomy of the origins and insertions in the total knee joint; hence, it is postulated that the fibre bundles could not deliver their full function and resulted in slightly larger variation in the kinematics. There was no consistent pattern in the I-E rotations during stair ascent within the 9 subjects for both HLS and ligament model. It would therefore appear that the variability in the applied I-E torque is responsible for the higher variability in the predicted kinematics for the stair ascent load case (Figure 7-9 and Figure 7-26).

In the stair ascent activity, simulation using the HLS model for subject 9 failed just before toe-off. By adding in the ligament constraint to the PFC Sigma model, the analysis for subject 9 was completed for a full stance phase of stair ascent activity. In this case, the ligaments coupled with the applied forces managed to effectively stop the femoral component from posteriorly subluxing from the tibial insert. With the ligaments model, a

sudden increased in the A-P displacements and I-E rotations were observed in subject 9, as at that stage the applied axial force was low but the applied anterior force and external torque were at their peak. The applied axial force was too small to resist the anterior movement and the external rotation of the tibial insert. It could be concluded that the outcome of the TKR is dependent on the complex articulation with non-linear relationship between surface geometry, contact forces, soft tissue balancing and alignment of the components. When comparing the predicted kinematics between PFC Σ ligaments model and HLS model during stair ascent activity, the ligaments model produced slightly larger I-E rotations (Table 7-5). The reason for this is not clear.

The predicted contact pressures are in general higher in the PFC Σ ligaments model than in the HLS model, for both activities. In addition, stair ascent activity showed larger range of maximum contact pressures in comparison with the less demanding activity of level gait. The ligaments restraint the vertical movement of the components and as a result hold the femoral component and the tibial insert tighter together and allowing more load transferred to the tibial insert. For example, during level gait, in the PFC Σ ligaments model, the standard deviations from the mean of 0.8 MPa – 8 MPa was estimated and compared to the HLS model the range was slightly less, i.e. from 1 MPa – 5 MPa. The variation in the contact pressure for the ligaments model during stair activity was ± 2.1 MPa – 9.2 MPa, slightly less than the HLS model but not to greater extent (Table 7-5).

For PLI ligaments model, in general, greater variability in the predicted kinematics and contact pressures were observed during the stair ascent activity than the level gait activity. For this design, the absolute magnitude and the variation in the predicted kinematics was larger compared to the PFC Σ ligament model. The polyethylene insert for PLI design has lower conformity as compared to the PFC Σ design. The less dished a polyethylene insert, the less constrain it has on the kinematics. Therefore, PLI design exhibited larger kinematics. From the kinematics results, it is clear that different TKR designs will result in different magnitude of kinematics as well as the kinematics trends. Both PFC Σ and PFC PLI designs were subjected to the same loading conditions and same ligamentous constraints, but PFC PLI design showed higher sensitivity (larger range of standard deviation from the mean, Table 7-6) in the predicted kinematics as a result of patient-to-patient variability in the applied forces.

PFC PLI ligaments model exhibited more consistent kinematics trends during level gait than during stair ascent activity. The analyses for six subjects during stair ascent activity using the PLI model did not start at the beginning of the stance phase as the simulations failed. This was probably due to the low axial load applied at the beginning of the stance phase of stair ascent activity (Figure 7-2 a) whereby the low axial load was not able to resist the movement of the femoral component which was flexed at high flexion angle,

causing it to ride up the posterior edge of the tibial insert and subluxing. As a result, the starting time for the six subjects was adjusted until a successful starting point was found. At the successful starting point, the applied axial load was higher than at the beginning of the stair ascent stance phase and was able to constraint the femoral component from falling-off of the tibial insert.

The PLI model has shallower polyethylene conformity as compared to the PFC Σ model. Low conformity of the PLI design has resulted in higher contact pressures and stresses in the polyethylene insert for both activities when compared to the PFC Σ model. The same femoral condylar geometry was used in the PLI and PFC Σ models and when examining the contact area in the PLI design, as expected, smaller contact areas were observed and the shape was more towards line contact. When examining the contour map of contact pressures of the PFC Σ model, on average a larger contact area was obtained and the shape was more elliptical. Contact stresses in the polyethylene insert for PLI knee design were significantly high, especially during stair ascent activity. The results strongly suggested that for this TKR design (PLI), it is more susceptible to polyethylene wear when undergoing more demanding activities, such as stair ascent. The wear volume has been shown to increase with an increase in kinematics and as well as stresses [6,152]. The lower conformity of the PLI model might be another reason for the unsuccessful simulations at the beginning of the stair ascent activity, as discussed earlier. The tibial insert dish was not deep enough to hold the femoral component in place and therefore, subluxation for the femoral component was observed.

The contact pressures for PFC Σ and PLI models during level gait were very sensitive to the changes in the axial loads and to a lesser extent to the kinematics. If A-P translations and I-E rotations were not included in the analysis, then the higher the axial force at a given flexion angle, the higher the contact pressures would be. For level gait load case, this is nearly the case, as there is little variation in the A-P translations and the I-E rotations between patients, the subjects generating the highest axial load tend to generate the highest contact pressures. Meanwhile, the contact pressures during stair ascent activity for both models were very sensitive to the AP forces and I-E torque and as well as the changes in the applied axial load. This may explain why in some subjects, for example subject 1 in Figure 7-10 a, generates higher than expected contact pressures that can be explained by the magnitude of the axial load alone. The predicted contact pressures during stair ascent activity were observed to be the highest in the first peak, rather than in the 2nd peak although the applied axial load during the 2nd peak was greater than the 1st. At higher flexion angle, the contact area between the femoral condyle and the tibia insert was small, resulting in higher contact pressures. In PFC Σ ligaments model, the high contact pressures resulting from higher flexion angles during stair ascent activity had caused the tibial insert to generate significant amount of plastic strain. This residual plastic strain

caused the peak Von Mises stresses to remain at constant values (Figure 7-28 b). Due to the lower conformity of the PLI design, higher maximum contact pressures were generated during level gait. From the predicted von Mises stresses during level gait, the PLI tibial insert generated significant amount pf plastic strain and causing residual stress. Similar residual stress was also observed in the PLI model during stair ascent activity (Figure 7-33).

The kinematics exhibited by the TKR are influenced by the surrounding soft tissue. Several selected subject specific level gait and stair ascent analyses' of the ligaments forces are shown in Appendix A. During level gait, for both TKR designs examined, the ligaments forces were no more than 160 N. There was no significant difference in the ligaments forces when compared to Shelburne et al. [133] study, whereby the knee ligaments forces were calculated over one cycle of normal level walking using a 3D knee model. From their study, the LCL carried the highest force of approximately 170 N and relatively small forces were observed in other ligaments. During stair ascent, the ligament forces were no more than 350 N. In general, these values (the peak force during level gait and stair ascent) were below 2% strain of all ligaments. Since complete failure of the ligament took place about 6% to 8% strain [110] (or maximum force 1000 N); the ligaments in this study were functioning properly and not over strained.

This study has several limitations, which should be taken into account when analysing the data. The forces used in this study have been predicted for a group of healthy, elderly subjects. Patients who have received a TKR may generate different load histories and this may also be design dependent. There are a number of potential sources of error related to predicting the magnitude of the joint contact force for subject specific level gait and stair ascent activity. Skin markers were used in order to identify bone landmarks while performing gait analysis. The researchers [31] reported that just a small error in locating the joint centre in the frontal plane would have significant effect on the estimated moment arm and as well as the calculated forces. The coordinates of the ligament insertion points were taken from several literature sources and they did not exactly fit the FE knee models in this study. The geometry of the limb and the prosthesis where the coordinates were taken varied from this study. As a result, the insertion points had to be adjusted in accordance to the geometry of the prosthesis used in this study. It was assumed that in this study there were no anatomical variations between individuals in their ligament attachment points. The axial force has been applied to the centre of the femoral component, leading to a 50:50 load distribution to the medial and lateral compartments of the knee. No varus-valgus moment has been applied to the TKR, which may lead to preferential loading for either the medial or lateral condyle. The performance envelope has been assessed for a relatively small number of subjects for each activity and ideally this should be expanded to a larger group. This work has only examined the influence of

subject specific loads and other parameters including implant orientation and ligament balancing are also likely to affect the performance envelope. Further work is required in this area, so that suitable assessment methods are developed in order to determine the performance envelope as a result of all the relevant parameters. Only this way can we effectively improve implant design and further reduce implant failure rates in the future.

Despite these limitations, this is the first time that the performance envelope of a TKR has been evaluated. For these particular TKR designs, the kinematics during level gait is relatively insensitive to variation due to subject specific loading, but greater variations were observed during stair ascent activity. This study has highlighted the need to assess the performance envelope of a TKR design, rather than the performance related to an isolated load case.

Summary of results

- Performance envelopes in the kinematics and contact pressures, as a result of patient-to-patient variability in the applied forces had been obtained for two TKR designs, for level gait and stair ascent activities.
- For both the PFC Σ and PLI designs, the kinematics during level gait are relatively insensitive to variation due to subject specific loading, but greater variations were observed during stair ascent.
- The lower conformity PLI design was shown to produce higher absolute value for the predicted kinematics as well as greater variation as compared to the higher conformity PFC Σ design.
- Low conformity design, i.e. PLI model generates smaller contact area and resulting in higher contact pressures. More conforming tibio-femoral geometry, i.e. the PFC Σ knee generates larger contact area and smaller contact pressures.
- By modelling the ligaments, the analyses for nine subjects during stair ascent activity were completed for full stance phase with the PFC Σ model. In comparing to the HLS model, only eight subjects analyses were completed.
- By assessing the kinematics and contact pressures, it is suggested that PLI knee design is more prone to polyethylene failure, especially when undergoing more demanding activity such as stair ascent gait.
- During level gait, the contact pressures are largely dependent on the changes in the applied axial load.
- During stair ascent activity, the contact pressures are dependent more on

the A-P forces and I-E torque than on the axial load applied.

- Based on the results, using full ligaments model provides higher constraint to the model and benefits especially when simulating higher range of flexion motion activity (stair ascent) or using low conformity design. However, for less range of flexion motion activity (level gait), using just the HLS model may be sufficient.

Chapter 8

THE EFFECT OF MISALIGNMENT ON THE PERFORMANCE OF TKR

In this chapter, the effect of malalignment of the TKR with respect to the ligaments in the knee joint system will be studied and discussed for two activities, level gait and stair ascent.

8.1 INTRODUCTION

Complications after TKR and the most common cause for revisions are polyethylene wear, loosening of the implants, knee instability and infection [27,36,45,57,85]. Polyethylene wear, loosening and instability are factors associated with altered kinematics of the knee joint that arises from misalignment of the TKR.

In a combined clinical and laboratory based study, Bargren et al. [9], which combined laboratory and clinical studies, demonstrated that malalignment of the TKR in the lower limb can lead to mechanical loosening of the tibial component and in some cases, failure of the knee component were observed as a result of repetitive loading at the knee joint. Of 32 patients examined (5 to 9 years follow-up studies), 11 showed varus alignment, 3 were in neutral position and 18 were in valgus. The knees that were in valgus showed the lowest failure rate whereby only 2 of the 18 valgus knees failed. From the clinical studies, it was observed that malalignment between 1° and 5° valgus produced the highest success rate. The knees presenting neutral and varus alignment (range from 1° to 10°) showed poor successful rate, with 12 of the 14 knees failed (only 2 successful varus knees). The results showed that the optimal femorotibial alignment at the knee seems to be 1° to 5° of valgus with components oriented perpendicular to the mechanical axis. This finding was supported by Clarke and Scott [27] in which intra-operatively, resection of the distal femur and proximal tibial should achieve a desirable axis of 5° to 8° of valgus alignment at the knee with the components oriented perpendicular to the mechanical axis of the femur and tibia.

Ritter et al. [126] evaluated 421 total knee arthroplasties (2 months to 13 years follow-up) in order to assess the alignment of the TKR at the lower limb. Varus malalignment of the

tibial component had been identified as a risk factor for prosthesis loosening after TKR. This finding further supported Bargren et al. [9] study. When loosening occurs, subsidence of the prosthesis may result, which also can contribute to the kinematics instability. From the clinical data, Ritter et al. [126] suggested that for good clinical results, the TKR should be installed at 5° to 8° of anatomic valgus alignment in the lower limb.

Hsu et al. [64] have analysed, by means of experimental tests, the influence of overall and individual component alignment upon the load distribution on the tibial insert, for two different total knee designs (Kinematic and Total Condylar). Their results suggest that for the Kinematic design, a tibial cut of 2° varus would produce the best force distribution between the medial and lateral condyle. For the Total Condylar knee, the best force distribution was observed when the tibial insert was perpendicular to the mechanical axis of the tibia. Nonetheless, it should be noticed that the validity of these results might be limited by the fact that, in all experiments, the magnitude of the load applied was constant and in real knees, this may not be the case.

Scuderi et al. [132] assessed the positioning of the femoral component in TKR, clinically. From their examination, it was agreed that internal malrotation of the femoral component increased the stresses on the tibial component leading to wear or loosening. Scuderi et al. [132] concluded that well implanted TKR could only be achieved by appropriate ligament releases and surgical techniques (i.e. bone resection to create equal and symmetrical flexion and extension gaps). Griffin et al. [57] also shared the similar findings.

From Scuderi et al. and Griffin et al. studies, both found that implant alignment and soft tissue balancing in the knee joint are interrelated. Ligament balancing is an integral part of TKR and is highly dependent on correct alignment of the knee in flexion and extension. A well-implanted TKR is said to have a balance between stability and motion and also a balance ligaments tension. However, when an implant is misaligned, this could place a different strain on the collateral ligaments and/or cruciate ligament. In some cases, the ligaments might be too tight and in some cases, too loose. Insufficient laxity of the soft tissues and ligaments hinders motion and excessive laxity causes instability. The unequal tension of the collateral ligament may also produce unequal tibiofemoral contact pressures with obvious implications for polyethylene wear and loosening. From a retrieval analysis by Wasielewski et al. [153], an asymmetric polyethylene wear that began at the posteromedial part of the component was a common pattern. This asymmetric wear indicated the non-equal stress distribution on the TKR contact surface, which was likely caused by misalignment of the TKR. Progressive femoral-tibial subluxation [45] and fracture of the medial tibia tray [87], which both resulted in polyethylene failure was also demonstrated to be associated with post-operative extremity alignment and excessive varus positioning of the tibial component [45,87].

Biomechanical studies have demonstrated a close link between the performance of the TKR and the alignment of the TKR in the lower limb post-operatively. Experimental measurements [5,59,128] and finite element method [85] have been used to investigate the sensitivity of TKR kinematics to misaligned installation. However, to date, only a few researchers had investigated the contact characteristics under misalignment conditions. Haider et al. [59] used the Stanmore knee simulator to assess the effects of installing TKR in varus (whereby the axial load was offset by 5 mm from the centre towards the medial side of the TKR) and as well as the effect of installing the tibial component internally rotated up to 10° and externally 10°, with respect to the femoral component. Their results showed that by offsetting the axial load 5 mm away from the centre, to simulate varus knee resulting in very little changes in the A-P displacements and I-E rotations, as compared to the neutral alignment of the knee (axial load applied at the centre and no pre-rotation of the tibial component). Meanwhile, rotation of tibial component of 10° internal or 10° external had a small effect on the A-P displacements but bigger changes in the rotational data when compare to the neutral position. Their report did not publish the kinematics data for this experiment conducted under these conditions. In a static finite element analysis, Liau et al. [85] conducted simulations on three misalignment conditions including the medial translation (up to 1.0 mm), internal rotation (up to 5°) and varus tilt (up to 5°) of the femoral component relative to the tibial component. A compression load of 3000 N was applied to the tibiofemoral joint at 0° of flexion. Overall, they found that each misalignment condition significantly increased the maximum contact stress in the polyethylene component. The most severe situation, which significantly increases the risk of polyethylene wear, was varus tilt, followed by medial mistranslation and internal malrotation.

Misalignment of TKR post-operatively is a well-discussed but not well-investigated (especially in finite element analysis) subject. There are three translational degrees of freedom (medial-lateral, proximal-distal, anterior-posterior) and three rotational degrees of freedom (varus-valgus, flexion-extension, internal-external) for each total knee component. From literature review, most researchers only investigate the misalignment of either one component relative to another component. No studies have yet examined the misalignment of both TKR components at the same time in relation to the ligaments and the consequences on the ligament forces. The study by Liau et al. [85] has limitation as it was a static FE analysis and thus, the tibiofemoral kinematics was not reported in their study. The aim of this study is to examine the effect of altering TKR components orientation relative to the ligaments position on the kinematics of the total knee system. Two different conformities of FE knee models were assessed. Two different activities loads were applied to the FE models. The sensitivity of these two designs to malalignment and to the changes in loading was investigated. The effects on the ligament forces were also examined.

8.2 METHOD

PFC Σ knee and PLI knee models as described in Section 7.4, Chapter 7 were used in this misalignment study. Simulations were performed by offsetting the femoral component and the tibial component, each time 3 mm in the proximal-distal and anterior-posterior directions with respect to the ligamentous structures. The centre of gravity for the femoral and tibial components was also moved along with the offset. An envelope of misalignment positions was defined and shown in Figure 8-1 below. Malrotation of the tibial component including 5° internal rotation and 5° external rotation with respect to the femoral component and varus-valgus tilt (5°) of both femoral and tibial components along the frontal axis were also simulated. The values of 3 mm and 5° were chosen as they were in the range of malalignment values reported in several clinical studies [17,122]. For example, through computed tomography (CT) scan, Berger and Rubash [17] observed that some patients' tibial component was in 5° of excessive internal rotation. Varus or valgus knee usually found to range from 5° up to 10° [9,17,122,126]. The positions of the ligamentous structures remained the same. A total of 12 misaligned positions were examined and results were compared to the neutrally aligned model. Figure 8-2 shows 2 examples of the malrotated positions.

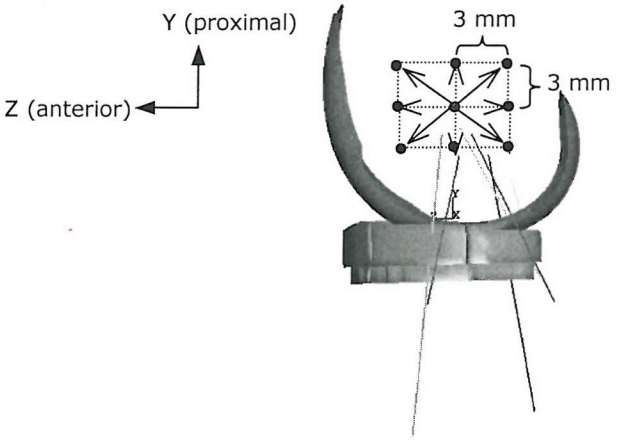

8 misaligned positions:

- Y-distal
- Y-proximal
- Z-posterior
- Z-anterior
- Y-distal, Z-posterior
- Y-distal, Z-anterior
- Y-proximal, Z-anterior
- Y-proximal, Z-posterior
- Neutral (control model)

Figure 8-1: (a) The envelope of misalignment installations of the total knee replacement components.

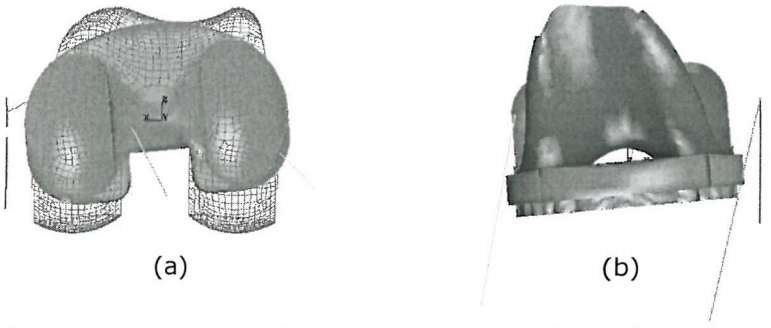

(a) (b)

Figure 8-2: (a) Internal 5° malrotated tibial component relative to the femoral component. (b) Valgus 5° malrotated femoral and tibial components along the frontal axis.

Average loads from subject specific level gait and subject specific stair ascent were calculated and applied to the FE models. The average data for axial force, A-P force, I-E torque and flexion angles, for subject specific level gait and stair ascent are shown in Figure 8-3. The direction of the applied forces remained the same despite changes in the components position. From the averaged force data, Figure 8-3, the stance phase of gait cycle for level gait is between 0% and 60%, while for stair ascent is between 40% and 100% of the activity cycle. Only the stance phase for both activities was simulated. For all cases, the kinematics (A-P translations and I-E rotations), maximum contact pressures and von Mises stresses were calculated. All kinematics are reported from the initial equilibrium position at the beginning of the analyses.

Figure 8-3 (a)

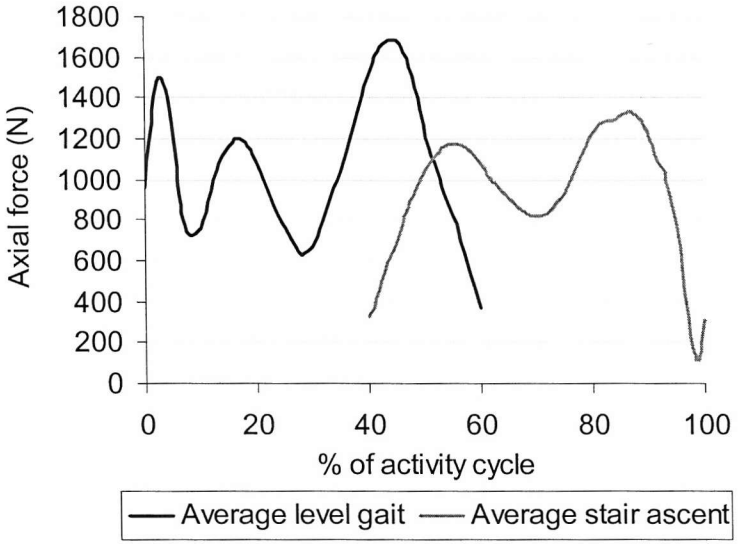

Figure 8-3 (b)

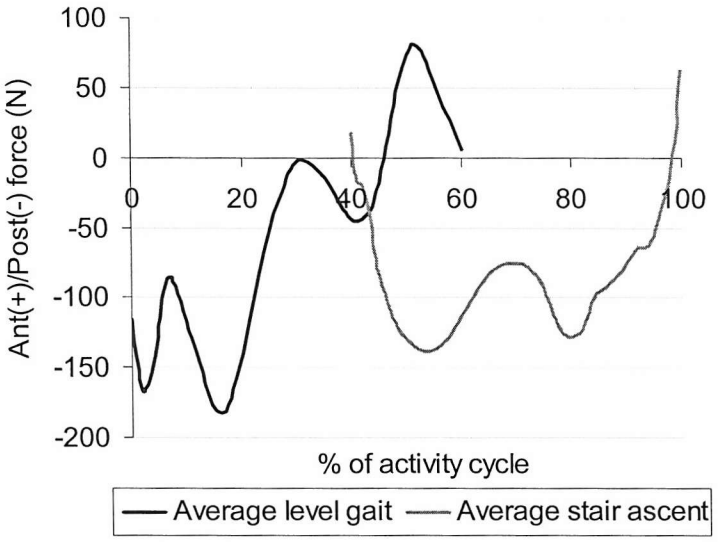

Figure 8-3 (c)

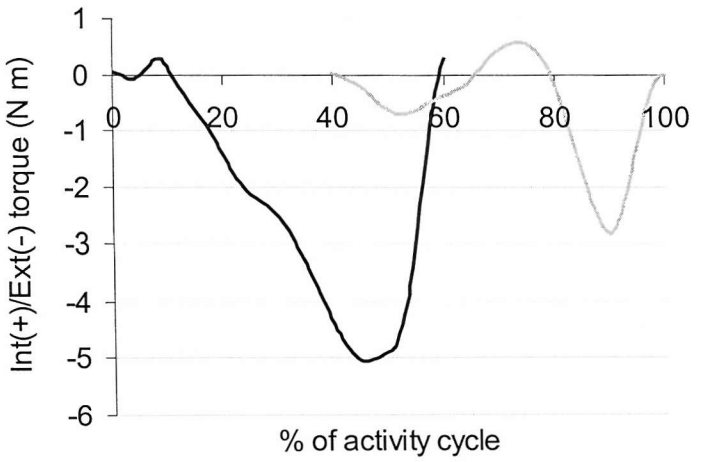

Figure 8-3 (d)

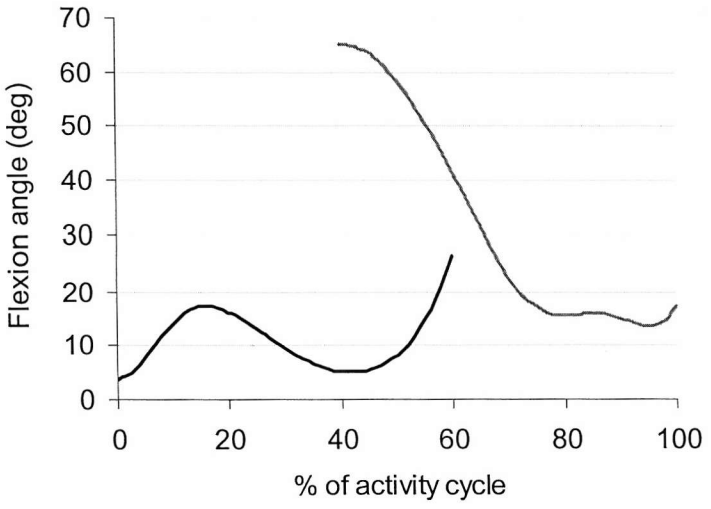

Figure 8-3: The calculated average subject specific level gait and stair ascent knee joint forces: a) axial force; b) A-P force; c) I-E torque and d) flexion angle.

8.3 RESULTS – AVERAGE LEVEL GAIT

8.3.1 PFC Σ Knee

All the misalignment simulations exhibited similar trend of A-P displacements by showing anterior tibia translation with respect to the femur for the first 5% of the gait cycle and then moved posteriorly from 5% to 20% of the gait cycle (Figure 8-4 a). At 20% of the gait cycle, all the simulations displaced anteriorly towards the initial starting position. The tibia insert then translated posteriorly just prior to toe-off, i.e. between 50% and 60% of the gait cycle. When the TKR was maltranslated in Y proximal and then Z posterior (yprox-zpost) directions, the model exhibited the least peak posterior displacement of 2.3 mm. There was no significant difference when compared to the normal alignment model, which showed peak posterior displacement of 2.9 mm. All 12 misalignment simulations, in general, showed a very small offset in the A-P displacements in comparison to the neutral alignment model. There was a 0.1 mm – 2 mm range of A-P displacements during the stance phase of gait cycle. The most significant differences in the A-P displacements occurred between 10% and 40% of the gait cycle. Pre-rotation of the tibial insert internally and externally, relative to the femoral component, did not significantly affect the A-P displacements performance, either in the trend or the magnitude. Similarly, varus or valgus tilt of the TKR also did not affect the A-P displacements.

There was a similar pattern of I-E rotations for all the malorientation simulations (Figure 8-4 b). Misalignment of the TKR did not show any significant changes in the I-E rotations as compared to the neutrally positioned model. From the beginning to 30% of the gait cycle, the tibia externally rotated. Then, the tibia tended to remain at similar position and occurred between 30% and 50% of the gait cycle. Just before toe-off, the tibia internally rotated. When comparing varus-valgus tilt of the TKR to the neutral alignment model, there was an approximately ± 0.2° offset in I-E rotations. The starting position of the tibial insert for externally and internally malrotated cases was different from the other misalignment simulations. At the beginning of the gait cycle, the tibial insert for the externally malrotated model rotated internally 4° (Figure 8-4 b) with respect to the femur. On the other hand, for the internally malrotated model, the tibial insert externally rotated 4° relative to the femur at the beginning of the gait cycle. The rotational changes of the tibial insert relative to the femoral component at the starting of the gait cycle was due to the axial load applied at the beginning of the gait cycle that caused the tibial insert to rotate either in external or internal direction, to find the neutral starting position (the femoral component and the tibial insert come in contact at the lowest contact point on the contact surfaces). The predicted I-E rotations for internal and external malrotated models were zeroed out to make a fair comparison with the other misalignment models (Figure 8-4 c). From Figure 8-4 (c), for the first 30% of the gait cycle, both external and internal

malrotated models did not show any significant changes as compared to the neutral alignment model. Major differences were observed for both models between 30% and 60% of the gait cycle. The internally malrotated model (of the tibia relative to the femur) produced slightly higher peak external rotation (3.8°), whereas externally malrotated model exhibited less peak external rotation (2.6°) as compared to the neutral alignment model (3.1°).

Figure 8-4(a)

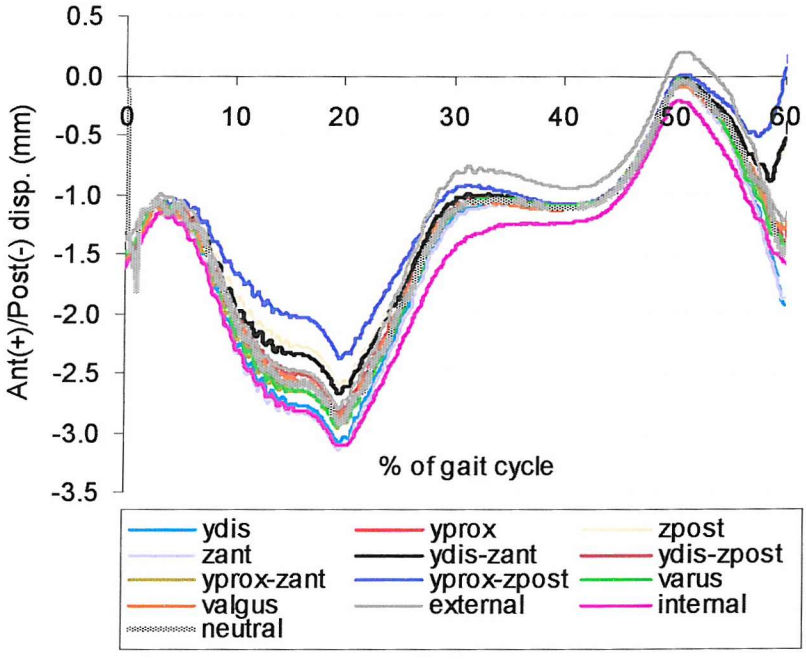

Figure 8-4(b)

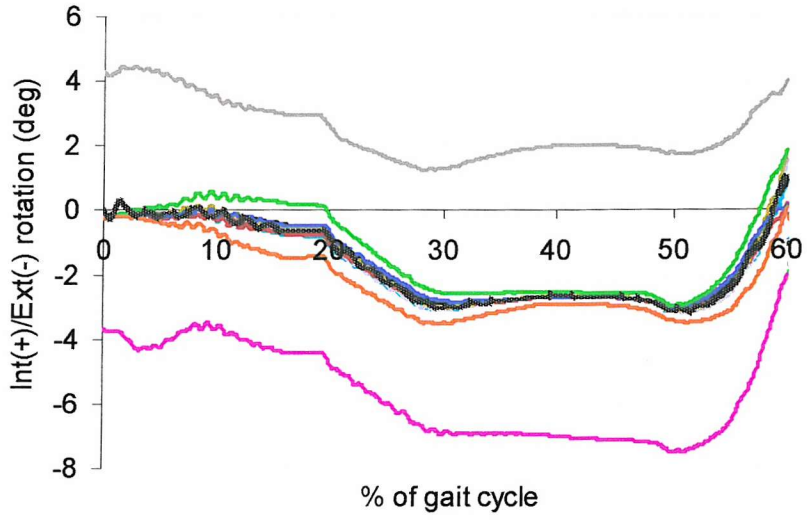

Figure 8-4(c)

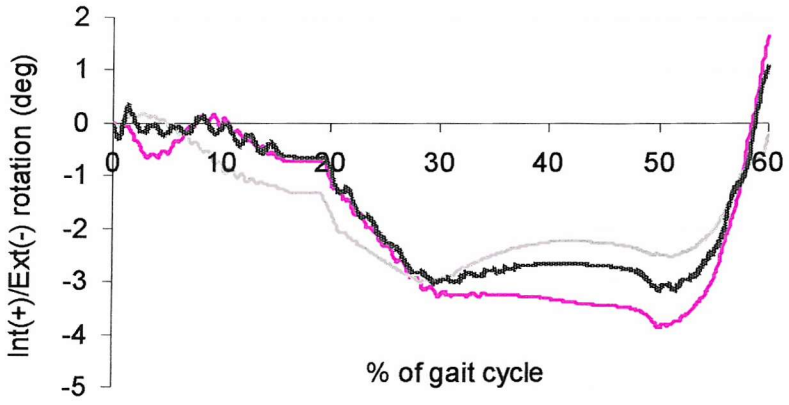

Figure 8-4: The predicted: a) A-P displacements; b) I-E rotations for the 12 misaligned cases during level gait and c) the zeroed I-E rotations for the external and internal malrotated models as compared to neutral alignment model, for the PFC Σ design.

All simulations exhibited a consistent pattern of maximum contact pressures (Figure 8-5 a). There were three peaks occurring, one just after heel strike (0% - 5% of the gait cycle) and a second between 15% and 20% of the gait cycle and the third between 40% and 45% of the gait cycle. The third peak was always the largest, with peak contact pressures varying from 20 MPa – 27 MPa. Valgus tilt of the TKR exhibited the highest peak maximum contact pressure of 27 MPa as compared to all the simulations. Varus tilt of the TKR produced lower contact pressures when compared with neutral alignment model. The peak contact pressure for neutrally aligned model was approximately 24 MPa. Malrotating the tibial component externally and internally with respect to the femoral component did not significantly change the contact pressures in the tibial insert. The maximum contact pressures varied from 10 MPa to 27 MPa throughout the stance phase of gait cycle, with the biggest variation occurring between 20% and 50% of the level gait cycle.

There was a consistent pattern in the maximum von Mises stresses with three peaks occurring (Figure 8-5 b). The first occurred just after heel strike, a second between 15% and 20% of the gait cycle and a third which was generally the largest, occurred between 40% and 45% of the gait cycle. All misalignment and malrotation orientations except varus tilt showed similar value of maximum von Mises stresses throughout the stance phase of gait cycle. As expected, valgus tilt of the TKR exhibited the highest maximum von Mises stress with peak stress value of 20.7 MPa. The rest of the simulations showed peak maximum von Mises stress of approximately 17.5 MPa.

Figure 8-5(a)

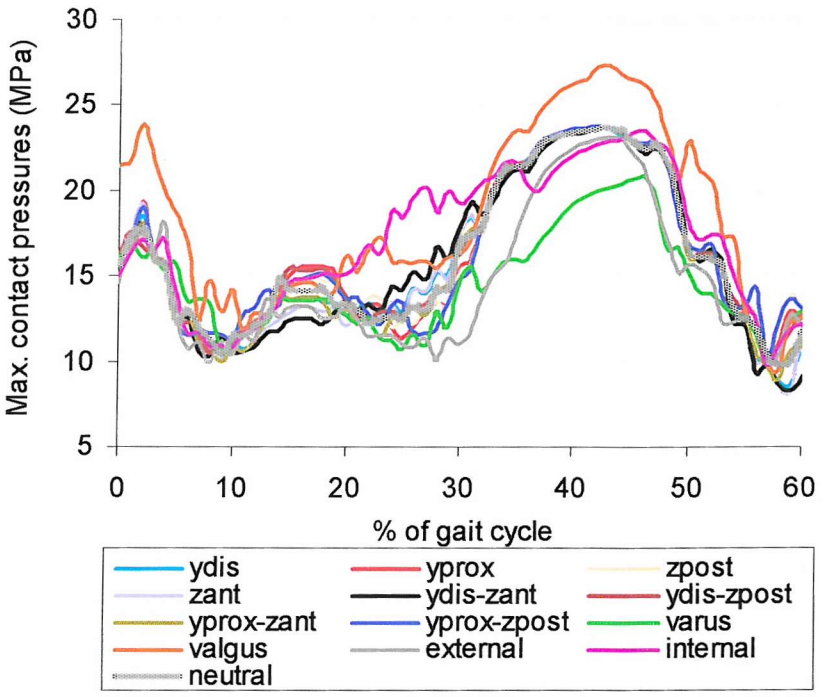

Figure 8-5(b)

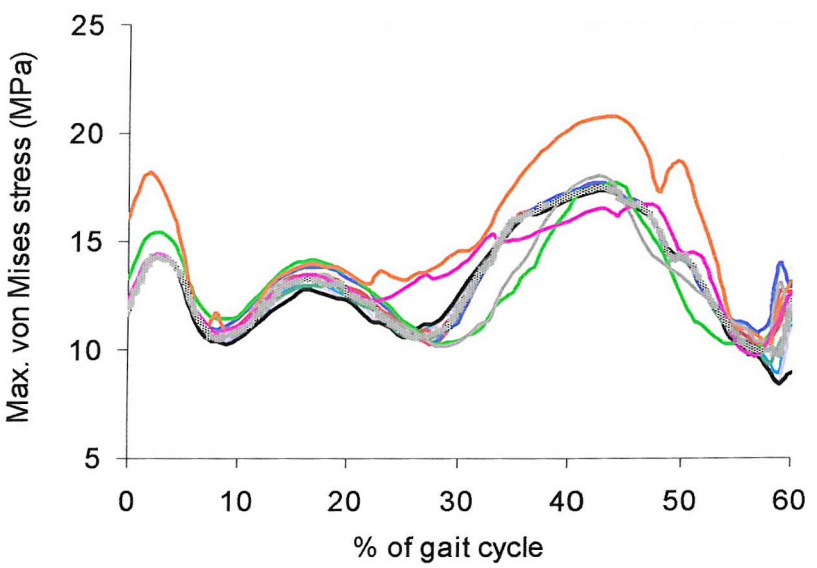

Figure 8-5: The predicted: a) maximum contact pressures and b) maximum von Mises stresses for the 12 misaligned cases during level gait, for the PFC Σ design.

8.3.2 PFC PLI Knee

There was a consistent trend of A-P displacements observed from all the misalignment simulations using the PLI design (Figure 8-6 a). At heel strike, i.e. at the first 5% of the gait cycle, the tibia translated posteriorly with respect to the femur. From 5% - 10% of the gait cycle, the tibia then moved anteriorly towards the initial starting position. Then, the tibia displaced in the posterior direction and reached peak posterior displacement at approximately 20% of the gait cycle. There was no significant difference when comparing the peak posterior displacement value of each simulation to the neutral alignment model. From 20% of the gait cycle, the tibia translated anteriorly and moved just anterior of the initial starting position (between 25% and 30% of the gait cycle). The tibia tended to stay at anterior position and when reached approximately 45% of the gait cycle, the tibia further translated in the anterior direction. Just before toe-off, the tibia translated posteriorly. The peak anterior translation occurred at approximately 55% of the gait cycle. In general, there were no significant changes in the A-P displacements when comparing all misalignment simulations. A range of A-P displacement varying from 0.5 mm – 2 mm was observed during the stance phase of gait cycle (Figure 8-6 a).

In general, a consistent trend of I-E rotations was observed for all the orientations (Figure 8-6 b). The effect of malalignments in the I-E rotations was small compared to the neutral alignment model. Pre-rotation of the tibial insert internally and externally relative to the femur as expected changed the starting position of the rotation. External rotation of the tibial insert at 5° with respect to the femoral component exhibited internal rotation at the beginning of the stance phase of gait cycle, in order to start at an equilibrium position between the articular surfaces of the femoral component and the tibial insert. For the same reason, internally malrotated the tibial insert caused the tibial insert to externally rotated at the beginning of the stance phase. The I-E rotations data for the internal and external malrotated models were zeroed (so that the starting position similar to all the misalignment cases) to make a fair comparison with the neutral alignment model. The adjusted I-E rotations for internal and external malrotated model are shown in Figure 8-6 (c). From the plot, both malrotated models did not produce huge changes in the I-E rotations when compared with the neutral alignment model. The peak external rotation of the 5° externally malrotated, 5° internally malrotated and neutrally aligned models was 7.6°, 8.6° and 9.5°, respectively.

Figure 8-6(a)

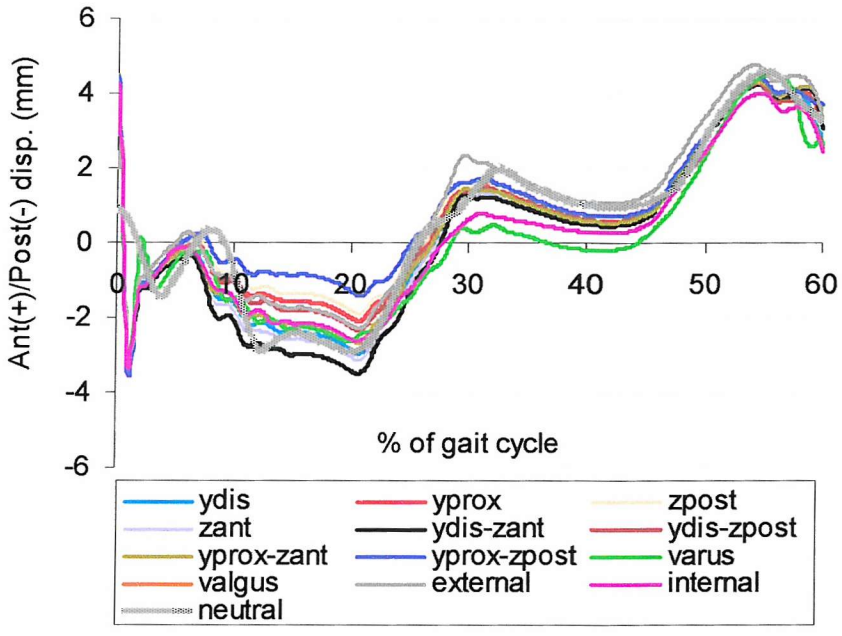

Figure 8-6(b)

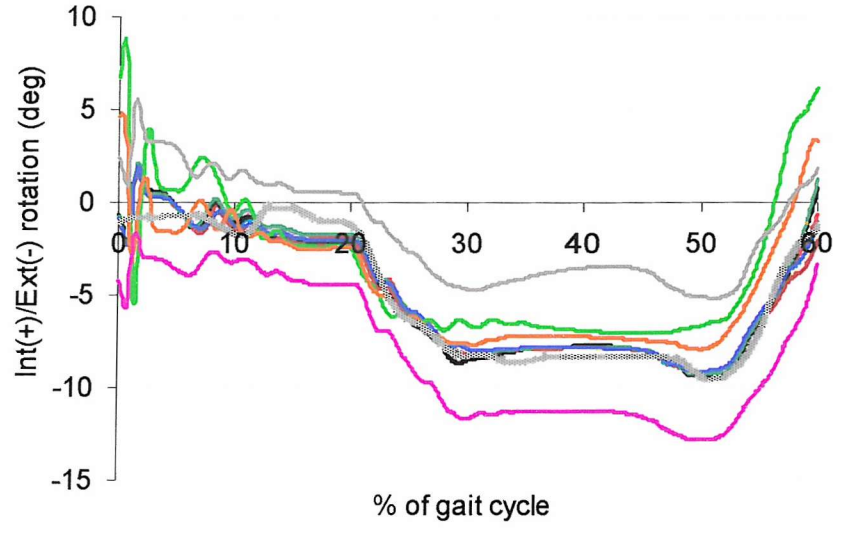

Figure 8-6(c)

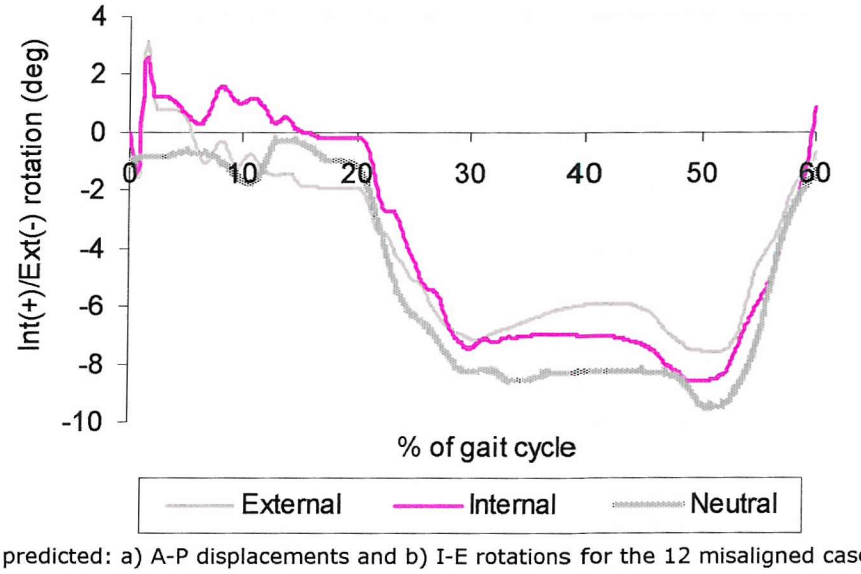

Figure 8-6: The predicted: a) A-P displacements and b) I-E rotations for the 12 misaligned cases during level gait. c) the zeroed I-E rotations for the external and internal malrotated models as compared to neutral alignment model, for the PLI design.

Transients were observed in the contact pressures data for PLI knee model (Figure 8-7 a). This probably was due to too large time step used in these particular models. The time step used in all the analyses was 0.001 ms. The simulation time for each analysis took nearly 36 hours to complete. Due to long computational time, time step 0.001 ms was selected and used in all the analyses. All simulated cases exhibited quite similar value of maximum contact pressures and only very small differences as compared to the neutral alignment model. Higher contact pressures were observed to occur between 30% and 50% of the gait cycle and was due to an increase in the applied axial load (Figure 8-3 a). Malrotated the tibial component, externally and internally with respect to the femoral component did not significantly affect the contact pressures. The highest maximum contact pressure was just over 45 MPa. This was 4 MPa higher than the neutral alignment model.

There was a consistent pattern of maximum von Mises stress (Figure 8-7 b) with three peaks occurring. The peak maximum von Mises stress of each peak was as high as 25 MPa. No significant differences between the simulated cases and the neutral positioned model. Since the maximum von Mises stress was greater than the yield stress of polyethylene (14.5 MPa), local plastic deformation would occur. Majority of the maximum von Mises stresses remained at constant value, 25 MPa and therefore, it would be ideal to refer to maximum contact pressures data for comparisons between misalignment cases. Similar plastic strain was observed as shown in Figure 7-24.

Figure 8-7 (a)

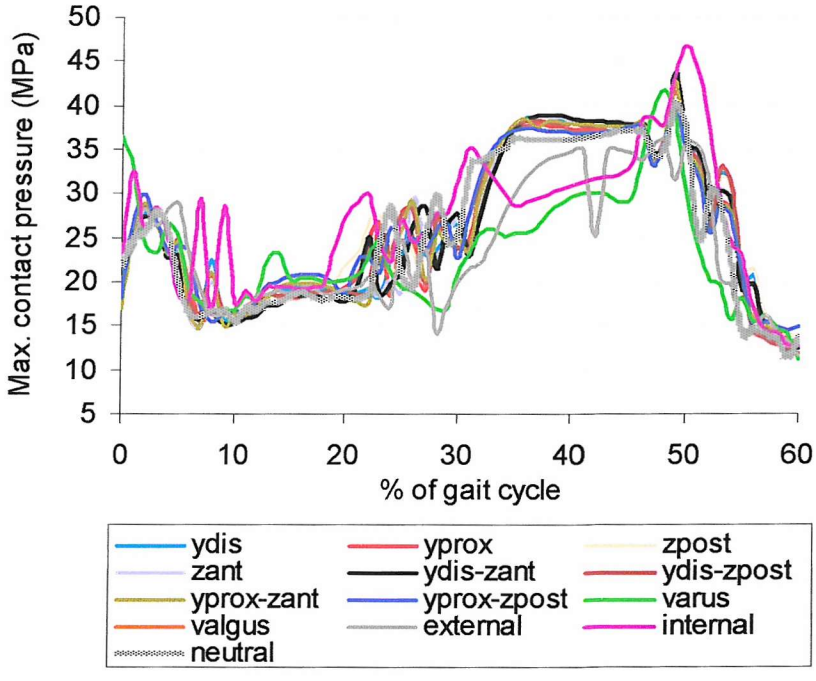

Figure 8-7 (b)

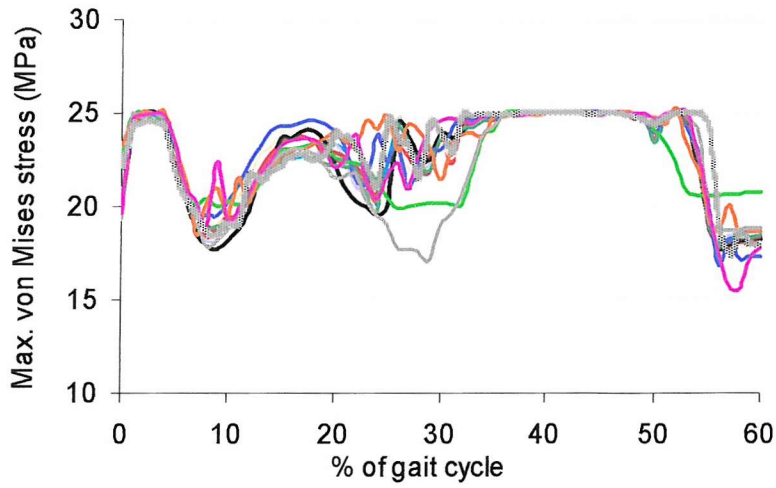

Figure 8-7: The predicted: a) maximum contact pressures and b) maximum von Mises stresses for the 12 misaligned cases during level gait, for the PLI design.

8.4 RESULTS – AVERAGE STAIR ASCENT

8.4.1 PFC Σ Knee

The predicted kinematics, contact pressures and maximum von Mises stresses for the misalignment installation are discussed here. Note that only the stance phase of stair ascent cycle, i.e. from 40% to 100% of the activity cycle is simulated. All results are compared to the neutral positioned model.

Figure 8-8 (a) shows that the PFC Σ knee model is sensitive to the misalignment installation when undergoing stair ascent loads. Larger variations in the A-P displacement were observed when compared to the neutral positioned model, especially between 40% and 70% of the stair ascent cycle. When the TKR was simulated as a maltranslation in the Y distal and then Z anterior (ydis-zant) directions; and Y proximal and then Z posterior (yprox-zpost) directions relative to the ligamentous structures, the changes in the A-P displacements were the maximum in comparing to the neutral alignment model. Offsetting the components position to simulate maltranslation had shifted the neutral position for the A-P displacements during stair ascent activity. When applying the averaged level gait data to simulate maltranslation (Figure 8-4 a), it did not change the neutral position for the A-P displacements. The trend of the A-P displacements during stair ascent was consistent. Model that was maltranslated 3mm in the Y proximal and then 3 mm in Z posterior directions (yprox-zpost) did not complete full stance phase of stair ascent. The analysis failed at the very early stage of the stance phase. It was

observed that as the knee flexed, the lateral condyle tracked to the posterior inner edge of the tibial insert and subluxed. On the other hand, for model that was maltranslated 3 mm in the Y distal and then 3 mm in Z anterior (ydis-zant) directions showed a posterior offset of no more than 2 mm throughout the stair ascent cycle in comparing to the neutral alignment model. The peak posterior displacement was 4.5 mm exhibited by the model maltranslated in the Y distal – Z anterior (ydis-zant) direction. An estimated range of 1.2 mm to 4 mm was observed within the simulations. All the models displaced posteriorly from the beginning of the activity till about 65% of the activity cycle and then translated anteriorly towards the initial starting position just prior to toe-off.

In comparison to the I-E rotations of misalignment simulations using the averaged level gait force data (Figure 8-4 b), the misalignment of the PFC Σ knee showed larger variations in the I-E rotations when the averaged stair ascent force data were applied (Figure 8-8 b). The I-E rotations ranged from internal 8° to external 8°. The analysis for the model maltranslated in the yprox-zpost directions failed at the very early stage of the stair ascent activity. Pre-rotation of the tibial insert at 5° internal and 5° external with respect to the femoral component, as expected, shifted the starting position for rotation, but the pattern for I-E rotations remain unchanged. Externally and internally rotated the tibial insert showed a + 4 ° offset and - 4° offset in the I-E rotations, respectively, when compared with the neutral alignment model in the stance phase of stair ascent cycle. 5° valgus tilt of the PFC Σ knee significantly increased the internal tibial rotation, occurring mainly between 40% and 45% of the activity cycle. There was a small amount of internally directed torque applied to the model at the beginning of the activity cycle. When the model was tilted in valgus position, the MCL was observed to exert higher pulling forces than the LCL, therefore produced larger internal rotation. By comparing the valgus alignment to the neutrally positioned model, the greatest increase in the peak internal rotation was 11°, occurring at approximately 42% of the activity cycle. Varus tilt of the TKR did not show sharp increase in the I-E rotation at the beginning of the stance phase as compared to the valgus malrotated model. All maltranslation simulations caused greater rotational magnitude changes between 40% and 70% of the stair ascent cycle. From 70% to the end of the stair ascent cycle, the rotational changes reduced and close to the neutrally aligned model. In order to make a fair comparison between internal and external malrotated models with the neutral alignment model, the I-E rotations data for internal and external malrotated tibial insert were adjusted to make the starting point similar as the neutral alignment model (Figure 8-8 c). From Figure 8-8 (c), pre-rotation of the tibial insert internally and externally did not show huge affect in the I-E rotations. Internal pre-rotation the tibia insert exhibited the highest peak external rotation (4.5°), followed by neutral alignment model (3.4°) and external pre-rotation of the tibia insert (2.7°).

Figure 8-8 (a)

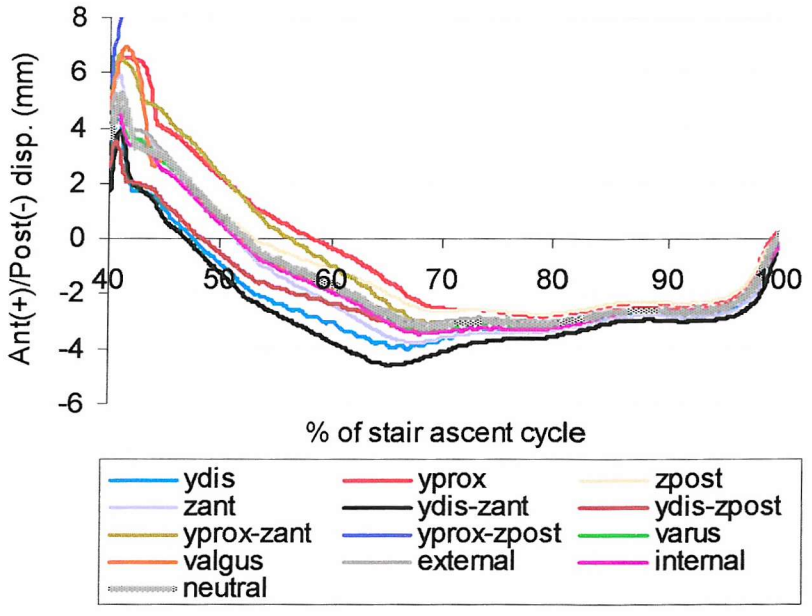

Figure 8-8 (b)

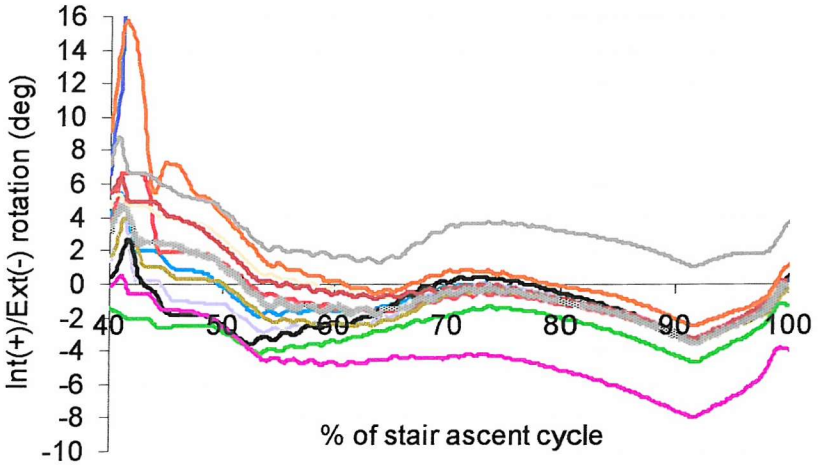

Figure 8-8 (c)

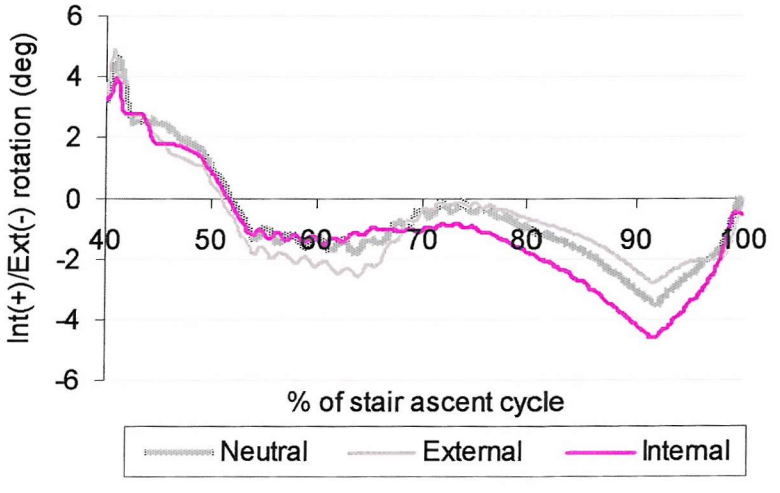

Figure 8-8: The predicted: a) A-P displacements and b) I-E rotations for the 12 misaligned cases during stair ascent. c) The adjusted I-E rotations for external and internal malrotated models as compared to neutral alignment model, for the PFC Σ design.

In general, a consistent range of maximum contact pressures was obtained with 2 peaks occurring (Figure 8-9 a). The changes in pressure magnitude mainly occurred in the first peak between 50% and 60% of the stair ascent cycle, with peak contact pressures varying from 20 MPa – 30 MPa. Between 70% and 100% of the stair ascent cycle, the contact pressures plateaud out with peak contact pressures varying from 13 MPa – 16 MPa for all the misaligned and malrotated simulations. From Figure 8-9 (a), the Y proximal (yprox) and Y proximal – Z posterior (yprox-zpost) maltranslated models exhibited the highest peak maximum contact pressures, just after heel strike (between 40% and 45% of the stair ascent gait). When the TKR was offset to Y proximal (yprox) direction, the peak maximum contact pressure was approximately 38 MPa, and when offset to Y proximal – Z posterior direction, the peak maximum contact pressure was the highest just before the analysis failed. In both analyses, the high contact pressures at the first 5% of the stance phase was observed to have caused by small contact area resulted from the lateral condyle that tracked to the posterior edge of the tibial insert.

In general, there were two peaks occurring (Figure 8-9 b) in the predicted von Mises stress. The first peak, which was the largest, occurred between 50% and 60% of the activity cycle, with peak stresses varying from 22 MPa to 25 MPa. A second peak tended to plateau out and occurred between 85% and 90% of the stair ascent cycle and varying from 13.5 MPa – 16.6 MPa. Several misaligned and malrotated cases exhibited peak maximum von Mises stress of approximately 25 MPa. A constant value of maximum von Mises stress, 13 MPa was observed when the TKR was translated 3 mm in the Y proximal direction. The residual plastic strain in the polyethylene causes residual stress, thus the von Mises remain at constant value. Less changes in the von Mises stress was observed from 70% till 100% of the stance phase when compared to the neutral alignment model.

Figure 8-9 (a)

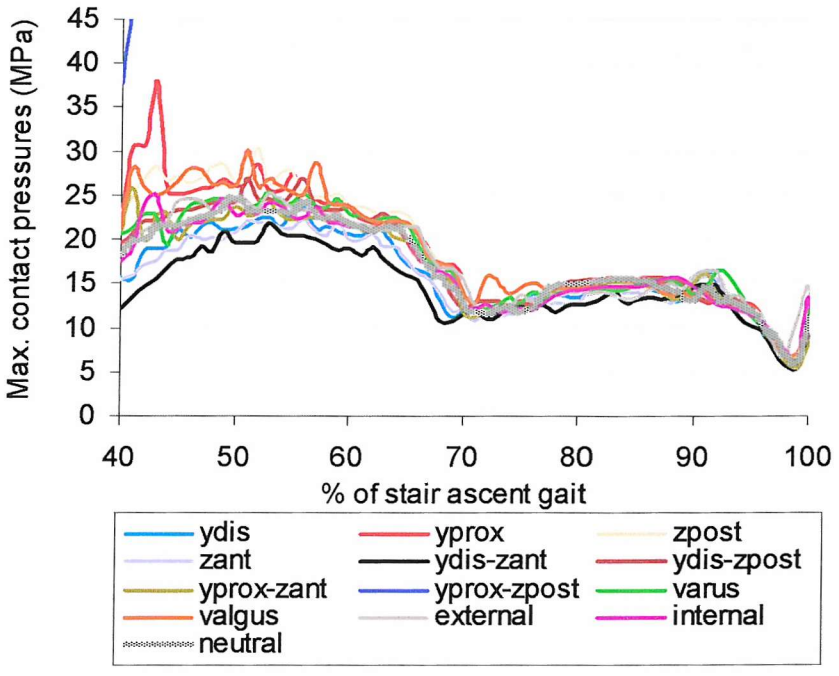

Figure 8-9 (b)

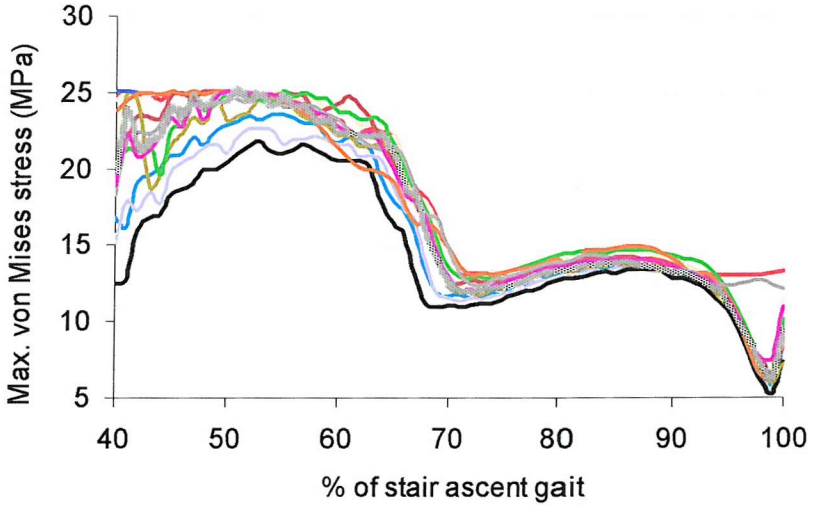

Figure 8-9: The predicted: a) maximum contact pressures and b) maximum von Mises stresses for the 12 misaligned cases during stair ascent, for the PFC Σ design.

8.4.2 PLI Knee

The predicted A-P displacements showed that PLI design was sensitive to the misalignment and malrotation installation when loaded with the stair ascent data (Figure 8-10 a). In general, all simulations showed anterior tibia insert translation relative to the femur at the first 5% of the stair ascent cycle. Then, the tibial insert moved posteriorly and passed the initial starting position. The tibial insert tended to stay posteriorly and this occurred between 48% and 80% of the stair ascent cycle. When reached 80% of the activity cycle, the tibial insert then translated anteriorly relative to the femur. When the PLI knee was offset 3 mm in the y proximal and then z posterior (yprox-zpost) directions, the simulation failed at the early stage of stance phase. It was observed that the lateral condyle of the femoral component displaced and rode up to the posterior edge of the tibial insert, and subluxed. Maltranslated the PLI knee automatically shifted the starting position for A-P displacement and I-E rotation using stair ascent activity load. From Figure 8-10 (a), when the TKR was simulated at y proximal (yprox) direction, it showed the most anteriorly offset in the A-P displacements when compared to the neutral alignment model. The most posteriorly offset in the A-P displacements was when the TKR was maltranslated in the y distal – z anterior (ydis-zant) directions. A range of A-P displacements was observed and this ranged from 1.5 mm to 10 mm.

For the I-E rotations (Figure 8-10 b), most of the changes occurred between 40% and 70% of the activity cycle. The effect of varus and valgus tilt of the PLI knee on the I-E rotations was small when compared to the neutral alignment model. Misalignment the prosthesis by 3 mm in the Y proximal and then Z posterior directions (yprox-zpost) caused earlier failure in the simulations. From the analysis of yprox-zpost misaligned model, it was observed that the MCL-A and MCL-D fibre bundles hold the medial condyle in place but the LCL did not hold the lateral condyle so tightly. The lateral condyle displaced to the posterior part the tibia insert and as the tibia insert continually internally rotated, the lateral condyle rode up to posterior edge of the insert and subluxed. For the other simulations, there was some degree of inconsistency in the I-E rotations between 40% and 70% of the stair ascent stance phase. Overall, the I-E rotations ranged from internal 15° to external 10.5°. Pre-rotation of the tibial insert, internally and externally changed the starting position of the I-E rotations. Externally and internally malrotated the tibial insert with respect to the femur, exhibited internal and externally rotation of the tibial insert, respectively, at the beginning of the stair ascent cycle, in order to start at an equilibrium position. The I-E rotations data for the internal and external malrotated models were adjusted so that the starting position was similar to the neutral alignment model (Figure 8-10 c). From the plot, there was no significant difference when compared the external and internal malrotated models with the neutrally aligned model.

Figure 8-10 (a)

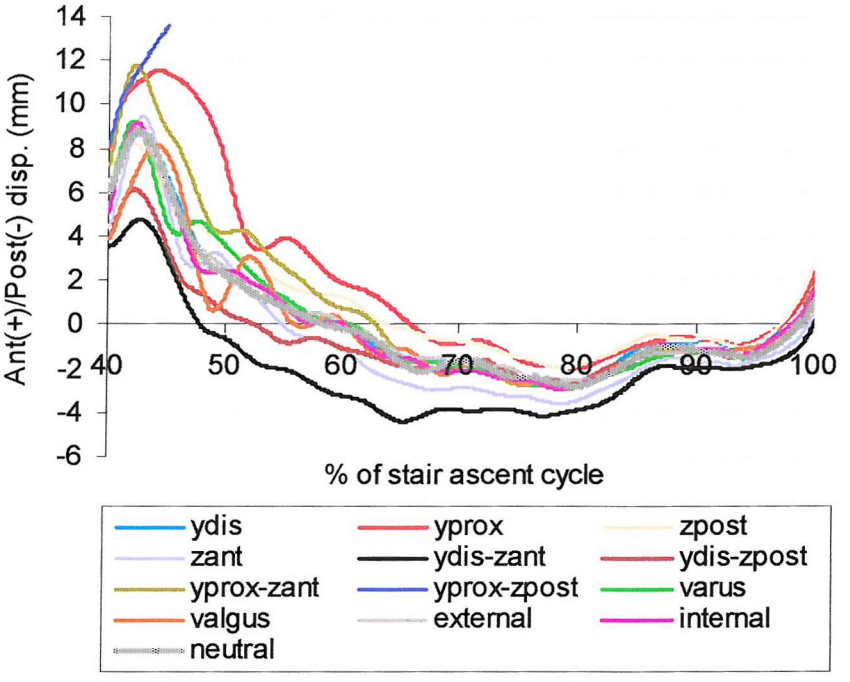

Figure 8-10 (b)

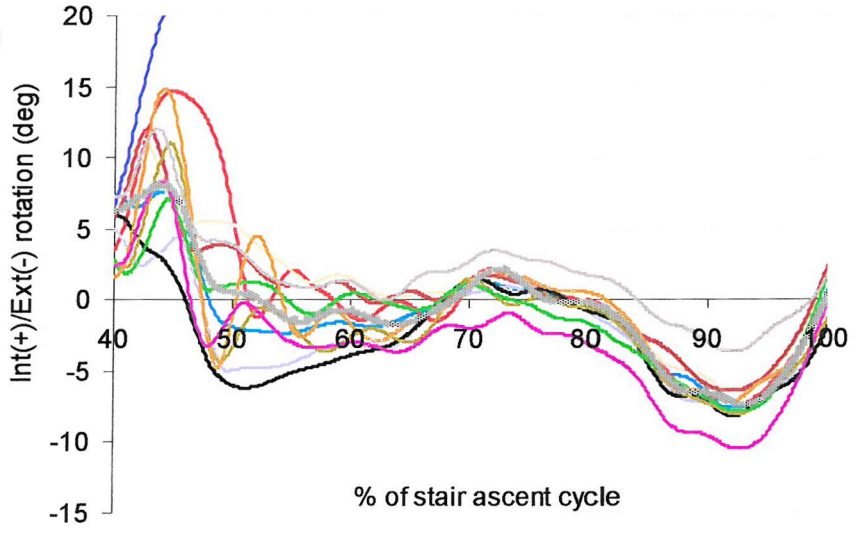

Figure 8-10 (c)

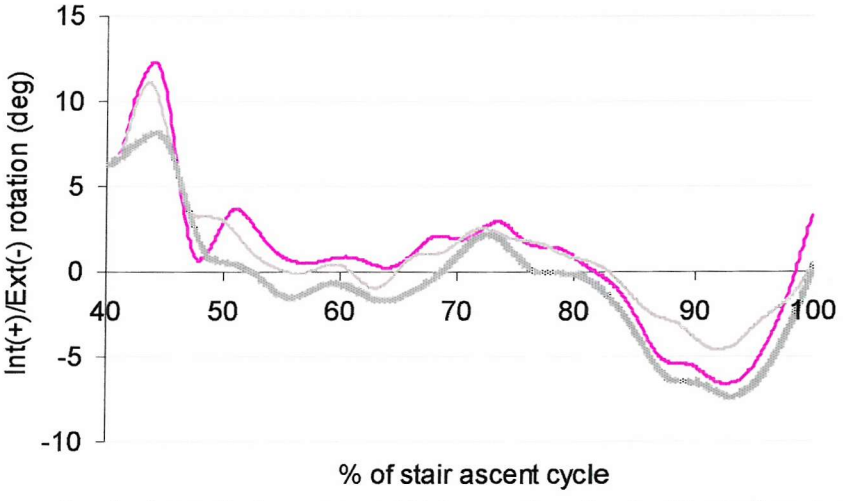

Figure 8-10: The predicted: a) A-P displacement and b) I-E rotations for the 12 misaligned cases during stair ascent. c) the adjusted I-E rotations for external and internal malrotated models as compared to neutral alignment model, for the PLI design.

There was a general trend of contact pressures with two peaks occurring (Figure 8-11 a). The first peak occurred between 50% and 60% of the stair ascent cycle, with peak contact pressures varying from 25 MPa – 30 MPa. A second peak was slightly smaller value compared to the first peak, with peak value varying from 20 MPa – 25 MPa. When the PLI total knee was at the ideal contact alignment (neutral), the maximum contact pressure was approximately 30 MPa (Figure 8-11 a). The worst case was when the TKR was misaligned at Y proximal – Z posterior (yprox-zpost) positions. At Y proximal (yprox) position, the tibial insert showed extremely high contact pressures at the beginning of the stair ascent cycle. As the knee flexed, the lateral condyle was observed to move posteriorly and rode up to the posterior edge of the tibial insert. The contact area at this stage was small and thus, produced high contact pressures. The peak maximum contact pressure for yprox analysis was as high as 40 MPa. This is an increase of 10 MPa as compared to the neutral alignment model. Apart from these two maltranslated cases, all the other simulations did not significantly increase or decrease the maximum contact pressures when compared to the neutral alignment model. Small oscillations were observed in all the analyses.

In general, there were two peaks in the predicted maximum von Mises stress with small changes in the stresses within the misalignment simulations (Figure 8-11 b). Misaligned the prosthesis at Y proximal position gave a constant value of maximum von Mises stress, i.e. 25 MPa. Small transients were observed in the plots. Overall, maltranslation and malrotation of the PLI knee prosthesis exhibited a considerably high maximum von Mises stress. Most of the simulations reached value of approximately 25 MPa. This value was greater than the yield stress of polyethylene and therefore, plastic deformation would occur.

Figure 8-11 (a)

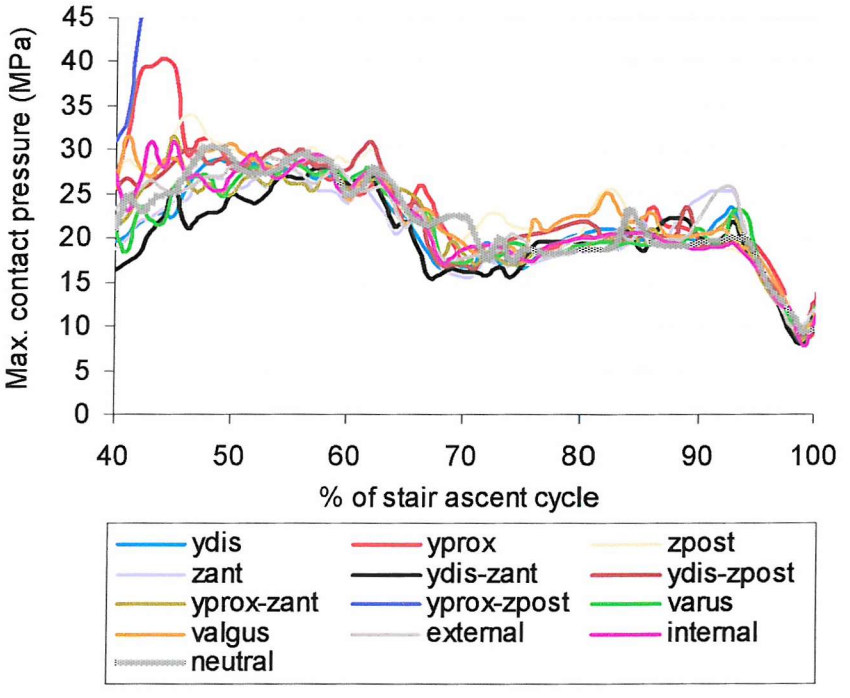

Figure 8-11 (b)

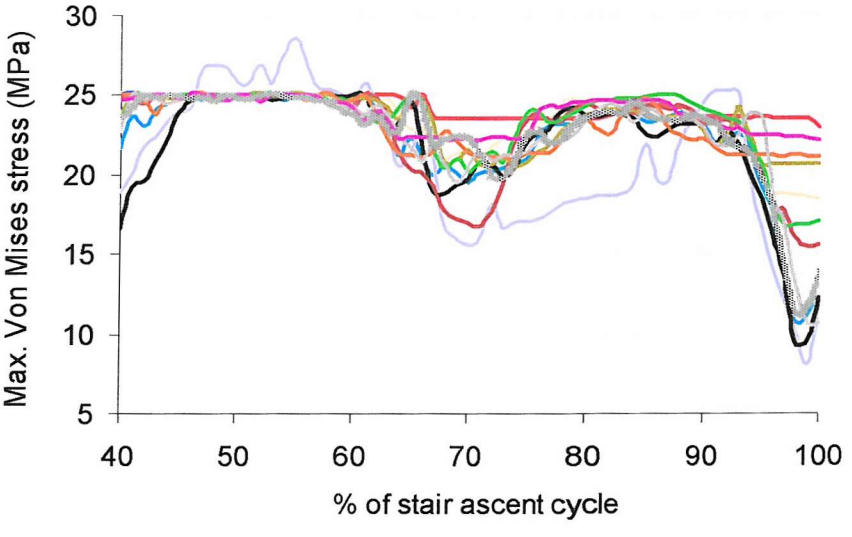

Figure 8-11: The predicted: a) maximum contact pressures and b) maximum von Mises stresses for the 12 misaligned cases during stair ascent, for the PLI design.

8.5 DISCUSSIONS

The kinematics performance and the durability of TKR are dependent on several well-known factors such as patient related (gait pattern) parameters, design of TKR (shape of the articulating surfaces) and surgery related parameters. Surgery related parameters such as implant positioning and soft tissue balancing may be the most important factors in deciding the outcome of the TKR surgery. These two parameters are controllable by surgeons. Pre-operative planning of implants orientation in the patient lower limb and appropriate soft tissue balancing is particularly essential as this could aid in avoiding or at least reducing the severity of misalignment occurring during TKR surgery. Perfect alignment of total knee components in the lower limb is very difficult to achieve [87,93]. There bound to be some degree of misalignment while implanting the prosthetic components. The occurrence of misalignment is mostly due to the handling of surgical instruments while performing TKR surgery by the surgeons. A highly skilled surgeon, who has extensive experience in total knee surgery, would result in less occurrence of total knee misalignment. Surgical instruments that are used in aiding and guiding in the total knee surgery may vary from one design of total knee to another. This may also mean there are differences in surgical techniques depending on the TKR types [64], manufactured by different companies. Hence, for a surgeon, it is particularly important for not just familiar with one design of total knee surgical instruments handling technique, but also be able to switch to other total knee design surgical techniques. There is also possibility that the surgical technique is not always perfect [93] and thus causes balancing problem.

In this study, the simulations were carried out by displacing the implants each time in a 3 mm offset, in a pre-defined envelope of misalignment positions (Figure 8-1). All these orientations could be used to represent the amount of bone being cut during TKR surgery. For example, offsetting the implant in the Y proximal direction was used to represent a situation where the femur is being cut 3 mm more than it should be. Varus-valgus tilt of the implants at the fixed frontal axis of the model and internal-external rotation of the tibial insert with respect to the femur were also examined. Orientating the implant in selected directions in this study has also changed the implant positioning with respect to the insertion points of the ligaments. The centre of flexion-extension axis at the femur and the centre of I-E rotation at the tibial insert were moved along with the implant positioning, i.e. both centres were not affected by the misalignment, varus-valgus malrotation and also the external-internal malrotation of the tibial insert relative to the femur.

For the two TKR designs examined (PFC Σ and PLI), there was little variation in the predicted kinematics for all the simulated cases during level gait activity. The PFC Σ knee exhibited a range of A-P displacement, from 1.2 mm – 2 mm. For the I-E rotation, ignoring

the external and internal malrotated tibial insert cases, a range of 0.3° - 1.7° was observed. The PLI design exhibited a similar range of A-P displacement as compared to the PFC Σ knee, i.e. ranged from 0.5 mm – 2 mm. By ignoring the two internal and external malrotated cases, the I-E rotations for PLI knee ranged from 1° - 8.5°. Greater variability in the I-E rotations of PLI design as compared to the PFC Σ design was observed. The kinematics was a result of the interaction of the applied loads. During the stance phase of level gait cycle, the axial forces were high (Figure 8-3 a) and it constrained the knee from moving too much. The changed in implant positioning did not have a significant effect on the kinematics. Fewer changes in the kinematics were also due to the small knee flexion angle during the stance phase of level gait. Pre-rotation of the tibial insert internally and externally altered the starting position in the I-E rotation (Figure 8-4 b and Figure 8-6 b) for both TKR designs, but the shape of the rotational curves was not affected. The adjusted I-E rotations data for the internal and external malrotated models represented the total amount of the I-E rotations produced by the tibial insert with respect to the femur (Figure 8-4 c and Figure 8-6 c). As compared to the neutral alignment model, there were no significant changes in the I-E rotations.

Although the kinematics for the two TKR designs remained reasonably constant, greater variability was seen in the contact pressures. The contact pressures were quite sensitive to the malpositioning of the components and larger changes were observed to occur between 20% and 60% of the gait cycle (Figure 8-5 a and Figure 8-7 a). Some malpositioning models showed an increase of approximately 2 to 3 MPa in the contact pressures. Although the increase was small, it was enough to accelerate polyethylene wear. Studies [6,46,152] had shown that the amount of wear increased with sliding distance (kinematics), pressures and wear factor.

Contact pressures for PLI knee (Figure 8-7 a) showed three peaks occurring but less obvious shapes compared to the PFC Σ knee (Figure 8-5 a). Transients were observed in the contact pressures data of PLI knee and this was probably due to the mesh type of the tibial insert and the time step. The is because the tetrahedral mesh generates higher contact pressures and this has been discussed in Chapter 4. Greater contact pressures were generated in the PLI knee than the PFC Σ knee, as a result of smaller conformity in the PLI knee, which tended to have smaller contact area. During level gait, the tibial insert for the PLI design suffered local plastic deformation. This plastic strain caused the von Mises stress to remain at 25 MPa from 35% of the gait cycle onwards. Figure 8-12 shows the residual plastic strain in the polyethylene insert for 2 selected misalignment simulations. This was not observed in the PFC Σ design.

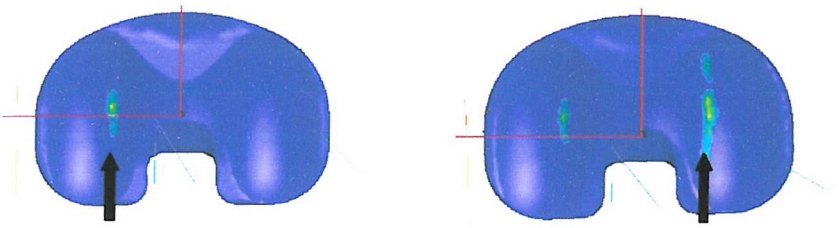

yprox-zant misaligned model Varus tilted model

Figure 8-12: The polyethylene insert showed permanent plastic strain (arrows), from 35% of the gait cycle onwards. The maximum von Mises stresses remained at a constant value. This permanent stress is known as residual stress.

Greater variability in the kinematics as a result of malorientation was observed for the two TKR designs during stair ascent activity as compared to level gait activity. The range of A-P displacements for PFC Σ design and PLI design was, 1.2 mm – 4 mm and 1.5 mm - 15 mm, respectively. For the I-E rotations, both designs exhibited a wide range of I-E rotation, with PFC Σ design ranging from 0.5° - 10° and PLI design ranging from 0.5° - 15° (not including the external and internal malrotation cases of the two designs). Higher changes in the kinematics at the beginning of the stair ascent cycle were probably due to the higher flexion angle and interaction of the applied forces at the early stage of stair ascent activity. Internally and externally rotating the tibia insert with respect to the femur for both designs had changed the starting position for I-E rotation but had only small effect in the A-P displacements. Adjusted I-E rotations data for internal and external malrotated models did not show any significant changes in the rotations when compared to the neutral alignment model.

Altering the alignment of both the PFC Σ design and PLI design 3 mm in the Y proximal and then Z posterior (yprox-zpost) directions in relation to the ligaments caused the model to fail at the very early stage of the stair ascent activity. This could be that at this malpositioning, the ligaments were not able to generate enough constraint to stop the femoral condyle to track to the posterior edge of the tibial insert and it subluxed. At the same time, the tibial insert exhibited large internal rotation.

The forces in each ligament fibre, for all the analyses were checked to ensure that acceptable amount of forces were generated. Under consistent tensile loading, a ligament can sustain a strain of 6% to 8% [47]. After this strain, the ligament starts to fail. By examining the forces generated in each fibre, the maximum force obtained was no more than 600 N. When comparing this value to the force-strain curve representing the ligament property (Figure 7-12, Chapter 7), it was confirmed that each fibre was not over strained. Therefore, the ligaments were functioning within the physiological range reported in the

literature. The amount of forces generated in each ligament for several misalignment cases are shown in Appendix B.

The contact pressures and von Mises stresses were also affected during the stair ascent activity as a result of malorientating the component. From the results (Figure 8-9 a and Figure 8-11 a), positioning the two TKR designs in the Y proximal (and also Y proximal – Z posterior) direction created extremely high contact pressures at the beginning of the stair ascent gait. When both the components were moved proximally at 3 mm, the new components' position relative to the ligaments' femoral insertion point become closer to the articulating contact surface. At this new position, the PCL-P fibre bundle exhibited higher forces than the neutrally aligned model (Appendix A). The was an increased of 150 N and together with small contact areas created as a result of reduces in curvature radius at the femoral component when the knee was flexed at high angle, hence, high contact pressures were observed. Maltranslation of the two TKR designs in the Y proximal direction(s) should be avoided. The contact pressures of all other simulations were the highest at the first peaks and then gradually decreased in the second peak. When examining the axial force data, the first peak was lower than the second peak. Hence, the contact pressures for the TKR designs examined were highly affected by the flexion-extension angles than the axial loads.

Both the TKR designs exhibited fairly similar contact pressures. However, due to the greater variability in the kinematics and lower conformity of the PLI knee when compared to the PFC Σ knee, higher contact pressures and von Mises stresses were reported for PLI design. The contact area of PLI knee was smaller than the PFC knee. Local plastic deformation was observed in all misalignment analyses using the PLI model during stair ascent activity. Plastic yielding was observed in the PFC Σ knee when it was misaligned 3 mm in the Y proximal (yprox) direction.

The effect of misalignment on the performance of total knee replacement is a topic of significant interest, and has been the focus in a variety of experimental [59,64,85,93,154] or finite element studies [36,85]. Direct comparisons of varus-valgus misalignment results from this study with other studies [59,64,154] are not possible. For instance, Liau et al. [85] performed varus tilt of 1°, 3° and 5° of the femoral component relative to the tibial component using a static FE analysis. A compression load of 3000 N was applied to the tibiofemoral joint at 0° of flexion. They found that the contact stresses and von Mises stresses increase as the varus tilt angle getting bigger. The kinematics were not predicted. Direct comparisons of results from this study with Liau et al. [85] study were not possible. This could be explained by the difference in the component positioning. Our study simulated the varus and valgus misalignment by tilting both femoral component and tibial

insert at the fontal axis. However, Liau et al. simulated the misalignment of the femoral component with respect to the neutrally fixed tibial component.

The predicted kinematics by internally and externally malrotating the tibial component relative to the femoral component from this study exhibited similar findings as Haider et al. [59]. In their study, ISO standard load was applied using a knee simulator and the kinematics (A-P displacements and I-E rotations) of PFC Sigma knee when the tibial component was rotated internally by 10° relative to the femoral component, then externally by 10° were examined. They found that internally or externally malrotated the tibial component relative to the femoral component did not have a significant effect on the A-P displacements. Malrotating the tibial component in this way only shifted the neutral position for rotation. This study showed good agreement with Haider's findings.

To our knowledge, there are very limited misalignment studies that have yet examined the mal-positioning of both femoral component and tibial component at the same time, and the effect of this misalignment on TKR kinematics. Haider et al. [59] reported the kinematics of various TKR designs when misaligned at different positions. However, results obtained from their study could not directly be compared to ours, typically for the envelope of misalignment position that had been discussed.

Comparisons of the maximum contact pressures and maximum von Mises stresses obtained from this study with previous analyses is complicated by design, material properties, methods (FE or experimental) and boundary condition. However, in general, the maximum contact pressures and maximum von Mises stresses obtained are similar to other studies [36,51,85,92,93,137]. Szivek et al. [137] reported contact pressures of between 15 MPa and 20 MPa for PFC Sigma knee when flexed at 15° with an applied vertical load of 2000 N. The contact pressures were measured by inserting pressure sensor films in between the femoral component and tibial insert. When comparing PFC Sigma knee contact pressures during level gait obtained from this study to Szivek et al., there were no significant differences observed. Liau et al. [85] performed static FE analysis by applying 3000 N load to three different conformity designs. From their observation, model with the lowest conformity (flat-on-flat) exhibited the highest maximum contact pressure (32.6 MPa) and von Mises stress (13.4) than the more conforming ones. Similarly, PLI design being less conforming than PFC Sigma design and hence, higher contact pressures and von Mises stresses were obtained. Nonetheless, it should be noticed that comparisons of results from this study and previously reported studies are limited by the differences as mentioned earlier.

It should be pointed out there are a number of limitations with this study. The averaged forces used in this study are from a group of healthy subjects. Patient who went through

TKR surgery might have different load histories. The axial force has been applied to the centre of the femoral component in the misalignment simulations and leading to a 50:50 load distribution to the medial and lateral compartments of the knee. In the misalignment knees, the axial load would not have been applied at the centre of the femoral component. The insertion points of the ligaments were approximately positioned according to the size of the TKR and this did not accurately represent the physiological model. Despite these limitations, this is the first attempt to examine the effect of misalignment on the performance envelope of TKR during level gait and stair ascent activities. For the TKR designs examined, the kinematics during level gait are relatively insensitive to the misalignment. Although the kinematics are not affect significantly, some malalignment positions do increase the contact pressures. However, the kinematics are sensitive towards misalignment during stair ascent activity. The main reason for these is the degree of knee flexion-extension angles during level gait and stair ascent. This study could be used to test the sensitivity of TKR designs by altering the implant positions.

Summary of results
▪ The kinematics of PFC Σ and PLI designs were less sensitive to the misalignment when the level gait loads were applied. Conversely, the kinematics was more sensitive to the misalignment orientations when stair ascent activity loads were applied. ▪ Contact pressures of PFC Σ and PLI designs were influenced by malalignment for both level gait and stair ascent. ▪ Higher knee flexion angles during stair ascent activity had been proved to be the main factor contributing to the high contact pressures seen in the tibial inserts for both TKR designs. ▪ Varus-valgus misalignment of the tibial component relative to the femoral component did not show significant effects on the A-P displacements, but only shifted the starting position for the I-E rotations. The trend of the predicted kinematics remained similar to the neutral alignment model. ▪ Under stair ascent loading, misaligned the total knee components 3 mm in the y proximal and then 3 mm in the z posterior resulted in subluxation of the model. ▪ During level gait and stair ascent, misalignment in the PFC Sigma knee did not significantly affect the kinematics as compared to the neutrally aligned model. However, in some analyses, contact pressures were observed to have increase slightly. Increased in contact pressures would speed up the process of polyethylene wear and hence, increased failure rate of the TKR.

Chapter 9

DISCUSSIONS AND CONCLUSIONS

Total knee replacement (TKR) is the treatment of choice for severe degenerative knee joint disease. Opting for TKR helps the patient to regain normal kinematics in daily activities. The purpose of the TKR is to relief pain, to restore motion and eventually give the patients normal life again. The performance of the TKR is highly dependent on TKR design, patient-to-patient variability and surgery related parameters. To assess the *in vivo* functional performance of the different TKR designs, careful quantitative analyses especially *in vivo* tests must be carried out. The measurement techniques that are most commonly used are video fluoroscopy and radio-stereophotogrammetric analysis (RSA). Through these techniques, patients with TKR can be examined post-operatively (follow-up examination) to assess their kinematics such as flexion-extension angles, abduction-adduction, anterior-posterior translations and internal-external rotations of the implants. These methods provide information on the magnitude and pattern of motion of implants but give no information on the contact pressures or stresses acting on the articulating surfaces of the implant. Knowledge of the contact pressures or stresses imposed by the implant are very important for assessing the durability and the effect these have on the wear of the polyethylene insert. Mechanical testing such as a knee simulator [10,13,150] has been used to simulate the kinematics performance of a knee implant and assess wear. Experimental wear studies [10,13,15,16,24,150] are dynamic testings, of which load profiles or combined load-displacement profiles are used as input. These dynamic experimental studies are not capable of predicting the contact pressures within the TKR. The contact pressures have been evaluated in static studies [36,92,93,155], i.e. an amount of load transferred through the opposite component is measured by the thin pressure sensor film after an amount of axial load is applied at a specific component position. Pressure sensor film could also provide information on the contact patch/area generated. Early static FE analyses [11,12,85,130,131] only examined the contact pressure distributions. However, the development of explicit FE models has allowed the kinematics as well as the pressures or stresses to be calculated for a whole activity, for example level gait. So far, the assessment of performance of TKR has been conducted based in an idealised gait cycle, using either FE or experimental methods.

The knee joint experiences a variety of loads during daily living. Apart from level walking, stair ascent and descent are the activities encountered in our daily life. Squatting activity is particularly common among Asian countries [63]. These activities are thought to apply higher loads (being more demanding activities) at the knee joint as compared to the

conservative level gait activity. Current assessment methods have yet to use other dynamic joint contact forces to simulate other daily activities. Although using the idealised load case allows for direct comparison of implant designs, it gives no indication of the sensitivity of a design regarding activity variability and patient-to-patient variability. In Chapter 5, four daily activities were simulated: level gait, stair ascent and descent, and squatting. Stair descent force data was based on results from three separate studies as summarised in DesJardins et al. [33]. The four inputs were flexion angle [95], compression load [115], anterior-posterior force [95] and internal-external torque [3]. The limitation of using these inputs was that it did not realistically represent a specific individual during stair descent activity as the measurements were taken from different individual in each of the studies. A squatting activity was also examined as it involved greater knee flexion than level gait, stair descent and stair ascent. The force data and flexion angle data were obtained from Dahlkvist et al. [32] study. Only the compression load and anterior-posterior force were calculated from their studies (average of 6 subjects). Torque was not reported, as the 2-D analysis was not able to calculate this force component. Furthermore, in Chapter 5, stair ascent was also simulated. The force data were kindly provided by Professor Patrick Costigan, Queen's University, Canada. The force data were the average of knee joint loadings from 9 healthy elderly subjects whom were asked to perform a step-up task. The ISO forces were used as the input for the level gait simulation.

The forces of each of these activities were plotted against percentage for one full activity cycle and were shown in Figure 5-1. The axial forces for stair descent and squatting activities were higher than level gait. The peak axial force during stair descent was approximately 6 times BW; whereas the peak axial force during squatting was approximately 7.5 times BW. Level gait exhibited a lower axial force with the peak value approximately 3.6 times BW. Stair ascent had the lowest axial force as compared to the other three activities, with peak value of approximately 1.9 times BW. For anterior-posterior force (Figure 5-1 b), squatting activity exhibited continually increase posterior force of the tibia relative to the femur. The peak posterior force was 2900 N (4.1 times BW). Stair descent exhibited anterior-posterior force ranged from + 110 N to - 120 N. Stair ascent exhibited anterior-posterior force ranged from + 550 N to - 140 N. The A-P force during level gait ranged from + 110 N to -120 N. Three of the activities showed external torque of the tibia relative to the femur for most of the activity cycle (Figure 5-1 d). Stair descent activity exhibited the highest peak external torque, 15.5 N m; followed by level gait with peak external torque of 7.2 N m and stair ascent with peak external torque of 2.7 N m. No torque component was recorded for squatting activity. Knee flexion angle varies within these activities. All activities were observed to have larger range of flexion angles under load as compared to level gait. Over 120° of knee flexion angle was observed during the squatting activity. The highest flexion angle during stair ascent and stair descent was 88° and 80°, respectively.

Each activity exhibited different kinematics pattern and magnitude, dependent on the applied forces. All three activities exhibited more A-P translations than level gait. Among the activities, stair descent exhibited the highest range of A-P displacements, I-E rotations and also the highest contact pressures and von Mises stresses. The A-P displacement for stair descent and level gait ranged from + 4 mm to - 9.3 mm and from 0 mm to - 4 mm, respectively (Figure 5-2 a). Squatting exhibited large posterior tibial displacement with respect to the femur with peak posterior displacement reaching 10 mm. The large posterior displacement was due to large applied posterior force. The analysis for squatting stopped at 115°, occurring at 84% of the activity cycle. The femoral component was seen to ride up the anterior lip of the tibial insert and as the tibial insert continued to translate posteriorly, the femoral component finally fell off from the tibial insert anterior lip. For stair ascent activity, only the stance phase, i.e. from 40% to 100% of the activity cycle was simulated. When compared with level gait, there was no significant difference in the A-P displacement. Stair ascent recorded a peak posterior tibial translation with respect to the femur of 4.6 mm. Stair descent with the highest external torque exhibited the largest external tibia rotation (7.5°), then followed by level gait (4.9°) and stair ascent (3°). No I-E rotation was recorded for squatting activity as no torque was applied.

One very important limitation that should be taken into account is that the force data for the different activities has been taken from a variety of sources using different methods. This may account for the large variation in force magnitudes between stair descent and stair ascent. Since total knee replacements are being put in younger and more active patients, this study on more demanding activities other than level walking is essential in evaluation of TKR performance. It must be borne in mind that the squatting force data did not take into account the torque at the knee joint. Nagura et al. stated [108] that greater range of motion in TKR is of particular concern for an increased risk of mechanical failure, since the mechanics of the knee in higher flexion angle (or deep knee flexion) are likely a factor causing problems of instability in TKR.

In Chapter 5, for the TKR design examined, the high contact pressures during level gait, stair descent, stair ascent and squatting activities all occurred at higher flexion angles (Figure 5-3), as a result of smaller contact area (smaller radius of femoral condyle curvature as the knee flexed). For each of the activities examined, the maximum von Mises stress was greater than the yield stress of the polyethylene insert (14.5 MPa) and local plastic deformation occurred. For stair descent and squatting activities, in particular, the higher axial loads (5 - 6.5 times BW) resulted in the polyethylene insert to be permanently deformed and residual stresses were observed (Figure 5-2 d). As surface damage is associated to stresses, this could lead to higher potential for adhesive and delamination wear development [85]. The loads during stair ascent were lower compared to level gait. It was more likely to be due to the way the forces were calculated in the

different studies. The study of simulating different activities encountered in daily life not only benefits in the area of the performances of the TKR, but also important in the design of prostheses towards the selection of the most suitable implant for patients with different demands. This study has emphasized that level gait is a very conservative activity. Simulations using stair descent and deep flexion activities joint contact forces could push the performance of this TKR design to the maximum limit, in terms of kinematics and contact stresses.

From the literature search, relatively little is known about the magnitude and distribution of the forces in the knee. However, *in vivo* kinematic studies suggest that there is considerable variation in the forces as there is a wide range of kinematics reported for a given design. For instance, Rittman et al. [127] performed the analysis of patterns of knee motion during walking for four types of total knee implants implanted in four groups of patients. They recorded the kinematics pattern in three planes (sagittal, coronal and transverse) and then carried out cross-relation analysis on each group of patient with the same implant. This technique was described as 'degree of similarity' in comparison of the patterns of knee motion exhibited by the same total knee implant or comparison between different total knee implants. Comparisons were then indicated in terms of cross-correlation coefficients. The highest coefficient being 1.00 and this means the patterns of two curves would be exactly the same. From the results, they found no exact correlation in the motions pattern within the patient group with the same implant. For instance, for the nine Geometric knees implanted in seven patients, the cross-correlation coefficients in the sagittal plane, coronal plane and transverse plane were 0.96, 0.71 and 0.70, respectively. The cross-correlation coefficients for six Shiers knees implanted in five patients in each of the planes were 0.87, 0.72 and 0.62, respectively. There were always some degree of differences in the kinematics performance in all three planes. These analyses of functional *in vivo* TKR motions have shown that for the same implant, different kinematics was obtained. Further analyses towards these kinematics ranges suggested one of the major factors is the difference in the joint contact forces between patients. The relation between the kinematics of the TKR and the forces apply is well understood. The kinematics produced (magnitude) is a resultant of various components of the joint contact force, e.g. axial force, A-P force and I-E torque. These joint contact forces are dependent on patient parameters, such as the weight, gait pattern and quality of bone after TKR, and as well as surgery related parameters, i.e. alignment of the implant and soft tissues balance. Therefore, the knee joint forces of a TKR patient will be different from another TKR patient. In Chapter 7, the influence of patient-to-patient variability was assessed.

No direct measurement of the joint contact force has been reported and we rely on predicted values from inverse dynamic studies [102,103]. The joint contact forces applied in this study (Chapter 7, section 7.2) were kindly provided by P. Costigan. The joint contact

forces were calculated by means of inverse dynamic method. The joint contact forces during level gait were obtained from 6 females and 1 male and during stair ascent, the joint contact forces were from 3 females and 6 males. These two groups of subjects were unrelated. The average age and average weight of subject in the level gait group was 63 years (range from 46 - 72 years) and 68.8 kg (range from 47.8 - 99.8 kg), respectively. The average age and weight of subject in the stair ascent group was 69 years (range from 66 - 72 years) and 72 kg (range from 55 - 93 kg), respectively. Overall, a range of joint contact forces was observed for the two activities (Figure 7-1 and Figure 7-2). For subject specific level gait, the maximum axial force was estimated up to 4 times BW. In general, a consistent pattern of axial load, I-E torque and flexion angle was observed, but less well defined in the A-P force. Meanwhile, for subject specific stair ascent, the estimated maximum axial load was up to 3.8 times BW. When comparing to level gait, the loading pattern during stair ascent was less well defined within the subjects. This study has shown variations in the magnitude of the joint contact force *in vivo* and range of flexion-extension movements and are due to differences in gait pattern and loading conditions.

The joint contact forces during level gait and stair ascent activities obtained from two different groups of healthy subjects were applied to two total knee designs in order to examine the performance envelope of TKR, as summarized in Chapter 7. The results showed that the kinematics of total knee designs examined (PFC Σ and PFC PLI) do vary from one individual to another individual. A performance envelope of kinematics, contact pressures and stresses was obtained as a result of patient-to-patient variability. Overall, for both PFC Σ and PLI total knees, the kinematics during level gait were less sensitive to variation of subject specific loading, but greater variations were observed during stair ascent. Simulations were performed with and without representation of collateral ligaments. For PFC Σ ligaments model, during level gait, the standard deviations from the mean ranged from 0.3 mm - 1.2 mm and 0.4° - 3.2° for the A-P displacements and I-E rotations, respectively; whereas during stair ascent, the standard deviations from the mean ranged from 0.6 mm - 2.5 mm and 2.0° - 6.1° for the A-P displacements and I-E rotations, respectively. The variation in the PFC Σ model kinematics for stair ascent loading was two times higher than level gait. Overall, the PLI design show higher magnitude and greater variability in the kinematics as compared to the PFC Σ design. During level gait, the standard deviations from the mean for PLI design were 0.6 mm - 2.3 mm and 1.0° - 5.2° for the A-P displacements and I-E rotations, respectively. On the other hand, during stair ascent, the respective A-P displacements and I-E rotations standard deviations from the mean was 1.0 mm - 3.0 mm and 3.9° - 7.0°. From the observations, there are no subjects that exhibited same kinematics performance. The amount of A-P displacements and I-E rotations produced are totally dependent on the applied load. The kinematics are also strongly affected by the surface geometry of the TKR design. From the predicted kinematics, it is clear that different TKR designs will result in different magnitude of

kinematics as well as the kinematics trends. Both PFC Σ and PLI designs were subjected to the same loading conditions and same ligamentous constraints, but PLI model showed higher sensitivity than PFC Σ model. DesJardins et al. [34] had shown that the kinematics altered with implant designs. They examined the kinematics over 8 different implant designs by utilizes the same loading regime across all implant designs to establish a standard by which the TKR mechanics could be compared. TKR kinematics were shown to vary between designs. For example, the maximum and minimum anterior(+)/posterior(-) displacement and internal(+)/external(-) rotation for the high conformity IB (Insall-Burstein I, Zimmer) design were -0.6 mm/-4.1 mm and +8.1°/+1.0°, respectively; the low conformity SPRO (Sulzer Protek Gueper) were +0.5 mm/-6.4 mm and +14.1°/-6.0°, respectively. The results in Chapter 7 showed that the motion pattern between PFC Σ and PLI designs also varies due to the different degree of constraint provided by the tibial insert. But, it also shows that the PLI design is more sensitive to variability in the loads applied by different patients. Analyses like that of DesJardins et al. [34], in using a single load case, with the maximum load of only 3 times BW, are unable to determine patient-to-patient variability sensitivity. Gait studies [31],[103] have proven that a TKR design will experience a range of loading conditions *in vivo* due to differences in gait pattern. The calculated knee joint forces could be as high as 6 times BW.

The PLI design has a lower conformity than the PFC Σ design. As a result, smaller contact area is observed and this generates higher contact pressures (Figure 7-15). For PLI model during level gait activity, the standard deviations from the mean for the contact pressures ranged from 1.8 MPa to 15.8 MPa (Figure 7-22 b). For stair ascent activity, the maximum contact pressures standard deviations from the mean varying from 1.0 MPa to 11.5 MPa (Figure 7-32 b). However, PFC Σ knee generates less contact pressures due to higher conformity (as compared to PLI design) with larger contact area (Figure 7-15). For PFC Σ model, the contact pressures were observed to vary from 0.8 MPa – 8.0 MPa during level gait. For stair ascent activity, the contact pressures varying from 2.1 MPa – 9.2 MPa. The contact pressures during level gait for the two total knee designs examined were more affected by the axial loading and to lesser extend of the kinematics. This is consistent with the result obtained in Chapter 5. The maximum contact pressures during level gait (results from Chapter 5 and Chapter 7) increases and decreases with the changes in the applied axial load. However, the contact pressures during stair ascent activity were more affected by the degree of A-P translation and I-E rotation leading to smaller contact areas. During stair ascent, smaller femoral condylar curvature radius was in contact with the polyethylene insert when the knee was flexed. This resulted in smaller contact area and higher contact pressures. The high contact pressures during stair ascent (typically for PLI design) were also likely to be due to high I-E rotations. Similar effect was observed in Chapter 5, i.e. during stair descent and squatting activities.

The maximum von Mises stresses from Chapter 7, in general, was greater than the yield stress of polyethylene insert (14.5 MPa) and local plastic deformation occurred. For PLI design, both level gait and stair ascent activities exhibited constant maximum von Mises stress value at 25 MPa throughout the activity cycle. Therefore, for this TKR design, it would be better referring to the maximum contact pressures data for comparisons between patient-to-patient variability. When assessing the von Mises stresses, it was suggested that PLI knee design has a higher risk of polyethylene wear, especially when patient with this design requires 'deep knee' flexion in daily activities. The PLI design is more sensitive than PFC Σ design towards kinematics changes for a more demanding activity. As Blunn and co-workers [20,21] have suggested that relative sliding distance, as well as stress, played an important role in the surface damage to TKR, increasing the sliding distance and stress would ultimately increased the wear volume. Delamination or fatigue wear of polyethylene has been reported to be a function related to the strain accumulation [131]. This study has shown residual stress to remain in the PLI model (maximum von Mises stresses remain at constant value for most of the level gait and stair ascent cycle), caused by residual plastic strain. If load continued to apply at this model, delamination wear is more likely to occur.

The envelope of active knee motions from level gait and stair ascent activities provide an idea of what performance range of the PFC Σ and PLI designs would have when the implant is perfectly aligned. This is the first attempt to obtain the performance envelope of a TKR design using subject specific load case and this study agrees with clinical observations whereby the TKR experiences a range of kinematics *in vivo*. No experimental or computational studies have yet investigated the kinematics changes of the TKR due to patient variability. One major reason to this limitation is the difficulty to find suitable joint contact force data. Current methods for assessing the performance of TKR designs needs improvement. Wear analyses either experimentally or computationally, should also include multiple subjects load cases and not just be biased to a single idealised load case. The result of this study clearly demonstrates that there is need to use more demanding dynamic loads on the mechanical testing of TKR design in order to obtain the optimal performances. Based on the results, modelling the ligaments provides higher constraint to the model and benefits especially when simulating activity with larger range of flexion motion (for example stair ascent). By modelling the ligaments, the analyses for nine subjects during stair ascent activity were completed for full stance phase with the PFC Σ model. When compared to HLS model (without ligaments), only analyses for eight subjects were completed. It was also postulated that modelling the ligaments provided more constraint when using low conformity TKR design such as the PLI design. One limitation of using ligaments model was that the ligaments orientations were approximately positioned in the FE model in this study. The positioning of the ligaments fibre bundles may not be

accurate and unable to represent the actual anatomy of the origins and insertions in the total knee joint. This could ultimately affect the kinematics.

Besides patient related factors, surgical parameters such as implant alignment and soft tissues balancing also plays an important role in TKR performance. Both chapters, 6 and 8, discussed the role of implant positioning. Chapter 6 investigated the effect of eccentric loading on the performance of TKR. The alignment of femoral component and tibial component were kept in their neutral position, as suggested by the manufacturer surgical procedure. Eccentric loading was simulated by adjusting the point of application of the axial load to either medial or lateral side of the TKR thus simulating the effect of a varus or valgus knee. Medial eccentric loading of the PFC Σ model has been previously studied [139]. Here, the analyses were repeated by also modelling collateral ligaments and also considered the effect of lateral eccentric loading. The collateral ligaments were represented by membrane elements and were assigned with their respective mechanical properties obtained from literature review (section 6.2). The anatomic femoral and tibia insertion points of these collateral ligaments were ignored. The alignment of these collateral ligaments were assumed to be that the femoral insertion point was collinear with the flexion-extension axis of the femoral component and vertically orientated. From this study, it was shown that the collateral ligaments have a significant effect on the predicted kinematics of TKR. Without the collateral ligament (HLS model), the worst loading case was medial uni-condylar loading. For medial uni-condylar load case, the HLS model showed the maximum increase in the posterior displacement of the tibial insert relative to the femoral component (2 times more than bi-condylar or 50:50 load case) and as well as the highest external tibial rotation relative to the femoral component (4 times more than the 50:50 load case). The femoral component was observed to nearly sublux. However, inclusion of the collateral ligaments significantly reduced the A-P displacements and I-E rotations for medial uni-condylar loading as compared with HLS model. For the ligament model, the medial uni-condylar load case showed an increased of 0.6 mm in the posterior displacement of the tibia and an increased of 1.6° external rotation of the tibia, both relative to the femur. The collateral ligaments acted to resist abnormal vertical motion and produced more desirable femoral component tracking on the tibial insert.

Lateral eccentric loading did not show extensive variations in the kinematics as compared to the medial eccentric loading even for the worst loading case, i.e. uni-condylar loading, with or without the collateral ligaments model.

Although the structures of the collateral ligaments in Chapter 6 did not directly represent the physiological reality, both medial and lateral collateral ligaments did affect the contact pressures in the articulating surfaces. In the HLS model (i.e. without collateral ligaments), the contact pressures increased significantly as the offset increased from 0 mm to medial

20 mm (Figure 6-6 a). For HLS medial uni-condylar load case, the maximum contact pressure was 42.4 MPa. Using static FE analysis, Bartel et al. [12] applied a 3000 N axial load to only one condyle of the PFC Σ knee and the recorded contact pressure was 57 MPa. The value is slightly higher than our study mainly due to the higher applied axial load in Bartel's study. For the ligaments model, the increased in contact pressures were consistent throughout the medial offset loading (Figure 6-6 b). Between HLS model and ligaments model, the most significant difference in the contact pressures was during the swing phase of gait cycle. The ligaments model, in general, exhibited slightly higher maximum contact pressures, with average value of 15 MPa (Figure 6-6 b). Meanwhile, the average maximum contact pressures for HLS model during the swing phase was 10 MPa (Figure 6-6 a). This showed that the collateral ligaments constrained the femoral component and tibial insert, and resulted more load being transferred to the insert. For lateral eccentric loading study, there were no significant difference in the contact pressures between HLS model and ligaments model apart from during the swing phase. Similarly, the ligaments model exhibited higher contact pressures (average 13 MPa) than the HLS model (average 10 MPa).

Overall, from the predicted kinematics and contact pressures, it seemed that if patient subjected their TKR to valgus loading (by offsetting of the applied axial load laterally), they might still be able to perform with reasonable kinematics. However, as the applied load tended to concentrate only at one side of the condyle, the lateral side of the polyethylene insert would experience high contact pressures and be more susceptible to wear. This result could well correlate with retrieval analyses [9,153], which saw asymmetric wear in the polyethylene insert. If patients subjected their TKR to varus loading, the kinematics may lie somewhere in between the collateral ligament model and the HLS model. The patient might still be able to perform with reasonable kinematics in varus loading only if the soft tissues are properly balanced or there is no laxity. The medial uni-condylar loading for the HLS model acted as the worst case scenario. In any situation, medial uni-condylar loading should be avoided. For this case, not only do the contact pressures increase significantly, but the kinematics get worse. This would accelerate the wear rate.

In Chapter 7, these simple membrane collateral ligaments were then improved by representing each collateral ligament with different fibre bundles each with different material properties. The methods involved were discussed in section 7.5. The PCL was also modelled. With these improved ligaments model, the kinematics performance when using subject specific loading was investigated (Chapter 7). The most significant difference was for the PFC Σ TKR; analysis for one particular subject (subject 9) was completed for the full stance phase of stair ascent activity. Conversely, without the ligaments, analysis for

that particular subject failed. This shows that ligaments in the TKR provide proper constraint in the motions of TKR by trying to avoid abnormal kinematics.
Minor degrees of misalignment and malrotation may cause less than optimal knee function. In some conditions, manifested by pain, instability and reduced range of motion. More serious misalignment in any anatomical plane can result in early failure of TKR. Misalignment in the sagittal plane usually affects flexion-extension range of motion, with resultant tightness or laxity of the soft tissues. Chapter 8 investigated the effect of misalignment on the performance of TKR. A range of TKR orientations were considered including offsetting both femoral and tibial component in an envelope of misalignment positions as described in section 8.2. In addition, internal 5° and external 5° malrotation were performed on the tibial component with respect to the femoral component, for PFC Σ and PLI designs.

The major differences in the kinematics as a result of malalignment occurred in the stair ascent study, with PLI design showing a wider range in the predicted kinematics as compared to the neutral alignment model and PFC Σ design. From the predicted kinematics during stair ascent activity, misaligning the PFC Σ model and PLI model 3 mm in the y proximal – z posterior directions resulted in subluxation of the femoral component at the early stage of stance phase of stair ascent cycle. For both analyses, the lateral condyle of the femoral component displaced and rode up to the posterior inner edge of the tibial insert and subluxed. The tibial insert for both the models exhibited internal rotation relative to the femur. Other orientations showed consistent increase or decrease in the A-P displacements and I-E rotations. Displacing the total knee components in the proximal and distal, anterior and posterior or combinations of both directions (section 8.2) could be used to represent installation of implants caused by surgical error, such as excessive bone resection during TKR surgery. Bone cuts are performed on the worn surface of femur and tibia to the desire dimension and then replace with knee implant. The bone cuts are performed to establish a symmetrical extension and as well as flexion gap with the aid of surgical instruments. Although with the guidance of these instruments, technical errors in surgery can happen, either due to improper use of the alignment tool or inexperience surgeon [122]. Surgical approaches have changed in accordance with design developments. Hence, knee surgeons have to be kept inform with any of the changes and trained on the new techniques. In a report by Lotke et al. [87], surgical experience in total knee replacement was proven to be very important. In their clinical assessment, early cases TKR performed by a surgeon showed lower roentgenographic scores (perfect positioned knee prosthesis received 100 points) than those in the later ones.

Changing the orientation of the TKR within the envelope described in section 8.2, did not significantly affect the contact pressures when the averaged subject specific level gait load was applied. There were only small increase or decrease (less than 5 MPa) in the

maximum contact pressures as compared to the neutrally aligned PFC Σ model or PLI model (Figure 8-5 a and Figure 8-7 a). PLI model exhibited higher contact pressures than PFC model due to its lower conformity. Although there were no significant changes in the contact pressure in PLI model, its lower conformity had caused large plastic strain and residual stress to be generated within the polyethylene insert (Figure 8-7 b and Figure 8-11 b). The maximum von Mises stress remained at constant value (25 MPa) and this stress was known as residual stress.

A performance envelope from the misalignment of TKR was obtained in this study (Chapter 8). Direct comparisons of the kinematics were complicated with differences in the methods of simulation and material properties assigned to the ligaments. No studies have yet investigated the misalignment of the TKR relative to the ligaments. To the author's knowledge, this is the first attempt to obtain the performance envelope of misaligned TKR.

Excessive bone cut during TKR surgery and misalignment of total knee prosthesis have resulted in tightness or laxity of the soft tissues [17,121,158]. From this study (Chapter 8), it was observed that altering the implant orientations changed in the relative position with respect to the ligaments (for example, when the femoral and tibial components were displaced 3 mm in the anterior direction relative to the ligaments, the ligaments would be at more posterior side of the FE model when compared to the neutrally aligned model). This then affected the forces transmitted in the knee ligaments. It was assumed that in this study, the ligaments tension remained constant. The length and position of the ligaments were kept at original value. For instance, in this study- shifting both the knee components 3 mm in the y proximal and then 3 mm in the z posterior direction relative to the ligaments was seen to have altered the forces transmitted in the ligaments when compared to the neutrally aligned model (Figure B-5, Appendix B). Overall, the peak forces for all the ligaments increased when the model was misaligned. Several selected analyses from Chapter 9 are shown in Appendix B. In some orientations, coupled with the kinematics and changed in ligament forces, had caused failure to the models (for example, in the 'y proximal-z posterior' model when applied with stair ascent load case). The force in each of the ligaments (Chapter 7 and Chapter 8) was examined to ensure the ligament was not over strained. The peak force observed was approximately 500 N (less than 6% strain) and was consistent with previous study made [133].

Limitations Of This Work

There are several limitations with the finite element models used in thesis. First, in Chapter 5, the forces during stair descent were obtained from different sources and did not represent the knee joint forces for a specific individual. Besides that, the 4 sets of forces (all activities) data came from 4 different sources using different methods to calculate the joint reaction force (JRF). So far, there is no single study that has reported all four loading input parameters for a variety of activities (axial load, anterior-posterior force, internal-external torque and flexion-extension angle). For the squatting activity [32], due to the 2-dimensional model used to predict the forces, the internal-external torque was not available and thus, the I-E rotations were not predicted. One major limitation in Chapter 5 is the absence of collateral ligaments and posterior cruciate ligaments. Stability and kinematics in the knee are controlled by these ligament structures, and if they were modelled, the predicted kinematics and contact pressures may have been different.

In Chapter 6, the FE model was improved by modelling the medial and lateral collateral ligaments. However, posterior cruciate ligament was ignored. The insertion points of the collateral ligaments were roughly positioned (the femoral origin sites were collinear with femoral component flexion-extension axis) and did not represent the physiological structure. Next, in Chapter 7, more realistic ligaments were modelled to improve the existing FE model (used in Chapter 6). Although the coordinates for femoral origin sites and tibia insertion sites were adapted from the literature, the coordinates were adjusted to best fit the FE models used in this work. The new positions of the femoral origin sites and tibia insertion sites might not exactly represent the anatomical/physiological model. There are bound to be errors in the positioning. Furthermore, it was assumed that for subject specific loading study, there were no anatomical variations between individuals in their attachment points and as well as in the stiffness and stresses present within the ligaments. In addition to this, the forces used in the study of subject specific loading have been predicted from healthy subjects. The performance envelope has only been assessed for a small number of subjects for each activity and ideally this should be expanded to a larger group. The axial load has been applied to the centre of the femoral component, which would lead to an even load distribution between medial and lateral compartment of the tibial insert. No varus or valgus moment has been applied to the TKR, which may lead to preferential loading for either the medial or lateral condyle.

In Chapter 8, again the applied axial load was centred on the femoral component and in misaligned TKR this may not have been the case. The maximum distance for misalignment study was 3 mm and the maximum malrotation angle was 5°. To approach the actual

condition *in vivo*, the larger translation distance and larger rotation angle may need to be further investigated. Furthermore, the effect of misalignment simulation including maltranslation, malrotation and varus-valgus tilt of the TKR components was studies in isolation. In actual situation of knee prosthesis *in vivo*, it would be a combination of these malalignment conditions and this may act to magnify the affects of malpositioning. These effects need to be further investigated.

In addition to these limitations, the set-ups of FE model used in this study were those used in the Stanmore simulator. It is a semi-constrained knee model. Ideally, the need is to model a fully unconstrained knee with kinematics totally dependent on the ligaments, geometry of the TKR design and applied loads.

Conclusions

This work has shown that the FE method can be used as an effective tool in assessing the performance envelope of TKR under several loading activities and varying the orientations of the TKR components relative to the ligaments. This work developed from the necessity of examining the TKR under a wider range of loading conditions and not just limited to one idealised load case as have been done so far in experimental testing and several FE analyses. The FE analyses performed have produced the following results:

- Total knee joint replacement underwent different types of daily activities and produced different kinematics trends and values. When compared to level gait activity, more demanding activities resulted in higher contact pressures. This indicates that there is need not only to examine the performance of a TKR under single load case but also to extend to other more demanding activities such as stair ascent and stair descent. By doing so, the functionality of the TKR could be examined to a more optimal level.

- Medial uni-condylar and lateral uni-condylar loadings are the most destructive load case (typically the medial uni-condylar loading). Both load cases altered the load distributions and with most load concentrated on one side of the polyethylene insert, increasing the risk of polyethylene wear.

- For the medial uni-condylar loading, the kinematics are sensitive to the quality of the lateral collateral ligament. A lax or absent LCL can result in extreme kinematics.

- This work is the first time that the performance envelope of a TKR has been evaluated under subject specific loading for two activities. For the TKR designs examined, the kinematics during level gait is relatively insensitive to variation due to subject specific loading, but greater variations were observed during stair ascent activity. Although the kinematics remained fairly similar during level gait, some orientations show an approximately 3 MPa increase in the contact pressure. This increase can lead to more wear of polyethylene and earlier failure of TKR. This study has shown the need to assess the performance envelope of a TKR design, rather than the performance related to an isolated load case (or single idealised load case).

- This is also the first time the performance envelope of a TKR has been assessed through the simulations of various misalignment orientations, under the loading of two different activities. For the TKR designs examined, the kinematics was less sensitive to the misalignment when level gait loads were applied. However, larger variations in the predicted kinematics were observed when stair ascent activity loads were applied.

- From the study conducted (Chapter 7 and Chapter 8), it could be concluded that implant orientation does not significantly affect either the kinematics or contact pressures of the TKR. The greater variability in kinematics is influenced more by the forces in the knee joint that vary between patients.

- The tension of ligaments in all the studies remained constant. Therefore, the only factor that these ligaments can affect the kinematics outcomes is their positioning in the knee model. This work has not looked at soft tissues balancing, soft tissues stiffness and laxity that could have influenced the performance of the TKR.

- This study has been able to improve the existing FE model by modelling more realistic ligaments, which includes the collateral ligaments and posterior cruciate ligament.

- Based on the results, using full ligaments model provides higher constraint to the model and benefits especially when simulating higher range of flexion motion activity (stair ascent) or using low conformity design. However, for less range of flexion motion activity (level gait), using just the HLS model might be sufficient.

- The lower conformity design (PLI design) exhibited a larger range kinematics than the higher conformity design (PFC Σ design), for both level gait and stair ascent activities examined.

- The lower conformity design also produced higher contact pressures and von Mises stresses. The maximum von Mises stress for PLI design remained at constant value and this indicated that local plastic deformation would occur. Hence, it had the maximal risk of polyethylene wear.

RECOMMENDATIONS FOR FUTURE WORK

The limitations in this work have been discussed and there are needs to further investigate and improve this study. Here are some recommendations for future work based on the limitations discussed:

- FE model: The femoral origin sites and tibial insertion sites for the FE model needs to be adjusted in order to best represent physiological model. There is need to re-mesh the polyethylene insert of PLI design, preferably with hexahedral element. Ideally, the aim is to model a fully unconstrained total knee joint model with the bony structures such as femur, tibia and patellar, and as well as the soft tissues and ligaments. The stability of this knee model would be total dependent on the ligaments and the kinematics on the load applied.

- Load cases: Given that suitable joint contact force data can be found, FE models have the potential to assess the kinematics and contact stresses as a result of multiple activities (Chapter 5) and subject specific load cases (Chapter 7). The number of subjects needs to be enlarged in order to make a better and solid conclusion for subject specific loading studies (Chapter 7).

- Misalignment: As has been discussed in the limitations of this work, in actual situation of knee prosthesis *in vivo*, there would be a combination of malalignment conditions. Studies on combine malalignments (such as maltranslation together with malrotation) need to be further investigated.

- Load application: In malalignment knee, the axial load is not necessarily applied through the centre of the TKR. There is need to further examine the malalignment conditions by differing point of application of axial load. Similarly, in subject specific loading study, not all subjects would have centrally located axial loading. The loading is dependent on the alignment of the lower limb.

If the improvements on the FE model could be done, analyses from this study need to be repeated. This would provide us more reliable results with the used of more physiological representative TKR model. Nevertheless, this work is the first time in assessing the performance envelope of TKR, using subject specific load cases and by orientating the positions of the TKR. Furthermore, it has highlighted the need to examine the performance of TKR design to other activities and not just limited to single load case (ISO standard load case). If possible, the author would like to repeat some of the works in experimental set-up, in order to validate the FE results obtained.

LIST OF REFERENCES

1. Abdel-Rahman EM and Hefzy MS. Three-dimensional dynamic behaviour of the human knee joint under impact loading. *Medical Engineering & Physics* 20: 276-290,1998.
2. Amstutz HC, Campbell PA, Kossovsky N and Clarke IC. Mechanism and clinical significance of wear debris-induced osteolysis. *Clin Orthop Rel Res* 276: 7-18,1992.
3. Andriacchi TP, Andersson GBJ, Fermier RW, Stern D and Galante JO. A study of lower-limb mechanics during stair-climbing. *J. Bone Jt Surg.* 62-A(5): 749-757,1980.
4. Andriacchi TP, Stanwyck TC and Galante JO. Knee biomechanics and total knee replacement. *J Arthroplasty* 1(3): 211-219,1986.
5. Anouchi YS, Whiteside LA, Kaiser AD and Milliano MT. The effects of axial rotational alignment of the femoral component on knee stability and patellar tracking in total knee arthroplasty demonstrated on autopsy specimens. *Clin Orthop* 287: 170-177,1993.
6. Archard JF. Contact and rubbing of flat surfaces. *J Applied Physics* 24(8): 981-988,1953.
7. Banks SA, Markovich GD and Hodge WA. *In Vivo* kinematics of cruciate-retaining and -substituting knee arthroplasties. *J Arthroplasty* 12(3): 297-304,1997.
8. Barbour PSM, Barton DC and Fisher J. The influence of contact stress on the wear of UHMWPE for total replacement hip prostheses. *Wear*: 250-257,1995.
9. Bargren JH, Blaha JD and Freeman MAR. Alignment in total knee arthroplasty. *Clin Orthop* 173: 178-183,1983.
10. Barnett PI, McEwen HMJ, Auger DD, Stone MH, Inghan E and Fisher J. Investigation of wear of knee prostheses in a new displacement/force-controlled simulator. *Proc Instn. Mech Engrs Part II: J Engineering in Medicine* 216: 51-61,2002.
11. Bartel DL, Bicknell VL and Wright TM. The effect of conformity, thickness and material on stresses in ultra-high-molecular weight components for total joint replacement. *J Bone Jt Surg* 68-A: 1041-1051,1986.
12. Bartel DL, Rawlinson JJ, Burstein AH, Ranawat CS and Flynn WF. Stresses in polyethylene components of contemporary total knee replacements. *Clin Orthop* 317: 76-82,1995.
13. Beaule PE, Campbell PA, Walker PS, Schmalzried TP, Dorey FJ, Blunn GW, Bell CJ, Yahia L'H and Amstutz HC. Polyethylene wear characteristics *in vivo* and in a knee simulator. *J Biomed Mater Res* 60(3): 411-419,2002.

14. Bellemans J, Victor J, Westhovens R, Dequeker J and Fabry G. Total knee arthroplasty in the young rheumatoid patient. *Acta Orthop Belg* 63(3): 189-193,1997.

15. Benson L, DesJardins J and LaBerge M. Stair descent loading pattern for TKR wear simulation. 48th Annual Meeting of the Orthopaedic Research Society, Texas, US., 2002.

16. Benson LC, DesJardins JD, Harman MK and LaBerge M. Effect of stair descent loading on ultra-high molecular weight polyethylene wear in a force-controlled knee simulator. *Proc Instn Mech Engrs Part H* 216: 409-418,2002.

17. Berger RA and Rubash HE. Rotational Instability and malrotation after total knee arthroplasty. *Orthop Clin North America* 32(4): 639-647,2001.

18. Bert JM. Dislocation/subluxation of meniscal bearing elements after New Jersey Low-Contact Stress total knee arthroplasty. *Clin Orthop* 254: 211-215,1990.

19. Blunn GW, Joshi AB, Lilley PA, Englebrecht E, Ryd L, Lidgren L, Hardinge K, Nieder E and Walker PS. Polyethylene wear in unicondylar knee prostheses: 106 retrieved Marmor, PCA and St. Georg tibial components compared. *Acta Orthop Scand* 63(3): 247-255,1992.

20. Blunn GW, Joshi AB, Minns RJ, Lingren L, Lilley P, Ryd L, Engelbreck E and Walker PS. Wear in retrieved condylar knee arthroplasties: a comparison of wear in different designs of 280 retrieved condylar knee prostheses. *J Arthroplasty* 12: 281-290,1997.

21. Blunn GW, Walker PS, Joshi A and Hardinge K. The dominance of cyclic sliding in producing wear in total knee replacements. *Clin Orthop* 273: 253-260,1991.

22. Brantigan OC and Voshell AF. The mechanics of the ligaments and menisci of the knee joint. *J Bone Jt Surg* 23(1): 44-66,1941.

23. Bull AMJ and Amis AA. Knee joint motion:description and measurement. *Proc Instn Mech Engrs* 212: 357-372,1998.

24. Burgess IC, Kolar M, Cunningham JL and Unsworth A. Developement of a six station knee wear simulator and preliminary wear results. *Proc Instn Mech Engrs Part H* 211: 37-47,1997.

25. Callaghan JJ, Squire MW, Goetz DD, Sullivan PM and Johnston RC. Cemented rotating-platform total knee replacement. A nine to twelve-year follow-up study. *J Bone Jt Surg* 82-A: 705-711,2000.

26. Cameron HU and Hunter GA. Failure in total knee arthroplasty. *Clin Orthop* 170: 141-146,1982.

27. Clarke HD and Scott WN. KNEE. Axial Instability. *Orthop Clin North America* 32(4): 627-637,2001.

28. Colizza WA, Insall JN and Scuderi GR. The posterior stabilized total knee prosthesis assessment of polyethylene damage and osteolysis after a ten-year-minimum follow-up. *J Bone Jt Surg* 77-A: 1713-1720,1995.

29. Cooke T, Derek V, Kelly B and Li J. Posthetic reconstruction of the arthritic knee: considerations for limb alignment, geometry and soft tissue reconstruction. *The Knee* 5: 165-174,1998.

30. Cooke TDV, Sorbie C, Scudamore RA, Bryant JT, Siu D and Fisher B. A quantitative approach to radiography of the lower limb. *J Bone Jt Surg* 73-B: 715-720,1991.

31. Costigan PA, Deluzio KJ and Wyss UP. Knee and hip kinetics during normal stair climbing. *Gait and Posture* 16: 31-37,2002.

32. Dahlkvist NJ, Mayo P and Seedhom BB. Forces during squatting and rising from a deep squat. *Engineering in Medicine* 11(2): 69-76,1982.

33. DesJardins JD, Banks SA, Pace T, Benson LC and LaBerge M. A direct comparison of patient and simulator total knee replacement kinematics. 47th Annual Meeting, Orthopaedic Research Society, San Francisco, California, 2001.

34. DesJardins JD, Walker PS, Haider H and Perry J. The use of a force-controlled dynamic knee simulator to quantify the mechanical performance of total knee replacement designs during functional activity. *J Biomech* 33(11): 1231-1242,2000.

35. Diduch DR, Insall JN, Scott WN, Scuderi GR and Font-Rodriguez D. Total knee replacement in young, active patient. Long term follow-up and functional outcome. *J Bone Jt Surg* 79-A: 575-582,1997.

36. D'Lima DD, Chen PC and Colwell CW. Polyethylene contact stresses, articular congruity and knee alignment. *Clin Orthop* 392: 232-238,2001.

37. Draganich LF, Andersson GBJ, Andriacchi TP and Galante JO. The effect of the cruciate ligaments in femoral-tibial contact movement during knee flexion. In Transactions of the 30th Annual Meeting of the Orthopedic Research Society., Atlanta, 1984.

38. Elftman H. The measurement of external forces in walking. *Science* 88: 152-153,1938.

39. Emmerson KP, Moran CG and Pinder IM. Survivorship analysis of the kinematic stabilizer total knee replacement. *J Bone Jt Surg* 78-B(3): 441-445,1996.

40. Engh GA. Failure of the polyethylene bearing surface of a total knee replacement within four years. *J Bone Jt Surg* 70-A(7): 1093-1096,1988.

41. Engh GA, Dwyer KA and Hanes CK. Polyethylene wear of metal-backed tibial components in total and unicompartmental knee prostheses. *J Bone Jt Surg* 74-B(1): 9-17,1992.

42. Estupinan JA, Bartel DL and Wright TM. Residual stresses in ultra-high molecular weight polyethylene loaded cyclically by a rigid moving indenter in nonconforming geometries. *J Orthop Research* 16(1): 80-88,1998.

43. Ewald FC, Jacobs MA, Walker PS, Thomas WH, Scott RD and Sledge CB. Accuracy of total knee replacement component position and relation to bone-cement interface reaction. The Knee. Baltimore, University Park Press, 1990.

44. Fagan MJ. Finite Element Analysis: Theory and Practise. Essex, Longman Group UK Limited, 1992.

45. Feng EL, Stulberg SD and Wixson RL. Progressive subluxation and polyethylene wear in total knee replacements with flat articular surfaces. *Clin Orthop* 299: 60-71,1994.

46. Fisher J, McEwen HMJ, Barnett PI, Bell CJ, Stewart TD, Stone MH and Ingham E. (i) Wear of polyethylene in artificial knee joints. *Current Orthop* 15: 399-405,2001.

47. Frankel VH. Biomechanics of Collagenous Tissues. Basic Biomechanics of the Skeletal System. Philadelphia, Lea & Febiger. 1: 87-110, 1980.

48. Fu FH, Barner CD, Johnson DL, Miller MD and Woo SL. Biomechanics of knee ligaments. *J Bone Jt Surg* 75-A(11): 1716-1727,1993.

49. Fukubayashi T, Torzilli PA, Sherman MF and Warren RF. An *in Vitro* Biomechanical Evaluation of Anterior-Posterior Motion of the Knee. *J Bone Jt Surg* 64-A(No. 2): 258-259,1982.

50. Gebhard JS and Kilgus DJ. Dislocation of a posterior stabilized total knee prosthesis. *Clin Orthop* 254: 225-229,1990.

51. Giddings VL, Kurtz SM and Edidin AA. Total knee replacement polyethylene stresses during loading in a knee simulator. *Trans ASME* 123: 842-847,2001.

52. Godest AC, Beaugonin M, Haug E, Taylor M and Gregson PJ. Simulation of a knee joint replacement during a gait cycle using explicit finite element analysis. *J Biomech* 35: 267-275,2002.

53. Godest AC, de Cloke CS, Taylor M, Gregson PJ, Keane AJ, Sathasivam S and Walker PS. A computational model for the prediction of total knee replacement kinematics in the sagittal plane. *J Biomech* 33: 435-442,2000.

54. Gollehon DL, Torzilli PA and Warren RF. The role of the posterolateral and cruciate ligaments in the stability of the human knee. A biomechanical study. *J Bone Jt Surg* 69-A: 233-242,1987.

55. Grace JN and Rand JA. Patellar instability after total knee arthroplasty. *Clin Orthop* 237: 184-186,1989.

56. Gray H. Anatomy of the human body. Lea & Febiger, 1918. www.bartleby.com, 2000.

57. Griffin FM, Insall JN and Scuderi GR. Accuracy of soft tissue balancing in total knee arthroplasty. *J Arthroplasty* 15(8): 970-973,2000.

58. Grood ES, Noyes FR, Butler DL and Suntay WJ. Ligamentous and capsular restraints precenting straight medial and lateral laxity in intact human cadaver knees. *J Bone Jt Surg* 63-A(8): 1257-1269,1981.

59. Haider H, Walker PS, Blunn GW and Bell CJ. The sensitivity of total knee replacement kinematics to misaligned installation. 47th Annual Meeting, Orthopaedic Research Society, San Francisco, California, 2001.

60. Hallen LG and Lindahl O. The "screw-home" moment in the knee joint. *Acta Orthop Scand* 37: 97-106,1966.

61. Halloran JP and Rullkoetter PJ. Development of an explicit-finite-element-based total knee replacement model. 2001 Bioengineering Conference ASME, Snowbird, Utah, 2001.

62. Hay JG and Reid JG. Anatomy, mechanics and human motion. 2nd edition New Jersey, Prentice-Hall, 1988.

63. Hefzy MS, Kelly BP and Cooke DV. Kinematics of the knee joint in deep flexion: a radiographic assessment. *Medical Engineering & Physics* 20: 302-307,1998.

64. Hsu HP, Garg A, Walker PS, Spector M and Ewald FC. Effect of knee component alignment on tibial load distribution with clinical correlation. *Clin Orthop* 248: 135-144,1989.

65. Huang CH, Liau JJ, Cheng CK and Huang CH. Could mobile bearing knee prosthesis reduce stress concentration under surgical malalignment? IV World Congress of Biomechanics., Calgary, Canada, 2002.

66. Hui FC and Fitzgerald RH Jr. Hinged total knee arhtroplasty. *J Bone Jt Surg* 62-A(4): 513-519,1980.

67. Insall JM, Lachiewicz PF and Burstein AH. The posterior-stabilized condylar prosthesis: A modification of the total condylar design. *J Bone Jt Surg* 64-A: 1317-1323,1982.

68. Insall JN, Binazzi R, Soudry M and Mestriner LA. Total knee arthroplasty. *Clin Orthop* 92: 13,1985.

69. Insall JN and Dethmers DA. Revision of total knee arthroplasty. *Clin Orthop* 170: 123-130,1982.

70. Iseki F and Tomatso T. The biomechanics of the knee joint with special reference to the contact area. *Keio J Med* 25:37,1976.

71. Jones SMG, Pinder IM, Moran CG and Malcolm AJ. Polyethylene wear in uncemented knee replacements. *J Bone Jt Surg* 74-B(1): 18-22,1992.

72. Kapandji IA. The physiology of the joints. The lower limb. London, Churchill Livingstone. II, 1970.

73. Karrholm J, Jonsson H, Nilsson KG and Soderqvist I. Kinematics of successful knee prostheses during weight-bearing: three-dimensional movements and positions of screw axes in the Tricon-M and Miller-Galante designs. *Knee Surgery, Sports Traumatology, Arthroscopy* 2: 50-59,1994.

74. Kettelkamp DB. An electrogoniometric study of knee motion in normal gait. *J Bone Jt Surg* 52-A: 775-790,1970.

75. Kilgus DJ, Funahashi TT and Campbell PA. Massive femoral osteolysis and early disintegration of a polyethylene-bearing surface of a total knee replacement. *J Bone Jt Surg* 74-A(5): 770-774,1992.

76. Kim H, Pelker RR, Gibson DH, Irving JF and Lynch JK. Rollback in posterior cruciate ligament-retaining total kne arthroplasty. *J Arthroplasty* 12(5): 553-561,1997.

77. Kim W, Rand JA and Chao EYS. Biomechanics of the knee. Total Knee Arthroplasty. J. A. Rand. New York, Raven Press Ltd.: 9-57, 1993.

78. Kleinbart FA, Bryk E, Evangelista J, Scott WN and Vigorita VJ. Histologic comparison of posterior cruciate ligaments from arthritic and age-matched knee specimens. *J Arthroplasty* 11: 726-731,1996.

79. Knutson K, Lewold S, Robertsson O and Lidgren L. The Swedish knee arthroplasty register. *Acta Orthop Scand* 65(4): 375-386,1994.

80. Kowalk DL, Duncan JA and Vaughan CL. Abduction-Adduction moments at the knee during stair ascent and descent. *J Biomech* 29(3): 383-388,1996.

81. Krachow KA. Approaches to planning lower extremity alignment for total knee arthroplasty and osteotomy about the knee. *Adv Orthop Surg*: 69-88,1983.

82. Lafortune MA, Cavanagh PR, Sommer HJ and Kalenak A. Three-dimensional kinematics of the human knee during walking. *J Biomech* 25(4): 347-357,1992.

83. Laubenthal KN, Smidt GL and Kettelkamp DB. A quantitative analysis of knee motion during activities of daily living. *Phys Ther* 52(1): 34-43,1972.

84. Lewis P, Rorabeck CH, Bourne RB and D. P. Posteromedial tibial polyethylene failure in total knee replacements. *Clin Orthop* 299: 11,1994.

85. Liau JJ, Cheng CK, Huang CH and Lo WH. The effect of malalignment on stresses in polyethylene component of total knee prostheses. *Clin Biomech* 17: 140-146,2002.

86. Lombardi AV Jr, Mallory TH, Vaughn BK, Krugel R, Honkala TK, Sorscher M and Kolczun M. Dislocation following primary posterior-stabilized total knee arthroplasty. *J Arthroplasty* 8(6): 633-639,1993.

87. Lotke PA and Eeker ML. Influence of positioning of prosthesis in total knee replacement. *J Bone Jt Surg* 59-A: 77,1977.

88. Mains DB, Andrews JG and Stonecipher T. Medial and anterior-posterior ligament stability of the human knee, measured with a stress apparatus. *Am. J. Sports Med.* 5: 144-153,1977.

89. Markolf KL, Gorek JF, Kabo JM and Shapiro MS. Direct measurement of resultant forces in the anterior cruciate ligament. An in vitro study performed with a new experimental technique. *J Bone Jt Surg* 72-A(4): 557-567,1990.

90. Markolf KL, Mensch JS and Amstutz HC. Stiffness and laxity of the knee - the contributions of the supporting structures. *J Bone Jt Surg* 58-A: 583-593,1976.

91. Matsuda S, Miura H, Nagamine R, Urabe K, Matsunobu T and Iwamoto Y. Knee stability in posterior cruciate ligament retaining total knee arthroplasty. *Clin Orthop* 366: 169-173,1999.

92. Matsuda S, White SE, Willams VG, McCarthy DS and Whiteside LA. Contact stress analysis in meniscal bearing total knee arthroplasty. *J Arthroplasty* 13: 699-706,1998.

93. Matsuda S, Whiteside LA and White SE. The effect of varus tilt on contact stresses in total knee arthroplasty: A biomechanical study. *Orthopedics* 22(3): 303-307,1999.

94. Matsuda S, Whiteside LA, White SE and McCarthy DS. Knee kinematics of posterior cruciate ligament sacrified total knee arthroplasty. *Clin Orthop & Rel Res* 341: 257-266,1997.

95. McFadyen BJ and Winter DA. An integrated biomechanical analysis of normal stair ascent and descent. *J Biomech* 21(9): 733-744,1988.

96. Mitts K, Muldoon MP, Gladden M and Padgett DE. Instability after total knee arthroplasty with the Miller-Gallante II total knee. *J Arthroplasty* 16(4): 422-427,2001.

97. Mommersteeg TJA, Blankevoort L, Huiskes R, Kooloos JGM and Kauer JMG. Characterization of the mechanical behaviour of human knee ligaments: A numerical-experimental approach. *J Biomech* 29(2): 151-160,1996.

98. Mommersteeg TJA, Blankevoort L, Huiskes R, Kooloos JGM, Kauer JMG and Hendriks JCM. The effect of variable relative insertion orientation of human knee bone-ligament-bone complexes on the tensile stiffness. *J Biomech* 28(6): 745-752,1995.

99. Mommersteeg TJA, Huiskes R, Blankevoort L, Kooloos JGM and Kauer JMG. A global verfication study of a quasi-static knee model with multi-bundle ligaments. *J Biomech* 29(12): 1659-1664,1996.

100. Moreland JR, Basselt LW and Henker GJ. Radiographic analysis of the axial alignment of the lower extremity. *J Bone Jt Surg* 69-A: 745-749,1987.

101. Morlock M, Schneider E, Bluhm A, Vollmer M, Bergmann G, Mueller V and Honl M. Duration and frequency of every day activities in total hip patients. *J Biomech* 34: 873-881,2001.

102. Morrison JB. Bioengineering analysis of force actions transmitted by the knee joint. *Bio-medical Engineering* 3(4): 164-170,1968.

103. Morrison JB. Function of the knee joint in various activities. *Bio-Med Eng* 4(12): 573-580,1969.

104. Morrison JB. The mechanics of the knee joint in relation to normal walking. *J Biomech* **3**(1): 51-61,1970.

105. Mottershead JE, Edwards PD and Whelan MP. Finite element analysis of a total knee replacement by using Gauss point contact constraints. *Proc Instn. Mech Engrs, Part H. Journal of Engineering in Medicine.* 210: 51-63,1996.

106. Murray D, Webb J, Price A, Topf H, Dodd C and Goodfellow J. Minimally invasive Oxford unicompartmental knee replacement. In Proceedings of the International Engineering Publishing, London, Professional Engineering Publishing, London, 1999.

107. Murray MP, Drought AB and Kory RC. Walking patterns of normal men. *J Bone Jt Surg* 46-A: 335-360,1964.

108. Nagura T, Dyrby CO, Alexander EJ and Andriacchi TP. Mechanical loads at the knee joint during deep flexion. *J Orthop Res* 20: 881-886,2002.

109. Nicholas JA and Hershman EB. The lower extremities and spine in sports medicine. St Louis, C.V. Mosby.:,1986.

110. Nordin M and Frankel VH. Biomechanics of the knee. Basic Biomechanics of the Skeletal System. Frankel VH and Nordin M. Philadelphia, Lea & Febiger: 113-148, 1980.

111. Noyes FR and Grood ES. The strength of the anterior cruciate ligament. Age and species-related changes. *J Bone Jt Surg* 58-A: 1074-1082,1976.

112. Otto JK, Callaghan JJ and Brown TD. A multiple-interface contact finite element analysis of a rotating platform total knee. 47th Annual Meeting, Orthopaedic Research Society, San Francisco, California, 2001.

113. Otto JK, Callaghan JJ and Brown TD. Influence of soft tissue constraints and friction on full walking cycle simulations of a rotating platform total knee replacement. 48th Annual Meeting of the Orthopaedic Research Society, Dallas, Texas, 2002.

114. Parks NL, Topoleski LD, Engh GA and Emperado J. Modular tibial insert micromotion. A concern with comtemporary knee implants. Read at the Interim Meeting of the Knee Society, New York City, 1997.

115. Paul JP and Poulson J. The analysis of forces transmitted by joints in the human body. Fifth International Conference on Experimentral Stress Analysis., Udine, Italy, 1974.

116. Perry J, Norwood L and House K. Knee posture and biceps and semimembranosis muscle action in running and cutting (an EMG study). *Trans Orthop Res Soc* 2: 258,1977.

117. Peters PC, Engh GA, Dwyer KA and Vinh TN. Osteolysis after total knee arthroplasty without cement. *J Bone Jt Surg* 74-A(6): 864-876,1992.

118. Piazza SJ and Cavanagh PR. Measurement of the srew-home motion of the knee is sensitive to errors in axis alignment. *J Biomech* 33: 1029-1034,2000.

119. Plante-Bordeneuve P and Freeman MAR. Tibial high-density polyethylene wear in conforming tibiofemoral prostheses. *J Bone Jt Surg* 75-B(4): 630-636,1993.

120. Prietto MP, Bain JR, Stonebrook SN and Settleage R. Tensile strength of the human posterior cruciate ligament (PCL). Trans Orthop Res Soc, 1988.

121. Ranawat CS, Padgett DE and Ohashi Y. Total knee arthroplasty for patients younger than 55 years. *Clin Orthop* 248(27),1989.

122. Ranawat CS and Rodriguez JA. Malalignment and malrotation in total knee arthroplasty. Current concepts in primary and revision total knee arthroplasty. Insall JN, Scott WN and S. GR. Philadelphia, Lippincott-Raven: 115-122, 1996.

123. Rawlinson J, Furman B, Li S and Bartel D. Finite element analysis of TKR captures device-dependent kinematics and wear potential. 48th Annual Meeting of the Orthopaedic Research Society, Dallas, Texas, 2002.

124. Reeves EA, Barton DC, FitzPatrick DP and Fisher J. A two-dimensional model of cyclic strain accumulation in ultra-high molecular weight polyethylene knee replacements. *Proc Instn. Mech Engrs, Part H, Journal of Engineering in Medicine* 212(H): 189-198,1998.

125. Rhoades DD, Noble PC, Reuben JD, Mahoney OM and Tullos HS. The effect of femoral component positioning on patellar tracking after total knee arthroplasty. *Clin. Orthop.* 260: 43-51,1990.

126. Ritter MA, Faris PM, Keating EM and Meding J. Postoperative alignment of total knee replacement. Its effect on survival. *Clin Orthop* 299: 153-156,1994.

127. Rittman N, Kettelkamp DB, Pryor P, Schwartzkopf GL and Hillberry B. Analysis of patterns of knee motion walking for four types of total knee implants. *Clin Orthop* 155: 111-117,1981.

128. Romero J, Duronio JF, Sohrabi A, Alexander N, MacWilliams BA, Jones LC and Hungerford DS. Varus and valgus flexion laxity of total knee alignment methods in loaded cadaveric knees. *Clin Orthop* 394: 243-253,2002.

129. Rorabeck CH. The unstable total knee: cause and cures. *The Knee* 8: 179-186,2001.

130. Sathasivam S and Walker PS. A computer model with surface friction for the prediction of total knee kinematics. *J Biomech* 30: 177-184,1997.

131. Sathasivam S and Walker PS. Computer model to predict subsurface damage in tibial inserts of total knees. *J Orthop Res* 16(5): 564-571,1998.

132. Scuderi GR and Insall JN. Rotational positioning of the femoral component in total knee arthroplasty. *American J Knee Surgery* 13(3): 159-161,2000.

133. Shelburne KB, Pandy MG, Anderson FC and Torry MR. Pattern of anterior cruciate ligament force in normal walking. *J Biomech* 37: 797-805,2004.

134. Shoemaker SC, Markolf KL and Finerman GAM. In vitro stability of the implanted total condylar prosthesis. *J Bone Jt Surg* 64-A: 1201,1982.

135. Stiehl JB, Komistek RD, Dennis DA and Paxson RD. Fluoroscopic analysis of kinematics after posterior-cruciate-retaining knee arthroplasty. *J Bone Jt Surg* 77-B(6): 884-889,1995.

136. Swany MR and Scott RD. Posterior polyethylene wear in posterior cruciate ligament-retaining total knee arthroplasty. *J Arthroplasty* 8(4): 439-447,1993.

137. Szivek JA, Anderson PL and Benjamin JB. Average and peak contact stress distribution evaluation of total knee arthroplasties. *J Arthroplasty* 11(8): 952-963,1996.

138. Tasker T and Waugh W. Articular changes associated with internal derangement of the knee. *J Bone Jt Surg* 64: 486-488,1982.

139. Taylor M and Barrett DS. Explicit finite element simulation of eccentric loading in total knee replacement. *Clin Orthop* 414: 162-171,2003.

140. Taylor S, Walker PS, Perry J, Cannon SR and Woledge R. The forces in the distal femur and the knee during walking and other activities measured by telemetry. *J Arthroplasty* 13(4): 428-437,1998.

141. Thatcher JC, Zhou XM and Walder PS. Inherent laxity in total knee prostheses. *J Arthroplasty* 2: 199,1987.

142. Toksvig-Larsen S. Minimaly-invasive surgery for the next decade? In Proceedings of the International Conference on Knee Replacement, London, Professional Engineering Publishing, London, 1999.

143. Torzilli PA, Greenberg RL and Insall J. An in vivo biomechanical evaluation of anterior-posterior motion of the knee. *J Bone Jt Surg* 63-A(6): 960-968,1981.

144. Townley CO. The anatomic total knee resurfacing arthroplasty. *Clin Orthop* 192: 82,1985.

145. Trent PS, Walker PS and Wolf B. Ligament length patterns, strength, and rotational axes of the knee joint. *Clin Orthop & Rel Res*: 263-270,1976.

146. Tsao A, Mintz L, McRae CR, Stulberg SD and Wright T. Failure of the porous-coated anatomic prosthesis in total knee arthroplasty due to severe polyethylene wear. *J Bone Jt Surg* 75-A(1): 19-26,1993.

147. Turek SL. Orthopaedics. London, J.B. Lippincott Co., 1984.

148. Uvehammer J, Kaerrholm J and Brandson S. In vivo kinematics of total knee arthroplasty. *J Bone Jt Surg* 82-B(4): 499-505,2000.

149. Vaughan CL, Davis BL and O'Conner JC. The three-dimensional and cyclic nature of gait. Dynamics of human gait. Illinois, Human Kinetics Publishers: 7-14, 1992.

150. Walker PS, Blunn GW, Broome DR, Perry J, Watkins A, Sathasivam S, Dewar ME and Paul JP. A knee simulating machine for the performance evaluation of total knee joint replacements. *J Biomech* 30: 83-89,1997.

151. Walker PS and Sathasivam S. Design Forms of Total Knee Replacement. *Proc Instn. Mech Engrs* 214,2000.

152. Wang A, Essner A and Klein R. Effect of contact stress on friction and wear of ultra-high molecular weight polyethylene in total hip replacement. *Proc Instn. Mech Engrs* 215(Part H): 133-139,2001.

153. Wasielewski RC, Galante JO, Leighty RB, Natarajan RN and Rosenberg AG. Wear patterns on retrieved polyethylene tibial inserts and their relationship to technical considerations during total knee arthroplasty. *Clin Orthop* 299(31-43),1994.

154. Werner FW, Ayers DC, Maletsky L, Fifolt D, Yanagida H and Weiner MM. The effect of coronal malalignment on load distribution in total knee replacements. 46th Annual Meeting, Orthopaedic Research Society, Orlando, Florida, 2000.

155. Werner FW, Ayers DC, Maletsky LP and Rullkoetter PJ. The effect of valgus/varus malalignment on load distribution in total knee replacements. *J Biomech* in press,2004.

156. Whelan MP, Mottershead JE, Edwards PD and Little EG. Modelling an orthopaedic knee prosthesis as a layered elastic system. Part 2: Finite element analysis. *J Strain Analysis* 30(3): 195-203,1995.

157. Whiteside LA. Positioning the femoral component. *American J Knee Surgery* 13(3): 173-180,2000.

158. Whiteside LA. Soft tissues balancing. *J Arthroplasty* 17(3): 23-27,2002.

159. Whiteside LA and Amador DD. The effect of posterior tibial slope on knee stability after Ortholoc total knee arthroplasty. *J Arthroplasty* 3: S51,1988.

160. Woo SLY, Hollis JM, Douglas JA, Lyon RM and Takai S. Tensile properties of the human femur-anterior cruciate ligament-tibia complex. *American J Sports Med* 19: 217-224,1991.

161. Wright TM, Rimnac CM, Faris PM and Bansal M. Analysis of surface damage in retrieved carbon fiber-reinforced and plain polyethylene tibial components from posterior stabilized total knee replacements. *J Bone Jt Surg* 70-A(9): 1312-1319,1988.

162. Yoshioka Y, Siu D and Cooke DV. The anatomy and functional axes of the femur. *J Bone Jt Surg* 69-A: 873-880,1987.

163. Young SK, Keller TS, Greer KW and Gorhan MC. Wear Testing of UHMWPE tibial components: Influence of Oxidation. *J Tribology* 122: 323-331,2000.

164. Yu CH, Walker PS and Dewar ME. The effect of design variables of condylar total knees on the joint forces in step climbing based on a computer model. *J Biomech* 34: 1011-1021,2001.

165. Zavatsky AB and O'Conner JJ. A model of human knee ligaments in the sagittal plane. Part 1: response to passive flexion. *J Engineering in Medicine* 206(H3): 125-134,1992.

166. Zhang LQ, Shiavi R, Limbird TJ and Minorik JM. Six degrees-of-freedom kinematics of ACL deficient knees during locomotion - compensatory mechanism. *Gait and Posture*: 1-9,2002.

APPENDIX A

Subject Specific Level Gait

Ligament forces for several selected subject specific level gait load cases will be discussed here. Figure A-1 shows the ligament forces for three subjects, using the PFC Σ knee and Figure A-2 shows the ligament forces, also for three subjects using the PLI knee. Figure A-1, with the PFC Σ model, in general, the LCL for subject 2, subject 3 and subject 7 carried the highest forces during level gait. These fibre bundles were assumed to carry load only when they are in tension. Overall, the forces in these ligaments were no more than 120 N. The forces varied with the applied loads and as well as the non-linear correlation with the kinematics. For PLI knee (Figure A-2), similarly, each ligament exhibited different forces dependent on the applied load and the kinematics of TKR. In general, the LCL showed the highest forces than other ligament elements. For both TKR designs, the MCL-A did not carry any force throughout the gait cycle.

Subject Specific Stair Ascent

Figure A-3 and Figure A-4 show the ligament forces for several selected subjects during stair ascent activity. In general, the ligament forces during stair ascent were higher in value than during level gait activity. In the first 20% of the stair ascent cycle (i.e. from 40% to 60%), PCL-P was observed to carry the highest force than other ligament elements. At this stage, the knee was flexed at the highest flexion angle during stair ascent with the help of PCL. Thus, PCL-P exhibited the highest forces. Overall, the ligaments forces during stair ascent activity were below 350 N.

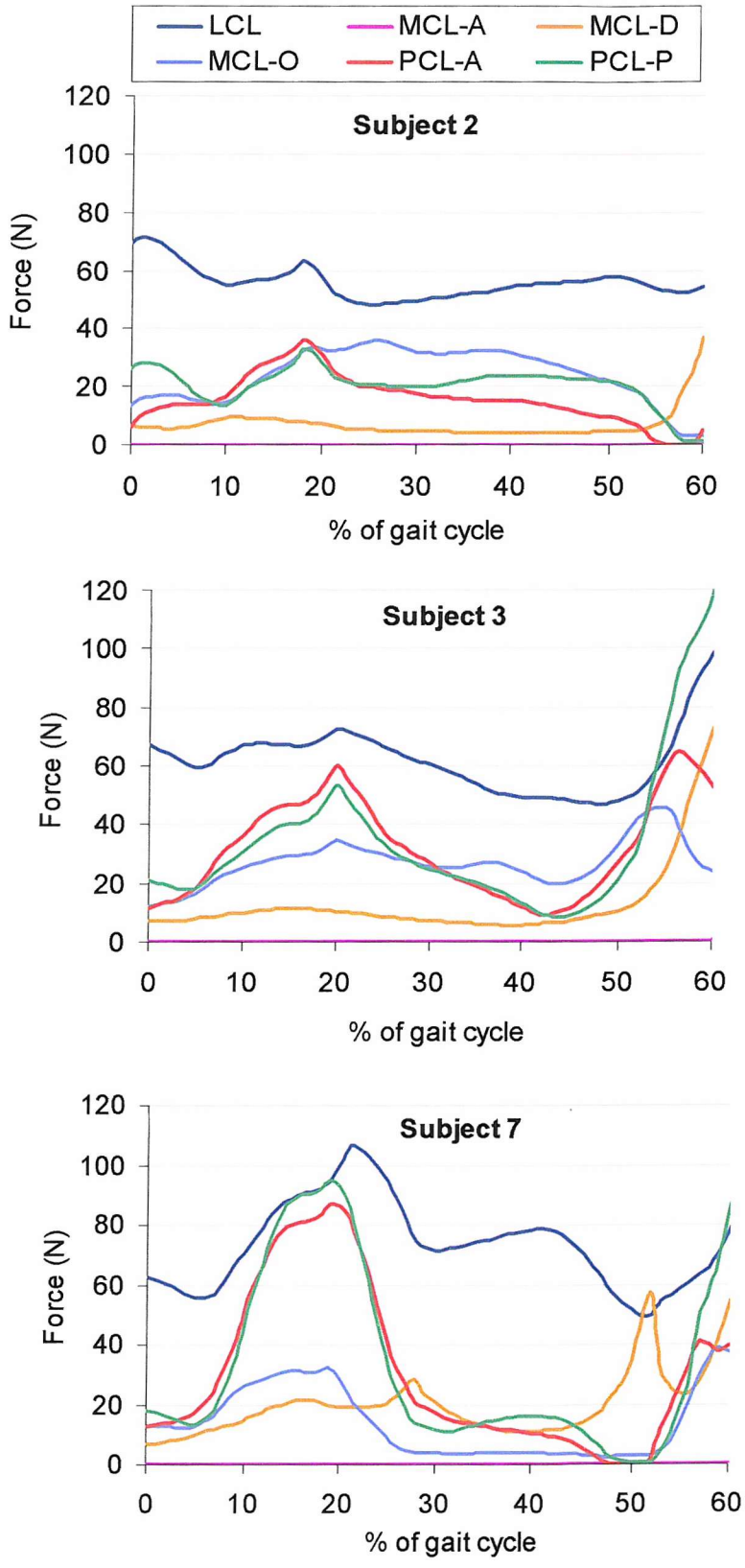

Figure A-1: Ligament forces for three selected subjects during level gait using PFC Σ knee.

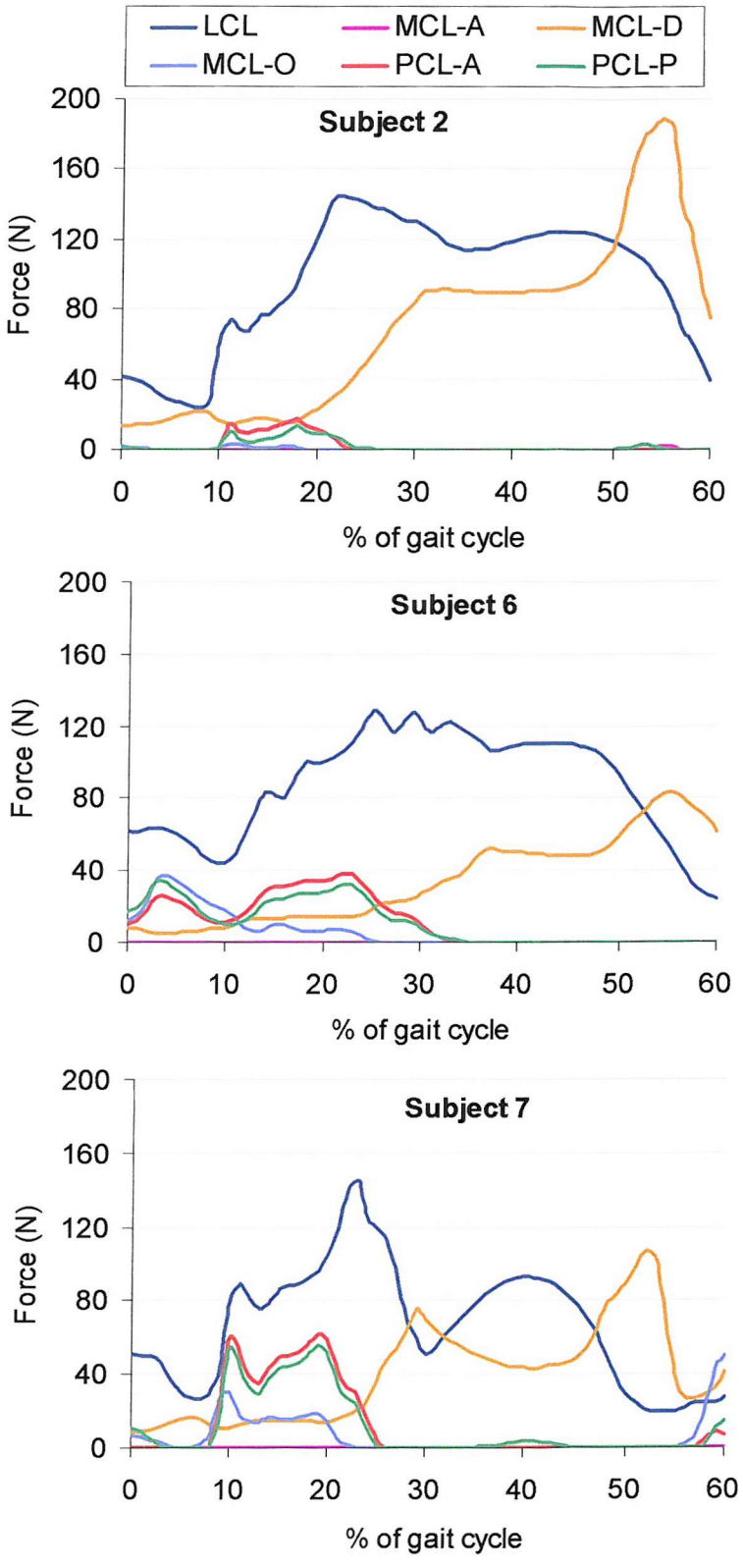

Figure A-2: Ligaments forces for three selected subjects during level gait using PLI knee.

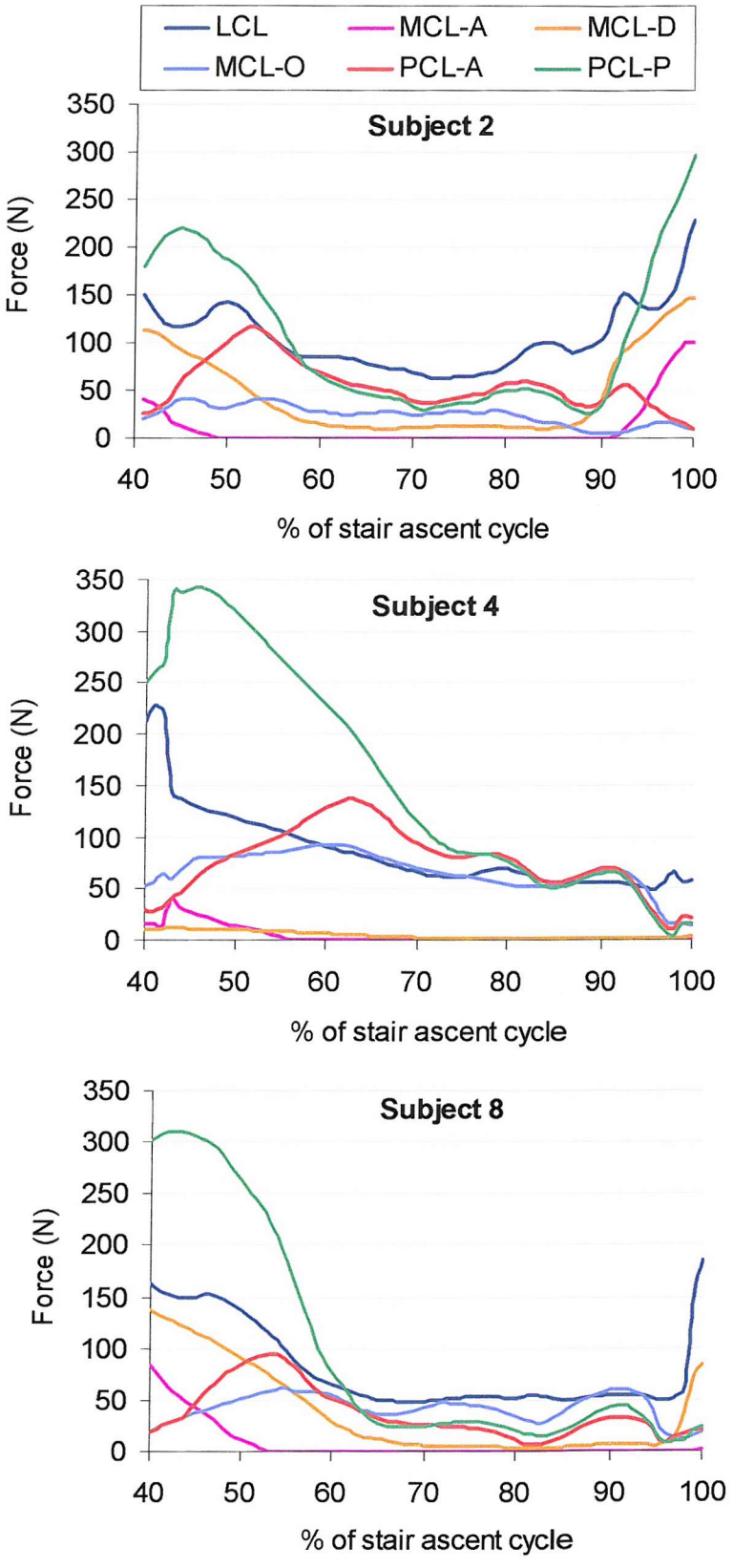

Figure A-3: Ligament forces for three selected subjects during stair ascent activity using PFC Σ knee.

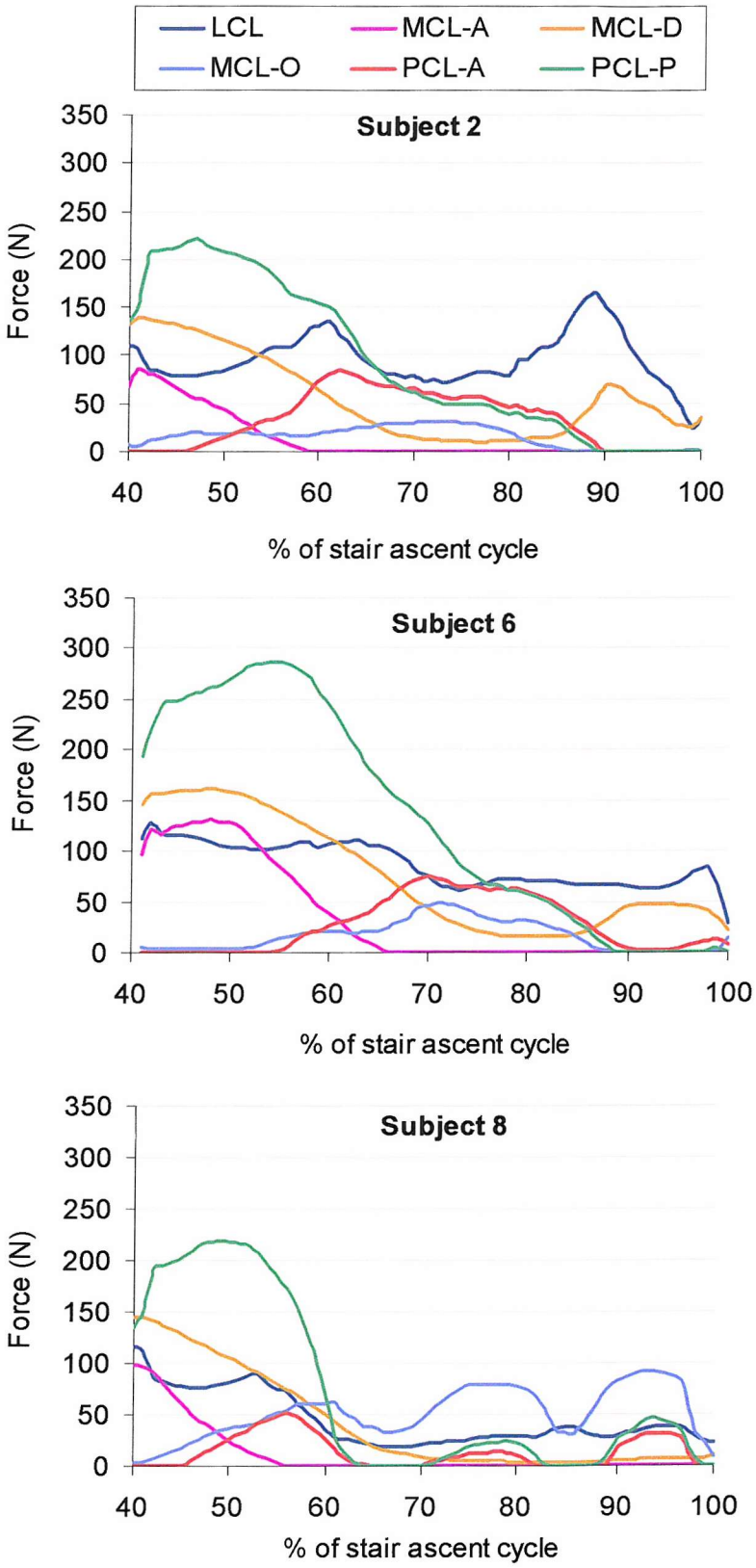

Figure A-4: Ligament forces for three selected subjects during stair ascent activity using PLI knee.

APPENDIX B

The Effect Of Misalignment On The Performance Of TKR

Misaligned the orientation of the TKR relative to the ligaments have been shown to affect the forces sustained by the ligaments. Figure B-1, Figure B-2, Figure B-3 and Figure B-4 show the ligament forces for misalignment study using PFC Σ design and PLI design during level gait and stair ascent activity. During level gait (Figure B-1 and Figure B-2), the amount of forces in each ligament element for PFC Σ design and PLI design were fairly similar. Although both designs were applied to the same loading condition, the differences observed in ligament forces probably due to the implant type. During stair ascent activity (Figure B-3 and Figure B-4), PCL-P exhibited the highest forces in both TKR designs. In general, the forces carried in each ligament were higher than level gait.

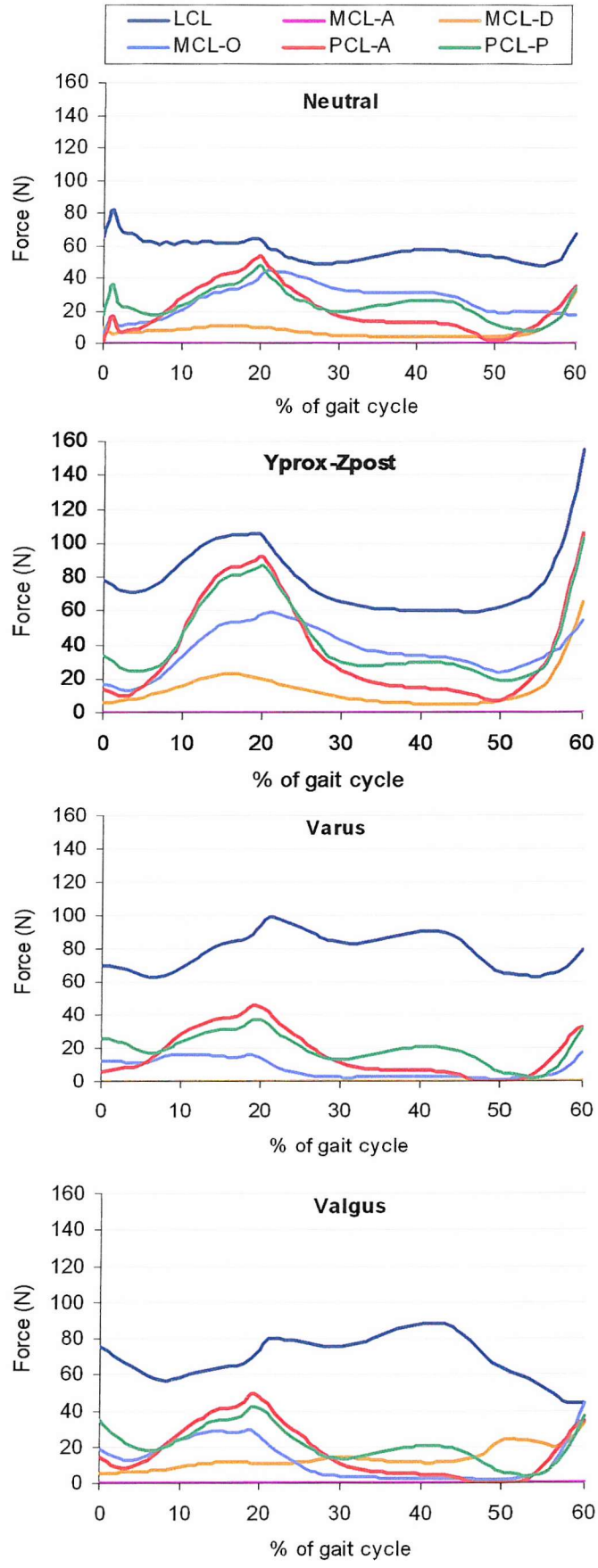

Figure B-1: Ligament forces for 3 selected misalignment cases with comparisons to the neutral alignment model using PFC Σ design during level gait activity.

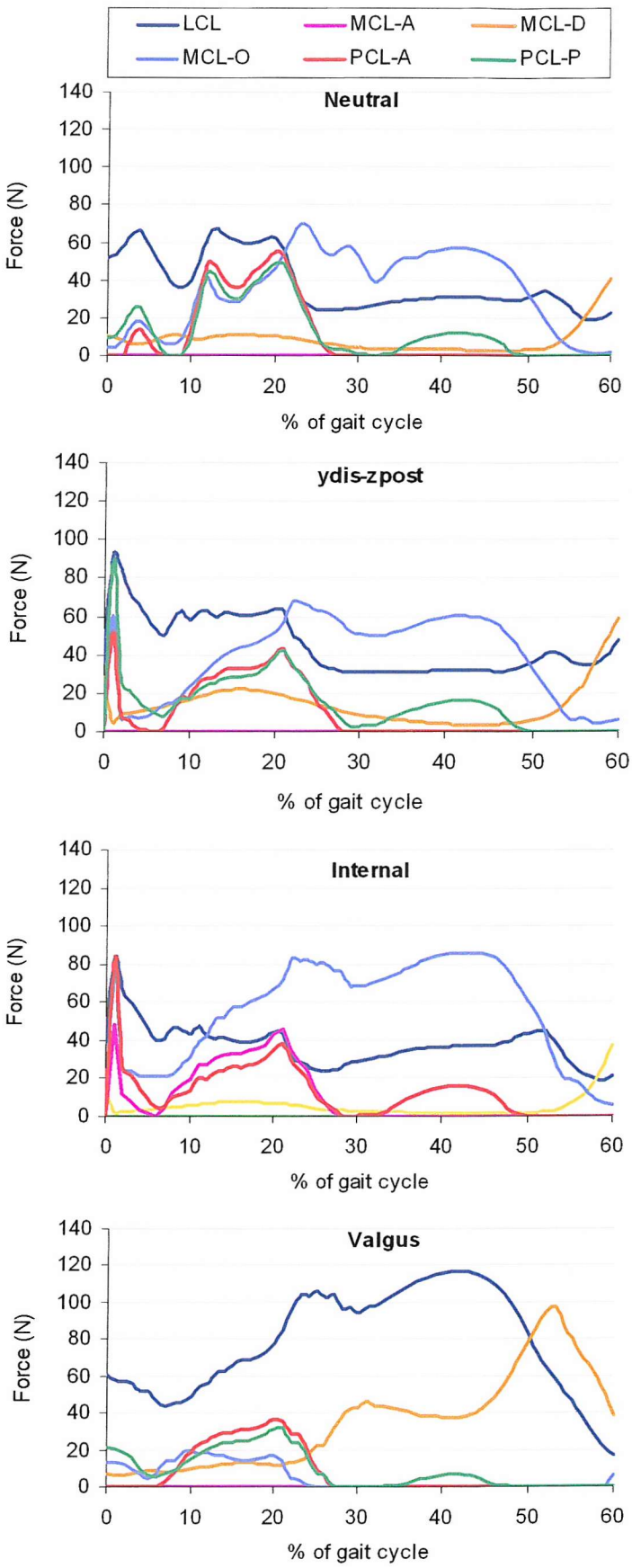

Figure B-2: Ligament forces for 3 selected misalignment cases with comparisons to the neutral alignment model using PLI design during level gait activity.

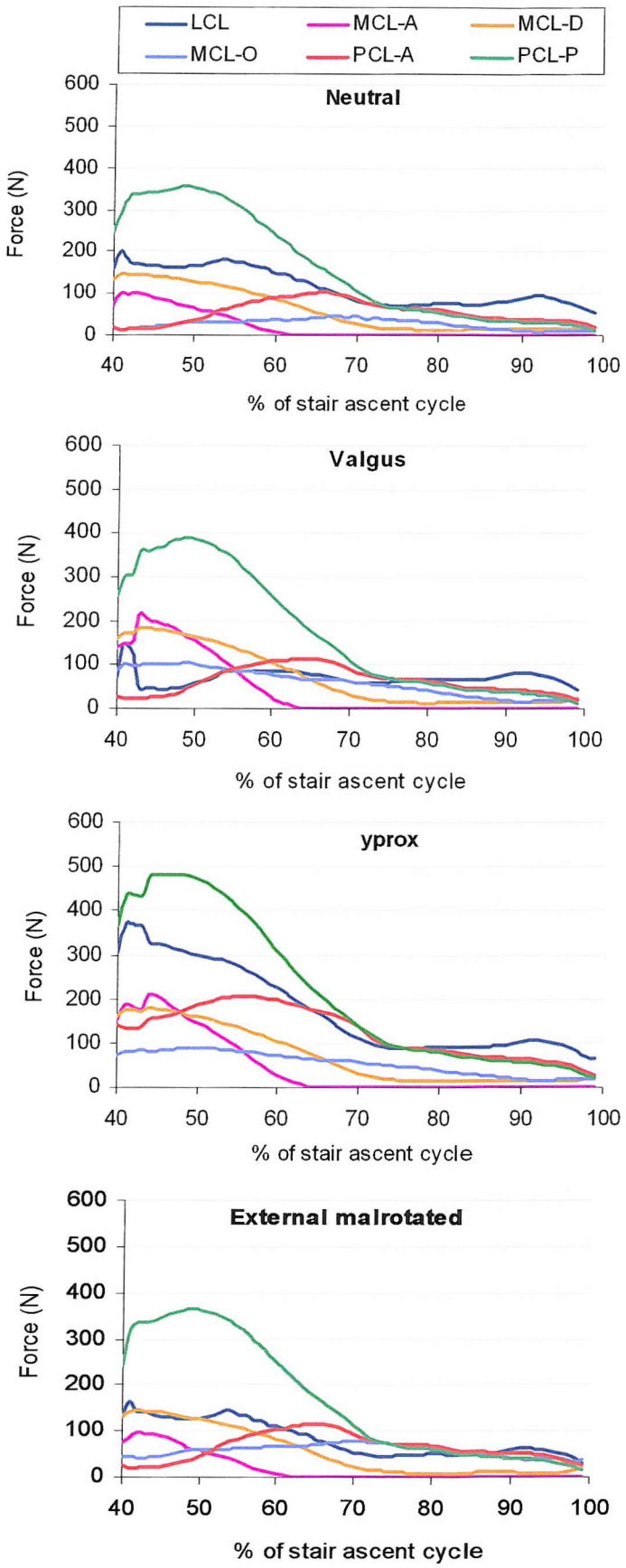

Figure B-3: Ligament forces for 3 selected misalignment cases with comparisons to the neutral alignment model using PFC Σ design during stair ascent activity.

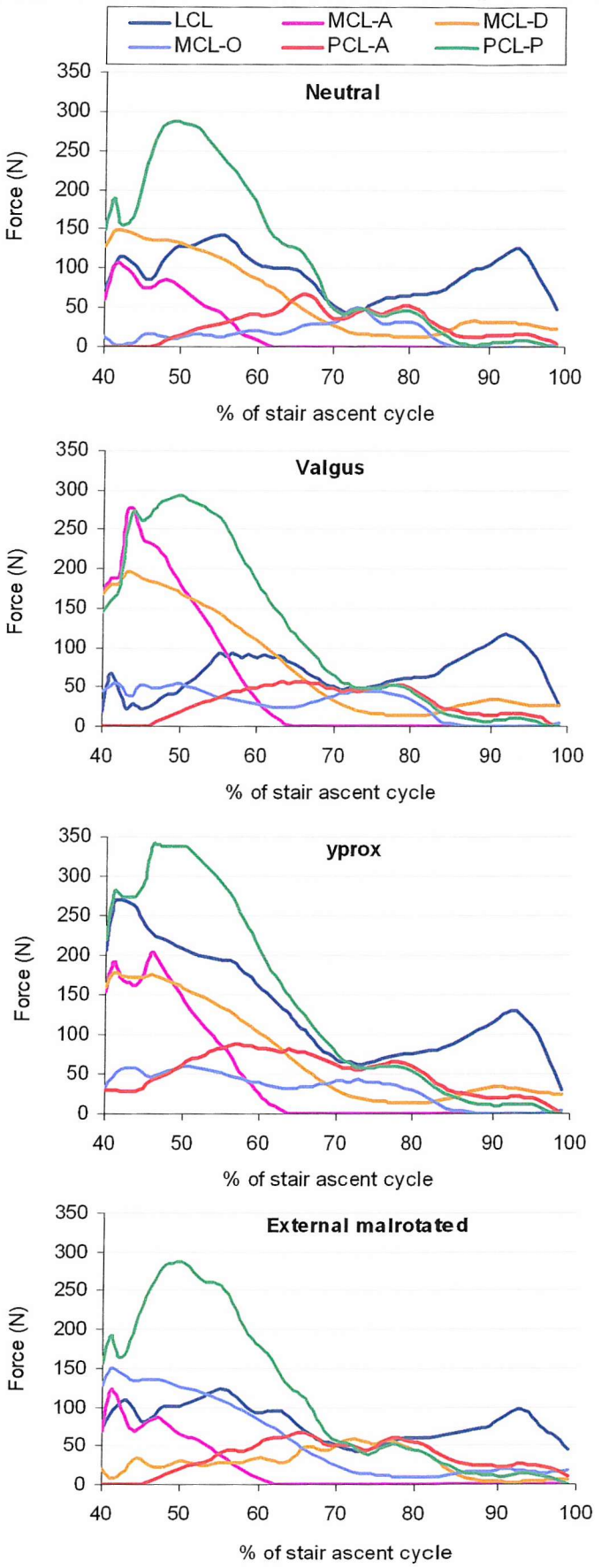

Figure B-4: Ligament forces for 3 selected misalignment cases with comparisons to the neutral alignment model using PLI knee during stair ascent activity.

APPENDIX C

Use Of Explicit FE In The Pre-Clinical Testing Of Total Knee Replacement

Mark Taylor[1], Rachael Tan[1], Jason Halloran[2] and Paul Rullkoetter[2]

1. Bioengineering Science Research Group, School of Engineering Sciences, University of Southampton, Highfield, Southampton, SO17 1BJ, UK.

2. Computational Biomechanics Group, School of Engineering and Computer Science, University of Denver, Denver, CO, USA.

(Book title: Explicit FE analysis of total knee replacement.
in press, 2004.)

Use of explicit FE in the pre-clinical testing of total knee replacement

Mark Taylor[1], Rachael Tan[1], Jason Halloran[2] and Paul Rullkoetter[2]

[1] *Bioengineering Science Research Group, School of Engineering Sciences, University of Southampton, Highfield, Southampton, SO17 1BJ. UK.*

[2] *Computational Biomechanics Group, School of Engineering and Computer Science, University of Denver, Denver, CO, USA.*

Introduction

The short and long term behaviour of total knee joint replacement is dependent on obtaining the optimal stress distribution within the bone-implant construct. The stress distribution within the prosthetic components, the bone-implant interface and within the supporting bone are ultimately dependent on the kinematics of the replaced knee. In turn, the kinematics are dependent on a number of factors including the geometry of the implant, particularly of the articulating surfaces, the relative alignment of the components, both with respect to each other and with respect to the bone, and tensions of the surrounding soft tissues. Of particular interest is the potential for wear of the polyethylene insert. Fatigue damage is likely to result in pitting or delamination and gross failure of the polyethylene component, whereas abrasive/adhesive wear may lead to an

adverse osteolytic reaction and potential for implant loosening. Both failure modes will be influenced by the magnitude of the polyethylene stresses and the overall kinematics of the joint. Retrieval studies have shown that, unlike hips, the wear of TKR is highly variable [1, 2] and this is probably due to the diverse kinematics which occur *in vivo*.

Fatigue damage and abrasive/adhesive wear of total knee replacements is a multi-factorial problem and is dependent on the material properties (including the molecular weight, degree of cross-linking, processing, sterilisation technique and counterface roughness), patient related variables (activity levels, which influence kinematics and loading), surgery related variables (orientation of the components and ligament balancing) and design related parameters (retention/resection of the posterior cruciate ligament, fixed or mobile bearing, degree of congruency). The relative contributions of these various factors to TKR wear are difficult to assess.

Currently, TKR designs are only subjected to a limited range of pre-clinical validation to assess their function, in terms of their kinematics and their potential long term wear performance. At the design stage, rigid body analyses may be performed to evaluate the kinematics of the design. At the prototype stage, a design will undergo wear testing. A number of experimental knee wear simulators have been proposed [3, 4] with the aim of replicating the *in vivo* mechanical environment. The most complex simulators are capable of applying loads and motions in four principal directions (flexion-extension; inferior-superior and anterior-posterior translation and internal-external rotation). At present, TKR designs are evaluated under idealized conditions, typically simulating the bi-condylar loading of an average weight patient during level gait.

Knee simulators are important in pre-clinical assessment of the initial kinematics and wear of both new designs and materials. They have been used to examine the kinematics of different implant designs [5] and the long-term wear

behaviour [3, 6, 7]. Although this gives a necessary benchmark for comparing different designs, it gives no indication of how a prosthesis is likely to perform in the diverse conditions likely to be experienced *in vivo*.

In addition to experimental studies, computer simulations can provide useful information to aid in the design process by evaluating potential TKR performance for a wider range of implant geometry and loading/kinematic conditions than can be examined experimentally. Until recently, simulations to predict implant kinematics and the stress distribution within the polyethylene insert were performed separately. However, as discussed earlier, the polyethylene stresses are intimately related to the kinematics of the joint. Early attempts to predict the polyethylene stresses were based on static FE analyses, which simulated the peak forces during the gait cycle. In these studies, the position of the femoral component relative to the tibia at that particular instant of the gait cycle had to be estimated and was assumed to be either in the deepest part of the polyethylene insert [8, 9] or by estimating where contact would occur in a well function natural knee [10]. In an attempt to develop more realistic models, the relative positions of the prosthetic components at various stages of the gait cycle was derived from either rigid body kinematic analyses [11] or from fluoroscopy data [12]. For example, Sathasivam *et al.* [13] developed a three dimensional rigid body model with that reproduced the motions of the experimental Stanmore knee simulator [14]. The predicted motions were then were used to define the relative positions of the prosthetic components within a three dimensional FE model and a series of static FE analyses were performed at various flexion angles to calculate the contact pressures and estimate sub-surface damage [11].

Only Estupinan *et al.* [15] and Reeves *et al.* [16] have modelled dynamic loading. Estupinan *et al.* used an idealized, two-dimensional model of a non-conforming knee replacement to simulate the influence of cyclic loading on polyethylene stresses. A 200 N load was applied to the femoral indentor which

was then displaced 4mm across the polyethylene surface, the load was removed and the indentor returned to its original position. Reeves *et al.* used a two dimensional sagittal plane model to examine the development of plastic strain in the polyethylene due to repetitive loading. The anterior-posterior motion of the femoral component was controlled by applying a displacement history from the literature.

The major limitation of all of these analyses are that they either assume the replaced knee to be statically loaded or in the rare cases where motion has been included, the motions are imposed by controlled displacements. *In vivo*, the motions of the knee are controlled by imposed forces, either directly by the joint reaction force or indirectly through the restraints of the surrounding ligaments.

At the University of Southampton and the University of Denver, we have been exploring the use of explicit FE analysis to study the performance of total knee replacement. Explicit finite element analysis has been specifically developed to simulate multi-contact and highly non-linear problems. It has been used extensively in the automotive industry to simulate impacts and to aid the development of occupant safety systems. The main advantage of explicit finite element analysis is that it is capable of calculating the kinematics and the implant stresses from a single analysis at a relatively low computational cost. The work described here will focus on the large body of work performed to date between the two laboratories on a particular TKR design (PFC Sigma, DePuy).

Simulation of a gait cycle in a knee wear simulator

The initial explicit FE studies [17-21] were aimed at replicating the mechanical environment within the Stanmore knee simulator in order simulate a gait cycle [14]. The femoral component was modelled as rigid body using four-noded shell elements. The polyethylene was modelled as a deformable continuum assuming

elastic-plastic material behaviour and meshed using continuum hexahedral elements (Figure 1). The boundary conditions applied to the model were aimed at reproducing the mechanical environment existing in the Stanmore knee simulator [14]. The femoral component was allowed to translate in the inferior-superior direction, to rotate about a frontal axis to simulate valgus - varus rotation and to rotate about a transverse axis to simulate flexion-extension. The tibial insert was allowed to translate in the anterior-posterior direction and rotate about a fixed vertical axis located in the middle of the tibial condyles to simulate internal-external rotation.

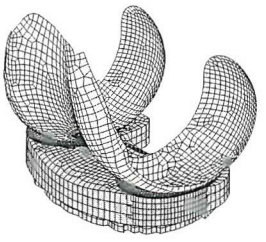

Figure 1 - Explicit FE model of tibiofemoral articulation.

In the experimental wear simulator, the horizontal component of the soft tissue restraints are represented by four springs, two anteriorly and two posteriorly. These springs were replicated within the FE model and assigned a stiffness of 10.4 Nmm^{-1}, and a corresponding rotational constraint of 0.3 $Nm\text{-}deg^{-1}$. The boundary condition loading histories for the axial force, internal-external torque, anterior-posterior force and the flexion-extension angle were defined according to the experimental protocol of the Stanmore knee simulator. The finite element simulations are typically performed at between 0.5 and 1 Hz. The models are then used to evaluate the resulting kinematics (anterior-posterior displacement, internal-external rotations), the contact pressures and areas, the polyethylene stresses and plastic strains. Analyses have been performed using either Pam-Crash-Safe or Abaqus explicit.

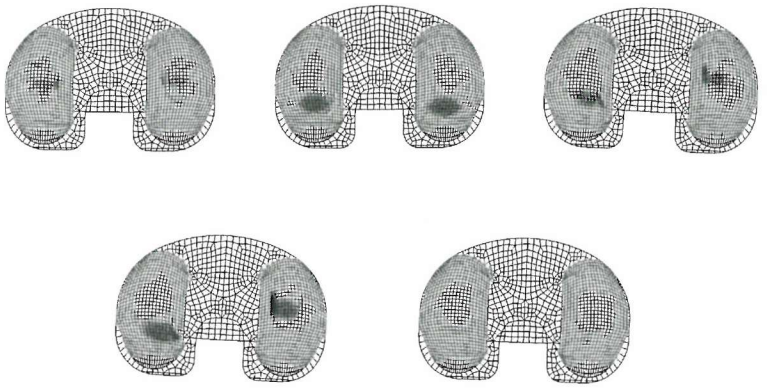

Figure 2 – Contact pressure distribution at 5, 17, 35,45 and 65% of the gait cycle (0% heel strike, 60% toe-off and 100% heel-strike). Light gray corresponds to 0 MPa and black to pressures in excess of 20 MPa

The predicted contact pressure distribution on the proximal surface of the polyethylene insert from a typical analysis are shown in Figure 2. At the beginning of the simulation, the medial and lateral condyles are slightly anterior of the neutral position. In the first 20% of the gait cycle the femoral condyles moved posteriorly on the polyethylene component and the peak contact pressures rose to approximately 15 MPa. Between 20% and 45% of the gait cycle, the lateral femoral condyle moved anteriorly. During this phase, the peak contact pressure decreased to 10 MPa at approximately 30% of the gait cycle and then rose again to the maximum of 22 MPa at 45% of the gait cycle. Between 45% and 60% the lateral condyle returned to a posterior position on the tibial component and the peak contact pressures decreased to 10 MPa. Both condyles remained in a slightly posterior position during the swing phase of gait (60%-100%) and the peak contact pressures remained constant at 5-6 MPa. In general, the predicted motions are similar to those seen experimentally, both in terms of general trends and the absolute magnitudes [17]. The influence of mesh density and contact algorithm on the predicted kinematics and contact stresses has been studied [17]. The kinematics were shown to be relatively insensitive to

changes in mesh density, but the predicted peak contact pressure and contact area were found to be mesh dependent. To date, this technique has been used to examine the performance of TKR as a result of a range of parameters including eccentric loading [21], patient specific loading and tibial slope angle.

Influence of unicondylar loading on the kinematics and stresses generated in a TKR

Normal alignment of the lower extremity is approximately 0 degree of mechanical alignment or 7 to 9 degrees of tibiofemoral anatomic valgus. The main objectives of total knee replacement (TKR) surgery are to alleviate pain and restore function by lower extremity re-alignment and soft-tissue balance. However, perfect knee alignment is not always obtained in total knee replacement. Varus-valgus malalignment has been shown to cause high contact stresses within the polyethylene insert [22] and in some cases may cause severe damage to the component.

The effects of eccentric loading, as a result of varus malalignment, were simulated by displacing the point of application of the axial load medially, along the flexion and extension axis. Two loading cases were simulated; loading offsets of 0 and 20 mm that resulted in medial:lateral loading ratios of 50:50 and 95:5 respectively, i.e bi-condylar and unicondylar loading, respectively. Because the femoral component is represented as a rigid body, offsetting the point of application of the vertical load meant that the center for varus and valgus rotations also was offset by the same amount.

In the knee joint, the collateral ligaments are positioned in the vertical direction to resist varus-valgus rotations. Therefore, two models were considered; the standard horizontal linear spring model (HLS model), which replicates the mechanical environment of a knee wear simulator, and a model in which the springs were replaced by representations of the collateral ligaments (CL model). The collaterals were modelled as membrane elements, which allow

buckling under compressive loads. . The MCL and LCL had stiffnesses of 130 and 110 N/mm, respectively [23]. The proximal ends of both ligaments were rigidly attached to the femoral component and the distal ends were attached to the tibial component. The origins of the collateral ligaments were assumed to be approximately parallel to the vertical loading axis. Again, the predicted AP translations and the IE rotations of the prosthetic components were compared for the different models.

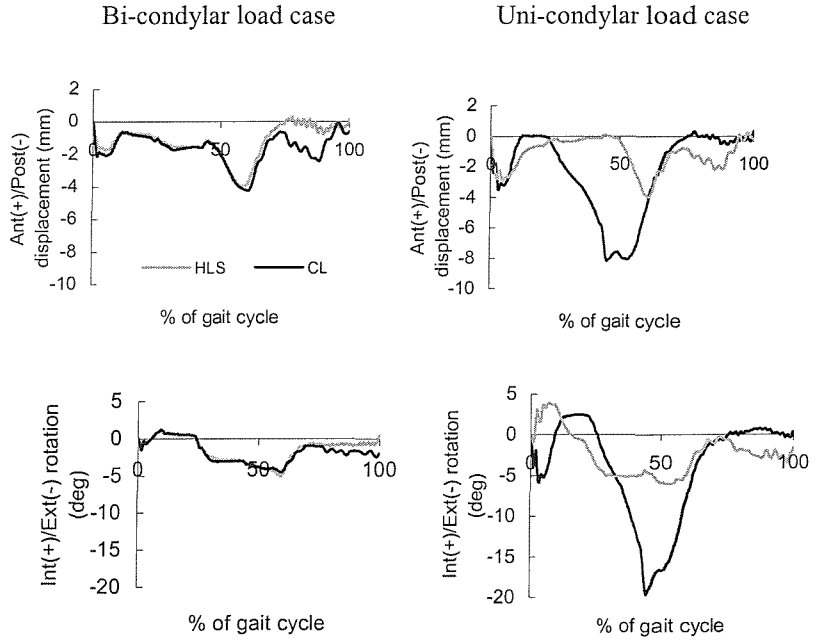

Figure 3: Predicted kinematics of the HLS and CL models when subjected to bi-condylar and uni-condylar load cases. Top row corresponds to the AP translations and the bottom row the IE rotations.

For the bi-condylar load cases, there was no significant difference in the kinematics of the TKR during the stance phase of gait between the HLS and CL models, although there were small differences during the swing phase (Figure 3). For the unicondylar load case, there was a significant difference in the kinematics (figure 3). For both models, at the beginning of the simulation to 15

% of the gait cycle, the medial condyle moved from being centrally located to a slightly posterior position and the lateral condyle translated from the anterior edge to the posterior edge of the tibial component. As the simulation progressed to 45 % of the gait cycle, the position of the medial condyle for the two models still remained constant. However, the HLS model internally rotated more than the CL model. The lateral condyle of the HLS model rode up the anterior lip of the tibial insert, nearly subluxing, between 45 % and 50 % of the gait cycle. The lateral condyle of the HLS model then moved back towards the center position at about 60% of the gait cycle. During the swing phase, both condyles for this model remained at a slight posterior position. For the CL model, a similar pattern of motion was observed for the lateral condyle, but the degree of internal rotation was significantly less, with peak internal rotations of 18 and 7 degrees respectively for the HLS and CL models. The presence of the collateral ligaments constrains the vertical motion of the femoral component, reducing the amount the lateral condyle of the femoral component is able to ride up the anterior lip of the polyethylene, and hence limits the degree of internal rotation.

The maximum contact stresses for the HLS model were generally less than the CL model for the bi-condylar load case. The peak contact stress for the HLS model was approximately 22 MPa and occurred at 47% of the gait cycle, as compared to the peak contact stress for the CL model of 27 MPa. There were only minor variations in the maximum contact stresses for the CL model between the unicondylar and bi-condylar load cases. However, for the HLS model, there was a significant increase between the bi-condylar and unicondylar load cases. The peak contact stress was 42.4 MPa at for the unicondylar load case and this was 12.4 MPa higher than the CL model.

The simple HLS model has been shown to be adequate for evaluating the ISO standard bi-condylar loading configuration. However, when considering abnormal loading, like uni-condylar loads, it is important to include representations of the collateral ligaments, so as to include the vertical constraint

that they provide. If these are not included, such models tend to over-predict the amount of internal rotation and consequently over-predict the peak contact pressures that occur.

Influence of patient specific loading

Although it is well understood that a TKR design will experience a range of loading conditions, at present they are evaluated under a limited range of idealised loading conditions. In order to assess the influence of variability in the kinematics and polyethylene stress a series of analyses were performed using subject-specific load cases. The knee joint reaction forces during walking for seven healthy subjects were calculated using an inverse dynamics method (Dr Patrick Costigan, Queen's University, Canada – Personal communication). The axial and anterior-posterior forces, internal-external torques and flexion angles calculated for these seven subjects are shown in Figure 4, and these were used to drive the knee replacement model. The peak axial force was typically in the range of 1000-2000 N, although the predicted peak axial force for one individual was 2800N. The anterior-posterior forces ranged from a posteriorly directed force of 250N to an anteriorly directed force of 200 N. A consistent pattern of torque was observed, with the peak value for each individual ranging from 2 to 8 Nm. From Figure 4, it can be seen that not all the subjects started at 0° of flexion. Two subjects started with a slightly hyperextended knee at approximately 2° and 5°, respectively. The other subjects began between 4° and 8.5° of flexion. Again, the anterior-posterior displacement, internal-external rotations and contact stress distributions of the knee prosthesis were reported for each individual.

In general, each individual's model produced a similar trend in both the anterior-posterior translations and the internal rotations. During the stance phase, the femoral component tended to translate posteriorly and internally

rotate (figure 5). This was followed by an anterior translation and an external rotation during swing phase. Averaging this data and plotting the mean and standard deviation (figure 5) showed relatively minor variations between the kinematics of each individual. During the stance phase of the gait cycle, the standard deviation is on the order of 0.5 to 1mm for the AP translations and 0.4 and 1 degree for the IE rotations.

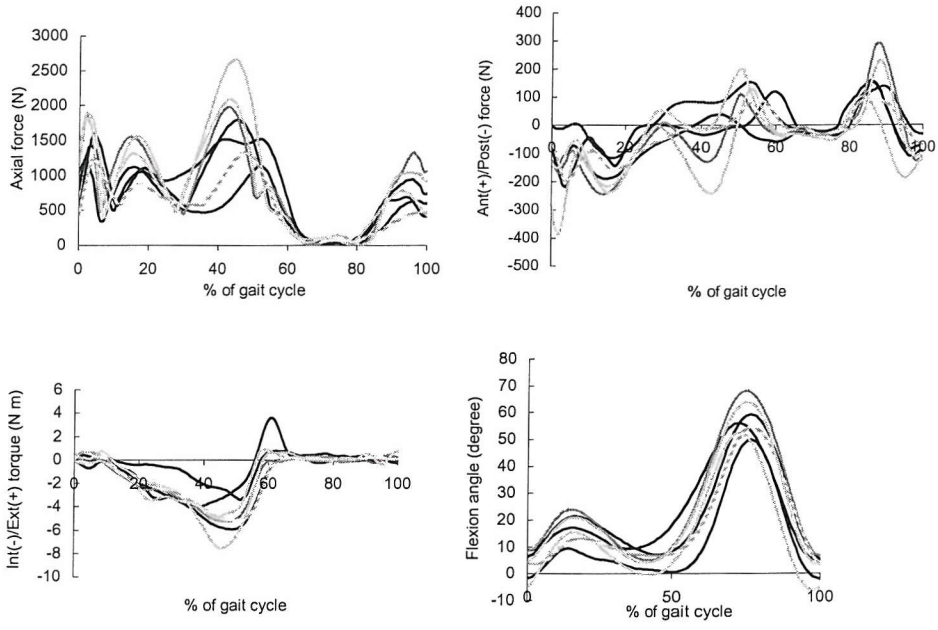

Figure 4 – Force data for seven healthy individuals applied to the TKR model (Dr P. Costigan, Queen's University, Canada – Personal communication).

Although the kinematics appear to be fairly consistent for this design for level gait, there was a larger range in the predicted maximum contact stresses (figure 5). The variation of the peak contact pressure during the gait cycle was fairly consistent, however, the magnitude was sensitive to the magnitude of the axial force. During the first 30% of gait cycle the standard deviation was

between 2 and 5 MPa and between 30 and 60% of the gait cycle it varied from 1 to 4 MPa.

For this particular design it has been shown that during level gait the kinematics are relatively insensitive to variation between patients, whereas substantial variations may occur in the predicted peak contact pressure. Other designs may be more or less sensitive to patient related variability. It may also be true that there will be greater variability between subjects for different activities, for example stair ascent. By using patient specific forces, it is possible to assess the performance envelope for a total knee replacement design.

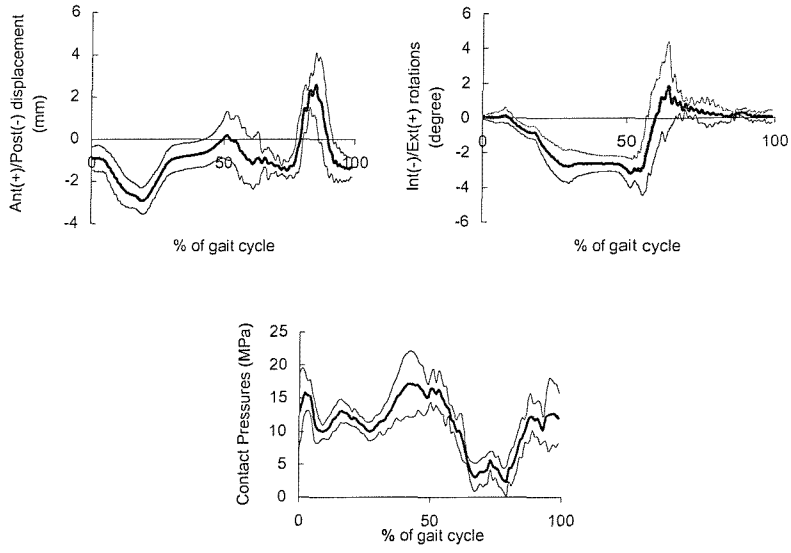

Figure 5 – Variation in the predicted kinematics and the peak contact pressures as a result of patient specific loading. The thick line represents the mean for the 7 patients and the thin line represents ± one standard deviation of the mean.

Influence of posterior tibial slope

Posterior tilting of the tibial tray and insert is frequently used clinically to facilitate a greater range of flexion by promoting natural femoral rollback, and to resist anterior tibial subsidence by optimizing the underlying bone strength following resection. Significant posterior tilt angles may also be included unintentionally. As a result of the altered tibiofemoral constraint and conformity, relative motion and insert stresses will also change. Since, as mentioned previously, the joint kinematics and contact mechanics will play a large role in the long-term success of total knee arthroplasty, it is important to quantify the effect of posterior tilting on these measures. Thus, the effect of posterior tilt on joint mechanics during *in vitro* physiological loading and the sensitivity of various current TKR devices to these changes were evaluated.

The TKR was analyzed during gait simulation at successive, even posterior tilt angles from 0° (no posterior slope) until component dislocation occurred during the gait cycle. In each analysis, the femoral component was loaded at full extension to find a stable initial position before applying the simulated gait loading cycle. During the initial loading cycle, a nominal load was applied to the femoral component while it was unconstrained in the AP and varus-valgus degrees of freedom. This initial loading resulted in settling of the femoral component into the lowest point in the tibial dish. For every tilt angle the simulated soft-tissue constraint remained in the original, 0° plane in order to evaluate changes in joint mechanics as a result of the changing posterior tilt. Again, tibiofemoral AP displacement, IE rotation, insert stresses, and contact area were recorded as a function of the gait cycle for each analysis.

Changes in the posterior tibial slope varied tibiofemoral constraint and hence, relative kinematics. Both changes in relative kinematics and tibiofemoral

conformity were factors in increasing surface and subsurface insert stresses. The semi-constrained PCR design showed only small changes in AP motion from 0° to 10° tilt, generally less than 0.5 mm (Figure 6). From 12° to 16° tilt the peak anterior tibial motion increased by 3.1 mm due to the decrease in anterior constraint. The total range of AP motion was very consistent throughout the range of tilt angles studied (Figure 6). Femoral component subluxation occurred posteriorly during the gait cycle at 18° tilt. Both the total range and peak internal rotation decreased steadily with increasing tilt. The peak internal rotation decreased from 5.2° with no posterior slope to 2.3° at 16° tilt (Figure 6). The total IE range of motion decreased nearly linearly from 6.3° to 2.7°, or approximately –0.22° IE/°tilt (Figure 6). Peak contact pressures during the cycle were steady, then increased linearly after 10° tilt due to variation in kinematics creating posterior edge loading (Figures 7 and 8). Near 55% of the gait cycle the 0°, 2°, and 4° analyses experienced a spike in the contact pressure results due to relatively high IE rotation creating poor-conformity contact. The reduction in IE rotation with posterior tilt angle reduced this peak by approximately 25% for the 8° and 10° analyses (Figure 7). Although there were only small changes in AP kinematics for the range of tilt studied, the composite von Mises stress distribution (all stress contours added for each increment of the gait cycle) shows a progressive posterior motion of the peak stresses with increasing posterior tilt (Figure 8).

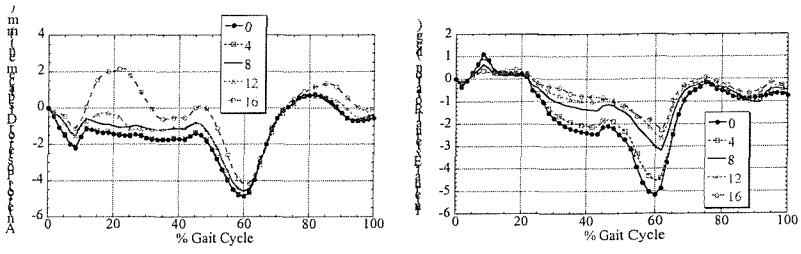

Figure 6 – Influence of posterior slope of on the predicted kinematics

This particular design of TKR was found to be relatively accommodating to changes in tilt in the range that would be used clinically.

Peak contact pressure remained steady until beyond 10° of posterior tilt. Predicted joint kinematics were fairly consistent, again, especially through 10° of tilt. The peak and range of IE rotation decreased consistently with tilt. Increased anterior insert motion marked the rise in contact pressure realized at 16° posterior tilt as a result of posterior edge contact. The single sagittal insert radius was relatively insensitive to changes in tilt that could occur when surgically reproducing the anatomic tibial slope in TKA.

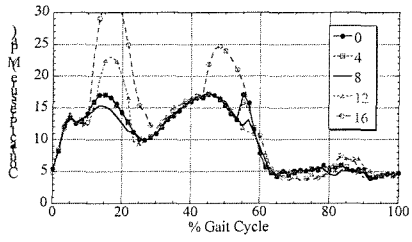

Figure 7 – Influence of posterior slope of on the predicted peak contact pressures

Wasielewski and coauthors [24] found a statistically significant correlation between tibial insert posterior slope and increasingly posterior articular wear track location with an unconstrained insert. This is consistent with the composite von Mises and contact stress distributions. The results from this study demonstrate that posterior tilting of the tibial tray and insert in the range used clinically may alter the tibiofemoral AP and IE constraint, and result in significant changes in stability and predicted kinematics during gait simulation. Corresponding contact mechanics may also be substantially altered due to variation in conformity, especially when edge-loading conditions appear. Additionally, the unconstrained PCR designs, which are frequently implanted with a posterior tilt, may be more sensitive to these changes.

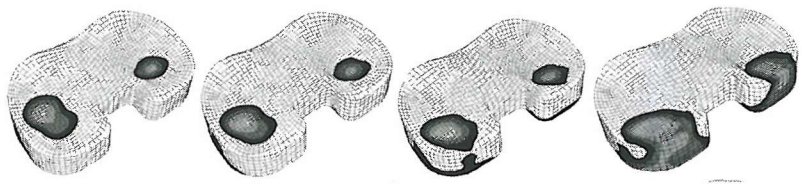

Figure 8 – Composite von Mises stress distribution (summation of all the stress contours for each increment of the gait cycle)

Rigid body analysis

Although the deformable, explicit FE models are reasonably efficient, reported CPU time is still in the range of 6 hours to more than a day for a full gait cycle [17, 25]. Parametric analysis of component positioning, numerical wear simulation of TKR components, or other studies which require many repeated analyses or real-time feedback can therefore be cost prohibitive. Modelling the polyethylene insert as a rigid body, together with an elastic contact definition, has been reported to reduce the solution times to less than thirty minutes. However, potential differences in predicted kinematics between rigid and deformable insert representations are currently not well understood, and it is unclear if the estimates of contact pressure distribution are acceptable given the significant reduction in computational time. The explicit analysis permits the polyethylene insert to be easily characterized as a deformable or rigid body. In order to estimate the contact pressure distribution during a rigid body analysis, softened contact capability was employed. A relationship between contact pressure and surface overclosure (penetration) was estimated for the rigid-body contact definition based on the polyethylene material data. The "bed of springs" method from elastic foundation theory was used:

$$Pressure = \frac{(1-\nu)E}{(1+\nu)(1-2\nu)} \cdot \frac{overclosure}{thickness} \qquad (1)$$

where E is the Young's modulus of the insert and ν is Poisson's ratio. The initial slope of the elastic-plastic material model (571.6 MPa), Poisson's ratio (0.45), and average thickness of the insert (10 mm) were used to calculate the linear pressure-overclosure relationship.

The deformable material behavior is nonlinear, and therefore beyond the initial linear region the rigid-body pressures calculated using the linear pressure-overclosure relationship will be overestimated.

In order to most accurately perform parametric or repetitive studies using the rigid body approximations, such as numerical wear simulation with many identical repeated analyses, more precise predictions of contact pressures and areas are required. In an effort to enhance the results with the rigid-body simulations, the pressure-overclosure relationship was optimized by minimizing the difference between the contact pressure and area results determined using a rigid and deformable analysis. To accomplish this, a nonlinear constrained optimization routine in the IMSL library (Visual Numerics, Inc., San Ramon, CA) was used in conjunction with a C program to integrate IMSL and Abaqus. The objective function to be minimized calculated the sum of the percent difference between the rigid and deformable results for twenty points along the contact pressure and area results curves.

The rigid body and fully deformable analyses predicted very similar kinematics. The AP motion was nearly identical, and the IE rotation had a maximum difference of less than 0.5° (Figure 9). Peak contact pressures were found near 15%, 45% and 55% of the gait cycle, and were approximately 17 MPa for the deformable analysis (Figure 10). The initial, 'bed-of-springs' estimate of the pressure-overclosure relationship resulted in very close agreement for the contact area and consistent overestimation of the peak pressures, although the general trends were acceptable (Figure 10). Once the rigid body pressure-overclosure relationship had been optimized, there was close agreement with the fully deformable analysis results. The contact pressure

contours for positions throughout the cycle were compared and closely match (Figure 10). CPU time for the full deformable analysis was 6 hours, yet it was only 8 minutes for the rigid body analysis, nearly a 98% reduction.

The pressure-overclosure model had little bearing on the predicted kinematics. Thus, if only kinematics are of interest in an analysis, an efficient rigid body model would provide acceptable results in this range of physiological loading conditions. The linear, 'bed-of-springs' contact pressure-surface overclosure relationship was a reasonable, first-order approximation to the deformable pressure distribution. Optimising the overclosure parameters resulted in excellent agreement between the deformable and rigid analyses. Limitations of the rigid body approach include significant overprediction of contact pressure with low conformity contact situations, such as the edge-loading conditions. Also, internal insert stresses and strains are not calculated in any of the rigid body analyses, nor is there currently the potential for including any time-dependent material properties, such as creep. In addition, the relationship was optimized for a particular mesh and loading conditions, and may change with significantly higher loads or variation in geometry or mesh density. However, given the vast reduction in computational time of approximately 98%, the rigid body approach will be useful in a variety of situations, such as numerical wear simulation that repeatedly applies the same loading conditions, or investigating the effects of variable component positioning.

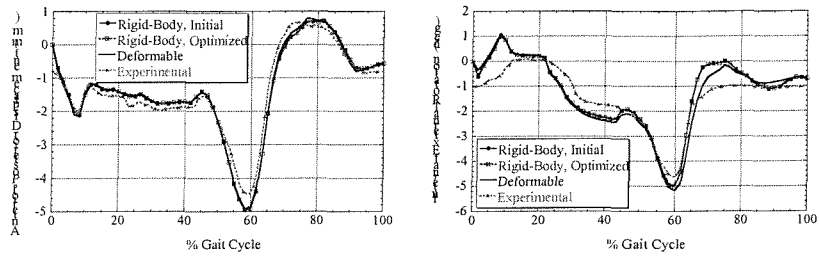

Figure 9 – Comparison of the kinematics predicted by a rigid body model and a deformable model.

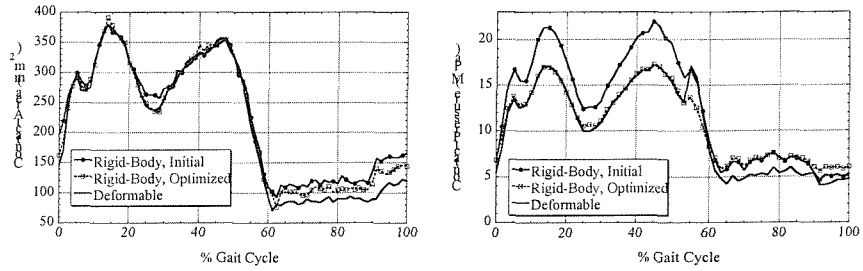

Figure 10 – Comparison of the contact areas and pressures predicted by a rigid body model and a deformable model

Numerical wear simulation

Mechanical wear simulators have been developed to this end, but require long testing times and are not ideal for investigating variables of implant geometry or effects of relative implantation locations. In addition, wear tests are slow and have a high associated cost. Tests are performed at a frequency of 1 hertz, which equates to 11.5 days/million loading cycles or 115 days for a typical 10 million cycle test. The average person with a joint replacement walks 1-2 million steps per year [26], so current tests equate to 5-10 years of normal activity. In order to simulate 20 years of service life, typical for a young TKR patient, these tests should be extended to at least 20-40 million cycles. This is clearly impractical with current knee wear simulators. Current test methods

only simulate the gait cycle and recently stair descent [27]. In everyday life, the knee is subjected to a range of activities, including ascending stairs and rising from a chair. These activities, although less frequent, are more demanding than level gait, as they have higher flexion angles and higher loads. The experimental wear simulators may be considered to be semi-constrained. The flexion-extension and internal-external axes of rotation are fixed, where as the knee is free to decide the point about which it rotates. This artificial constraint may influence the wear process, particular for higher flexion activities like ascending/descending stairs. Current experimental wear tests are performed under 'ideal' conditions, with respect to the implant orientation and the applied loading and boundary conditions (simulated soft-tissue constraints and axes of rotation). The prosthetic components are orientated within the machine in a neutral position. The loads are assumed to be for an average individual with a mass of approximately 70 kg and are typically distributed 50:50 to the medial and lateral condyles. The constraints representing the soft-tissue assume that the medial and lateral sides are balanced.

These ideal conditions are rarely achieved *in vivo*. Fluoroscopy studies have shown that lift-off often occurs, causing uni-condylar loading of either the medial or lateral compartment. Gait studies have shown that the gait patterns can vary significantly between individual strides within same patient and between patients, particularly in the early post-operative period. This will lead to variations in the ratios of the axial force to the anterior-posterior loads and internal-external torques. Patient mass can vary significantly, with masses in excess of 100 kg frequently occurring. In order to address these issues there is a need to develop numerical simulations to compliment experimental wear testing.

In an effort to produce results efficiently, numerical wear simulation methods have been developed based on Archard's law [28], and used in conjunction with implicit FE analyses [29]. The development of the explicit FE analysis has now made it practical to simulate the wear of knee joint

replacements during force-controlled loading conditions. The explicit FE wear simulation can include important changes in relative kinematics due to changes in insert geometry during evaluation of long-term wear behaviour.

Although it is of future interest to perform long-term wear simulation, the initial rigid and deformable analyses discussed previously were used to estimate wear of the tibial inserts for 1 million loading cycles from a single gait cycle analysis. Predicted wear was enforced on a nodal basis, and linear penetration at each node was estimated using Archard's law [28]:

$$W = k \times s \times p \qquad (2)$$

where W is the linear wear penetration, s is the tangential sliding distance, p is the contact stress, and k is the wear coefficient. k was adapted from Wang et al. [30] for the TKR analyses. Using a custom script, the sliding distance and contact stress data were extracted from the FE results and were used to estimate linear wear values for each node on the articular surface of the polyethylene component. Linear wear was applied to each node in a direction normal to the surface. The nodal positions were recorded before and after application of the simulated wear and the linear and volumetric wear were estimated.

Maximum linear penetration was determined for two designs, the semi-constrained PFC Sigma and an unconstrained TKR for a simulated 1 million gait cycles (Figure 11). The unconstrained insert experienced greater contact pressures and smaller contact areas due to lesser tibiofemoral conformity. This resulted in larger predicted linear wear, but a 10% decrease in wear volume when compared to the more conforming, semi-constrained device. For the semi-constrained insert, a 3.2% difference was found in the peak penetration using rigid and deformable insert representations. For the unconstrained insert, the difference was only 2.2%. Corresponding volumetric wear predictions varied by 6.2% (semi-constrained) and 4.2% (unconstrained). A significant reduction in

CPU time was realized using the rigid body approach with optimized pressure-overclosure relationship, which completed in approximately 15 minutes compared to more than 6 hours for the deformable model.

The predicted wear trends of increasing volumetric wear with larger areas of contact is similar to results found on retrieved TJR components, and determined using mechanical simulators [31, 32]. Work is currently in progress to develop adaptive FE simulations of wear, which will be able to account for the changes in geometry, and the corresponding changes in kinematics and contact pressures, that occur during extended wear testing (20+ million cycles). In addition, experimental validation by comparison with a knee wear simulator is ongoing, and will include both volumetric wear measurement (from weight loss) and surface profile measurement (includes linear wear and creep).

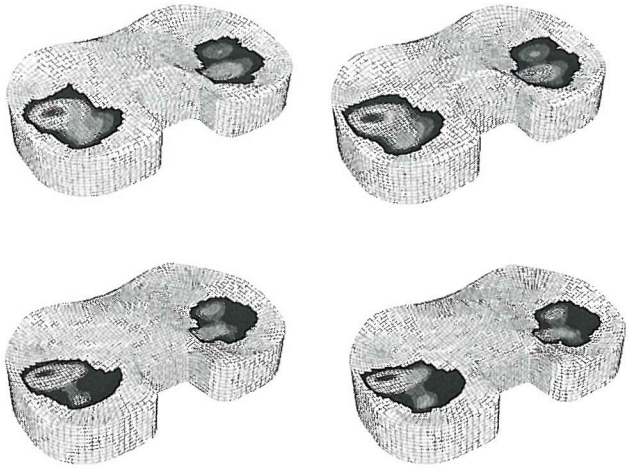

Figure 11 - Wear contours determined using deformable (left column) and rigid body (right column) analyses for semi-constrained (top) and unconstrained (bottom) designs.

Full TKR model: Analysis of the patello-femoral kinematics and stresses

Solid models of the femur, patella, tibia, and fibula were developed from computed tomography (CT) scan data, obtained from the Visible Human Female dataset. The bone models were imported, placed appropriately and trimmed using standard surgical technique, and meshed with rigid elements (Figure 12). Membrane elements were chosen to represent the quadriceps tendon and ligamentous structures (Figure 12). These structures include contact to capture the effects of soft-tissue wrapping on the implant and bone [23, 33]. Bony protrusions of the solid models were used as insertion sites for the soft-tissue structures. Nonlinear elastic material definitions for the soft-tissue structures were also adopted from available literature [34, 35]. Separate load-displacement analyses were used to validate the response of each ligament, including the quadriceps tendon, patellar ligament, lateral and medial collaterals, and posterior cruciate ligament.

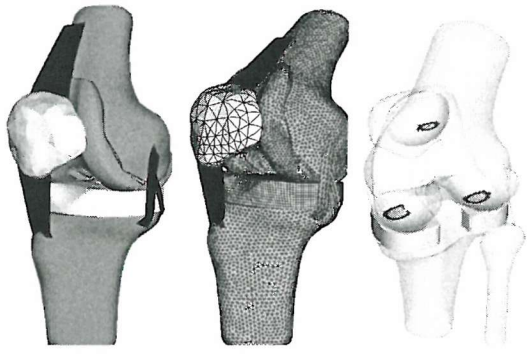

Figure 12. TKR model solid models (left), finite element mesh (middle), and transparent view showing patellar button and contact pressures (right).

In order to describe the relative kinematics for the TKR model in a manner consistent with experimental studies, a three-cylindric model of joint motion was incorporated for both tibio- and patello-femoral motion [36].

Coordinate frames were created with nodes placed on the femur, tibia, and patella, and relative kinematics were be measured and described as three rotations and three translations. The model of joint motion was implemented with a post-processing script written in Python to interface with the output results database.

Experimental kinematic data were obtained from articulation of the TKR device during gait simulation using the Purdue knee simulator [37]. Two implanted cadaveric knees were run under level walking conditions in the knee simulator. The Purdue simulator applies a vertical load and flexion angle at a simulated hip, and a tibial torque and a medial-lateral directed force at the representative ankle. A quadricep actuator balances the vertical load through the patellar ligament. Six-degree-of-freedom spatial linkages were mounted between the femur and the patella and femur and tibia. Provided experimental data, therefore, included tibio-femoral and patello-femoral kinematics and measured feedback of quadricep load as a percent of gait cycle. Hence, in order to verify model-predicted patellar motion the experimental tibio-femoral motion and quad load were used as inputs to the TKR model, and predicted patellar kinematics were compared to experimental data.

Boundary conditions were applied to reproduce the Purdue knee simulator environment. Measured tibial flexion-extension and internal-external rotations, anterior-posterior and medial-lateral translations, and vertical and quadriceps loading were applied to the model. In order to simulate the changing orientation, the applied quadriceps load is coupled to the flexion-extension angle as occurs in the experimental simulator. The Q-angle of the simulator was also included. The predicted patello-femoral kinematics were compared with the experimentally determined six degree-of-freedom kinematics using both a relatively coarse and a fine button mesh. A deformable as well as a rigid body analysis was performed using each mesh. Finally, contact area and contact pressure were compared between rigid body and deformable analyses.

Patello-femoral kinematic verification showed good agreement between experimental and model predicted results for both trends and magnitudes (Figures 13). The plotted experimental data is the average of the two measured knees. Predicted patellar flexion matched experimental results to within approximately 1.3°. Flexion results from both meshes and both rigid and deformable analyses were very similar (Figure 13). Model predicted and experimental patellar spin were both near 1°. The largest discrepancy between model and experimental data is seen in the medial-lateral tilt of the patella. The model over predicted medial tilt during flexion by up to 2.7° (Figure 13). The two data sets were consistent in all degrees of freedom except tilt; one knee demonstrated a similar pattern to the model but the other exhibited almost no tilt. Predicted relative translations also correlated well with the experimental data, with peak differences of 1.7 mm along the femoral inferior-superior axis, and 2.7 mm along the femoral anterior-posterior direction. Predicted and experimental medial-lateral shift were both under 1 mm. Again, kinematic predictions resulting from the rigid body and deformable analyses were almost indistinguishable.

CPU time for the patello-femoral verification deformable analysis (coarse mesh) required approximately 18 hours and the corresponding rigid body representation required 2 hours.

Use of the explicit code allows 'buckling' of the soft tissues to occur without the stability problems that would take place with implicit analyses. During flexion activity this can act to simulate the recruitment of different ligament fibers (Blankevoort et al., 1991). This initial use of explicit FE modeling of soft-tissue structures is advantageous and will likely continue to progress. The addition of time-dependent material models for the soft tissues should be an area of future development.

In order to perform a rigorous experimental verification, the tibio-femoral and patello-femoral articulations were initially examined separately.

Additionally, although the collaterals and posterior cruciate load-displacement behaviour was verified independently, the knee constraint provided was not included in the present experimental verification. The rigid bone models were used primarily for soft-tissue attachment sites. Futher development of the knee model will include a distribution of bone material properties, and a focused study on verification of soft-tissue constraint before thorough experimental verification of predicted simultaneous, force-controlled articulation.

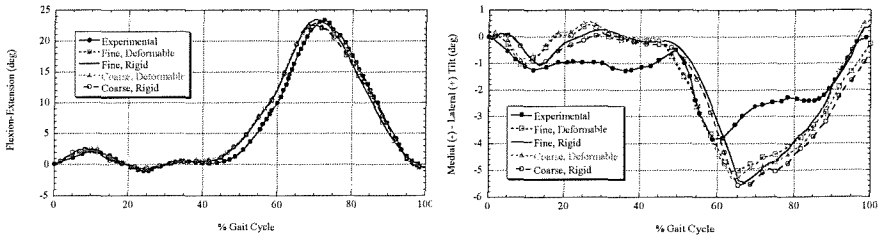

Figure 13. Experimental (Purdue knee simulator) and model predicted patello-femoral a) flexion-extension and b) medial-lateral tilt as a function of gait cycle.

Conclusions

Joint kinematics and contact mechanics substantially influence the short- and long-term performance of current total knee replacement devices. Although a multifactorial problem, implant contact stresses and relative motion play a significant role in wear and fatigue damage to the polyethylene insert, potentially limiting the useful life of the implant. Fatigue damage, such as pitting or delamination, can lead to catastrophic insert failure, while excessive abrasive/adhesive polyethylene wear may initiate an osteolytic reaction to particulate debris, contributing to eventual loosening and revision surgery. A volume of recent research has, therefore, focused on the prediction of kinematics at the joint interfaces and contact stresses and areas due to articulations as an indication of potential clinical performance.

Until recently, TKR stress analyses were generally performed using implicit FE analysis to predict surface and subsurface implant stresses during displacement-controlled conditions, and kinematic analyses were frequently formulated as rigid body dynamics problems to estimate relative motion during various loading conditions. Explicit FE models may be advantageous due to their stability during general, force-controlled analysis and ability to simultaneously predict implant stresses and relative motion. In addition, explicit FE formulations are unique in that they generally allow for either rigid or deformable representations of meshed components.

In our work, explicit FE formulations have been developed for both tibiofemoral and combined tibio- and patellofemoral articulations. Verification results from the computational TKR models showed that the predicted patellofemoral and tibiofemoral kinematics were in good agreement with experimental knee simulator measurements. Current studies have demonstrated the significance of eccentric loading and posterior tilting, and ongoing research includes the analysis of implant design parameters, sensitivity to implantation position, and effects of surgical procedures.

References

1. Engh GA: Failure of the Polyethylene Bearing Surface of a Total Knee Replacement within 4 Years. Journal of Bone and Joint Surgery-American Volume 70A:1093-1096, 1988.
2. Blunn GW, Joshi AB, Lilley PA, Engelbrecht E, Ryd L, Lidgren L, Hardinge K, Nieder E, Walker PS: Polyethylene Wear in Unicondylar Knee Prostheses - 106 Retrieved Marmor, Pca, and St-Georg Tibial Components Compared. Acta Orthopaedica Scandinavica 63:247-255, 1992.
3. Burgess IC, Kolar M, Cunningham JL, Unsworth A: Development of a six station knee wear simulator and preliminary wear results. Proceedings of the Institution of Mechanical Engineers, Part H 211, 1997.

4. Walker PS, Blunn GW, Perry J, Bell CJ, Sathasivam S, Andriacchi TP, Paul JP, Haider H, Campbell PA: Methodolgy for long-term wear testing of total knee replacements. Clinical Orthopaedics and Related Research 372:290-301, 2000.
5. DesJardins JD, Walker PS, Haider H, Perry J: The use of a force-controlled dynamic knee simulator to quantify the mechanical performance of total knee replacement designs during functional activity. Journal of Biomechanics 33:1231-1242, 2000.
6. Barnett PI, McEwen HMJ, Auger DD, Stone MH, Ingham E, Fisher J: Investigation of wear of knee prostheses ina new displacement/force controlled simulator. Proceedings of the Institution of Mechanical Engineers, Part H 216:51-61, 2002.
7. McGloughlin T , Kavanagh A: Wear of ultra-high molecular weight polyethylene (UHMWPE) in total knee prostheses: a review of key influences. Proceedings of the Institution of Mechanical Engineers, Part H 214:349-359, 2000.
8. Bartel DL, Bicknell VL, Ithaca MS, Wright TM: The effect of conformity, thickness and material on stresses in ultra-high molecular weight components for total joint replacement. Journal of Bone and Joint Surgery 68A:1041-1051, 1986.
9. Mottershead JE, Edwards PD, Whelan MP, English RG: Finite element analysis of a total knee replacement by using Gauss point contact constraints. Proceedings of the Institution of Mechanical Engineers, Part H 210:51-63, 1996.
10. Bartel DL, Rawlinson JJ, Burstein AH, Ranawat CS, Flynn WF: Stresses in polyethylene components of contemporary total knee replacements. Clinical Orthopaedics and Related Research 317:76-82, 1995.
11. Sathasivam S , Walker PS: Computer model to predict subsurface damage in tibial inserts of total knees. Journal of Orthopaedic Research 16:564-571, 1998.
12. Ishikawa H, Fujiki H, Yasuda K: Contact analysis of ultrahigh molecular weight polyethylene articular plate in artificial knee joint during gait movement. Journal of Biomechanical Engineering-Transactions of the Asme 118:377-386, 1996.

13. Sathasivam S , Walker PS: A computer model with surface friction for the prediction of total knee kinematics. Journal of Biomechanics 30:177-184, 1997.
14. Walker PS, Blunn GW, Broome DR, Perry J, Watkins A, Sathasivam S, Dewar ME, Paul JP: A knee simulating machine for the performance evaluation of total knee joint replacements. Journal of Biomechanics 30:83-89, 1997.
15. Estupinan JA, Bartel DL, Wright TM: Residual stresses in ultra-high molecular weight polyethylene loaded cyclically by a rigid moving indentor in non-conforming geometries. Journal of Orthopaedic Research 16:80-88, 1998.
16. Reeves EA, Barton DC, FitzPatrick DP, Fisher J: A two-dimensional model of cyclic strain accumulation in ultra-high molecular weight polyethylene knee replacements. Proceedings of the Institution of Mechanical Engineers, Part H 212:189-198, 1998.
17. Godest AC, Beaugonin M, Haug E, Taylor M, Gregson PJ: Simulation of a knee joint replacement during a gait cycle using explicit finite element analysis. Journal of Biomechanics 35:267-276, 2002.
18. Halloran J, Patrella A, Rullkoetter P. *Explicit finite element model predicts TKR mechanics.* in *49th ORS.* 2003.
19. Halloran J , Rullkoetter P. *A dynamic finite element model for prediction of TKR mechanics.* in *48th ORS.* 2002.
20. Halloran J , Rullkoetter PJ. *Development of an explicit finite element based total knee replacement model.* in *ASME Bioengineering Conference.* 2001.
21. Taylor M , Barrett DS: Explicit finite element simulation of eccentric loading in total knee replacement. Clinical Orthopaedics and Related Research 414:162-171, 2003.
22. Liau JJ, Cheng CK, Huang CH, Lo WH: The effect of malalignment on stresses in polyethylene component of total knee prosthese - a finite element analysis. Clinical Biomechanics 17:140-146, 2002.
23. Mommersteeg TJA, Blankevoort L, Huiskes R, Kooloos JGM, Kauer JMG, Hendriks JCM: The Effect of Variable Relative Insertion Orientation of Human Knee Bone-Ligament-Bone Complexes on the Tensile Stiffness. Journal of Biomechanics 28:745-752, 1995.

24. Wasielewski RC, Galante JO, Leighty RM, Natarajan RN, Rosenberg AG: Wear patterns on retrieved polyethylene tibial inserts and their relationship to technical considerations during total knee arthroplasty. Clin Orthop 299, 1994.
25. Giddings VL, Kurtz SM, Edidin AA: Total knee replacement polyethylene stresses during loading in a knee simulator. Journal of Tribology 123:842-847, 2001.
26. Wallbridge N , Dowson D: The walking activities of patients with artificial joints. Eng. Med. 11:96, 1982.
27. Benson L, DesJardins JD, LaBerge M. *Stair descent loading pattern for TKR wear simulation.* in *48th Annual Meeting of theOrthopaedic Research Society.* 2002. Dallas, USA.
28. Archard JF: Contact and rubbing of flat surfaces. Journal of Applied Physiology:981-988, 1953.
29. Maxian TA, Brown TD, Pedersen DR, Callaghan JJ: A sliding-distance-coupled finite element formulation for polyethylene wear in total hip arthroplasty. Journal of Biomechanics 29:687-692, 1996.
30. Wang A: Lubrication and Wear of Ultra-High Molecular Weight Polyethyelene Total Joint Replacements. Tribology International 31:17-33, 1998.
31. Gillis AM , and Li S, "," , , p.: A Quantitative Comparison of Articular Surface Damage Areas and Types in Retrievals From 4 Different Knee Designs. Trans 45th Annual Meeting ORS 45:861, 1999.
32. Harman MK, Banks SA, Hodge WA: The Influence of Femoral Geometry on In-Vivo Kinematics and Wear in Two Designs of PCL-Retaining Total Knee Arthroplasty. Trans 45th Annual Meeting 45:148, 1999.
33. Blankevoort L , Huiskes R: Ligament-bone interaction in a three-dimensional model of the knee. J. Biomech. Eng. 113:263-269, 1991b.
34. Staubli HU, Schatzmann L, Brunner P, Rincon L, Nolte LP: Mechanical Tensile Properties of the Quadriceps Tendon and Patellar Ligament in Young Adults. American Journal of Sports Medicine 27:27-34, 1999.
35. Quapp KM , Weiss JA: Material characterization of human medial collateral ligament. J. Biomech. Eng. 120:757-763, 1998.

36. Grood ES , Suntay WJ: A Joint Coordinate System for the Clinical Description of Three-Dimensional Motions: Application to the Knee. Transactions of the Associated Society of Mechanical Engineers 105:136-144, 1983.
37. Zachman NJ, Hillberry BM, Kettlekamp: Design of a Load Simulator for the Dynamic Evaluation of Prosthetic Knee Joints. ASME publication n 78-DET-59: 1978.